Chen CA, Chang MC, Sun WZ, Chen YL, Chiang YC, Hsieh CY, Chen SM, Hsiao PN, and Cheng WF. 2009. Noncarrier naked antigen-specific DNA vaccine generates potent antigen-specific immunologic responses and antitumor effects. Gene Ther. 16(6):776-87.

Huang CY, Chen CA, Lee CN, Chang MC, Su YN, Lin YC, Hsieh CY, and Cheng WF. 2007. DNA vaccine encoding heat shock protein 60 co-linked to HPV16 E6 and E7 tumor antigens generates more potent immunotherapeutic effects than respective E6 or E7 tumor antigens. Gynecol Oncol. 107(3):404-12.

Hung HF, Wang BW, Chang H, and Shyu KG. 2008. The molecular regulation of resistin expression in cultured vascular smooth muscle cells under hypoxia. J Hypertens. 26(12):2349-60.

Lai MD, Chen CS, Yang CR, Yuan SY, Tsai JJ, Tu CF, Wang CC, Yen MC, and Lin CC. 2009. An HDAC inhibitor enhances the antitumor activity of a CMV promoter-driven DNA vaccine. Cancer Gene Ther. 1-9.

Lai MD, Yen MC, Lin CM, Tu CF, Wang CC, Lin PS, Yang HJ, and Lin CC. 2009. The effects of DNA formulation and administration route on cancer therapeutic efficacy with xenogenic EGFR DNA vaccine in a lung cancer animal model. Genet Vaccines Ther. 7:2.

Lou PJ, Cheng WF, Chung YC, Cheng CY, Chiu LH, and Young TH. 2009. PMMA particle-mediated DNA vaccine for cervical cancer. J Biomed Mater Res A. 88(4): 849-57.

Shyu KG, Chua SK, Wang BW, Kuan P. 2009. Mechanism of inhibitory effect of atorvastatin on resistin expression induced by tumor necrosis factor-alpha in macrophages. J Biomed Sci. 16:50.

Yen MC, Lin CC, Chen YL, Huang SS, Yang HJ, Chang CP, Lei HY, and Lai MD. 2009. A novel cancer therapy by skin delivery of indoleamine 2,3-dioxygenase siRNA. Clin Cancer Res. 15(2):641-9.

Yi-Ta Chen
Application Specialist
Email: info@wealtec.com

Wealtec Bioscience Co. Ltd.
27Fl. No. 29-1 Sec.2, Jungjeng E. Rd., Danshuei Jen, Taipei, Taiwan 25170
TEL: +886-2-8809-8587 FAX: +886-2-8809-8589; http://www.wealtec.com

Gene Therapy (2009) 16, 776–787

www.nature.com/gt

ORIGINAL ARTICLE

Noncarrier naked antigen-specific DNA vaccine generates potent antigen-specific immunologic responses and antitumor effects

C-A Chen[1], M-C Chang[2], W-Z Sun[2], Y-L Chen[1], Y-C Chiang[1], C-Y Hsieh[1], SM Chen[1], P-N Hsiao[2] and W-F Cheng[1,3]

[1]Department of Obstetrics and Gynecology, College of Medicine, National Taiwan University, Taipei, Taiwan; [2]Department of Anesthesiology, College of Medicine, National Taiwan University, Taipei, Taiwan and [3]Graduate Institute of Clinical Medicine, College of Medicine, National Taiwan University, Taipei, Taiwan

Genetic immunization strategies have largely focused on the use of plasmid DNA with a gene gun. However, there remains a clear need to further improve the efficiency, safety, and cost of potential DNA vaccines. The gold particle-coated DNA format delivered through a gene gun is expensive, time and process consuming, and raises aseptic safety concerns. This study aims to determine whether a low-pressured gene gun can deliver noncarrier naked DNA vaccine without any particle coating, and generate similarly strong antigen-specific immunologic responses and potent antitumor effects compared with gold particle-coated DNA vaccine. Our results show that mice vaccinated with noncarrier naked chimeric CRT/E7 DNA lead to dramatic increases in the numbers of E7-specific CD8+ T-cell precursors and markedly raised titers of E7-specific antibodies. Furthermore, noncarrier naked CRT/E7 DNA vaccine generated potent antitumor effects against subcutaneous E7-expressing tumors and pre-established E7-expressing metastatic pulmonary tumors. In addition, mice immunized with noncarrier naked CRT/E7 DNA vaccine had significantly less burning effects on the skin compared with those vaccinated with gold particle-coated CRT/E7 DNA vaccine. We conclude that noncarrier naked CRT/E7 DNA vaccine delivered with a low-pressured gene gun can generate similarly potent immunologic responses and effective antitumor effects has fewer side effects, and is more convenient than conventional gold particle-coated DNA vaccine.
Gene Therapy (2009) **16,** 776–787; doi:10.1038/gt.2009.31; published online 9 April 2009

Keywords: *noncarrier naked DNA vaccine; antigen; immunologic response; antitumor effect*

Introduction

Ideal cancer treatment should be able to eradicate systemic tumors at multiple sites of the body while having the specificity to discriminate between neoplastic and non-neoplastic cells. In this regard, antigen-specific cancer immunotherapy represents an attractive approach. The activation of antigen-specific T cell-mediated immune responses allows for the killing of tumors associated with a specific antigen and has become an important strategy for cancer immunotherapy.[1,2]

The DNA vaccine has emerged as a novel method and an attractive strategy for the generation of antigen-specific cancer vaccines and immunotherapy. It is a new and powerful approach to generate immunologic responses against various diseases.[3–6] A variety of human clinical trials and animal models using DNA vaccines have been carried out for various infectious diseases,[7,8] therapies against cancer[9,10] and therapies against autoimmune diseases and allergies.[11,12] In addition, they have also become a widely used laboratory tool for a variety of applications ranging from proteomics to understand antigen presentation and cross-priming. The use of DNA vaccine technology precludes the need for handling hazardous viral pathogens, as only the DNA encoding antigens are incorporated into the vaccine.[13] DNA vaccine technology also eliminates the need for biocontainment and the risk of exposure to live viral agents. Several modalities have been employed to deliver DNA vaccines, including intramuscular injection using conventional needle and syringe,[3] electroporation,[14] intradermally by the needle-free biojector[15] and epidermally through a gene gun.[16,17]

However, one of the concerns regarding DNA vaccines is their limited potency. This is characterized by two major properties: the low level of the antigen expression and the long-lasting expression. These two factors are believed to be responsible for the vaccination effect, which leads to a continuous stimulation of the immune system and training of memory cells.[18] Our earlier work has shown that a chimeric DNA vaccine coated with gold particles using the gene gun approach to rout the human papillomavirus (HPV) type 16 E7 model antigen results in enhanced E7-specific CD8+ T cell-mediated immune responses and antitumor effects through different strategies, including targeting antigens by fusing molecules to

Correspondence: Dr W-F Cheng, Department of Obstetrics and Gynecology, National Taiwan University Hospital, Taipei, Taiwan.
E-mail: wenfangcheng@yahoo.com
Received 4 September 2008; revised 24 February 2009; accepted 24 February 2009; published online 9 April 2009

enhance antigen processing,[19] directing antigens to APCs by fusion to ligands for APC receptors,[20] or to a pathogen sequence, such as domains of exotoxin in *Pseudomonas*,[10,21] intercellular spread[22] and prolonging dendritic cells (DCs) survival through antiapoptotic molecules.[9]

Safety issues and complicated preparation are two important concerns for the clinical application of gene gun-delivered gold particle-coated DNA vaccines. So, we utilized a new, low-pressured gene gun to evaluate whether a noncarrier naked DNA vaccine can be delivered efficiently by this method and to evaluate the possibility of using noncarrier naked DNA vaccines without gold particle coating in the development of cancer vaccines and immunotherapy. We first showed that noncarrier naked DNA could be delivered into the cells of the intradermal layer. The noncarrier naked chimeric CRT/E7 DNA vaccine could also enhance antigen-specific T cell immunity and antibody response, and generate as potent antitumor effects as the gold particle-coated chimeric CRT/E7 DNA vaccine did. In addition, the burning effect on bombarded skin was less on noncarrier naked DNA vaccinated mice than that on gold particle-coated DNA vaccinated mice. We concluded that noncarrier naked DNA vaccines can be delivered by a low-pressured gene gun to generate similar potent antigen-specific immunities and antitumor effects, but with fewer side effects compared with gold particle-coated DNA vaccines. This can help improve the utility of naked DNA vaccines and promote human clinical trials of naked DNA vaccines in cancer vaccines and immunotherapy in the future.

Results

Fluorescence examination on skins of noncarrier naked pEGFP-N2 DNA-vaccinated mice

We first evaluated whether noncarrier naked DNA could be delivered by a low-pressure gene gun to the intradermal cells that express the interested gene. Very few intradermal cells expressed green fluorescence protein (GFP) after being immunized with noncarrier naked pEGFP-N2 DNA vaccine in various solution media after 6 hours (Figures 1a–d). However, significantly higher numbers of intradermal cells expressed GFP protein after immunization with noncarrier naked pEGFP-N2 DNA vaccine in various solution media after 24 h (Figures 1e–h). The areas of distribution for GFP-expressed cells did not reveal a difference between different volumes or formulations (data not shown). The GFP-expressing cells showed a cluster phenomenon in noncarrier naked DNA regardless of the solution medium (Figures 1f–h). However, the epidermal growth factor (EGF)-expressing cells showed a scattered phenomenon in the gold particle-coated DNA group (Figure 1e).

Our results indicated that noncarrier naked DNA vaccine dissolved in various solutions, without gold particle coating, and could be delivered into the intradermis of mice to express the interested gene.

Vaccination with noncarrier naked CRT/E7 DNA four times generated the most optimal immunologic profiles and tumor preventive effects

We then determined the optimal number of vaccinations with noncarrier naked DNA to generate the most potent immune responses and antitumor effects. As shown in Figure 2a, the number of E7-specific $CD8^+$ T-cell precursors increased when the number of noncarrier naked CRT/E7 DNA vaccinations increased (10.5 ± 1.4 for naïve, 47.0 ± 7.0 for twice, 103.0 ± 9.9 for thrice, 157.5 ± 8.5 for four times, $P < 0.001$, one-way analysis of variance (ANOVA)). In addition, the titers of anti-E7 antibodies also correlated with the number of noncarrier naked CRT/E7 DNA vaccinations (Figure 2b; in 1:100 dilution, 0.447 ± 0.017 for naïve, 0.730 ± 0.035 for twice, 1.550 ± 0.047 for thrice and 1.688 ± 0.094 for four times, $P < 0.01$, one-way ANOVA).

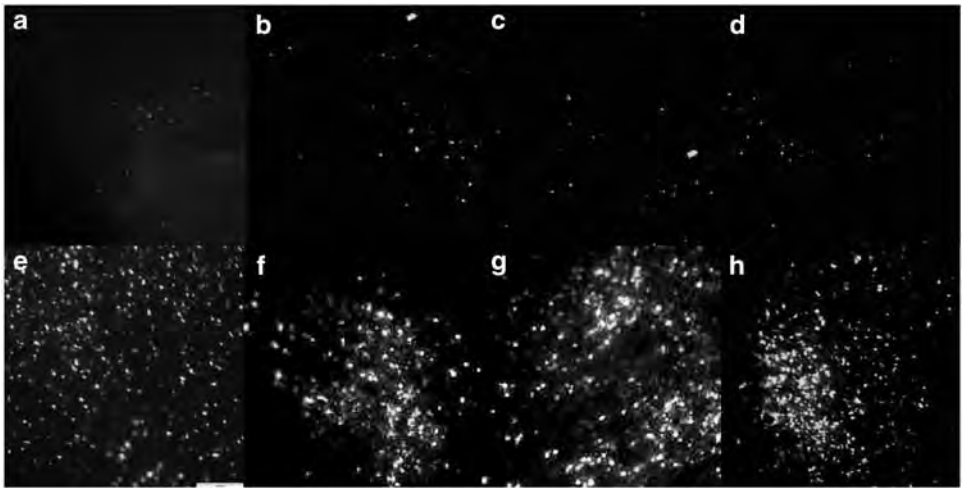

Figure 1 Fluorescence studies on skins of gold particle-coated or noncarrier naked pcDNA3-green fluorescence protein (GFP) DNA vaccinated mice. (**a**) Gold particle-coated DNA 6 h after immunization. (**b**) Noncarrier naked DNA in distilled H_2O (ddH_2O) solution 6 h after immunization. (**c**) Noncarrier naked DNA in phosphate-buffered saline (PBS) 6 h after immunization. (**d**) Noncarrier naked DNA in Tris-EDTA (TE) solution 6 h after immunization (note: only a few cells in the intradermis expressed the GFP protein). (**e**) Gold particle-coated DNA 1 day after immunization. (**f**) Noncarrier naked DNA in ddH_2O solution 1 day after immunization. (**g**) Noncarrier naked DNA in PBS solution 1 day after immunization. (**h**) Noncarrier naked DNA in TE solution 1 day after immunization (note: most of the cells in the intradermis expressed the GFP protein).

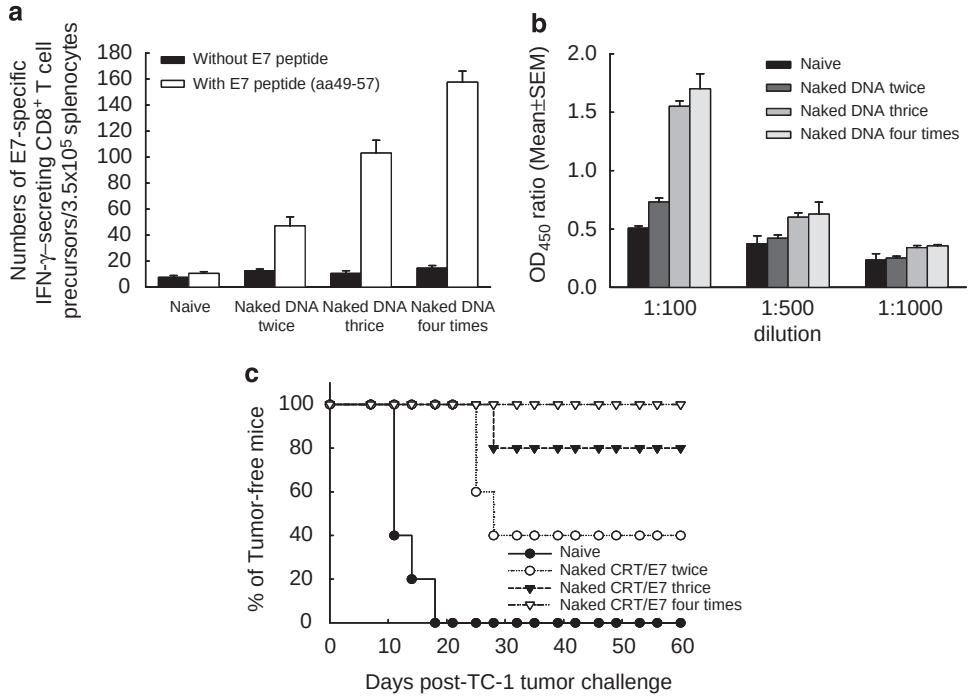

Figure 2 Immunologic profiles and *in vivo* tumor preventive effects of noncarrier naked CRT/E7 DNA vaccine with various times of vaccination. (**a**) Numbers of E7-specific $CD8^+$ T-cell precursors (note: the frequencies of E7-specific $CD8^+$ T-cell precursors correlated with the frequency of noncarrier naked CRT/E7 DNA vaccinations). (**b**) Titers of anti-E7 antibodies (note: the titers of anti-E7 antibodies increased when the number of noncarrier naked CRT/E7 DNA increased). (**c**) *In vivo* tumor preventive experiments (note: only 40 and 80% of mice receiving twice and thrice, respectively, noncarrier naked CRT/E7 DNA vaccine remained tumor-free for 60 days onward when challenged with TC-1 tumor cells). However, 100% of the mice that received noncarrier naked CRT/E7 DNA vaccine four times remained tumor-free 60 days after TC-1 tumor challenge.

For *in vivo* tumor protection experiments, all of the mice vaccinated four times with noncarrier naked CRT/E7 DNA vaccine were tumor-free after 60 days of TC-1 challenge. Only 40 and 80% of mice, which were vaccinated twice and thrice, respectively, remained tumor-free for 60 days onward when challenged with TC-1 tumor cells (Figure 2c).

Our results indicated that the number of noncarrier naked DNA vaccinations influenced the immune responses and tumor protective effects.

Noncarrier naked and gold particle-coated CRT/E7 DNA vaccines generate similar E7-specific immunity and antitumor effects

We further evaluated whether noncarrier naked DNA vaccine generates similar antigen-specific immunities and antitumor effects as gold particle-coated DNA vaccine. Mice vaccinated with noncarrier naked or gold particle-coated CRT/E7 DNA generated higher frequencies of E7-specific interferon (IFN)-γ-secreting $CD8^+$ T-cell precursors when compared with mice vaccinated with the noncarrier naked or gold particle-coated wild-type E7 DNA (12.0 ± 2.8 for noncarrier naked wild-type E7 group, 162.0 ± 10.5 for noncarrier naked CRT/E7 group, 14.0 ± 2.8 for gold particle-coated wild-type E7 group, 226.0 ± 10.0 for gold particle-coated CRT/E7, $P < 0.05$, one-way ANOVA; Figure 3a). The numbers of E7-specific $CD8^+$ T-cell precursors in noncarrier naked CRT/E7 DNA vaccinated mice were fewer than those in the gold particle-coated CRT/E7 DNA vaccinated group ($P < 0.05$, one-way ANOVA).

As shown in Figure 3b, mice vaccinated with noncarrier naked or gold particle-coated CRT/E7 DNA also showed significantly higher titers of anti-E7 antibodies compared with the wild-type E7 groups (for 1:100 dilution, naive 0.507 ± 0.019; noncarrier naked wild-type E7 0.496 ± 0.021; noncarrier naked CRT/E7 DNA 1.510 ± 0.149; gold particle-coated wild-type E7 0.511 ± 0.015; gold particle-coated CRT/E7 DNA 1.742 ± 0.223; $P < 0.01$, one-way ANOVA). However, there was no significant difference in the titers of E7 antibodies between the noncarrier naked and gold particle-coated CRT/E7 DNA groups ($P > 0.05$, one-way ANOVA; Figure 3b).

We further carried out *in vivo* tumor protection experiments to compare the antitumor effects between noncarrier naked and gold particle-coated CRT/E7 DNA vaccines. As shown in Figures 3c and d, all of the mice, which received noncarrier naked or gold particle-coated CRT/E7 DNA vaccines remained tumor-free 60 days and were still alive 90 days after TC-1 challenge. In contrast, the unvaccinated, noncarrier naked no insert DNA, noncarrier naked E7 DNA, noncarrier naked CRT DNA and noncarrier naked E7 mixed with CRT DNA groups developed tumors within 20 days and died within 60 days of tumor challenge.

Our results indicated that mice vaccinated with noncarrier naked CRT/E7 DNA vaccine could enhance similarly potent E7-specific immunities and protective antitumor effects from E7-expressing TC-1 tumor challenge as gold particle-coated CRT/E7 DNA vaccine.

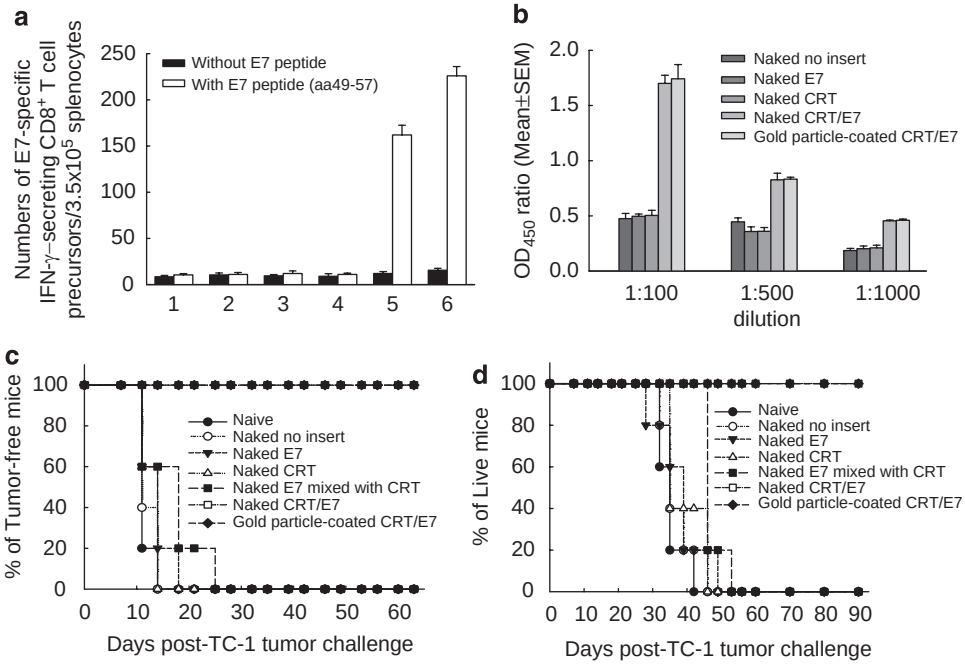

Figure 3 Immunologic profiles and tumor protection effects of noncarrier naked and gold particle-coated DNA vaccines. (**a**) Numbers of E7-specific interferon (IFN)-γ-secreting CD8+ T-cell precursors/3.5×10^5 splenocytes of various DNA vaccinated mice: 1, naive; 2, naked no insert; 3, naked E7; 4, naked CRT; 5, naked CRT/E7; 6, gold particle-coated CRT/E7 (note: mice vaccinated with noncarrier naked or gold particle-coated CRT/E7 DNA generated higher frequencies of E7-specific IFN-γ-secreting CD8+ T-cell precursors when compared with the other groups of mice). (**b**) Enzyme-linked immunosorbent assay (ELISA) showed E7-specific antibodies in mice vaccinated with various DNA vaccines (note: the titers of anti-E7 antibodies generated by the noncarrier naked or gold particle-coated CRT/E7 DNA showed significantly higher titers of anti-E7 antibodies compared with the other groups). (**c**) *In vivo* tumor preventive experiments for tumor-free. (**d**) *In vivo* tumor preventive experiments for survival of animals (note: both groups of mice that received noncarrier naked and gold particle-coated CRT/E7 DNA remained tumor-free 60 days, and were still alive 90 days after TC-1 challenge.

Noncarrier naked CRT/E7 DNA in various media generated E7-specific T-cell immunity and antitumor effects

We then evaluated whether the solution media influenced immune responses and antitumor effects. The representative figures of flow cytometric analysis of E7-specific IFN-γ-secreting CD8+ T-cell precursors are shown in Figure 4a. The numbers of E7-specific CD8+ T-cell precursors of noncarrier naked CRT/E7 DNA vaccinated mice, regardless of solution, were higher than those in naïve mice (11.5 ± 2.1; $P < 0.05$, one-way ANOVA). However, mice vaccinated with noncarrier naked CRT/E7 DNA in distilled H_2O (ddH_2O) (157.5 ± 8.5) or Tris-EDTA (TE) (150.0 ± 5.0) generated higher numbers of E7-specific CD8+ T-cell precursors compared to those immunized with noncarrier naked CRT/E7 DNA in phosphate-buffered saline (PBS; 94.0 ± 4.0; $P < 0.05$, one-way ANOVA; Figure 4b). As shown in Figure 4c, the titers of anti-E7 antibodies in mice vaccinated with noncarrier naked CRT/E7 DNA vaccine, regardless in which medium, were significantly higher than those in naive mice. However, the titers of anti-E7 antibodies were not different in mice vaccinated with noncarrier naked CRT/E7 DNA vaccine in different media ($P > 0.05$, one-way ANOVA; Figure 4c).

We further evaluated whether the immunity of noncarrier naked CRT/E7 DNA vaccine in various solution media could be translated to the antitumor effects. As shown in Figure 4d, 100% of the mice were tumor-free 60 days after TC-1 challenge when vaccinated with noncarrier naked CRT/E7 DNA vaccine in ddH_2O or TE buffer. However, only 60% of the mice were tumor-free after 60 days of TC-1 challenge when given noncarrier naked CRT/E7 DNA vaccine in PBS buffer.

Our results indicated that DNA vaccine in different solution media could generate antigen-specific immunity and potent antitumor effects through the delivery of a low-pressured gene gun, and that ddH_2O or TE solution could be more suitable media for the noncarrier naked DNA vaccine.

Noncarrier naked CRT/E7 DNA vaccinated with at least 50 psi was optimal for tumor protection against TC-1 E7-expressing tumor cells

To determine whether the delivery pressure in vaccination influenced the effect of noncarrier naked DNA vaccine, mice were vaccinated at various psi and challenged with TC-1 tumor cells to evaluate the antitumor effects. As shown in Figure 4e, only 40–60% of mice were tumor-free after 60 days of TC-1 challenge when given noncarrier naked DNA vaccine at 30 or 40 psi. However, when vaccinated at 50 or 60 psi, all of the mice were tumor-free 60 days after TC-1 challenge.

Our results indicated that the bombardment pressure of the gene gun influenced the potency of the noncarrier naked DNA vaccine.

The bombardment pressure influences the expression of the interested gene in vivo

The protein expressions of the interested gene at different bombardment pressures were further evaluated. The protein expression of luciferase was

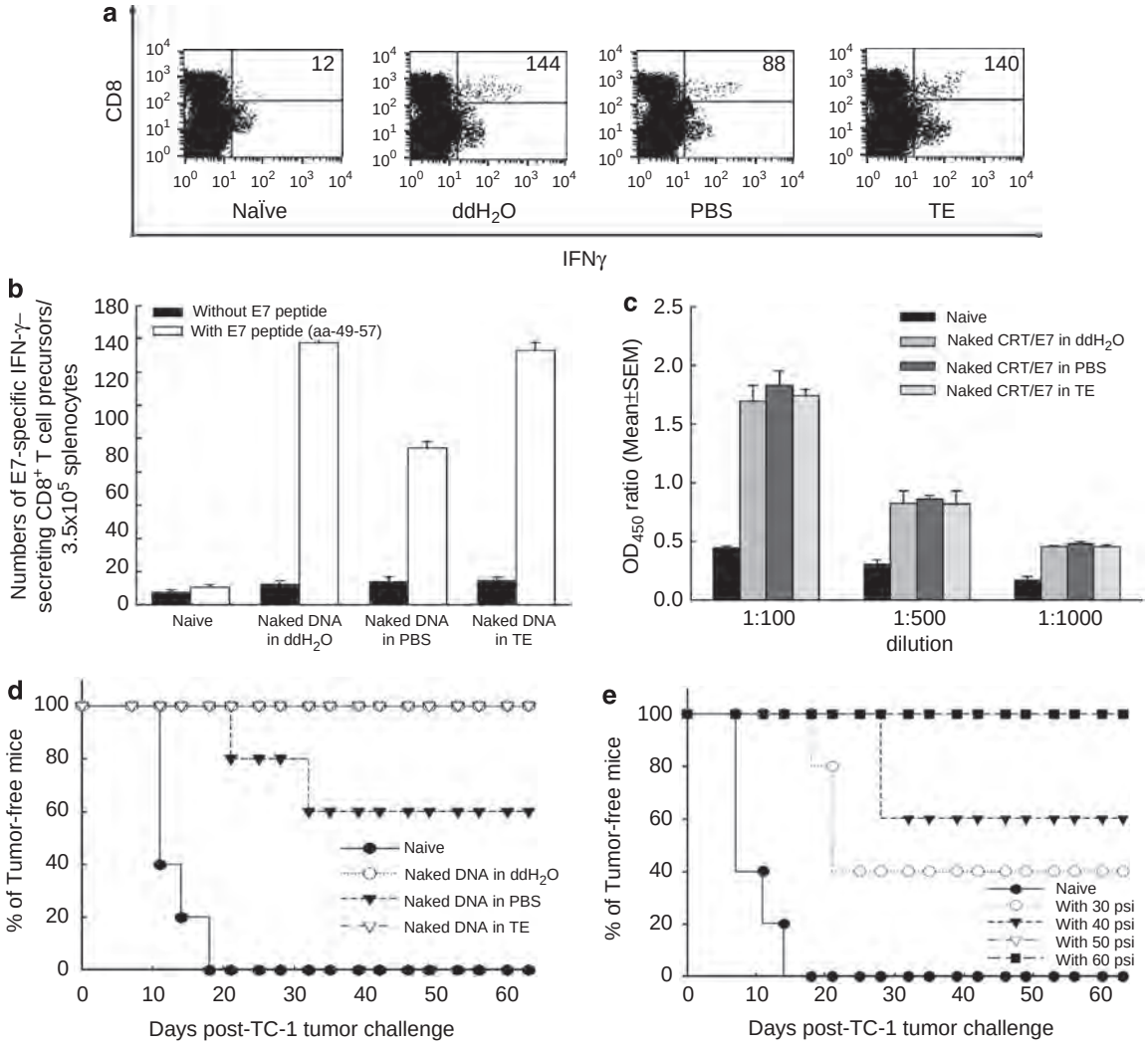

Figure 4 Immunologic profiles and *in vivo* tumor preventive effects of noncarrier naked CRT/E7 DNA vaccine dissolved in various media and bombarded at various pressures. (**a**) Representative figures of flow cytometry analysis of E7-specific $CD8^+$ T-cell precursors. (**b**) Frequencies of E7-specific $CD8^+$ T-cell precursors of noncarrier naked CRT/E7 DNA vaccine in various solutions (note: the numbers of E7-specific $CD8^+$ T-cell precursors for noncarrier naked CRT/E7 DNA vaccinated mice in distilled H_2O (ddH_2O) or Tris-EDTA (TE) solution were higher than those in phosphate-buffered saline (PBS) solution ($P<0.05$, one-way analysis of variance (ANOVA)). (**c**) Titers of anti-E7 antibodies in mice vaccinated with noncarrier naked CRT/E7 DNA in various media (note: the titers of anti-E7 antibodies were not significantly different between the noncarrier naked CRT/E7 DNA groups, regardless of which solution used ($P>0.05$, one-way ANOVA). (**d**) *In vivo* tumor preventive experiments in mice vaccinated with noncarrier naked CRT/E7 DNA vaccine in various solutions (note: mice vaccinated with noncarrier naked CRT/E7 DNA vaccine in ddH_2O or TE were 100% tumor-free after 60 days of TC-1 challenge). However, only 60% of mice vaccinated with noncarrier naked CT/E7 DNA vaccine in PBS were tumor-free after 60 days of TC-1 challenge. (**e**) *In vivo* tumor preventive experiments in mice that received noncarrier naked CRT/E7 DNA at various pressures (note: mice vaccinated at 50 or 60 psi were 100% tumor-free after 60 days of TC-1 challenge). However, only 40 and 60% of mice were tumor-free after being vaccinated at 30 and 40 psi, respectively.

significantly lower in the dermis of noncarrier naked luciferase DNA immunized mice with 30 psi bombardment pressure compared to those with higher bombardment pressures ($P<0.05$, one-way ANOVA; Figure 4f).

Our results indicated that mice receiving noncarrier naked DNA vaccine with higher bombardment pressures can express higher amounts of protein of the interested gene.

Treatment with noncarrier naked CRT/E7 DNA vaccine led to a significant reduction of pulmonary tumor nodules

We further assessed the therapeutic potential of noncarrier naked CRT/E7 DNA vaccine using a lung hematogeneous spread model. The representative pulmonary tumor nodules in various vaccinated groups are shown in Figure 5a. As shown in Figure 5b, mice treated four times with noncarrier naked or gold particle-coated CRT/E7 DNA showed significantly less pulmonary tumor nodules than the other groups (naïve 92.4 ± 7.4, noncarrier no insert 89.2 ± 5.4, noncarrier naked wild-type E7 90.4 ± 6.1, noncarrier naked CRT/E7 1.6 ± 1.1 and gold particle-coated CRT/E7 0.8 ± 0.8; $P<0.001$, one-way ANOVA). In addition, mice that received more vaccinations of noncarrier naked CRT/E7 DNA had lower numbers of pulmonary tumor nodules (twice 32.4 ± 4.3, thrice 15.2 ± 3.6, 4 times 1.6 ± 1.1; $P<0.01$, one-way ANOVA). However, the number of pulmonary tumor

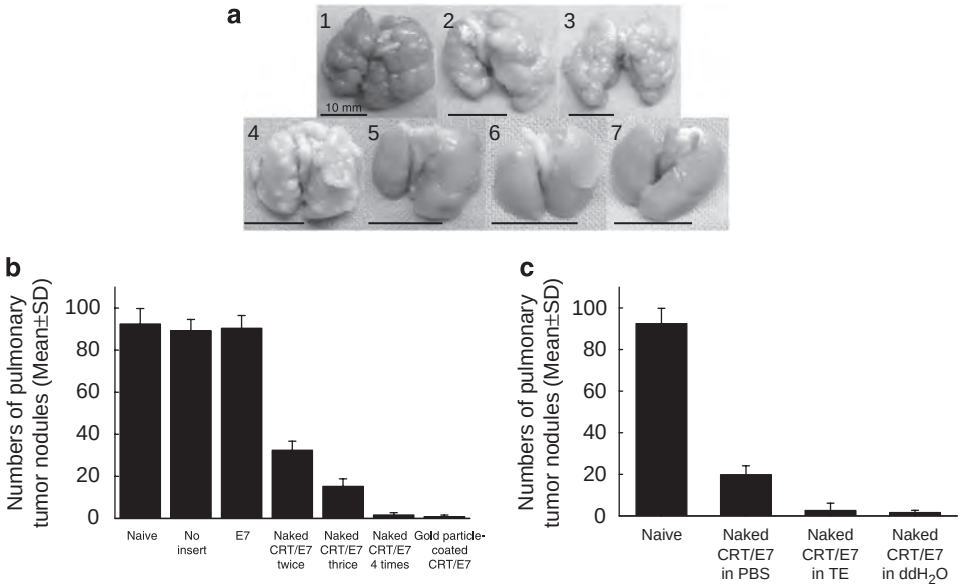

Figure 5 *In vivo* tumor treatment experiments in mice that received a high therapeutic dose of noncarrier naked or gold particle-coated DNA vaccine. (**a**) Representative figures of pulmonary tumor nodules in each group: 1, naïve; 2, no insert; 3, E7; 4, naked CRT/E7 twice; 5, naked CRT/E7 thrice; 6, naked CRT/E7 four times; 7, gold particle-coated CRT/E7. (**b**) Mean pulmonary tumor nodules in mice vaccinated with different frequencies of noncarrier naked CTGFCRT/E7 DNA vaccine and gold particle-coated CRT/E7 DNA vaccines (note: mice that received the noncarrier naked CRT/E7 DNA vaccine had less pulmonary tumor nodules than those that received the noncarrier naked wild-type E7 DNA vaccine). Mice that were treated with noncarrier naked CRT/E7 DNA four times showed significantly less pulmonary tumor nodules than those that were treated twice or thrice. The number of pulmonary tumor nodules was not different between mice immunized with noncarrier naked and gold particle-coated CRT/E7 DNA vaccine four times. (**c**) Mean pulmonary tumor nodules in mice vaccinated with noncarrier naked CRT/E7 DNA in various media (note: the mean pulmonary tumor nodules of mice vaccinated with noncarrier naked CRT/E7 DNA in distilled H_2O (ddH_2O) or Tris-EDTA (TE) solution was significantly lower than those in mice treated with noncarrier naked DNA vaccine in phosphate-buffered saline (PBS).

nodules was not different between mice immunized four times with noncarrier naked and those four times with gold particle-coated CRT/E7 DNA vaccine (1.6 ± 1.1 vs 0.8 ± 0.8; $P > 0.05$, one-way ANOVA).

Our results indicated that mice vaccinated more times with noncarrier naked DNA vaccine generated more potent therapeutic effects. In addition, mice vaccinated with noncarrier naked or gold particle-coated DNA vaccine generated similarly excellent therapeutic effects.

Noncarrier naked CRT/E7 DNA in various media generated different therapeutic effects

We then evaluated whether the solution media influenced the therapeutic effects of noncarrier naked CRT/E7 DNA vaccine. As shown in Figure 5c, mice treated with noncarrier naked CRT/E7 DNA in ddH2O (1.6 ± 0.5) or TE solution (2.6 ± 1.8) had less numbers of pulmonary tumor nodules compared to those in PBS solution (19.8 ± 2.1; $P < 0.05$, one-way ANOVA).

Our results indicated that different solution media influenced the therapeutic effects of noncarrier naked DNA vaccine.

CD11c-enriched cells from mice vaccinated with noncarrier naked CTGF/E7 DNA effectively enhanced the activation of an E7-specific CD8$^+$ T-cell line

Several studies have shown that following intradermal immunization, DCs migrate to draining lymph nodes where they play a major role in priming and stimulating antigen-specific T cells.[23,24] Therefore, it is important to determine whether DCs express the reporter gene in draining lymph nodes when noncarrier naked DNA is administered. The draining lymph nodes of mice vaccinated with various DNA vaccines and CD11$^+$ cells were first isolated as described in Materials and methods. The CD11c-enriched cells were then incubated with an E7-specific T-cell line to evaluate their ability to stimulate INF-γ secretion. The representative figures of flow cytometric analysis are shown in Figure 6a. As shown in Figure 6b, CD11c-enriched cells isolated from mice vaccinated with noncarrier naked and gold particle-coated CRT/E7 DNA vaccines were more effective in activating the E7-specific CD8$^+$ T-cell line to secrete IFN-γ compared with noncarrier naked wild-type E7 DNA vaccine (70 ± 15 for E7 group, 419 ± 11 for naked CRT/E7 in ddH2O group, 405 ± 12 for naked CRT/E7 in PBS group, 412 ± 14 for naked CRT/E7 in TE group, 380 ± 19 for gold particle-coated CRT/E7 group; $P < 0.001$, one-way ANOVA). However, there was no difference in the numbers of IFN-γ-secreting CD8$^+$ T cells between gold particle-coated and noncarrier naked CRT/E7 DNA vaccines in respective solution media ($P > 0.05$, one-way ANOVA). These results are consistent with the notion that *in vivo* DNA-transfected DCs from mice vaccinated with CRT/E7 DNA can enhance the activation of E7-specific CD8$^+$ T cells regardless of the noncarrier naked or gold particle-coated groups.

Noncarrier naked DNA vaccine generated less burning effect on the skin of mice compared with gold particle-coated DNA vaccine

We finally evaluated whether the local skin reaction would be similar on mice bombarded with noncarrier naked and gold particle-coated chimeric DNA vaccines.

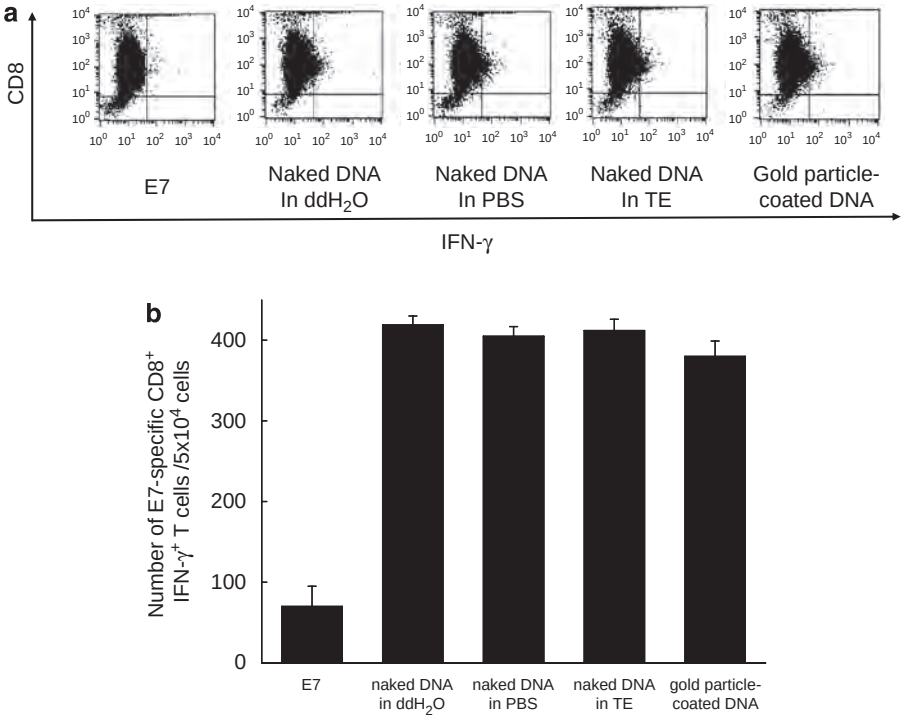

Figure 6 Activation of E7-specific $CD8^+$ T cells by CD11c-enriched cells isolated from the inguinal lymph nodes of noncarrier naked or gold particle-coated DNA vaccinated mice. (**a**) Representative figures of flow cytometry analysis. (**b**) Numbers of interferon (IFN)-γ-secreting E7-specific $CD8^+$ T cells stimulated by CD11c-enriched cells isolated from the inguinal lymph nodes of vaccinated mice (note: CD11c-enriched cells isolated from mice vaccinated with noncarrier naked and gold particle-coated CRT/E7 DNA vaccines were more effective in activating the E7-specific $CD8^+$ T-cell line to secrete IFN-γ compared with noncarrier naked wild-type E7 DNA vaccine). However, there was no difference in the numbers of IFN-γ-secreting $CD8^+$ T cells between gold particle-coated and noncarrier naked CRT/E7 DNA vaccines in respective solution media. The data collected from all of the above experiments are from one representative experiment of the two experiments that were carried.

As shown in Figures 7b, d, f, and h, no definite skin damage could be identified in mice vaccinated with noncarrier naked DNA. However, local skin damage was significant from 1 day after the gold particle-coated DNA vaccination (Figure 7e). The most severe skin damage was noted 3 days after vaccination (Figure 7g), and it took 7 days for the skin to heal (Figure 7i).

Our observation indicated that noncarrier naked DNA vaccination resulted in significantly less local skin damage than gold particle-coated DNA vaccination.

Discussion

DNA vaccination is a new and powerful approach to generate immunologic responses. Only a small quantity of DNA vaccine is required to enhance *in vivo* immune responses. Gregersen[25] showed that intradermal gene gun immunization needs smaller quantities of DNA compared with intramuscular injections,[25] which always requires large amounts of DNA (100 μg per mouse) to elicit the immune response. In contrast, the microparticulated bombardment system can induce an immune response using very small amounts of DNA (1 μg per mouse).[26] In addition, gene gun immunization has a 10- to 100-fold greater expression of the DNA-encoded protein than intramuscular vaccinations.[27,28]

Gold particle-coated DNA vaccines with a gene gun delivery system are currently widely used in immunopreventive and immunotherapeutic applications. Traditionally, DNA vaccines need to be coated with gold particles to be heavy enough to be bombarded into the intradermis and deliver the antigens of interest to the intradermal Langerhan's cells (antigen-presenting cells) to induce potent immunologic responses and antitumor effects. High efficiency and stability are two key points in these DNA vaccines coated with gold particles for *in vivo* use. Particle-mediated gene gun technology uses compressed helium to propel micrometer-sized colloidal gold particles coated with plasmid through the stratum corneum, where the particles lodge in the epidermal and dermal layers of the skin.[29] The gene gun technique has been used to immunize various animals for tumor prevention and regression, including prostate cancer, melanomas and cervical cancer.[25,30] The additional advantage of gene gun immunization is the application to a broad variety of cells, including Langerhan's cells, DCs and keratinocytes, which are transfected.[31] The DNA vaccine can then provide protein expression in the transfected cells, and the transfected Langerhan's cells and dermal DCs can migrate to local lymph nodes where presentation of antigens to T cells can occur, and thus start a variety of immunologic responses.[29,32]

Inconvenience in preparation and safety issues are concerns for the clinical applications of gene gun-delivered, gold particle-coated DNA vaccines. The conventional gene gun delivery system can only deliver dry DNA bullets instead of wet DNA bullets because of inherent limitations. In contrast, the noncarrier naked DNA vaccine can be delivered in the form of wet DNA

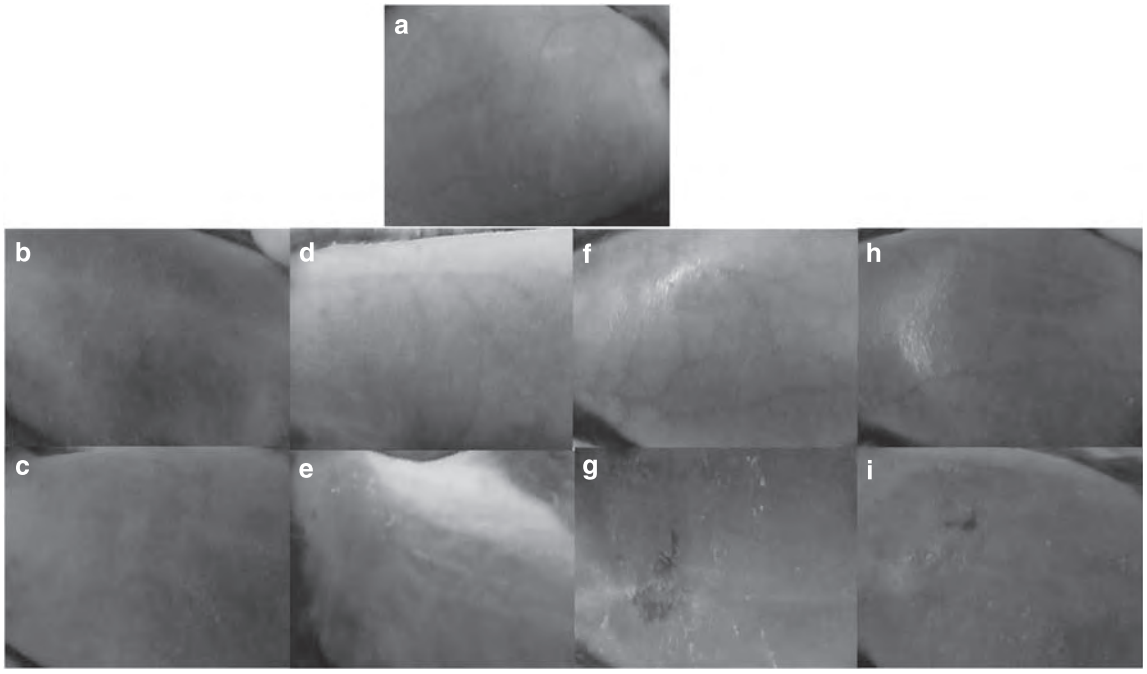

Figure 7 Burning effects on the skin of noncarrier naked and gold particle-coated DNA vaccinated mice. Mice were first given noncarrier naked CRT/E7 chimeric DNA or gold particle-coated CRT/E7 DNA at 50 psi as described in the Materials and methods section. **(a)** Shaved skin before vaccination. **(b)** Mice that received noncarrier naked DNA vaccine immediately. **(c)** Mice that received gold particle-coated DNA vaccine immediately. **(d)** Mice that received noncarrier naked DNA vaccine 24 h later. **(e)** Mice that received gold particle-coated CRT/E7 DNA vaccine 24 h later. **(f)** Mice that received noncarrier naked DNA vaccine after 3 days. **(g)** Mice that received gold particle-coated DNA vaccine after 3 days. **(h)** Mice that received noncarrier naked CRT/E7 DNA vaccine after 7 days. **(i)** Mice that received gold particle-coated CRT/E7 DNA vaccine after 7 days (note: the skin damage was noted from 24 h after being given the gold particle-coated DNA vaccine and the damage continued until 7 days postimmunization. There was no visible skin damage for mice that received noncarrier naked DNA immunization.

bullets. Moreover, the preparation of gold particle-coated DNA vaccines is hardly aseptic. However, the preparation of noncarrier naked DNA vaccines can be relatively aseptic and simpler. As such, safety concerns of gold particle-coated DNA vaccine is a major consideration in human clinical trials. Another disadvantage of gold particle-coated DNA vaccine is that non-biodegradable gold or tungsten may skew the immune response or cause adverse side effects when they accumulate.[33] Finally, gold particle-coated DNA vaccination always induces burning effects on bombarded skin, as shown presenting this and in earlier studies.[17,34,35] The novel technology of noncarrier naked DNA vaccination could resolve these above-mentioned concerns.

Noncarrier naked DNA vaccine can be as effective as gold particle-coated DNA vaccine to reach intradermal layer, to deliver the antigens of interest to the intradermal Langerhan's cells and to enhance the subsequent immune responses. Our earlier results have shown that gold particle-coated CRT/E7 DNA vaccine could generate more potent immune responses and antitumor effects than gold particle-coated wild-type E7 DNA vaccine.[34] We observed that noncarrier naked CRT/E7 DNA vaccine generates less numbers of E7-specific $CD8^+$ T-cell precursors than gold particle-coated CRT/E7 DNA vaccine, although 100% tumor protection effects were seen in both DNA formats (Figures 2a and 3c). We hypothesize that gold particle-coated DNA vaccination may induce non-specific immune responses to enhance the antigen-specific immune responses by the local burning effect on the bombarded skin, as shown in our earlier studies.[19,51] Another possible mechanism is that the gold beads alone can upregulate the antigen-presenting cells,[36] and these upregulated DCs can induce more potent antigen-specific immune responses when encountering specific antigens.

Different solution media can influence the antigen-specific immunity and antitumor effects of noncarrier naked DNA vaccine. Our results indicated that noncarrier naked CRT/E7 DNA in ddH2O or TE buffer can generate better E7-specific immune responses and antitumor effects than in PBS buffer (Figures 4b and d). Hartikka *et al*.[37] observed that the concentration, osmolarity and pH of sodium phosphate can influence plasmid DNA expression *in vivo*. The optimum sodium phosphate concentration was 150 mM and the luciferase expression was 4.3-fold compared with saline. The luciferase expression decreased significantly, when solved in sodium phosphate solution less than 40 mM, compared to that of saline.[37] The sodium concentration of PBS buffer was only 6.7 mM in this study. This might be the reason why the PBS group did not generate as potent antigen-specific immune responses and antitumor effects as the other two groups in this study. It is essential to test and identify the optimal buffer and its concentration for noncarrier naked DNA vaccine.

Dermal immunization methods target the epidermis, the dermis, or both, and include chemical modification,[38,39] transepidermal immunization,[40,41] gene gun technology,[31] electroporation[42,43] and intradermal injections.[42] Recently, intradermal administration with the RNA interference technique has also been reported.[44]

The benefit of intradermal administration by the gene gun technique is that it is less harmful and injurious to the host. Hirao *et al*.[42] observed higher cellular and humoral responses to an HIV DNA vaccine with electroporation compared with intradermal route alone. Electroporation may have importance as an immunization approach in larger animal models. More studies are needed to identify the optimal immunization approach in different animal models.

Multiple vaccinations are always needed for both noncarrier naked and gold particle-coated DNA vaccines delivered by a gene gun. Gold particle-coated, and especially, noncarrier naked DNA vaccine needs boosters to enhance immune responses and antitumor effects. One of the benefits of the dermal immunization technique is that it is needleless. However, the disadvantage is the requirement of frequent and multiple sites per immunization to elicit immune responses. Doria-Rose *et al*.[45] reported that a prime-boost strategy seems necessary for DNA vaccines. We also observed that more shots of noncarrier naked DNA vaccine were needed to generate comparable immune responses and antitumor effects compared with gold particle-coated DNA vaccine. Gregersen reported that frequent or multiple sites of application may be safe and acceptable from a scientific point of view, although they may not necessarily be tolerated and widely accepted by patients.[25] Peng *et al.* recently reported that cluster intradermal antigen-specific gold particle-coated DNA vaccination is capable of rapidly inducing antigen-specific $CD8^+$ T-cell immune responses leading to therapeutic anti-tumor effects.[46] The noncarrier naked DNA vaccine can also use a similar protocol to induce potent anti-tumor immune responses in a shorter interval.

Noncarrier naked DNA vaccine induces less tissue injury as compared to gold particle-coated DNA vaccine, where the gold particles can cause slight necrosis and mild to moderate tissue damage. Pilling *et al*. reported that gold particle-coated DNA bombardment with the gene gun system induced local skin reactions two days post-dosing in mini-pigs.[47] By 28 days, the skin lesions had regressed apart from a low grade peri-vascular mononuclear cell infiltration in the upper dermis, which persisted up to 141 days, together with a small number of phagocytosed gold particles.[47] We also observed that gold particle-coated DNA vaccine bombardment by a gene gun has definite local skin damage as compared to noncarrier naked DNA vaccine (Figure 6). In addition, the most severe local skin damage of the mice was seen three days after bombardment with gold particle-coated DNA vaccine. The bombardment pressure might be a factor in generating skin damage. DNA vaccines are always administered in 1–8 vaccinations on non-overlapping sites on shaved epidermis using 150–1200 psi with a majority of investigators favoring around 400 psi of helium pressure.[48] We bombarded the mice with a lower pressure of 50 psi of helium pressure for both gold particle-coated and noncarrier naked DNA vaccines in multiple sites on the shaved abdomen in this study. Our observations imply that noncarrier naked DNA vaccine could be effectively delivered by an intradermal gene gun at lower helium pressure so that damage to local skin can be minimized.

E7-specific antibody titers were significantly enhanced by noncarrier naked and gold particle-coated CRT/E7 DNA vaccines, although the mechanism for enhancement of antibody responses by CRT/E7 DNA vaccine is not clear. The titers of anti-E7 antibodies were similar between noncarrier naked and gold particle-coated DNA vaccines in this study. We also observed that the CRT/E7 proteins could be detected in the sera,[34] and the levels of CRT/E7 proteins were similar between noncarrier naked and gold particle-coated DNA vaccinated groups (data not shown). We hypothesize that the similar amounts of secreted CRT/E7 proteins, regardless of whether generated by noncarrier naked or gold particle-coated CRT/E7 DNA vaccine, might enhance the humoral-mediated immune response to generate similar anti-E7 antibodies. Even though antobody-mediated responses have not been shown to play an important role in controlling HPV-associated malignancies, antigen-specific antibodies are significant in other tumor models such as the breast cancer model with the HER-2/neu antigen. Lin *et al.* reported that noncarrier naked neu DNA vaccine can generate anti-neu antibodies and anti-tumor effects as much as gold particle-coated neu DNA vaccine,[49] and the titers of anti-neu antibodies correlated with the doses of noncarrier naked DNA vaccination.[49] The chimeric CRT/E7 DNA vaccine, regardless of whether in the noncarrier naked format, can significantly enhance higher titers of anti-E7 antibodies. This novel strategy can be utilized to generate the other oncogene-specific antibodies for the treatment of oncogene overexpressing tumor model.

In summary, our study showed that noncarrier naked chimeric CRT/E7 DNA vaccine, without gold particle coating, bombarded under low pressure by a gene-gun delivery system, can be delivered into the intradermis of mice to express the interested gene and enhance similar E7-specific immunities and antitumor effects compared with the gold particle-coated CRT/E7 DNA vaccine.

Materials and methods

Plasmid DNA constructs and preparation

The generation of pcDNA3 with no insert as well as pcDNA3-E7, pcDNA3-CRT, pcDNA3-CRT/E7 and pcDNA3-CRT/E7/GFP has been described earlier.[34] pEGFP-N2 was purchased from Clontech Laboratories (Palo Alto, CA, USA).

Mice

Six- to eight-week-old female C57BL/6J mice were bred in, and purchased from the animal facility of the National Taiwan University Hospital (Taipei, Taiwan). All animal procedures were carried out according to approved protocols and in accordance with recommendations for the proper use and care of laboratory animals.

DNA vaccination

For vaccination of noncarrier naked DNA or gold particle-coated DNA, a low pressure-accelerated gene gun (BioWare Technologies Co. Ltd, Taipei, Taiwan) was used as described previously.[9,49] Mice were immunized with respective DNA vaccine four times at 1 week intervals. Mice (five per group) were immunized with 2 μg of noncarrier naked or gold particle-coated DNA vaccine each time.

To test the influence of dissolved media in DNA vaccination, noncarrier chimeric pcDNA3-CRT/E7 or pEGFP-N2 DNA was dissolved in PBS (pH8.0), TE buffer (pH 7.0) or ddH_2O for vaccination. To evaluate the influence of the bombardment pressure of the gene gun, mice were immunized with noncarrier DNA vaccine at various pressures.

Immunofluorescence examination of the skin of noncarrier naked DNA vaccinated mice

The mice's (five per group) abdomens were shaved for the DNA vaccination (pEGFP-N2 in dd-H2O, PBS or TE buffer, respectively) through the gene gun at 50 psi as described earlier. Six or 24 h after, the mice were killed so that the abdominal skin could be observed under fluorescence microscope (BX60, Olympus Corp., Tokyo, Japan).

The detection of luciferase assay within the skin of mice vaccinated with various bombardment pressures

Mice were prepared and bombarded with the pCMV-Luciferase DNA vaccine at various bombardment pressures of the gene gun as described earlier. One day after DNA immunization, the mice were killed and the bombarded area of the abdominal skin was taken off and then homogenized with lysis buffer (Promega, Madison, WI, USA) into sample lysates. The lysates were centrifuged and the supernatant was collected for further analysis. The supernatants were then added to a 96-well plate, and an equal volume of Bright-Glo (Promega) luciferase assay reagent was added. The results were counted with a luminometer (TopCount NXT, PerkinElmer, Meriden, CT, USA). The known concentrations of recombinant luciferase (Promega) were used as standards to calculate the luciferase content in each sample. The contents of total protein in the samples were also assayed by using a BCA assay kit (Pierce, Rockford, IL, USA). Finally, the luciferase content in each sample was normalized by the total protein content.

Intracellular cytokine staining and flow cytometry analysis

Mice (five per group) were immunized with 2 μg of various noncarrier naked or gold particle-coated DNA vaccines, followed by a booster 1 week later, four times. Splenocytes were harvested 1 week later and incubated with either 1 μg ml^{-1} of E7 peptide (aa 49–57) overnight.[50] Cell surface marker staining of CD8 and intracellular cytokine staining for IFN-γ, as well as flow cytometry analysis, were carried out as described previously.[9]

Enzyme-linked immunosorbent assay (ELISA) for anti-E7 antibody

Mice (five per group) were immunized with 2 μg of the various DNA vaccines and a booster with the same regimen 1 week later. Sera were prepared from mice on day 14 after immunization. For the detection of HPV 16 E7-specific antibodies in sera, direct ELISA was used as described previously.[51,52] Briefly, a 96-microwell plate was coated with 100 μl of bacteria-derived HPV-16 E7 proteins (0.5 μg ml^{-1}) and incubated at 4 °C overnight. The wells were then blocked with PBS containing 20% fetal bovine serum. Sera were serially diluted in PBS, added to the ELISA wells and incubated at 37 °C for 2 h. After washing with PBS containing 0.05% Tween 20, the plate was incubated with a 1:2000 dilution of a peroxidase-conjugated rabbit antimouse immunoglobulin antibody (Zymed, San Francisco, CA, USA) at room temperature for 1 h. The plate was washed, developed with 1-step Turbo TMB-ELISA (Pierce, Rockford, IL, USA) and stopped with 1 M H2SO4. The ELISA plate was read with a standard ELISA reader at 450 nm.

TC-1 tumor cell line

The generation of TC-1 tumor cell line has been described previously.[53] Briefly, HPV-16 E6, E7 and *Ras* were used to transform primary C57BL/6 mice lung epithelial cells. This tumorigenic cell line was named TC-1. The TC-1 cells were grown in RPMI-1640, supplemented with 10% (vol/vol) fetal bovine serum, 50 U ml^{-1} penicillin/streptomycin, 2 mM L-glutamine, 1 mM sodium pyruvate, 2 mM non-essential amino acids, and 0.4 mg ml^{-1} G418 at 37 °C with 5% CO_2. On the day of tumor challenge, tumor cells were harvested by trypsinization, washed twice with 1 × Hank's buffered salt solution, and finally resuspended in 1 × Hank's buffered salt solution to the designated concentration for injection.

In vivo *tumor protection experiments*

For the tumor protection experiments, mice (five per group) were immunized with 2 μg of various noncarrier naked or gold particle-coated DNA vaccines and boosted 1 week later for a total of four times with a gene gun. One week after the last vaccination, the mice were subcutaneously challenged with 5×10^4 cells per mouse of TC-1 tumor cells in the right leg.[53] The mice were monitored for evidence of tumor growth by palpation and inspection twice a week until they were killed on day 60.

In vivo *tumor treatment experiments*

For *in vivo* tumor treatment experiments, the mice were injected with 5×10^4 cells per mouse TC-1 tumor cells through the tail vein as described previously.[9] Two days after tumor challenge, the mice were given 16 μg per mouse of various noncarrier naked or gold particle-coated DNA vaccines, followed by a booster with the same regimen every 7 days for 4 weeks (a total of two 64 μg DNA). Mice that were not vaccinated were used as a negative control. The mice were killed and the lungs were explanted on day 28. Pulmonary tumor nodules in each mouse were evaluated and counted by experimenters blinded to the sample identity.

Preparation of CD11c$^+$ cells in the inguinal lymph nodes from vaccinated mice

Mice (five per group) received multiple inoculations of non-overlapping intradermal administration with a gene gun on the abdominal region. The mice were vaccinated with 16 μg of noncarrier naked or gold particle-coated CRT/E7 DNA. Inguinal lymph nodes were harvested from vaccinated mice 3 days after vaccination with a gene gun. A single cell suspension from isolated inguinal lymph nodes was prepared as described previously.[9] CD11c$^+$ cells were enriched from lymph nodes using CD11c (N418) micro-beads (Miltenyi Biotec, Auburn, CA, USA). The purity of the CD11c$^+$ cells were further characterized using phycoerythrin-conjugated anti-CD11c antibody (PharMingen, San Diego, CA, USA)

and analyzed by flow cytometry analysis,[9] and samples of more than 90% of the CD11c$^+$ cells were utilized for the following experiments.

Activation of E7-specific CD8$^+$ T-cell line by CD11c-enriched cells

CD11c-enriched cells (2×10^4) were incubated with 2×10^6 of the E7-specific CD8$^+$ T-cell line for 16 h. The cells were then stained for both surface CD8 and intracellular IFN-γ and analyzed with flow cytometry analysis as described above.

Local skin burning effect on noncarrier naked and gold particle-coated DNA vaccines

To compare the local skin burning effect, mice were vaccinated with noncarrier naked or gold particle-coated CRT/E7 DNA vaccine as described earlier, and pictures of the shaved DNA-bombarded abdominal skin of the mice were taken before and after immunization at 1, 3, 5 or 7 days later.

Statistical analysis

The data expressed as mean ± s.e.m. or mean ± s.d. are representative of at least two different experiments. Data for intracellular cytokine staining with flow cytometry analysis and tumor treatment experiments were evaluated by ANOVA. Comparisons between individual data points were made using the Student's *t*-test. In the tumor protection experiment, the principal outcome of interest was the time to the development of a tumor. The event time distributions for different mice were compared by the Kaplan–Meier method, and by log-rank analysis.

Acknowledgements

This study was supported by a grant from the New Century Health Care Promotion Foundation and in part by the Department of Medical Research of NTUH. The E7-specific CD8$^+$ T-cell line and TC-1 tumor cell line were kindly provided by Dr TC Wu of Johns Hopkins Medical Institutes in Baltimore, MD, USA. The pCMV-Luciferase DNA was kindly provided by Dr MD Lai of National Cheng Kung University in Tainan, Taiwan.

References

1 Boyd D, Hung CF, Wu TC. DNA vaccines for cancer. *IDrugs* 2003; **6**: 1155–1164.
2 Ribas A, Butterfield LH, Glaspy JA, Economou JS. Current developments in cancer vaccines and cellular immunotherapy. *J Clin Oncol* 2003; **21**: 2415–2432.
3 Lin YL, Chen LK, Liao CL, Yeh CT, Ma SH, Chen JL *et al*. DNA immunization with Japanese encephalitis virus nonstructural protein NS1 elicits protective immunity in mice. *J Virol* 1998; **72**: 191–200.
4 Saravia NG, Hazbon MH, Osorio Y, Valderrama L, Walker J, Santrich C *et al*. Protective immunogenicity of the paraflagellar rod protein 2 of Leishmania mexicana. *Vaccine* 2005; **23**: 984–995.
5 Hedley ML, Curley J, Urban R. Microspheres containing plasmid-encoded antigens elicit cytotoxic T-cell responses. *Nat Med* 1998; **4**: 365–368.
6 Klencke B, Matijevic M, Urban RG, Lathey JL, Hedley ML, Berry M *et al*. Encapsulated plasmid DNA treatment for human papillomavirus 16-associated anal dysplasia: a Phase I study of ZYC101. *Clin Cancer Res* 2002; **8**: 1028–1037.
7 Capone S, Zampaglione I, Vitelli A, Pezzanera M, Kierstead L, Burns J *et al*. Modulation of the immune response induced by gene electrotransfer of a hepatitis C virus DNA vaccine in nonhuman primates. *J Immunol* 2006; **177**: 7462–7471.
8 Takamura S, Matsuo K, Takebe Y, Yasutomi Y. Ag85B of mycobacteria elicits effective CTL responses through activation of robust Th1 immunity as a novel adjuvant in DNA vaccine. *J Immunol* 2005; **175**: 2541–2547.
9 Hsieh CY, Chen CA, Huang CY, Chang MC, Lee CN, Su YN *et al*. IL-6-encoding tumor antigen generates potent cancer immunotherapy through antigen processing and anti-apoptotic pathways. *Mol Ther* 2007; **15**: 1890–1897.
10 Hung CF, Cheng WF, Hsu KF, Chai CY, He L, Ling M *et al*. Cancer immunotherapy using a DNA vaccine encoding the translocation domain of a bacterial toxin linked to a tumor antigen. *Cancer Res* 2001; **61**: 3698–3703.
11 Glinka Y, Chang Y, Prud'homme GJ. Protective regulatory T cell generation in autoimmune diabetes by DNA covaccination with islet antigens and a selective CTLA-4 ligand. *Mol Ther* 2006; **14**: 578–587.
12 Mannie MD, Abbott DJ. A fusion protein consisting of IL-16 and the encephalitogenic peptide of myelin basic protein constitutes an antigen-specific tolerogenic vaccine that inhibits experimental autoimmune encephalomyelitis. *J Immunol* 2007; **179**: 1458–1465.
13 Encke J, Geissler M, Stremmel W, Wands JR. DNA-based immunization breaks tolerance in a hepatitis C virus transgenic mouse model. *Hum Vaccin* 2006; **2**: 78–83.
14 Ahlen G, Soderholm J, Tjelle T, Kjeken R, Frelin L, Hoglund U *et al*. *In vivo* electroporation enhances the immunogenicity of Hepatitis C virus nonstructural 3/4A DNA by increased local DNA uptake, protein expression, inflammation, and infiltration of CD3+ T cells. *J Immunol* 2007; **179**: 4741–4753.
15 van Rooij EM, Haagmans BL, de Visser YE, de Bruin MG, Boersma W, Bianchi AT. Effect of vaccination route and composition of DNA vaccine on the induction of protective immunity against pseudorabies infection in pigs. *Vet Immunol Immunopathol* 1998; **66**: 113–126.
16 Cheng WF, Chen LK, Chen CA, Chang MC, Hsiao PN, Su YN *et al*. Chimeric DNA vaccine reverses morphine-induced immunosuppression and tumorigenesis. *Mol Ther* 2006; **13**: 203–210.
17 Cheng WF, Hung CF, Lin KY, Ling M, Juang J, He L *et al*. CD8+ T cells, NK cells and IFN-gamma are important for control of tumor with downregulated MHC class I expression by DNA vaccination. *Gene Therapy* 2003; **10**: 1311–1320.
18 Molling K. Naked DNA for vaccine or therapy. *J Mol Med* 1997; **75**: 242–246.
19 Cheng WF, Hung CF, Chen CA, Lee CN, Su YN, Chai CY *et al*. Characterization of DNA vaccines encoding the domains of calreticulin for their ability to elicit tumor-specific immunity and antiangiogenesis. *Vaccine* 2005; **23**: 3864–3874.
20 Hung CF, Hsu KF, Cheng WF, Chai CY, He L, Ling M *et al*. Enhancement of DNA vaccine potency by linkage of antigen gene to a gene encoding the extracellular domain of Fms-like tyrosine kinase 3-ligand. *Cancer Res* 2001; **61**: 1080–1088.
21 Liao CW, Chen CA, Lee CN, Su YN, Chang MC, Syu MH *et al*. Fusion protein vaccine by domains of bacterial exotoxin linked with a tumor antigen generates potent immunologic responses and antitumor effects. *Cancer Res* 2005; **65**: 9089–9098.
22 Hung CF, Cheng WF, Chai CY, Hsu KF, He L, Ling M *et al*. Improving vaccine potency through intercellular spreading and enhanced MHC class I presentation of antigen. *J Immunol* 2001; **166**: 5733–5740.
23 Weiss RA. ONg retroviral particles in chick cell grown vaccines [comment]. *J Clin Virol* 1998; **11**: 3–6.

24 Torres CA, Iwasaki A, Barber BH, Robinson HL. Differential dependence on target site tissue for gene gun and intramuscular DNA immunizations. *J Immunol* 1997; **158**: 4529–4532.
25 Gregersen JP. DNA vaccines. *Naturwissenschaften* 2001; **88**: 504–513.
26 Morel PA, Falkner D, Plowey J, Larregina AT, Falo LD. DNA immunisation: altering the cellular localisation of expressed protein and the immunisation route allows manipulation of the immune response. *Vaccine* 2004; **22**: 447–456.
27 Fynan EF, Webster RG, Fuller DH, Haynes JR, Santoro JC, Robinson HL. DNA vaccines: protective immunizations by parenteral, mucosal, and gene-gun inoculations. *Proc Natl Acad Sci USA* 1993; **90**: 11478–11482.
28 Tighe H, Corr M, Roman M, Raz E. Gene vaccination: plasmid DNA is more than just a blueprint. *Immunol Today* 1998; **19**: 89–97.
29 Condon C, Watkins SC, Celluzzi CM, Thompson K, Falo Jr LD. DNA-based immunization by *in vivo* transfection of dendritic cells. *Nat Med* 1996; **2**: 1122–1128.
30 Hung CF, Calizo R, Tsai YC, He L, Wu TC. A DNA vaccine encoding a single-chain trimer of HLA-A2 linked to human mesothelin peptide generates anti-tumor effects against human mesothelin-expressing tumors. *Vaccine* 2007; **25**: 127–135.
31 Steele KE, Stabler K, VanderZanden L. Cutaneous DNA vaccination against Ebola virus by particle bombardment: histopathology and alteration of CD3-positive dendritic epidermal cells. *Vet Pathol* 2001; **38**: 203–215.
32 Robinson HL, Torres CA. DNA vaccines. *Semin Immunol* 1997; **9**: 271–283.
33 Ariyo OA, Atiri GI, Dixon AG, Winter S. The use of biolistic inoculation of cassava mosaic begomoviruses in screening cassava for resistance to cassava mosaic disease. *J Virol Methods* 2006; **137**: 43–50.
34 Cheng WF, Hung CF, Chai CY, Hsu KF, He L, Ling M *et al.* Tumor-specific immunity and antiangiogenesis generated by a DNA vaccine encoding calreticulin linked to a tumor antigen. *J Clin Invest* 2001; **108**: 669–678.
35 Cheng WF, Hung CF, Pai SI, Hsu KF, He L, Ling M *et al.* Repeated DNA vaccinations elicited qualitatively different cytotoxic T lymphocytes and improved protective antitumor effects. *J Biomed Sci* 2002; **9**: 675–687.
36 Tanigawa K, Yu H, Sun R, Nickoloff BJ, Chang AE. Gene gun application in the generation of effector T cells for adoptive immunotherapy. *Cancer Immunol Immunother* 2000; **48**: 635–643.
37 Hartikka J, Bozoukova V, Jones D, Mahajan R, Wloch MK, Sawdey M *et al.* Sodium phosphate enhances plasmid DNA expression *in vivo*. *Gene Therapy* 2000; **7**: 1171–1182.
38 Li ZS, Zhao Y, Rea PA. Magnesium Adenosine 5[prime]-Triphosphate-Energized Transport of Glutathione-S-Conjugates by Plant Vacuolar Membrane Vesicles. *Plant Physiol* 1995; **107**: 1257–1268.
39 Shi SR, Cote RJ, Hawes D, Thu S, Shi Y, Young LL *et al.* Calcium-induced modification of protein conformation demonstrated by immunohistochemistry: What is the signal? *J Histochem Cytochem* 1999; **47**: 463–470.
40 Glenn GM, Scharton-Kersten T, Vassell R, Mallett CP, Hale TL, Alving CR. Transcutaneous immunization with cholera toxin protects mice against lethal mucosal toxin challenge. *J Immunol* 1998; **161**: 3211–3214.
41 Sedegah M, Hedstrom R, Hobart P, Hoffman SL. Protection against malaria by immunization with plasmid DNA encoding circumsporozoite protein. *Proc Natl Acad Sci USA* 1994; **91**: 9866–9870.
42 Hirao LA, Wu L, Khan AS, Satishchandran A, Draghia-Akli R, Weiner DB. Intradermal/subcutaneous immunization by electroporation improves plasmid vaccine delivery and potency in pigs and rhesus macaques. *Vaccine* 2008; **26**: 440–448.
43 Yan J, Harris K, Khan AS, Draghia-Akli R, Sewell D, Weiner DB. Cellular immunity induced by a novel HPV18 DNA vaccine encoding an E6/E7 fusion consensus protein in mice and rhesus macaques. *Vaccine* 2008; **26**: 5210–5215.
44 Huang B, Mao CP, Peng S, Hung CF, Wu TC. RNA interference-mediated *in vivo* silencing of fas ligand as a strategy for the enhancement of DNA vaccine potency. *Hum Gene Ther* 2008; **19**: 763–773.
45 Doria-Rose NA, Ohlen C, Polacino P, Pierce CC, Hensel MT, Kuller L *et al.* Multigene DNA priming-boosting vaccines protect macaques from acute CD4+-T-cell depletion after simian-human immunodeficiency virus SHIV89.6P mucosal challenge. *J Virol* 2003; **77**: 11563–11577.
46 Peng S, Trimble C, Alvarez RD, Huh WK, Lin Z, Monie A *et al.* Cluster intradermal DNA vaccination rapidly induces E7-specific CD8+ T-cell immune responses leading to therapeutic antitumor effects. *Gene Therapy* 2008; **15**: 1156–1166.
47 Curnow SJ, Scheel-Toellner D, Jenkinson W, Raza K, Durrani OM, Faint JM *et al.* Inhibition of T cell apoptosis in the aqueous humor of patients with uveitis by IL-6/soluble IL-6 receptor trans-signaling. *J Immunol* 2004; **173**: 5290–5297.
48 Peachman KK, Rao M, Alving CR. Immunization with DNA through the skin. *Methods* 2003; **31**: 232–242.
49 Lin CC, Yen MC, Lin CM, Huang SS, Yang HJ, Chow NH *et al.* Delivery of noncarrier naked DNA vaccine into the skin by supersonic flow induces a polarized T helper type 1 immune response to cancer. *J Gene Med* 2008; **10**: 679–689.
50 Feltkamp MC, Smits HL, Vierboom MP, Minnaar RP, de Jongh BM, Drijfhout JW *et al.* Vaccination with cytotoxic T lymphocyte epitope-containing peptide protects against a tumor induced by human papillomavirus type 16-transformed cells. *Eur J Immunol* 1993; **23**: 2242–2249.
51 Cheng WF, Chang MC, Sun WZ, Lee CN, Lin HW, Su YN *et al.* Connective tissue growth factor linked to the E7 tumor antigen generates potent antitumor immune responses mediated by an antiapoptotic mechanism. *Gene Therapy* 2008; **15**: 1007–1016.
52 Cheng WF, Hung CF, Hsu KF, Chai CY, He L, Ling M *et al.* Enhancement of sindbis virus self-replicating RNA vaccine potency by targeting antigen to endosomal/lysosomal compartments. *Hum Gene Ther* 2001; **12**: 235–252.
53 Lin K-Y, Guarnieri FG, Staveley-O'Carroll KF, Levitsky HI, August T, Pardoll DM *et al.* Treatment of established tumors with a novel vaccine that enhances major histocompatibility class II presentation of tumor antigen. *Cancer Res* 1996; **56**: 21–26.

Available online at www.sciencedirect.com
ScienceDirect
Gynecologic Oncology 107 (2007) 404–412
Gynecologic Oncology
www.elsevier.com/locate/ygyno

DNA vaccine encoding heat shock protein 60 co-linked to HPV16 E6 and E7 tumor antigens generates more potent immunotherapeutic effects than respective E6 or E7 tumor antigens

Chia-Yen Huang [a], Chi-An Chen [a], Chien-Nan Lee [a], Ming-Cheng Chang [a], Yi-Ning Su [b], Yi-Chun Lin [a], Chang-Yao Hsieh [a], Wen-Fang Cheng [a,b,*]

[a] *Department of Obstetrics and Gynecology, College of Medicine, National Taiwan University, Taipei, Taiwan*
[b] *Graduate Institute of Clinical Medicine, College of Medicine, National Taiwan University, Taipei, Taiwan*

Received 13 February 2007
Available online 1 October 2007

Abstract

Objective. Vaccination based on tumor antigen is an attractive strategy for cancer prevention and therapy. Cervical cancer is highly associated with human papillomavirus, especially type 16. We developed DNA vaccines encoding heat shock protein 60 (HSP60) linked to HPV16 E6 or E7 to test if HSP60 chimeric DNA vaccines may generate strong E6 and/or E7-specific immune response and anti-tumor effects in vaccinated mice.

Methods. In vivo antitumor effects such as preventive, therapeutic, and antibody depletion experiments were performed. *In vitro* assays such as intracellular cytokine stainings, ELISA for Ab responses, and direct and cross-priming effects, were also performed.

Results. HSP60 chimeric DNA vaccines generated strong E6- or E7-specific immune responses and anti-tumor effects in vaccinated mice via direct and cross-priming effects. HSP60 was also linked with both E6 and E7 antigens and the HSP60/E6/E7 chimeric DNA vaccine generated more potent immunotherapeutic effects on E6- and E7-expressing tumors than HSP60/E6 or HSP60/E7 chimeric DNA vaccine alone.

Conclusion. Utilization of both E6 and E7 tumor antigens can advance the therapy of tumors associated with HPV-infections. The DNA vaccine encoding heat shock protein 60 co-linked to HPV16 E6 and E7 tumor antigens can generate more potent immunotherapeutic effects than E6 or E7 tumor antigens alone.

Keywords: DNA vaccine; Heat shock protein 60; HPV16; E7 antigen; E6 antigen

Introduction

DNA vaccines have become an attractive approach for generating antigen-specific cancer vaccine and immunotherapy. Naked plasmid DNA can be repeatedly administered and easily prepared in large scale with high purity, and are highly stable relative to proteins and other biological polymers [1]. In addition, intra-dermal administration of DNA vaccines using a gene gun represents an efficient means of targeting dendritic cells, the most potent professional antigen-presenting cells that are specialized to prime T helper and cytotoxic cells *in vivo* [2,3].

One of the concerns about DNA vaccines is their limited potency, because they do not have the intrinsic ability to amplify *in vivo* as viral vaccines do [1]. Several strategies have been applied to increase their potency. For example, targeting antigens for rapid intracellular degradation [4], directing antigens to APCs by fusion to ligands for APC receptors [5], or fusing antigens to a pathogen sequence, such as fragment C of tetanus toxin [6] have been made. Linkage of antigens to HSP may be another potential approach for increasing the potency of DNA vaccines. HSP-based protein vaccine can also be administered by fusing antigens to HSP [7–9]. Furthermore, immune response can be induced in mice with MHC that is either identical or different to the MHC of donor HSPs [10–12]. These

* Corresponding author. Department of Obstetrics and Gynecology, College of Medicine, National Taiwan University, Chung-Shan South Road, Taipei, Taiwan. Fax: +886 2 393 4197.
E-mail address: wenfangcheng@yahoo.com (W.-F. Cheng).

0090-8258/$ - see front matter © 2007 Elsevier Inc. All rights reserved.
doi:10.1016/j.ygyno.2007.06.031

investigations have made HSPs more attractive to use in cancer vaccine and immunotherapy.

More than 99% of cervical cancers contain HPV, particularly the high-risk HPV type such as 16 and 18 [11]. Two HPV oncoproteins, E6 and E7, are consistently expressed in HPV-associated cancer cells and are responsible for their malignant transformation. These two oncogenic proteins therefore represent ideal target antigens for developing vaccines and immunotherapeutic strategies against HPV-associated neoplasia. Numerous pre-clinical studies and some clinical studies have targeted the HPV16 oncogenic proteins E6 or E7 for vaccine development to control HPV-associated lesions [13–15].

In the past, most HPV researchers focused on E7, and thus an E7 immuno-dominant epitope and its associated immune responses have been well characterized [6]. The gene gun approach was previously used to test several strategies that are able to rout the human papilloma virus type 16 E7 model antigen and result in enhanced E7-specific $CD8^+$ T cell-mediated immune response and anti-tumor effects [16–19]. Since E6 represents another important target for potential vaccines to control HPV-associated lesions, it is also crucial to develop vaccines targeting E6.

We therefore developed a DNA vaccine encoding HSP60 linked to E6 and/or E7 to elucidate if DNA vaccines encoding HSP60 with two tumor antigens (E6 and E7) have the potential to prevent HPV infection and provide therapeutic effects on HPV-related cancers.

Materials and methods

Plasmid DNA constructs and preparation

For the generation of pcDNA3-HSP60, HSP60 was first amplified with PCR using human placenta cDNA as template and a set of primers, 5′-CCGGTCTAGAAGAAATGCTTCGGTTACCCACAG-3′ and 5′-CGCGGATCCACACTGCCTTGGGCTTCCTGTCA-3′. The amplified product was then cloned into the *Xba*I/*Bam*HI sites of the pcDNA3 vector (Invitrogen Corp., Carlsbad, California, USA). For the generation of pcDNA3-HSP60/E6, E6 was first amplified with PCR using DNA of the CaSki cell line as template and a set of primers, 5′-CGCGGATCCATGCACCAAAAGAGAACTGCAATGT-3′ and 5′-CCCAAGCTTTTACAGCTGGGTTTCTCTACGTGTTCT-3′. E6 was then cloned into the *Bam*HI/*Hin*dIII sites of pcDNA3-HSP60 to generate pcDNA3-HSP60/E6.

To generate pcDNA3-HSP60/E7, E7 was first amplified using DNA of the CaSki cell line as template and with a set of primers, 5′-CCGGGATCCATG-GAGATACACCTA -3′ and 5′-CCCAAGCTTTTGAGAACAGATGG -3′, and cloned into the *Bam*HI/*Hin*dIII sites of pcDNA3-HSP60 to generate pcDNA3-HSP60/E7. To generate pcDNA3-HSP60/E6/E7, E7 was cloned into the *Hin*dIII/*Hin*dIII sites of pcDNA3-HSP60/E6. Plasmid constructs were confirmed by DNA sequencing.

Cell line

TC-1

The TC-1 tumor cell line was generated as described previously [20]. On the day of tumor challenge, tumor cells were harvested by trypsinization, washed twice with 1× Hanks buffered salt solution (HBSS), and finally re-suspended in 1× HBSS to the designated concentration for injection.

293 D^bK^b cells

293 D^bK^b cells (a human embryonic kidney 293 cell line expressing the D^b and K^b (293 D^bK^b), two C57BL/6 mouse MHC class I molecules) [21] were kindly provided by Dr. TC Wu, Johns Hopkins Medical Institutes, Baltimore, MD.

Transfection of 293 D^bK^b cells

293 D^bK^b were tansfected with various DNA, such as E6, E7, E6/E7, HSP60/E6, HSP60/E7, or HSP60/E6/E7 using LipofectAMINE reagent (Life Technologies) according to the manufacturer's instructions. The 293 D^bK^b cells were collected 48 h after transfection for further experiments.

Immunoblotting

Transfected 293 D^bK^b cells with various DNA constructs were lysed in immuno-precipitation assay buffer containing 137 mM NaCl, 2.7 mM KCl, 1 mM $MgCl_2$, 1 mM $CaCl_2$, 1% NP40, 10% glycerol, 1 mg/ml BSA, 20 mM Tris, pH 8.0, and 2 mM orthovanadate and analyzed as previously described [22]. Briefly, 50 μg of cell lysates was resolved on a sodium dodecyl sulfate (SDS)-containing 12% polyacrylamide gel, transferred to polyvinylidene difluoride nylon membranes (Millipore, Bedford, Mass.), and probed with antibodies specific to E6 (Abcam, Cambridge, UK) or E7 (Zymed, San Francisco, CA) or β-actin (Chemicon International, Temecula, CA). The membrane was then probed with either horseradish peroxidase-conjugated goat anti-mouse or anti-rabbit antibody.

The specific bands were visualized by an ECL (enhanced chemiluminescence) Western blot system (Amersham, Buckinghamshire, England). As shown in Fig. 1, the E6 (MW 18 kDa), E7 (MW 18 kDa), HSP60/E6 (MW 78 kDa), HPS60/E7 (MW 78 kDa), and HSP60/E6/E7 (MW 96 kDa) proteins showed similar expression levels.

Mice

Six to 8-week-old female C57BL/6J mice were purchased and kept in the animal facility of the School of Medicine, National Taiwan University. All animal procedures were performed according to approved protocols and in accordance with recommendations for the proper use and care of laboratory animals.

DNA vaccination

Preparation of DNA-coated gold particles and gene gun particle-mediated DNA vaccination were performed using a helium-driven gene gun according to a protocol described previously with some modifications [17,23]. Control plasmid (no insert), E6, E7, E6/E7, E6 mixed with E7, HSP60, HSP60 mixed with E6, HSP60 mixed with E7, HSP60/E6, HSP60/E7, HSP60/E6 mixed HSP60/E7, and HSP60/E6/E7-coated gold particles were delivered to the shaved abdominal region of mice using a low pressure-accelerated gene gun (BioWare Technologies Co. Ltd, Taipei, Taiwan) with a 50 psi discharge pressure of helium [23].

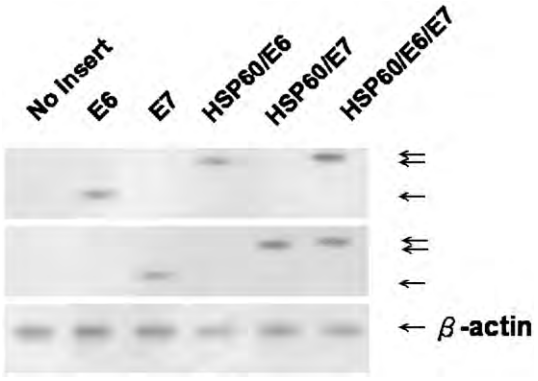

Fig. 1. The protein expression levels of respective constructs in transfected 293 D^bK^b cells. 293 D^bK^b cells were transfected with respective DNA. The E6 or E7 protein expression levels in various constructs are shown as follows: E6 (MW 18 kDa), E7 (MW 18 kDa), HSP60/E6 (MW 78 kDa), HPS60/E7 (MW 78 kDa), and HSP60/E6/E7 (MW 96 kDa).

Intracellular cytokine staining and flow cytometry analysis

Mice were immunized with 2 μg of the various DNA vaccines and received a booster with the same regimen 1 week later. Splenocytes were harvested 1 week after the last vaccination. Before intracellular cytokine staining, pooled splenocytes from each vaccination group were incubated for 16 h with either 1 μg/ml of E6 peptide (aa 50–57) [13] or E7 peptide (aa 49–57) [24], containing an MHC class I epitope for detecting E6- or E7-specific $CD8^+$ T cell precursors, or 50 μg/ml of E6 or E7 protein (kindly provided by Dr. CW Liao, Animal Technology Institute Taiwan, Miaoli, Taiwan) for detecting E6- or E7-specific $CD4^+$ T cell precursors. Cell surface marker staining of CD4 or CD8 and intracellular cytokine staining for IFN-γ, as well as flow cytometric analysis, were performed using conditions described previously [17,25].

Cytotoxic T lymphocyte assay using transfected 293 D^bK^b cells as target cells

Cytotoxic T lymphocyte (CTL) assays were performed by quantitative measurements of lactate dehydrogenase (LDH) using CytoTox96 non-radioactive cytotoxicity assay kits (Promega Corp., Madison, Wisconsin, USA) according to the manufacturer's protocol. Various DNA-transfected 293 D^bK^b cells served as target cells while a D^b-restricted E6- or E7-specific $CD8^+$ T cell line (provided by Dr. TC Wu, Johns Hopkins Medical Institutes, Baltimore, MD) was used as effector cells. Untransfected 293 D^bK^b cells were used as a negative control. The 293 D^bK^b cells were collected 40–44 h after transfection.

CTL assays were performed with effector cells and target cells mixed together at various effector/target (E/T) ratios, 1:1, 5:1, 15:1, and 45:1, in a final volume of 200 μl as described previously [16]. After a 5-h incubation at 37 °C, 50 μl of the cultured media was collected to assess the amount of LDH. The percentage of lysis was calculated from the following equation: $100\times(A-B)/(C-D)$, where A is the reading of experimental-effector signal value, B is the effector spontaneous background signal value, C is maximum signal value from target cells, and D is the target spontaneous background signal value.

CTL assay using dendritic cells pulsed with lysates of transfected 293 D^bK^b cells as target cells

CTL assays were performed using bone marrow-derived dendritic cells (DCs) pulsed with cell lysates as target cells and D^b-restricted E6- or E7-specific $CD8^+$ T cells as effector cells using the protocol described previously [26]. DCs were generated by culture of bone marrow cells in the presence of GM-CSF as described previously [27]. 293 D^bK^b cells were first transfected with various DNA constructs via lipofectamine. The protein concentration of lysates was determined using the BioRad protein assay (BioRad Laboratories Inc.) according to the vendor's protocol [16]. DCs were pulsed with different concentrations of cell lysates of various DNA-transfected 293 D^bK^b cells (50 μg/ml, 10 μg/ml, 2 μg/ml, and 0.4 μg/ml) in a final volume of 2 ml for 16–20 h. CTL assays were performed at a fixed E/T ratio of 9:1 using E7-specific T cells mixed with prepared DCs in a final volume of 200 μl. Cytolysis was determined by quantitative measurements of LDH as described earlier.

In vivo tumor protection experiments

For the tumor protection experiments, mice (five per group) either received no vaccination or were immunized with 2 μg/mouse of various DNA vaccines with a gene gun. They were boosted with the same regimen as the first vaccination one week later. One week after the last vaccination, the mice were subcutaneously challenged with 5×10^4 of TC-1 cells/mouse in the right leg. They were monitored for evidence of tumor growth by palpation and inspection twice a week until they were sacrificed on day 60.

In vivo antibody depletion experiments

In vivo Ab depletions were performed as described previously [27,28]. Briefly, mice (five per group) were vaccinated with 2 μg/mouse of HSP60/E6 or HSP60/E7 DNA with a gene gun, boosted 1 week later, and challenged with 5×10^4 cells/mouse TC-1 tumor cells. Depletion was started 1 week before tumor challenge.

mAb GK1.5 was used for CD4 depletion [29], mAb 2.43 was used for CD8 depletion [30], and mAb PK136 was used for NK1.1 depletion [31]. Depletion was terminated on day 40 after tumor challenge. Mice were monitored for evidence of tumor growth by palpation and inspection twice a week until they were sacrificed on day 60.

In vivo tumor treatment experiments

The therapeutic potential of each vaccine was assessed by performing an *in vivo* tumor treatment experiment using a previously described lung hematogenous spread model [16]. Two days after tumor challenge, mice received 16 μg/mouse of no insert DNA, E6 DNA, E7 DNA, E6 mixed with E7 DNA, HSP60 DNA, HSP60/E6 DNA, HSP60/E7 DNA, HSP60/E6 mixed with HSP60/E7 DNA, or HSP60/E6/E7 DNA by a gene gun, followed by a booster with the same regimen every 7 days for 4 weeks (a total of 64 μg DNA). Mice receiving no vaccination were used as negative control. The mice were sacrificed and the lungs were explanted on day 28. Pulmonary tumor nodules in each mouse were evaluated and counted by experimenters who were blinded to sample identity.

For the second *in vivo* tumor treatment experiment, mice were injected with 5×10^4 cells/mouse TC-1 tumor cells via the tail vein as described earlier. Seven days after tumor challenge, mice received various DNA vaccines such as HSP60/E6, HSP60/E7, HSP60/E6 mixed with HSP60/E7, and HSP60/E6/E7 as described earlier. The mice were sacrificed, and the lungs were explanted on day 28. The pulmonary tumors in each mouse were evaluated and counted as described earlier.

Statistical analysis

All data expressed as mean±SEM were representative of at least two different experiments. Data for intracellular cytokine staining with flow cytometry analysis and tumor treatment experiments were evaluated by analysis of variance (ANOVA). Comparisons between individual data points were made using Student's *t*-test. In the tumor protection experiment, the principal outcome of interest was the time to tumor development. The event time distributions for different mice were compared by the Kaplan and Meier and by log-rank analyses. A p value<0.05 was considered statistically significant.

Results

Vaccination with DNA encoding HSP60 linked to E6 alone, E7 alone, or both E6 and E7 significantly enhanced E6 and/or E7-specific $CD8^+$ T cell response

The representative figures of flow cytometric analysis are shown in Fig. 2A. As shown in Fig. 2B, vaccination with HSP60/E6 (140.0±14.1) or HSP60/E6/E7 (218.0±17.0) DNA generated higher frequencies of E6-specific IFN-γ-secreting $CD8^+$ T cell precursors when compared to mice vaccinated with E6 (6.5±2.1), E7 (4.0±1.4), E6/E7 (8.0±3.5), HSP60 mixed with E6 (12.5±2.8), or HSP60/E7 (39.0±5.7) DNA ($p<0.01$, one-way ANOVA). In addition, vaccination with HSP60/E7 (275.0±24.0), or HSP60/E6/E7 (987.5±27.6) DNA generated higher frequencies of E7-specific IFN-γ-secreting $CD8^+$ T cell precursors when compared to mice vaccinated with E6 (7.5±1.4), E7 (7.0±2.8), E6/E7 (12.0±2.8), HSP60 mixed with E7 (14.5±2.1), or HSP60/E6 DNA (40.5±7.0) ($p<0.01$, one-way ANOVA) (Fig. 2C). We further evaluated whether HSP60 could enhance the E6, or E7-specific $CD4^+$ T cell response when linked to E6, or E7 in a DNA vaccine, respectively. As shown in

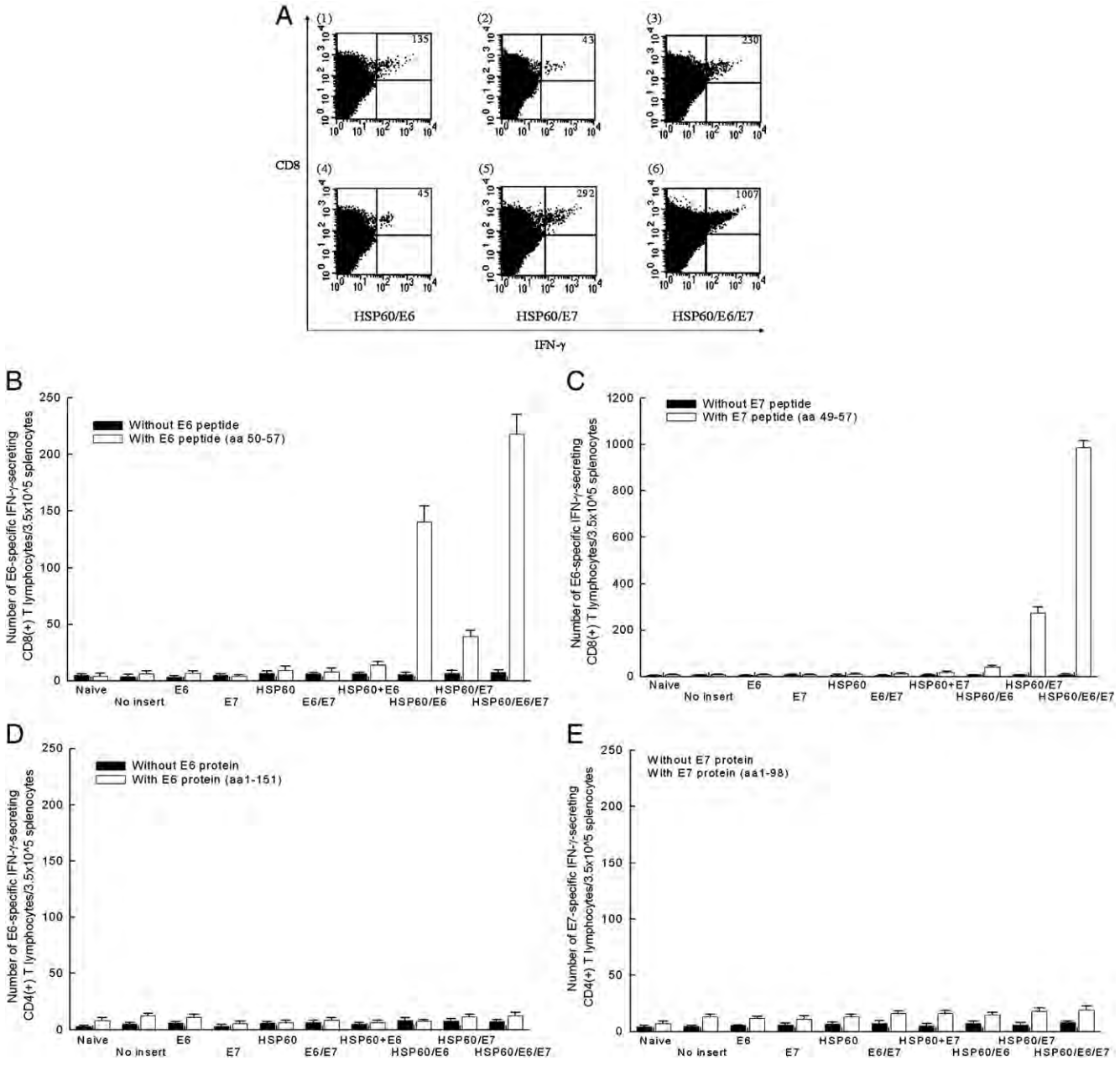

Fig. 2. Immunologic profiles of vaccinated mice using intracellular cytokine staining and flow cytometry analysis and ELISA. (A) Representative figures of flow cytometric analysis. (B) Bar graph depicting the number of E6-specific IFN-γ-secreting $CD8^+$ T cell precursors/3.5×10^5 splenocytes (mean±SEM). Mice vaccinated with HSP60/E6 or HSP60/E6/E7 DNA generated higher numbers of E6-specific IFN-γ-secreting $CD8^+$ T cell precursors than other vaccination groups ($p<0.01$, one-way ANOVA). (C) Bar graph depicting the number of E7-specific IFN-γ-secreting $CD8^+$ T cell precursors/3.5×10^5 splenocytes (mean±SEM). Mice vaccinated with HSP60/E7 or HSP60/E6/E7 DNA generated higher numbers of E7-specific IFN-γ-secreting $CD8^+$ T cell precursors than other vaccination groups ($p<0.01$, one-way ANOVA). (D) Bar graph depicting the number of E6-specific IFN-γ-secreting $CD4^+$ T cell precursors/3.5×10^5 splenocytes (mean±SEM). None of the vaccinated groups generated significantly higher number of E6-specific $CD4^+$ T cell precursors when compared with naive mice ($p>0.05$, one-way ANOVA). (E) Bar graph depicting the number of E7-specific IFN-γ-secreting $CD4^+$ T cell precursors/3.5×10^5 splenocytes (mean±SEM). None of the vaccinated groups generated significantly higher number of E7-specific $CD4^+$ T cell precursors when compared with naive mice ($p>0.05$, one-way ANOVA).

Figs. 2D and E, no increase in the number of E6- or E7-specific IFN-γ-secreting $CD4^+$ T cells in mice vaccinated with various DNA vaccines was observed.

Our data showed that physical linkage of HSP60 to E6 or E7 was required for enhancement of E6- or E7-specific $CD8^+$ T cell activity, since DNA encoding HSP mixed with E6 or E7 DNA did not generate enhancement of E6- or E7-specific $CD8^+$ T cell activity.

Enhanced presentation of E6, or E7, or E6 and E7 antigen through the MHC class I pathway in cells transfected with HSP60 linked with E6, or E7, or E6 and E7 DNA and in dendritic cells pulsed with various chimeric HSP60 proteins

We further explored potential explanations for the observed increase in E6 and/or E7-specific $CD8^+$ T cell precursors in mice vaccinated with HSP60/E6, HSP60/E7, or HSP60/E6/E7.

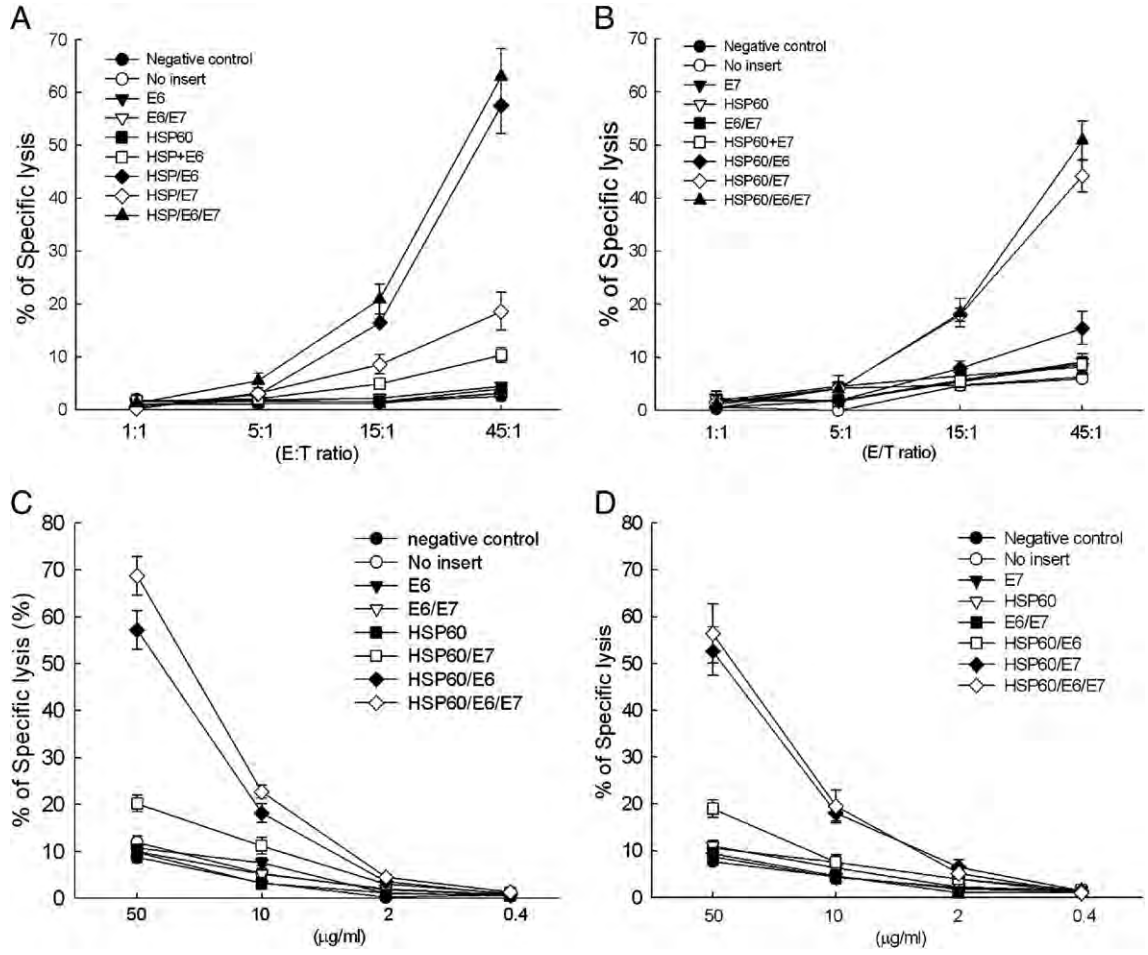

Fig. 3. CTL assays demonstrate enhanced presentation of E6 or E7 through the MHC class I pathway directly by 293 D^bK^b cells transfected with HSP60/E6, HSP60/E7, or HSP60/E6/E7 DNA constructs. (A) CTL assays with various E/T ratios (E/T = 1:1, 5:1, 15:1, 45:1) by using 293 D^bK^b cells transfected with various DNA constructs served as target cells and D^b-restricted E6-specific $CD8^+$ T cells as effector cells. (B) CTL assays with various E/T ratios (E/T = 1:1, 5:1, 15:1, 45:1) by using 293 D^bK^b cells transfected with various DNA constructs served as target cells and D^b-restricted E7-specific $CD8^+$ T cells as effector cells. CTL assays demonstrate enhanced presentation of E6, or E7 through the MHC class I pathway indirectly by bone marrow-derived DCs pulsed with cell lysates containing chimeric HSP60/E6, HSP60/E7, or HSP60/E6/E7 protein. (C) CTL assays at fixed E/T ratio (9:1) using bone marrow-derived DCs pulsed with different concentrations of cell lysates from various DNA-transfected 293 D^b cells, and D^b-restricted E6-specific $CD8^+$ T cells as effector cells. (D) CTL assays at fixed E/T ratio (9:1) using bone marrow-derived DCs pulsed with different concentrations of cell lysates from various DNA-transfected 293 D^bK^b cells and D^b-restricted E6-specific $CD8^+$ T cells as effector cells.

One was that there was direct enhancement of MHC class I presentation of E6 or E7 in cells expressing HSP60/E6, HSP60/E7, or HSP60/E6/E7. As shown in Fig. 3A, 293 D^bK^b cells transfected with HSP60/E6 (57.6±5.4%) and HSP60/E6/E7 (63.1±5.2%) DNA generated significantly higher percentages of specific lysis at 45:1 E/T ratios compared with cells transfected with E6 and HSP60 (10.3±1.4%), HSP60 (4.0±0.4%), E6/E7 (4.4±0.2%), or wild-type E6 (3.1±0.1%) DNA when the effector cells were the E6-specific $CD8^+$ T cell line ($p<0.001$, one-way ANOVA).

Similar phenomena were also observed in 293 D^bK^b cells transfected with HSP60/E7 (44.2±3.0%), and the HSP60/E6/E7 (50.9±3.6%) DNA also generated significantly higher percentages of specific lysis at 45:1 E/T ratios compared with cells transfected with E7 and HSP60 (8.7±1.4%), HSP60 (9.1±0.5%), E6/E7 (9.0±1.7%), or wild-type E7 (8.2±1.4%) DNA when the effector cells were changed to the E7-specific $CD8^+$ T cell line ($p<0.001$, one-way ANOVA) (Fig. 3B).

Another potential mechanism for the observed enhancement of E7-specific $CD8^+$ T cell immune responses *in vivo* was the so-called "cross-priming" effect [32], where the HSP70/E7 protein released from cells were taken up and processed by other antigen-presenting cells (APCs) via the MHC class I-restricted pathway [27]. As shown in Fig. 3C, DCs pulsed with lysates of 293 D^bK^b cells transfected with HSP60/E6 (57.2±4.0%) or HSP60/E6/E7 (68.7±4.1%) DNA generated a significantly higher percentage of specific lysis than DCs pulsed with lysates of 293 D^bK^b cells transfected with HSP60/E7 (20.2±1.8%) or the wide-type E6 (10.7±0.6%) DNA construct ($p<0.001$, one-way ANOVA), when the effector cells were the E6-specific $CD8^+$ T cell line.

In addition, DCs pulsed with 50 μg/ml lysates of 293 D^bK^b cells transfected with HSP60/E7 (52.6±5.2%) or HSP60/E6/E7 (56.4±6.3%) DNA generated a significantly higher percentage of specific lysis than DCs pulsed with lysates of 293 D^bK^b cells transfected with HSP60/E6 (19.0±1.8%) or the wide-type E7

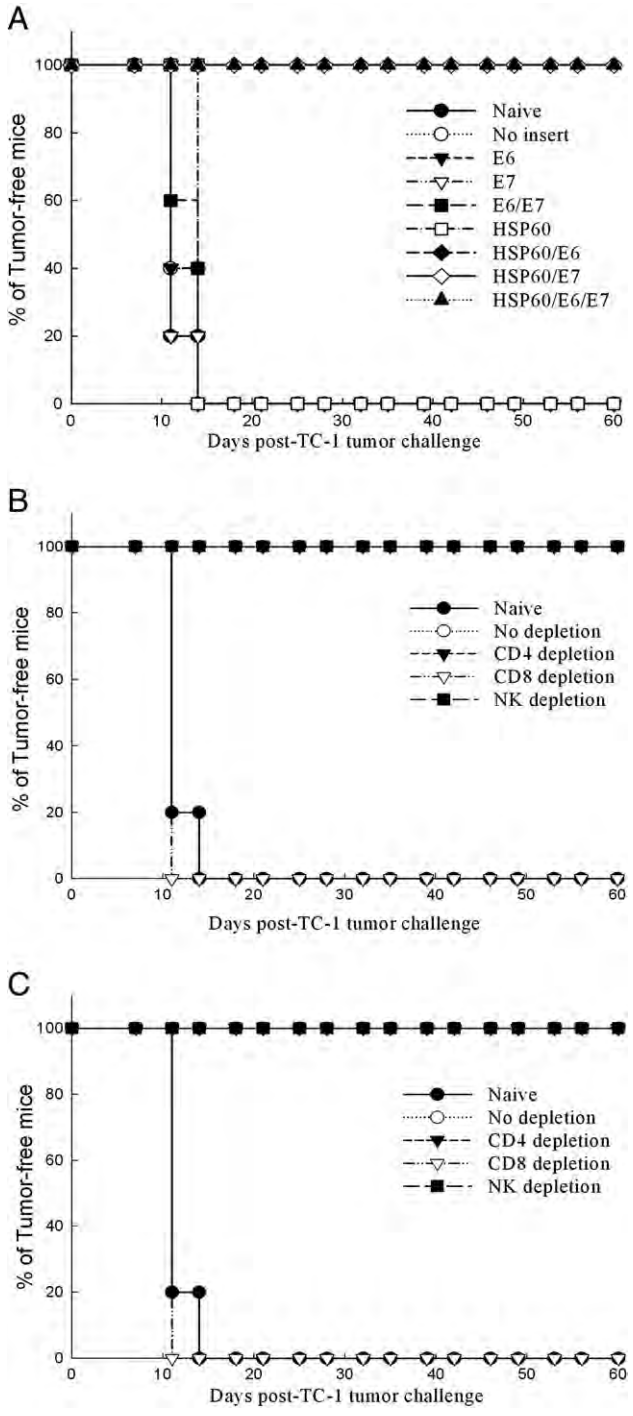

Fig. 4. *In vivo* tumor protection experiments in mice vaccinated with various protein vaccines and *in vivo* Ab depletion experiments in mice vaccinated with HSP60/E6 or HSP60/E7 DNA vaccines. (A) *In vivo* tumor protection experiments. 100% of mice receiving HSP60/E6, HSP60/E7, or HSP60/E6/E7 remained tumor-free 60 days after TC-1 challenge. (B) *In vivo* Ab depletion experiments of mice vaccinated with HSP60/E6 DNA vaccine. (C) *In vivo* Ab depletion experiments of mice vaccinated with HSP60/E7 DNA vaccine. All of the HSP60/E6 or HSP60/E7 vaccinated mice depleted with $CD8^+$ T lymphocytes, as well as naive mice, developed tumors within 14 days after TC-1 tumor challenge. All of the HSP60/E6 or HSP60/E7 vaccinated mice depleted of $CD4^+$ T lymphocytes or $NK1.1^+$ cells were tumor-free after 60 days of TC-1 tumor challenge.

(8.8±1.3%) DNA construct, when the effector cells were the E7-specific $CD8^+$ T cell line ($p<0.001$, one-way ANOVA) (Fig. 3D).

Our *in vitro* experiments revealed that HSP60/E6, HSP60/E7, and HSP60/E6/E7 chimeric molecules may enhance antigen-specific immunity via direct and/or cross-priming effects.

Vaccination with HSP60/E6, HSP60/E7, or HSP60/E6/E7 DNA enhanced tumor protection in mice challenged with an E6 and E7-expressing tumor cell line

To determine if the observed enhancement of E6- or E7-specific $CD8^+$ T cell response translated into a significant E6- or E7-specific protective anti-tumor effect, we performed an *in vivo* tumor protection experiment using a previously characterized E6- and E7-expressing tumor model, TC-1 [20]. As shown in Fig. 4A, 100% of mice receiving HSP60/E6, HSP60/E7, or HSP60/E6/E7 DNA vaccination, when challenged with TC-1 tumor cells, remained tumor-free 60 days after TC-1 challenge. In comparison, all mice vaccinated with the wild-type E6, E7, E6/E7, or HSP60 mixed with E6 or E7 DNA developed tumors within 14 days of challenge.

These results indicated that fusion of HSP60 to E6 and/or E7 antigens is required for anti-tumor immunity of E6 and E7-expressing TC-1 tumor cells.

$CD8^+$ T cells but not $CD4^+$ T cells or natural killer cells were essential for anti-tumor effect generated by HSP60/E6 or HSP60/E7 DNA

To determine the subset of lymphocytes important for the anti-tumor effect, we performed *in vivo* Ab depletion experiments [16]. As shown in Figs. 4B and C, depleted of $CD8^+$ T cells grew tumors within 15 days after tumor challenge in all naive mice and those vaccinated with HSP60/E6 or HSP60/E6 DNA vaccine. In contrast, all of the non-depleted mice and those depleted of $CD4^+$ T cells or NK1.1 cells remained tumor-free 60 days after tumor challenge.

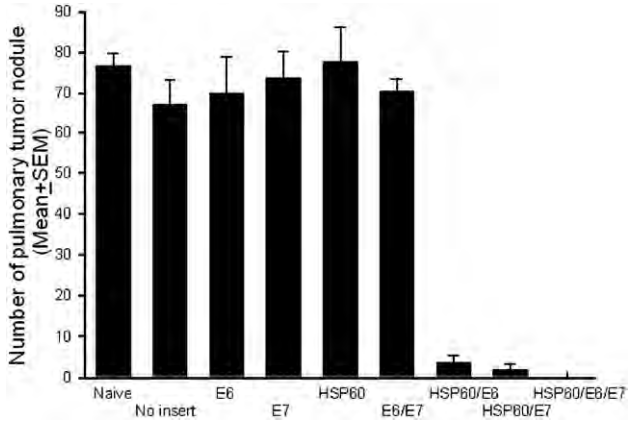

Fig. 5. *In vivo* tumor treatment experiments in mice at a high therapeutic dose. Mice treated with DNA encoding HSP60/E6, HSP60/E7, or HSP70/E6/E7 showed similar numbers of tumor nodules, all significantly lower than those in mice treated with DNA encoding E6, E7, or E6/E7. Data are expressed as mean number of pulmonary tumor nodules+SEM.

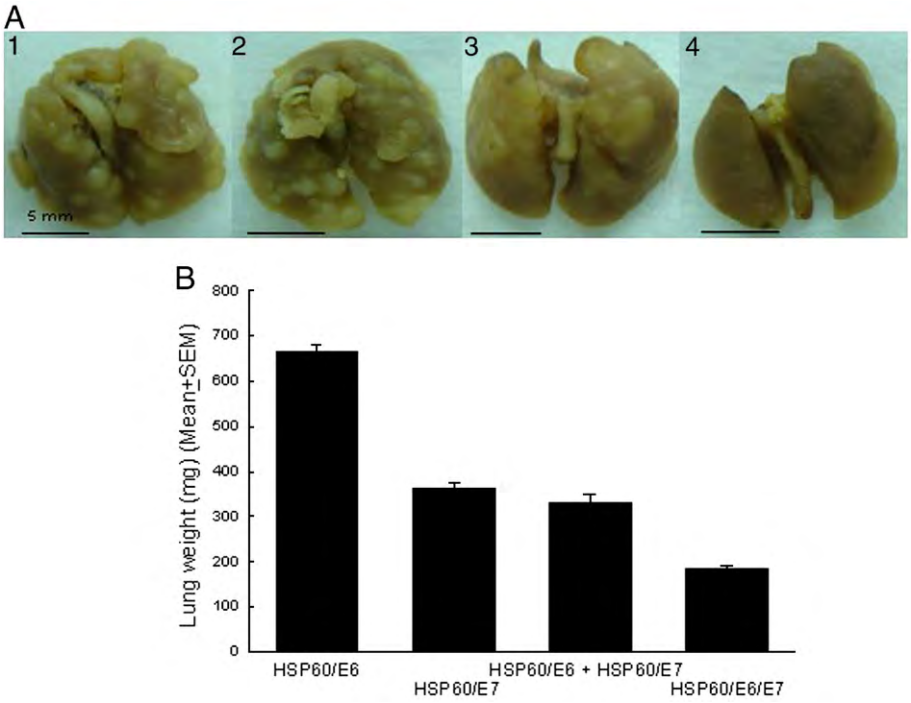

Fig. 6. *In vivo* tumor treatment experiments in mice with various therapeutic conditions. (A) Representative pulmonary tumor nodules in various DNA vaccinated groups. (1) HSP60/E6 group, (2) HSP60/E7 group, (3) HSP60/E6 mixed with HSp60/E7 group, (4) HSP60/E6/E7 group. (B) Mean lung weights in various DNA vaccinated groups. Mice treated with DNA encoding HSP60/E6/E7 showed significantly lower lung weights than those treated with either HSP60/E6 or HSP60/E7 DNA only. Mice vaccinated with HSP60/E7 DNA had lower lung weights than those vaccinated with HSP60/E6 DNA. Data are expressed as mean number of pulmonary tumor nodules ± SEM.

These results suggested that $CD8^+$ T cells are required for anti-tumor immunity generated by HSP60/E6 and HSP60/E7 DNA vaccines.

Treatment with HSP60/E6/E7 led to significant reduction of pulmonary tumor nodules

As shown in Fig. 5, mice treated with HSP60/E6 DNA (3.7 + 1.7), HSP60/E7 (1.8 ± 1.6), or HSP60/E6/E7 (0.0 ± 0.0) all exhibited significantly fewer pulmonary tumor nodules than mice treated with the wild-type E6 (70.0 ± 9.0), wild-type E7 (73.6 ± 6.7), or E6/E7 (70.4 ± 3.1) DNA vaccine ($p < 0.001$, one-way ANOVA), when started on treatment 2 days after tumor injection.

The representative figures of pulmonary tumor nodules treated with various DNA vaccines after 7 days of TC-1 tumor injection are shown in Fig. 6A. As shown in Fig. 6B, mice treated with HSP60/E6/E7 DNA led to significantly lower lung weights (185.0 + 7.1 mg) than those with HSP60/E6 mixed with HSP60/E7 (330.0 ± 20.3 mg), or HSP60/E7 (362.0 ± 13.8 mg), or HSP60/E6 DNA (665.2 ± 14.8 mg) (one-way ANOVA, $p < 0.05$), when started on treatment 7 days after tumor injection.

These data indicated that HSP60, when linked with either E6 or E7 tumor antigens, could generate more potent anti-tumor effects than wild-type E6 or E7 DNA vaccine in a lung hematogeous spread therapeutic model. Moreover, HSP60, when linked with E6 and E7 antigens together, could generate more potent anti-tumor effects than HSP60 linked with either E6 or E7 tumor antigen, or HSP60/E7 mixed with HSP60/E7.

Discussion

Mice vaccinated with HSP60/E6 or HSP60/E7 DNA enhanced E6- or E7-specific $CD8^+$ T cell responses. One possible mechanism for the enhancement of $CD8^+$ T cell responses was the effect of HSP60 in inducing direct-priming mechanism. Our *in vitro* data also revealed that HSP60 chimeric DNA vaccine might enhance $CD8^+$ T cell responses via this mechanism. Ballistic DNA delivery might introduce chimeric HSP60/E6 or HSP60/E7 DNA directly into the dermal precursors or professional APCs to enhance the antigen processing and presenting processes [33]. It was also shown that direct-priming of $CD8^+$ T cells by gene-transfected dendritic cells was the key event in gene gun-mediated DNA immunization [34]. We posit that HSP60/E6 or HSP60/E7 DNA vaccine was transfected into the DCs via the gene gun delivery system to directly enhance E6- or E7-specific T cell immunity.

Another possible mechanism for the enhancement of $CD8^+$ T cell responses by the chimeric HSP60 DNA vaccine was the "cross-priming" of HSP/peptide complexes, where the HSP led exogenous proteins to the MHC-I restricted antigen presentation pathway. We demonstrated that cross-priming might be one of possible mechanisms for the chimeric HSP60 DNA vaccine. HSP60/E6 and HSP60/E7 might be released from other cell types, such as keratinocytes (which were also transfected by gene gun vaccination) and then these chimeric HSP60/E6 or HSP60/E7 proteins were released exogenously to be taken up and processed by other APCs via the MHC class I-restricted pathway [35,36].

HSP complexes taken up by professional APCs are supposed to play an important role in introducing HSP-associated

peptides into the MHC-I antigen presentation pathway [37]. These mechanisms may provide an explanation for the observed enhancement of E6- or E7-specific T cell immunity. CD14 [38] and Toll-like receptors (TLR) 2 and 4 [39,40] are involved in HSP60-mediated cell activation. As regards HSP60, studies have shown that CD14, TLR2, and TLR4 are involved in signal transduction in macrophages [38,41]. It is interesting to evaluate the *in vivo* mechanism of HSP60/E7 and HSP60/E6 DNA vaccine using TLR2 or TLR4 deficient mice in the future.

Heat-shock proteins of the HSP60 family are molecular chaperones that enhance immune responses. HSP60 can transport antigens and after internalization, mediates antigen-specific cytotoxic T cell response [36,42] as observed in this study. HSP60 protein has also been identified in many infectious agents as an immuno-dominant antigen with a protective effect. Immunization of laboratory animals by selected HSP60, HSP70, or HSP90 isolated from several pathogens induces protective host immunity and significantly reduce the clinical manifestation of infection [43,44].

Self HSP60 protein and its derived peptide as carriers in a conjugated vaccine have been shown to protect against lethal *Streptococcus pneumoniae* [45,46]. Milan *et al.* reported that naked HSP60 DNA provides better protective effects than recombinant HSP60 protein [43]. Recently, naked HSP60 DNA has also been utilized to control adjuvant arthritis [47]. Naked human HSP60 DNA vaccine can also be used to inhibit insulitis and diabetes in the NOD mice by vaccination with a DNA construct encoding human HSP60 [48]. Mice, either unprimed or primed with *M. Tuberculosis var. bovis* (Bacillus Calmette-Guerin, BCG), produce a high and long-lasting titer of anti-peptide antibodies when immunized with repetitive malaria synthetic peptide (NANP) conjugated to mycobacterial HSP60 [49]. Although this carrier effect is associated with the risk of immune responses against self HSPs, it still provides a novel approach for the development of vaccines by a fusion of peptides or antigens to HSP60.

The $293K^bD^b$ cells are always used as the antigen-presenting cells in various immunologic assays. Ideally, immunologic assays that evaluate HPV-related vaccines are better used in actual HPV-generated tumor cells. However, it is impossible to create HPV-generated tumor cells in the animal system. Hence, we tried to use $293K^bD^b$ cells to test the immunogenicity of various HSP60 chimeric DNA vaccines. Although it is not relevant to actual HPV-generated tumor cells, 293 cells previously transfected and selected to stably express murine class I MHC molecules H2-K^b and H2-D^b (designated $293K^bD^b$) are good alternative target cells in evaluating the efficacy of DNA vaccine in the animal model.

DNA vaccine encoding heat shock protein 60 co-linked to HPV16 E6 and E7 tumor antigens generates more potent immunotherapeutic effects than E6 or E7 tumor antigens alone. Both E6 and E7 can be utilized as target antigens of cancer vaccine and immunotherapy. The fusion of HSP60 family to E6 or E7 enhances E6- or E7-specific $CD8^+$ T cell-mediated immune responses. In the past, most HPV researchers focused on E7 [50]. Since E6 represents another important target for potential vaccines to control HPV-associated lesions, it is crucial to develop vaccines targeting E6. To combine E6 and E7 as target tumor antigens is important in aiding the future development of HPV vaccines. In addition, the ability of HSP60 to enhance immune responses when linked to two different antigens in DNA vaccines also suggests that HSP60 may be broadly applicable as a strategy to enhance DNA vaccines encoding a variety of antigens. This possibility will be explored further in future DNA vaccination studies, in which HSP60 will be linked to other viral or tumor-specific antigens.

Acknowledgments

This work was supported by grants from the National Science Committee of Taiwan (NSC 94-2314-B-002-198 and NSC 95-2314-B-002-036).

References

[1] Pardoll DM. Exposing the immunology of naked DNA vaccines. Immunity 1995;3:165–9.
[2] Wang R, Epstein J, Charoenvit Y, Baraceros FM, Rahardjo N, Gay T, et al. Induction in humans of CD8+ and CD4+ T cell and antibody responses by sequential immunization with malaria DNA and recombinant protein. J Immunol 2004;172:5561–9.
[3] Ha SJ, Kim DJ, Baek KH, Yun YD, Sung YC. IL-23 induces stronger sustained CTL and Th1 immune responses than IL-12 in hepatitis C virus envelope protein 2 DNA immunization. J Immunol 2004;172:525–31.
[4] Rodriguez F, Zhang J, Whitton JL. DNA immunization: ubiquitination of a viral protein enhances cytotoxic T-lymphocyte induction and antiviral protection but abrogates antibody induction. J Virol 1997;71:8497–503.
[5] Boyle JS, Brady JL, Lew AM. Enhanced responses to a DNA vaccine encoding a fusion antigen that is directed to sites of immune induction. Nature 1998;392:408–11.
[6] King CA, Spellerberg MB, Zhu D, Rice J, Sahota SS, Thompsett AR, et al. DNA vaccines with single-chain Fv fused to fragment C of tetanus toxin induce protective immunity against lymphoma and myeloma. Nat Med 1998;4:1281–6.
[7] Suzue K, Zhou X, Eisen HN, Young RA. Heat shock fusion proteins as vehicles for antigen delivery into the major histocompatibility complex class I presentation pathway. Proc Natl Acad Sci U S A 1997;94:13146–51.
[8] Suzue K, Young RA. Adjuvant-free hsp70 fusion protein system elicits humoral and cellular immune responses to HIV-1 p24. J Immunol 1996;156:873–9.
[9] Enomoto Y, Bharti A, Khaleque AA, Song B, Liu C, Apostolopoulos V, et al. Enhanced immunogenicity of heat shock protein 70 peptide complexes from dendritic cell-tumor fusion cells. J Immunol 2006;177:5946–55.
[10] Srivastava PK, Menoret A, Basu S, Binder RJ, McQuade KL. Heat shock proteins come of age: primitive functions acquire new roles in an adaptive world. Immunity 1998;8:657–65.
[11] Przepiorka D, Srivastava PK. Heat shock protein–peptide complexes as immunotherapy for human cancer. Mol Med Today 1998;4:478–84.
[12] Chan T, Chen Z, Hao S, Xu S, Yuan J, Saxena A, et al. Enhanced T-cell immunity induced by dendritic cells with phagocytosis of heat shock protein 70 gene-transfected tumor cells in early phase of apoptosis. Cancer Gene Ther 2007;14:409–20.
[13] Peng S, Ji H, Trimble C, He L, Tsai YC, Yeatermeyer J, et al. Development of a DNA vaccine targeting human papillomavirus type 16 oncoprotein E6. J Virol 2004;78:8468–76.
[14] Blachere NE, Udono H, Janetzki S, Li Z, Heike M, Srivastava PK. Heat shock protein vaccines against cancer. J Immunother 1993;14:352–6.
[15] Liao CW, Chen CA, Lee CN, Su YN, Chang MC, Syu MH, et al. Fusion protein vaccine by domains of bacterial exotoxin linked with a tumor

antigen generates potent immunologic responses and antitumor effects. Cancer Res 2005;65:9089–98.
[16] Cheng WF, Hung CF, Chai CY, Hsu KF, He L, Ling M, et al. Tumor-specific immunity and antiangiogenesis generated by a DNA vaccine encoding calreticulin linked to a tumor antigen. J Clin Invest 2001;108:669–78.
[17] Cheng WF, Hung CF, Chen CA, Lee CN, Su YN, Chai CY, et al. Characterization of DNA vaccines encoding the domains of calreticulin for their ability to elicit tumor-specific immunity and antiangiogenesis. Vaccine 2005;23:3864–74.
[18] Hung CF, Cheng WF, He L, Ling M, Juang J, Lin CT, et al. Enhancing major histocompatibility complex class I antigen presentation by targeting antigen to centrosomes. Cancer Res 2003;63:2393–8.
[19] Hung CF, Cheng WF, Chai CY, Hsu KF, He L, Ling M, et al. Improving vaccine potency through intercellular spreading and enhanced MHC class I presentation of antigen. J Immunol 2001;166:5733–40.
[20] Lin KY, Guarnieri FG, Staveley-O'Carroll KF, Levitsky HI, August T, Pardoll DM, et al. Treatment of established tumors with a novel vaccine that enhances major histocompatibility class II presentation of tumor antigen. Cancer Res 1996;56:21–6.
[21] Bloom MB, Perry-Lalley D, Robbins PF, Li Y, el-Gamil M, Rosenberg SA, et al. Identification of tyrosinase-related protein 2 as a tumor rejection antigen for the B16 melanoma. J Exp Med 1997;185:453–9.
[22] Chen CH, Ji H, Suh KW, Choti MA, Pardoll DM, Wu TC. Gene gun-mediated DNA vaccination induces antitumor immunity against human papillomavirus type 16 E7-expressing murine tumor metastases in the liver and lungs. Gene Ther 1999;6:1972–81.
[23] Cheng WF, Chen LK, Chen CA, Chang MC, Hsiao PN, Su YN, et al. Chimeric DNA vaccine reverses morphine-induced immunosuppression and tumorigenesis. Molec Ther 2006;13:203–10.
[24] Feltkamp MC, Smits HL, Vierboom MP, Minnaar RP, de Jongh BM, Drijfhout JW, et al. Vaccination with cytotoxic T lymphocyte epitope-containing peptide protects against a tumor induced by human papillomavirus type 16-transformed cells. Eur J Immunol 1993;23:2242–9.
[25] Cheng WF, Hung CF, Hsu KF, Chai CY, He L, Polo JM, et al. Cancer immunotherapy using Sindbis virus replicon particles encoding a VP22-antigen fusion. Hum Gene Ther 2002;13:553–68.
[26] Hung CF, Cheng WF, Hsu KF, Chai CY, He L, Ling M, et al. Cancer immunotherapy using a DNA vaccine encoding the translocation domain of a bacterial toxin linked to a tumor antigen. Cancer Res 2001;61:3698–36703.
[27] Cheng WF, Hung CF, Chai CY, Hsu KF, He L, Rice CM, et al. Enhancement of Sindbis virus self-replicating RNA vaccine potency by linkage of Mycobacterium tuberculosis heat shock protein 70 gene to an antigen gene. J Immunol 2001;166:6218–26.
[28] Cheng WF, Hung CF, Lee CN, Su YN, Chang MC, He L, et al. Naked RNA vaccine controls tumors with down-regulated MHC class I expression through NK cells and perforin-dependent pathways. Eur J Immunol 2004;34:1892–900.
[29] Dialynas DP, Quan ZS, Wall KA, Pierres A, Quintans J, Loken MR, et al. Characterization of the murine T cell surface molecule, designated L3T4, identified by monoclonal antibody GK1.5: similarity of L3T4 to the human Leu-3/T4 molecule. J Immunol 1983;131:2445–51.
[30] Sarmiento M, Glasebrook AL, Fitch FW. IgG or IgM monoclonal antibodies reactive with different determinants on the molecular complex bearing Lyt 2 antigen block T cell-mediated cytolysis in the absence of complement. J Immunol 1980;125:2665–772.
[31] Koo GC, Dumont FJ, Tutt M, Hackett Jr J, Kumar V. The NK-1.1(−) mouse: a model to study differentiation of murine NK cells. J Immunol 1986;137:3742–7.
[32] Uger RA, Barber BH. Creating CTL targets with epitope-linked beta 2-microglobulin constructs. J Immunol 1998;160:1598–605.
[33] Flohe SB, Bruggemann J, Lendemans S, Nikulina M, Meierhoff G, Flohe S, et al. Human heat shock protein 60 induces maturation of dendritic cells versus a Th1-promoting phenotype. J Immunol 2003;170:2340–8.
[34] Porgador A, Irvine KR, Iwasaki A, Barber BH, Restifo NP, Germain RN. Predominant role for directly transfected dendritic cells in antigen presentation to CD8+ T cells after gene gun immunization. J Exp Med 1998;188:1075–82.
[35] Srivastava PK, Udono H, Blachere NE, Li Z. Heat shock proteins transfer peptides during antigen processing and CTL priming. Immunogenetics 1994;39:93–8.
[36] Castellino F, Boucher PE, Eichelberg K, Mayhew M, Rothman JE, Houghton AN, et al. Receptor-mediated uptake of antigen/heat shock protein complexes results in major histocompatibility complex class I antigen presentation via two distinct processing pathways. J Exp Med 2000;191:1957–64.
[37] Suto R, Srivastava PK. A mechanism for the specific immunogenicity of heat shock protein-chaperoned peptides. Science 1995;269:1585–8.
[38] Kol A, Lichtman AH, Finberg RW, Libby P, Kurt-Jones EA. Cutting edge: heat shock protein (HSP) 60 activates the innate immune response: CD14 is an essential receptor for HSP60 activation of mononuclear cells. J Immunol 2000;164:13–7.
[39] Ohashi K, Burkart V, Flohe S, Kolb H. Cutting edge: heat shock protein 60 is a putative endogenous ligand of the toll-like receptor-4 complex. J Immunol 2000;164:558–61.
[40] Vabulas RM, Ahmad-Nejad P, da Costa C, Miethke T, Kirschning CJ, Hacker H, et al. Endocytosed HSP60s use toll-like receptor 2 (TLR2) and TLR4 to activate the toll/interleukin-1 receptor signaling pathway in innate immune cells. J Biol Chem 2001;276:31332–9.
[41] Tsan MF, Gao B. Cytokine function of heat shock proteins. Am J Physiol Cell Physiol 2004;286:C739–44.
[42] Binder RJ, Han DK, Srivastava PK. CD91: a receptor for heat shock protein gp96. Nat Immunol 2000;1:151–5.
[43] Milan R, Alois R, Josef C, Jana B, Evzen W. Recombinant protein and DNA vaccines derived from hsp60 Trichophyton mentagrophytes control the clinical course of trichophytosis in bovine species and guinea-pigs. Mycoses 2004;47:407–17.
[44] Radwanska M, Magez S, Michel A, Stijlemans B, Geuskens M, Pays E. Comparative analysis of antibody responses against HSP60, invariant surface glycoprotein 70, and variant surface glycoprotein reveals a complex antigen-specific pattern of immunoglobulin isotype switching during infection by *Trypanosoma brucei*. Infect Immun 2000;68:848–60.
[45] Amir-Kroll H, Nussbaum G, Cohen IR. Proteins and their derived peptides as carriers in a conjugate vaccine for Streptococcus pneumoniae: self-heat shock protein 60 and tetanus toxoid. J Immunol 2003;170:6165–71.
[46] Konen-Waisman S, Cohen A, Fridkin M, Cohen IR. Self heat-shock protein (hsp60) peptide serves in a conjugate vaccine against a lethal pneumococcal infection. J Infect Dis 1999;179:403–13.
[47] Quintana FJ, Carmi P, Mor F, Cohen IR. DNA fragments of the human 60-kDa heat shock protein (HSP60) vaccinate against adjuvant arthritis: identification of a regulatory HSP60 peptide. J Immunol 2003;171: 3533–41.
[48] Quintana FJ, Rotem A, Carmi P, Cohen IR. Vaccination with empty plasmid DNA or CpG oligonucleotide inhibits diabetes in nonobese diabetic mice: modulation of spontaneous 60-kDa heat shock protein autoimmunity. J Immunol 2000;165:6148–55.
[49] Lussow AR, Barrios C, van Embden J, Van der Zee R, Verdini AS, Pessi A, et al. Mycobacterial heat-shock proteins as carrier molecules. Eur J Immunol 1999;21:2297–302.
[50] Feltkamp MC, Vierboom MP, Toes RE, Ossendorp F, ter Schegget J, Melief CJ, et al. Competition inhibition of cytotoxic T-lymphocyte (CTL) lysis, a more sensitive method to identify candidate CTL epitopes than induction of antibody-detected MHC class I stabilization. Immunol Lett 1995;47:1–8.

The molecular regulation of resistin expression in cultured vascular smooth muscle cells under hypoxia

Huei-Fong Hung[a], Bao-Wei Wang[a], Hang Chang[b] and Kou-Gi Shyu[a,c]

Objectives **Resistin has a potential role in atherosclerosis because resistin produces proinflammatory effects in the vascular wall. However, the molecular mechanism of resistin increase in atherosclerosis remains unclear. Hypoxia plays an important role in vascular remodeling and directly affects vascular smooth muscle cells functions. We sought to investigate the molecular regulation of resistin expression under hypoxia in cultured vascular smooth muscle cells.**

Methods **Vascular smooth muscle cells from thoracic aorta of adult Wistar rats were cultured and subjected to hypoxia at 2.5% oxygen in a hypoxic chamber. Western blot, real-time PCR, reactive oxygen species assay, and promoter activity were measured.**

Results **Hypoxia significantly increased the resistin protein (3.5-fold, $P<0.001$) and mRNA (4.8-fold, $P<0.001$) expression as compared with the control cells. The specific extracellular signal-regulated kinase (ERK) inhibitor PD98059, antioxidant *N*-acetylcysteine, and ERK siRNA attenuated the induction of resistin protein by hypoxia. It increased the phosphorylated ERK protein expression (3.2-fold, $P<0.001$), whereas pretreatment with PD98059 and *N*-acetylcysteine significantly blocked the increase of phosphorylated ERK by hypoxia. It also increased the reactive oxygen species production (9.3-fold, $P<0.001$), and pretreatment with *N*-acetylcysteine significantly blocked the induction of reactive oxygen species by hypoxia. Hypoxia increased resistin promoter activity (5.1-fold, $P<0.001$), and the activity was abolished when nuclear factor of activating T cells in the promoter area was mutated. Pretreatment with PD98059 and *N*-acetylcysteine significantly attenuated the resistin promoter activity induced by hypoxia.**

Conclusion **Hypoxia increases the resistin expression in cultured rat vascular smooth muscle cells under hypoxia. The hypoxia-induced resistin is mediated through reactive oxygen species, ERK mitogen-activated protein (MAP) kinase and nuclear factor of activating T cells pathway.**
J Hypertens **26:2349–2360 © 2008 Wolters Kluwer Health | Lippincott Williams & Wilkins.**

Journal of Hypertension 2008, **26**:2349–2360

Keywords: hypoxia, resistin, signal pathway, vascular smooth muscle cell

Abbreviations: EMSA, electrophoretic mobility shift assay; NAC, N-acetylcysteine; NFATc, nuclear factor of activating T cells; PCR, polymerase chain reaction; PDGF, platelet-derived growth factor; ROS, reactive oxygen species; TNF-α, tumor necrosis factor-α; VSMCs, vascular smooth muscle cells

[a]Division of Cardiology, [b]Department of Emergency Medicine, Shin Kong Wu Ho-Su Memorial Hospital and [c]Graduate Institute of Clinical Medicine, College of Medicine, Taipei Medical University, Taipei, Taiwan

Correspondence to Kou-Gi Shyu, Division of Cardiology, Shin Kong Wu Ho-Su Memorial Hospital, 95 Wen-Chang Rd, Taipei 111, Taiwan
Tel: +886 2 28332211; fax: +886 2 28365775; e-mail: shyukg@ms12.hinetnet

Received 15 February 2008 **Revised** 23 July 2008
Accepted 24 July 2008

See editorial commentary on page 2271

Introduction

Obesity and atherosclerosis are major public health problems in developed countries and are increasingly viewed as inflammatory states [1,2]. For clinical applications, biomarkers that integrate metabolic and inflammatory signals are powerful candidates for defining risk of atherosclerotic cardiovascular disease [3]. Rodent resistin is derived almost exclusively from fat tissue, and adipose expression and serum levels are elevated in models of obesity and insulin resistance [4–6]. Resistin was shown to have potent proinflammatory properties [7]. It promotes endothelial cell activation [8] and causes endothelial dysfunction of porcine coronary arteries [9]. Recently, resistin was found to have a potential role in atherosclerosis because resistin increased proinflammatory cytokine expression in vascular endothelial cells [10], and it promoted vascular smooth muscle cell (VSMC) proliferation [11]. In the atheroma, resistin may contribute to atherogenesis by virtue of its effects on vascular endothelial cells and smooth muscle cells [12]. Although resistin has been shown to increase in atherosclerosis, its molecular regulation mechanism remains unclear. Resistin may represent a novel link between metabolic signals, inflammation, and atherosclerosis [13].

Several lines of evidence indicate that hypoxia is a stimulus to VSMCs proliferation and migration, a process known as the vascular remodeling [14]. Blaschke *et al.* [15] have shown that hypoxia plays an important role in vascular remodeling and directly affects VSMCs functions. The effect of hypoxia on resistin expression in VSMCs has not been previously reported. Nuclear factor of activating T cells (NFAT) has been demonstrated to play a key role in various vasculopathies such as atherosclerosis and restenosis [16–19]. Hypoxia has been proved to stimulate the production of reactive oxygen

0263-6352 © 2008 Wolters Kluwer Health | Lippincott Williams & Wilkins DOI:10.1097/HJH.0b013e328311fa30

species (ROS) in VSMCs [20]. Furthermore, ROS can activate NFAT [21,22]. We hypothesized that hypoxia may regulate resistin expression in VSMCs via ROS and NFAT. Therefore, in this study, we designed to investigate the resistin expression in VSMCs under the hypoxia model and tried to seek the possible molecular mechanisms and signal pathways mediating the expression of resistin under hypoxia condition.

Materials and methods

Vascular smooth muscle cell culture

Primary cultures of VSMCs were grown by the explant technique from the thoracic aorta of 200-g to 250-g male Wistar rats, as described previously [23,24]. Cells were cultured in medium 199 containing 20% fetal calf serum, 0.1 mmol/l nonessential amino acids, 1 mmol/l sodium pyruvate, 4 mmol/l L-glutamine, 100 U/ml penicillin, and 100 μg/ml streptomycin at 37°C under 5% CO_2/95% air in a humidified incubator. When confluent, VSMC monolayers were passaged every 6–7 days after trypsinization and were used for experiment from the third to sixth passages. These third to sixth passage cells were incubated for an additional 2 days to render them quiescent before the initiation of each experiment. The study conforms to *Guide for the Care and Use of Laboratory Animals* published by the US National Institutes of Health (NIH Publication No. 85-23, revised 1996). The study was reviewed and approved by the Institutional Animal Care and Use Committee of the Shin Kong Wu Ho-Su Memorial Hospital.

Hypoxic stimulation

A humidified temperature controlled incubator Proox model 110 (BioSpherix, Redfield, New York, USA) was used as a hypoxic chamber. For hypoxia conditions, the concentration of oxygen was reduced to 2.5% by replacement with N_2, keeping CO_2 constant at 5%, and incubated at 37°C for different times. Control was defined as 95% air and 5% CO_2. For the investigation of signal pathways, cells were pretreated with inhibitors for 30 min, and then exposed to hypoxia without changing medium. SP600125 (20 μmol/l; Calbiochem, San Diego, California, USA) is a potent, cell-permeable, selective, and reversible inhibitor of JNK. SB203580 (3 μmol/l; Calbiochem) is a highly specific, cell-permeable inhibitor of p38 kinase. PD98059 (50 μmol/l; Calbiochem) is a specific and potent inhibitor of extracellular signal-regulated kinase (ERK) kinase. *N*-Acetylcysteine (NAC, 500 μmol/l; Calbiochem) is a free radical scavenger.

Western blot analysis

Western blot was performed as previously described [25]. Rabbit antiresistin rat polyclonal antibody (Chemicon, Temecula, California, USA), polyclonal anti-ERK and monoclonal antiphospho ERK kinase antibodies (Cell Signaling, Beverly, Massachusetts, USA), polyclonal anti-$NFAT_c3$, and antiphospho $NFAT_c3$ antibodies (Santa Cruz Biotechnology, Santa Cruz, California, USA) were used.

Real-time reverse transcription-PCR

Total RNA from cultured VSMCs was extracted using the single-step acid guanidinium thiocyanate/phenol/chloroform extraction method [26]. Real-time reverse transcription-PCR was performed as described previously [24]. The rat resistin primers were 5′-ACTT-CAGCTCCCTACTG-3′ and 5′-GTCTATGCTTCCG-CACT-3′.

RNA interference

Cultured VSMCs were transfected with 800 ng ERK annealed siRNA (Dharmacon Inc., Lafayette, Colorado, USA) or resistin siRNA oligonucleotide (Invitrogen, Carlsbad, California, USA). ERK or resistin siRNA is a target-specific 20–25 nt siRNA designed to knockdown gene expression. ERK sense and antisense of siRNA sequences were 5′-GACCGGAUGUUAACCUUUAUU and 5′-PUAAAGGUUAACAUCCGGUCUU, respectively. Resistin sense and antisense of siRNA sequences were ACACAUUGUAUCCUCACGGACGUCCC and GGACGUCCGUGAGGATACAAUGUGU, respectively. As a negative control, a nontargeting siRNA (scrambled siRNA) purchased from Dharmacon was used. VSMCs were transfected with siRNA oligonucleotides using Effectene Transfection Reagent as suggested by the manufacturer (Qiagen Inc., Valencia, California, USA).

Reactive oxygen species assay

ROS production was measured using the cell permeant probe 2′-7′-dichlorodihydrofluorescin diacetate, which passively diffuses into cells in which intracellular esterases cleave the acetate groups to form the impermeable $DCFH_2$ that remains trapped within the cell [27]. After hypoxia treatment, cells were collected by trypsinization and resuspended in phosphate-buffered saline medium. ROS assay was performed according to the manufacture's instruction (Invitrogen, Eugene, Oregon, USA). Fluorescence microscopy was used to detect the green fluorescence.

Electrophoretic mobility shift assay

Nuclear protein concentrations from cultured VSMCs were determined by Biorad protein assay. Consensus and control oligonucleotides (Research Biolabs, Singapore) were labeled by polynucleotides kinase incorporation of [γ^{32}P]-dATP. Oligonucleotides sequences of $NFAT_c$ were consensus 5′-CGCCCAAAGAGGAAAA-TTTGTTTCATA-3′. The mutant oligonucleotides sequences were 5′-CGCCCAAAGCTTAAAATTT-GTTTC-3′. Electrophoretic mobility shift assay (EMSA) was performed as previously described [26]. Controls were performed in each case with mutant oligonucleotides or cold oligonucleotides to compete with labeled sequences.

Promoter activity assay

A −741 to +22 bp rat resistin promoter construct was generated as follows. Rat genomic DNA was amplified with forward primer (ACGCGTCTCAGCGGTAGAGCTCTTG) and reverse primer (AGATCTGGAGAAATGAAAGGTTCTTCATC). The amplified product was digested with *Mlu*I and *Bgl*II restriction enzymes and ligated into pGL3-basic luciferase plasmid vector (Promega Corp., Madison, Wisconsin, USA) digested with the same enzymes. The resistin promoter contains $NFAT_c$ conserved sites (AGG) at −365 to −363 bp and HIF-1α conserved sites (CGT) at −112 to −114 bp. For the mutant, the $NFAT_c$ and HIF-1α binding sites were mutated using the mutagenesis kit (Stratagene, La Jolla, California, USA). Site-specific mutations were confirmed by DNA sequencing. Plasmids were transfected into VSMCs using a low pressure-accelerated gene gun (Bioware Technologies, Taipei, Taiwan) essentially following the protocol from the manufacturer. In brief, 2 μg of plasmid DNA was suspended in 5 μl of PBS and was delivered to the cultured VSMCs at a helium pressure of 15 psi. The transfection efficiency using this method is 30%. Following hypoxia treatment for 1.5 h, cell extracts were prepared using Dual-Luciferase Reporter Assay System (Promega) and measured for dual luciferase activity by luminometer (Turner Designs Inc., Sunnyvale, California, USA).

Glucose uptake in cultured vascular smooth muscle cells

VSMCs were seeded on ViewPlate for 60 min (Packard Instrument Co., Meriden, Connecticut, USA) at a cell density of 5×10^3 cells/well in serum free medium with transferrin 5 μg/ml, insulin 5 μg/ml for overnight. Recombinant mouse resistin 20 μg/ml (R&D Systems, Minneapolis, Minnesota, USA), resistin siRNA, or NAC were added to the medium. Glucose uptake was performed by adding 0.1 mmol/l glucose and 500 nCi/ml D-[3-^{3}H]-glucose (Perkin Elmer, Boston, Massachusetts, USA) for various periods. Cells were washed with PBS twice. Nonspecific uptake was performed in the presence of 10 μmol/l cytochalasin B and subtracted from all of the measured value. MicroScint-20 50 μl was added and the plate was read with TopCount (Packard Instrument Co.).

Measurement of resistin concentration

Conditioned media from cultured VSMCs under hypoxia and those from control cells (normoxia) were collected for resistin measurement. The level of resistin was measured by a quantitative sandwich enzyme immunoassay technique (R&D Systems). The lower limit of detection of resistin was 5 pg/ml. Both the intraobserver and interobserver coefficient of variance were less than 10%.

Balloon injury of rat carotid artery

Adult Wistar rats were anesthetized with isoflurane (3%) and subject to balloon catheter injury of the right carotid artery. Briefly, a 2F Forgarty balloon catheter (Biosensors International Inc., Newport Beach, California, USA) was inserted through the right external carotid artery, inflated and passed three times along the length of the isolated segment (1.5–2 cm in length), then the catheter was removed. Resistin siRNA was injected to the segment and electric pulses using CUY21-EDIT Square Wave Electroporator (Nepa Gene Co., Ltd, Chiba, Japan) were administered with five pulses and five opposite polarity pulses at 250 V/cm, 50 ms duration, 75 ms interval using Parallel fixed platinum electrode (CUY610P2-1, 1 mm tip, 2 mm gap). The injected siRNA was incubated for 10 min. After incubation, unbound siRNA was aspirated. The carotid artery was then tied off and the neck was closed. The rats were sacrificed at 14 days after balloon injury. The carotid artery was harvested and fixed in 10% formaldehyde and sliced into 5 μm paraffin sections. Then immunohistochemical study was performed as previously described [28].

Statistical analysis

The data were expressed as mean ± SD. Statistical significance was performed with analysis of variance (GraphPad Software Inc., San Diego, California, USA). The Dunnett's test was used to compare multiple groups to a single control group. Tukey–Kramer comparison test was used for pairwise comparisons between multiple groups after the analysis of variance. A value of $P < 0.05$ was considered to denote statistical significance.

Results

Hypoxia increases resistin expression in cultured vascular smooth muscle cells

To test the effect of hypoxia on the resistin expression, different degrees of hypoxia were used. As shown in Fig. 1a and b, hypoxia at 2.5% oxygen for 2 h significantly induced resistin expression, whereas hypoxia at 5 and 10% oxygen had no effect on resistin expression. We then used 2.5% oxygen as hypoxia to the following experiments. As shown in Fig. 1c and d, the level of resistin induction by 2.5% oxygen was similar to that induced by growth factor such as platelet-derived growth factor (PDGF) at 5 ng/ml (PeproTech Inc., Rocky Hill, New Jersey, USA) and proinflammatory stimuli, such as TNF-α at 100 pg/ml (R&D systems). We further showed that hypoxia at 2.5% oxygen induced resistin protein expression maximally at 2 h after hypoxia treatment and maintained elevated for 8 h (Fig. 2a and b). The levels of resistin mRNA also significantly increased from 1.5 to 6 h after hypoxia treatment (Fig. 2c). The immunohistochemical staining demonstrated that resistin was present in the smooth muscle cells in the atheroma induced by balloon injury for 14 days as shown in Supplementary I. We used resistin siRNA by electric pulse to deliver the resistin siRNA to the intimal area. As shown in Supplementary Fig. SI, the neointimal area decreased and resistin labeling decreased by siRNA in the atheroma.

Fig. 1

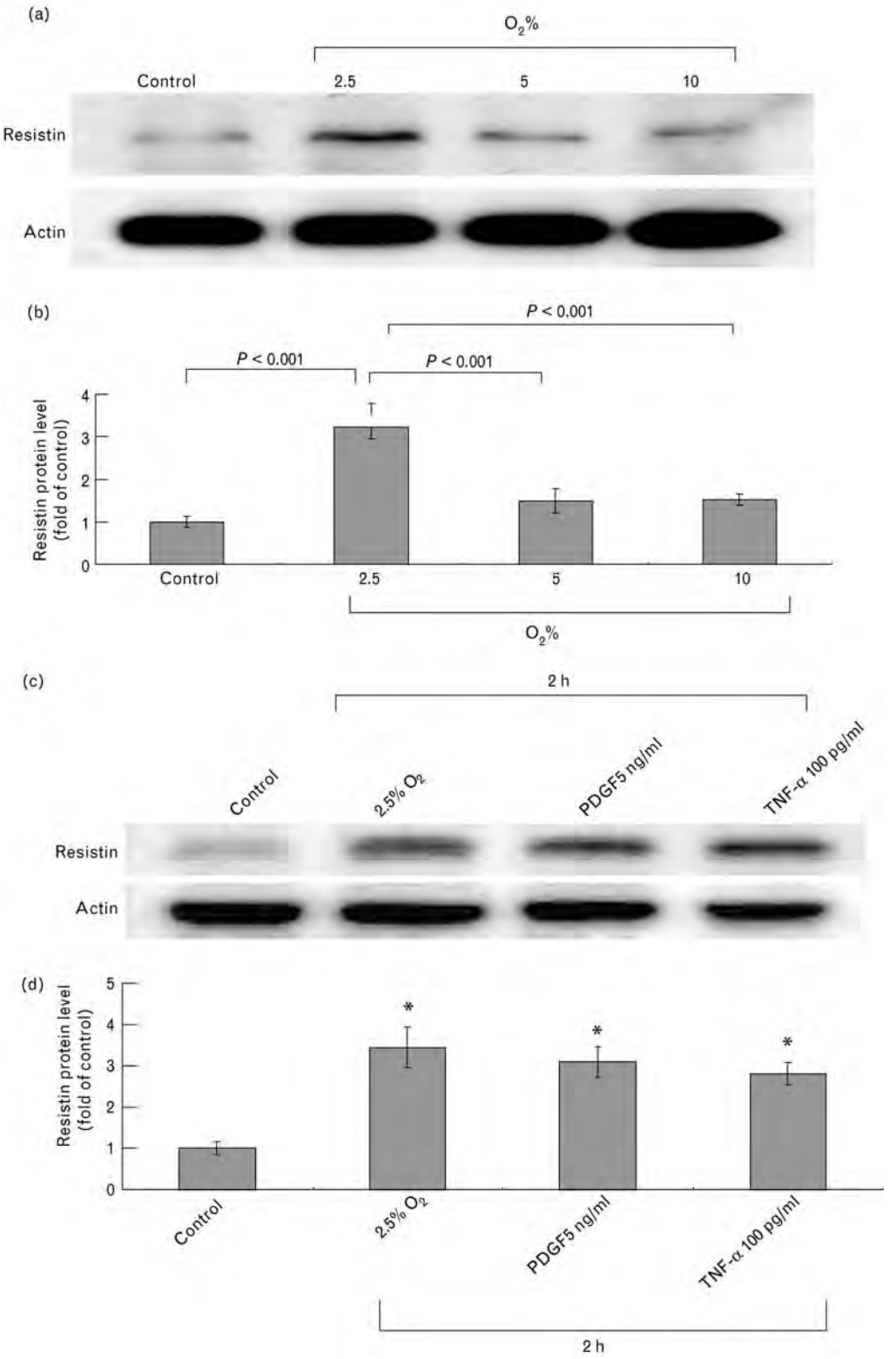

Effect of hypoxia and proinflammatory cytokines on resistin expression in cultured vascular smooth muscle cells. (a and c) Representative western blots for resistin in VSMCs treated with different concentrations of oxygen, platelet-derived growth factor, or TNF-α for 2 h. (b and d) Quantitative analysis of resistin protein levels. The values from treated VSMCs have been normalized to values in control cells ($n = 4$ per group). $^*P < 0.001$ vs. control. The *P*-value for comparing control with 5 and 10% O_2 is 0.170. The *P*-value for comparing PDGF, TNF-α with 2.5% O_2 is 0.125. PDGF, platelet-derived growth factor; VSMC, vascular smooth muscle cell.

Fig. 2

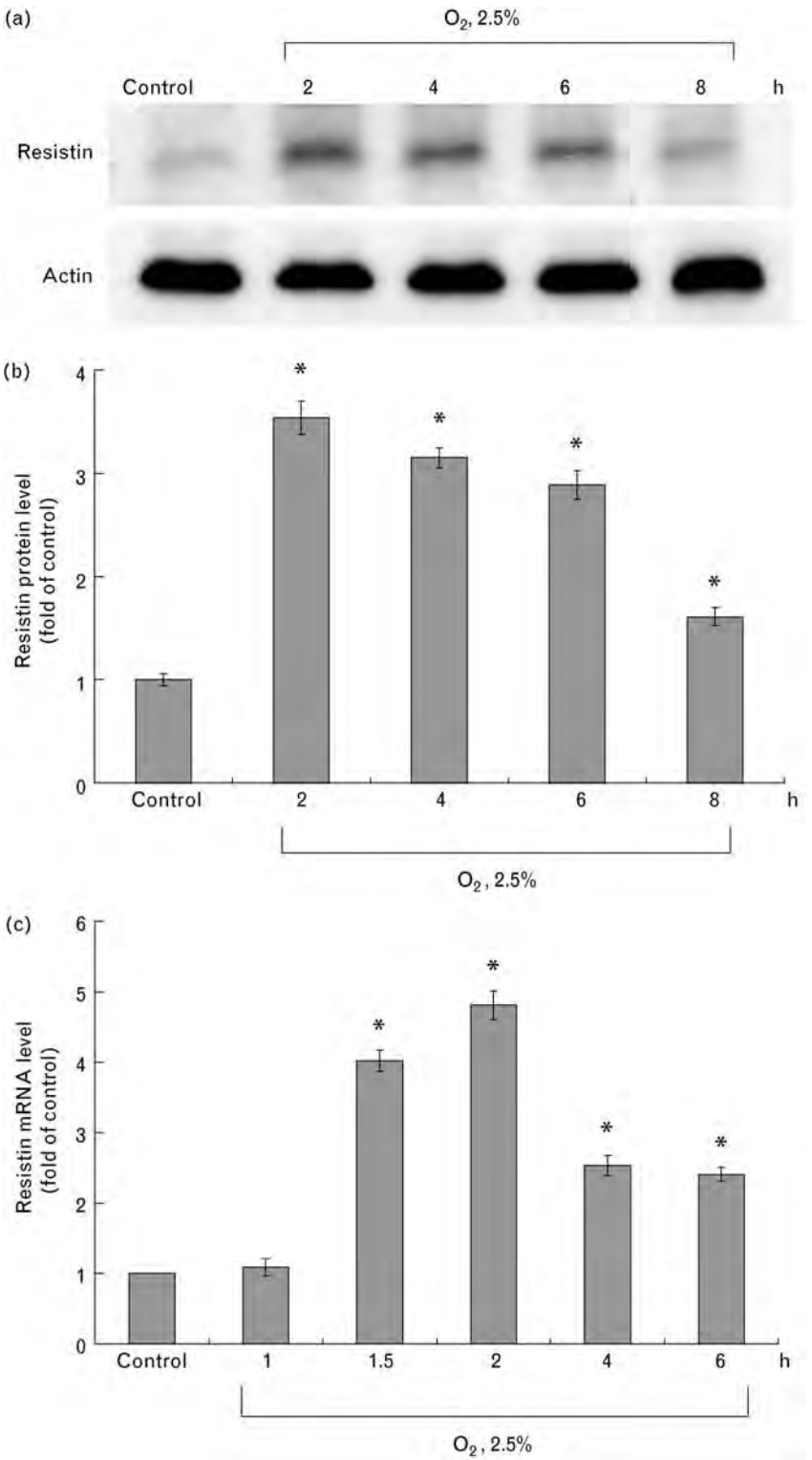

Hypoxia increases resistin protein and mRNA expression in vascular smooth muscle cells. (a) Representative western blots for resistin in VSMCs subjected to 2.5% oxygen stimulation for various periods. (b) Quantitative analysis of resistin protein levels. The values from hypoxic VSMCs have been normalized to values in control cells ($n = 3$ per group). $^*P < 0.001$ vs. control. (c) Quantitative analysis of resistin mRNA levels. The mRNA levels were measured by real-time PCR. The values from hypoxic VSMCs have been normalized to matched actin measurement and then expressed as a ratio of normalized values to mRNA in control cells ($n = 3$ per group). $^*P < 0.01$ vs. control. VSMC, vascular smooth muscle cell.

Fig. 3

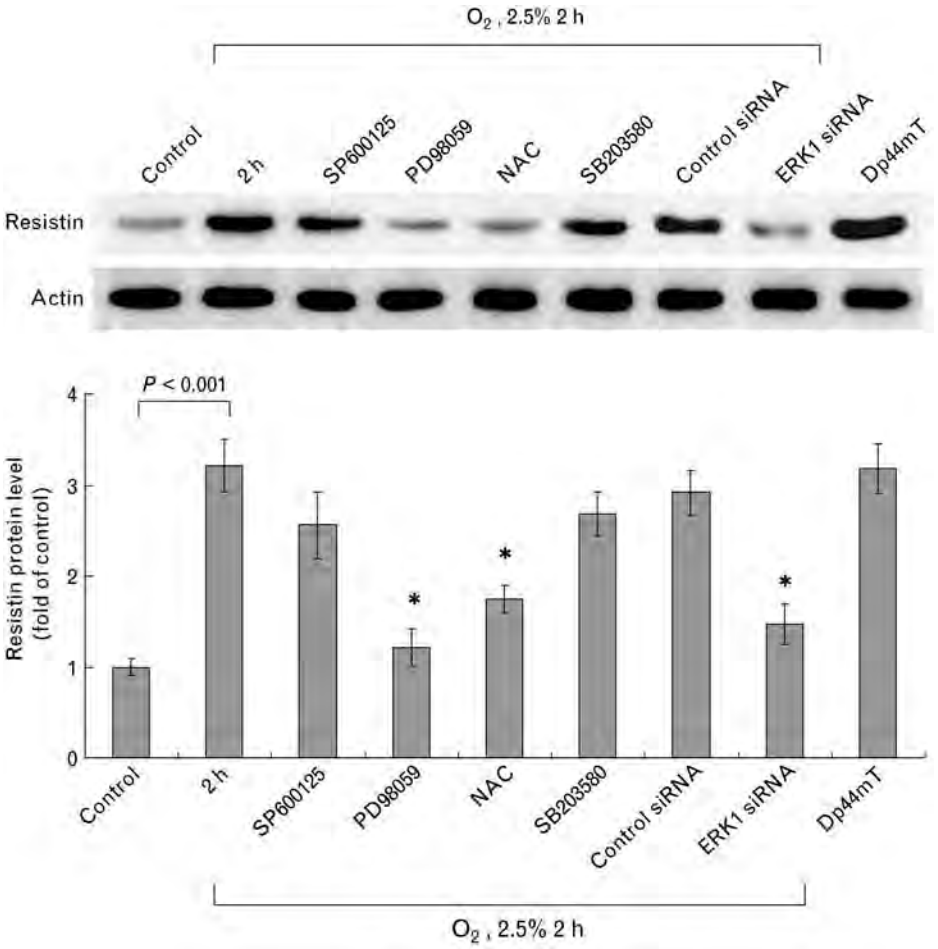

Reactive oxygen species and extracellular signal-regulated and mitogen-activated protein kinases are important regulators that mediate hypoxia-induced resistin expression in vascular smooth muscle cells. Upper panel, representative western blots for resistin protein levels in VSMCs subjected to hypoxia stimulation for 2 h or control cells without hypoxia in the absence or presence of inhibitors, and siRNA. Dp44mT was added to VSMCs without hypoxia. Lower panel, quantitative analysis of resistin protein levels. The values from stimulated VSMCs have been normalized to values in control cells ($n = 4$ per group). $^*P < 0.001$ vs. 2 h. VSMC, vascular smooth muscle cell.

Macrophage was also found in the atheroma with anti-CD68 antibody staining.

Hypoxia-induced resistin protein expression in vascular smooth muscle cells is mediated by reactive oxygen species and extracellular signal-regulated kinase

To investigate the possible signaling pathways mediating the hypoxia-induced resistin expression, different inhibitors were used. As shown in Fig. 3, the western blots demonstrated that the hypoxia-induced increase of resistin protein was significantly attenuated after the addition of PD98059 or NAC 30 min before hypoxia treatment. The resistin protein induced by hypoxia was not affected by the addition of SP600125 and SB203580. Dimethyl sulfoxide as the vehicle for PD98059 did not affect resistin expression induced by hypoxia. Addition of 2,2′-dipyridyl-*N*,*N*-dimethylsemicarbazone (Dp44mT, 30 μmol/l; Calbiochem) alone without hypoxia treatment significantly increased resistin expression. ERK siRNA also completely blocked the resistin expression induced by hypoxia. The control siRNA did not affect the resistin expression induced by hypoxia.

As shown in Fig. 4, hypoxia for 1.5 and 2 h significantly increased the ROS production by using ROS assay with fluorescent microscope. Pretreatment with NAC significantly blocked the induction of ROS by hyperbaric oxygen. In the control group with normoxia treatment, very few VSMCs expressed green fluorescence.

As shown in Fig. 5a and b, phosphorylated ERK protein was induced by hypoxia in a time-dependent manner. The phosphorylated ERK protein was maximally induced at 1.5 h of hypoxia treatment and remained elevated until 4 h. The pattern of increase in phosphorylated ERK protein after hypoxia was slightly earlier than

Fig. 4

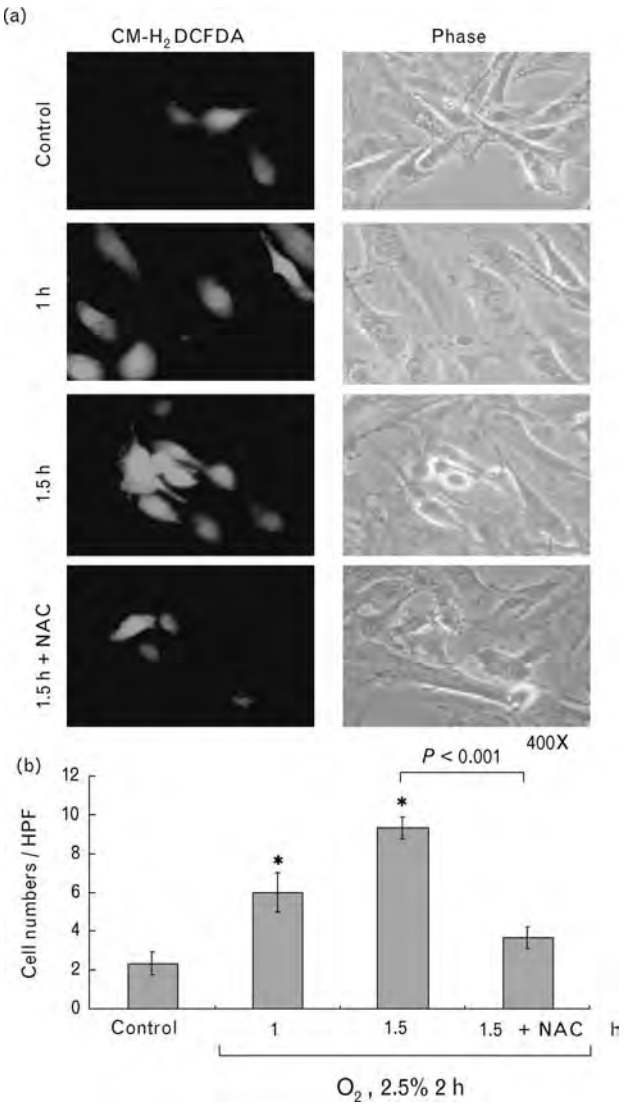

Effect of hypoxia on reactive oxygen species formation in vascular smooth muscle cells. (a) Representative microscopic image for ROS assay with (left panel) or without green fluorescence (right panel) in VSMCs subjected to hypoxia stimulation for 2 h or control cells without hypoxia in the absence or presence of NAC. (b) Quantitative analysis of the positive fluorescent cells. Control group indicates normoxia group ($n = 4$ per group). $^*P < 0.001$ vs. control. NAC, *N*-acetylcysteine; ROS, reactive oxygen species; VSMC, vascular smooth muscle cell.

that of resistin protein after hypoxia as shown in Fig. 2. The phosphorylated ERK was abolished by pretreatment with PD98059 or NAC. ERK siRNA knocked down the ERK protein expression by 72% (from 3.2-fold to 0.89-fold). The phosphorylated $NFAT_c$ protein activated by hypoxia was similar to the pattern of phosphorylated ERK activated by hypoxia. The phosphorylated $NFAT_c$ induced by hypoxia was attenuated by pretreatment with PD98059, NAC, or ERK siRNA (Fig. 5c and d). These data indicate that ROS was generated before the ERK activation and ERK was activated before $NFAT_c$ activation, clarifying the sequence of ROS generation, ERK and $NFAT_c$ activation.

Hypoxia increases nuclear factor of activating T cells binding activity

Hypoxia treatment for cultured VSMCs for 1–4 h significantly increased the DNA-protein binding activity of NFAT (Fig. 6). An excess of unlabeled NFAT oligonucleotide competed with the probe for binding NFAT protein, whereas an oligonucleotide containing a 3-bp substitution in the NFAT-binding site did not compete for binding. Addition of PD98059 30 min before hypoxia abolished the DNA-protein binding activity induced by hypoxia. DNA-binding complexes induced by hypoxia could be supershifted by a monoclonal $NFAT_c$ antibody, indicating the presence of this protein in these complexes.

Hypoxia increases resistin promoter activity

The rat resistin promoter construct contains Stat-3, AP-1, $NFAT_c$, NF-κB, and HIF-1α binding sites. Hypoxia for 1.5 h significantly increased the resistin promoter activity by 5.2-fold as compared with control without hypoxia (Fig. 7). When the $NFAT_c$-binding sites were mutated, the increased promoter activity induced by hypoxia was abolished. Addition of PD98059 and NAC 30 min before hypoxia abolished the increased resistin promoter. The promoter activity of HIF-1α mutant was significantly enhanced after hypoxia treatment and addition of PD98059 and NAC did not change the promoter activity. The promoter activity of wild resistin promoter after hypoxia was significantly higher than that of HIF-1α mutant resistin promoter. This finding indicates that hypoxia regulates resistin in VSMCs at transcriptional level and that $NFAT_c$-binding sites in the resistin promoter is essential for the transcriptional regulation. Combing mutation of NFATC and HIF-1α binding sites did not further reduce the promoter activity as compared with mutation of NFATC-binding site alone. This finding indicates that the HIF-1α binding site is not the major part for the transcriptional regulation of resistin expression in the hypoxic model of VSMC.

Recombinant resistin reduces glucose uptake

Recombinant mouse resistin at 20 μg/ml significantly reduced glucose uptake at various periods of incubation as compared with control VSMCs without treatment (Fig. 8). The dose of recombinant mouse resistin used in the study was according to the study by Graveleau *et al.* [29]. The glucose uptake in hypoxic cells was similar to that in exogenous addition of resistin. Addition of resistin siRNA or NAC before recombinant resistin treatment reversed the glucose uptake to baseline levels. Addition of Dp44mT, a ROS generating agent, reduced the glucose uptake in cultured VSMCs similar to exogenous addition of resistin. Using serum free medium in the

Fig. 5

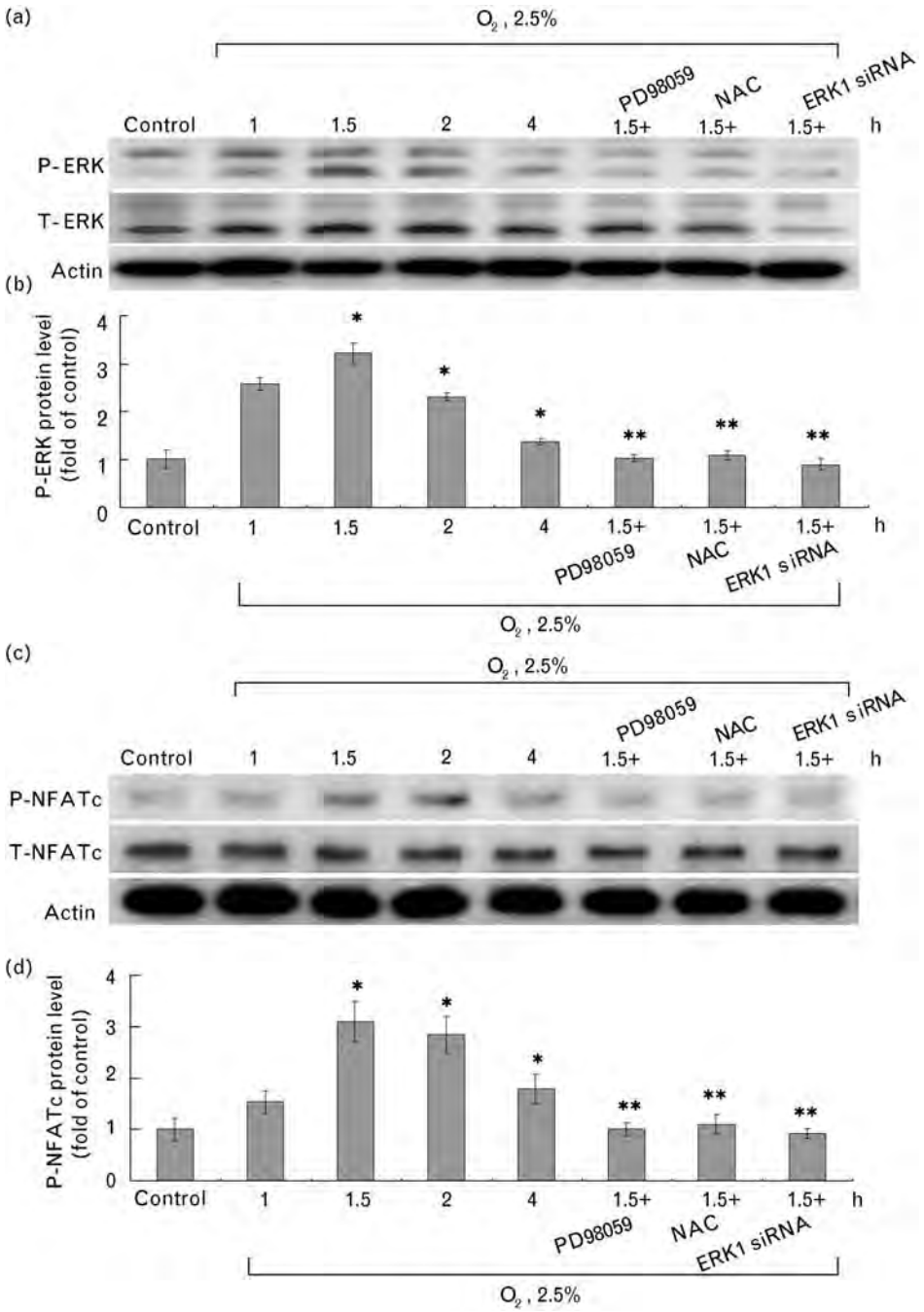

Expression of extracellular signal-regulated and mitogen-activated protein kinases and nuclear factor of activating T cells in vascular smooth muscle cells. (a and c) Representative western blot for phosphorylated and total ERK MAP and $NFAT_c$ in VSMCs after treatment with hypoxia for various periods with or without inhibitor. (b and d) Quantitative analysis of phosphorylated protein levels. The values from hypoxic VSMCs have been normalized to matched actin and corresponding total protein measurement and then expressed as a ratio of normalized values to each phosphorylated protein in control cells ($n = 3$ per group). $^{*}P < 0.001$ vs. control. $^{**}P < 0.001$ vs. 1.5 h. ERK, extracellular signal-regulated kinase; MAP, mitogen-activated protein; NAC, *N*-acetylcysteine; $NFAT_c$, nuclear factor of activating T cells; VSMC, vascular smooth muscle cell.

absence of insulin and resistin, the glucose uptake for VSMCs was 140 ± 10 cpm, whereas addition of resistin reduced the glucose uptake to 106 ± 8 cpm ($P < 0.05$, $n = 3$).

Hypoxia stimulates secretion of resistin from vascular smooth muscle cells

As shown in Fig. 9, hypoxia significantly began to increase the resistin secretion from VSMCs at 1 h after

Fig. 6

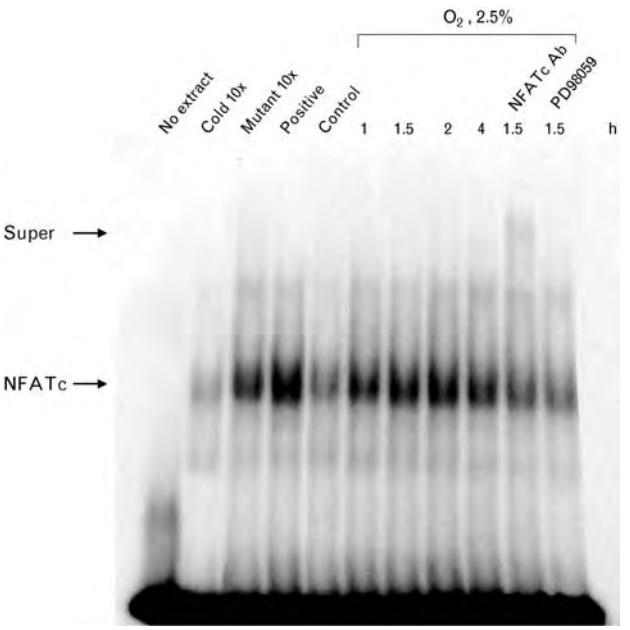

Hypoxia increases nuclear factor of activating T cells binding activity. Representative electrophoretic mobility shift assay showing protein binding to the $NFAT_c$ oligonucleotide in nuclear extracts of vascular smooth muscle cells after hypoxia stimulation in the presence or absence of inhibitors. Arrow indicates the mobility of the complex. Similar results were found in another two independent experiments. Cold oligo means unlabeled $NFAT_c$ oligonucleotides. A significant supershifted complex (S) after incubation with $NFAT_c$ antibody was observed. $NFAT_c$, nuclear factor of activating T cells.

hypoxia treatment and remained elevated for 6 h. The mean concentration of resistin rose from 102 ± 10 pg/ml before hypoxia to 540 ± 20 pg/ml after hypoxia for 2 h ($P < 0.01$).

Discussion

In this study, we demonstrated several significant findings. First, hypoxia at 2.5%, but not 5 and 10% oxygen upregulates resistin expression in VSMCs; second, ROS, ERK kinase and NFAT transcription factor are involved in the signaling pathway of resistin induction; third, resistin impairs glucose uptake in cultured VSMCs, and finally, hypoxia-induced resistin secretion from VSMCs. Our data clearly indicate that moderate hypoxia plays a crucial role in the modulation of resistin expression in VSMCs. Our data also demonstrated that functional consequence of resistin upregulation by hypoxia resulted in reduction of glucose uptake. We have demonstrated that secreted resistin is already elevated at 1 h after hypoxia; however, resistin RNA levels are not increased yet. The resistin mRNA increased at 2 h after hypoxia. There are possibly two purely hypothetical explanations. First, the sercretion of stored resistin protein may be a possible explanation for the finding that the secreted resisitn protein level is elevated before the increase in mRNA level. Second, hypoxia may first protect resistin protein degradation and then enhance resistin protein synthesis by increased mRNA. To date, no resistin receptor has been reported yet. The resistin functions as mediator of insulin resistance. In this study, we analyzed the expression of resistin after PDGF and TNF-α and found a remarkable induction of resistin protein level even after stimulation with low level of PDGF and TNF-α, comparable to the level after 2.5% hypoxia. This finding indicates that effect on resistin expression in VSMC by hypoxia at 2.5% oxygen is similar to that by PDGF and TNF-α. Hypoxia at 2.5% has proinflammatory and growth factor effect on VSMCs.

The induction of resistin protein by hypoxia was largely mediated by ROS and ERK kinase pathway because the potent antioxidant, NAC and specific and potent inhibitors of an upstream ERK kinase, PD98059, inhibited the induction of resistin protein. Hypoxia increased ROS formation in VSMCs and NAC reduced the ROS formation induced by hypoxia. A ROS generating agent, Dp44mT, increased resistin protein expression similar to hypoxia. The signaling pathway of ERK was further confirmed by the finding that ERK siRNA inhibited the induction of resistin protein by hypoxia. Hypoxia increased phosphorylated ERK protein and NAC attenuated the induction of phosphorylated ERK protein. Our finding indicates that hypoxia generates ROS first and then ROS activates ERK protein.

Hypoxia is an important stimulus for the neointimal angiogenesis in the vessel wall because neoangiogenesis develops in response to inadequate perfusion through the thickened atherosclerotic plaques [30]. Hypoxia may cause plaque thrombosis during atherosclerosis because of poor perfusion caused by thickened atherosclerotic plaques. Sato *et al.* [20] have demonstrated that hypoxia stimulates the production of ROS in VSMCs. In this study, we clearly demonstrated that hypoxia generated ROS in VSMCs. NFAT can be activated by ROS in mouse embryo fibroblast [21] and human colon cancer cell [22]. NFAT, a Ca^{2+}-dependent transcription factor that regulates the expression of genes in both immune and nonimmune cells [31,32], has been linked to smooth muscle phenotypic maintenance [33,34]. In this study, we demonstrated that hypoxia stimulation of NFAT–DNA binding activity required at least phosphorylation of the ERK as ERK inhibitor abolished the NFAT-binding activity. $NFAT_c$ monoclonal antibody shifted the NFAT–DNA binding complex, indicating the specificity of the NFAT–DNA binding activity induced by hypoxia. We further demonstrated that hypoxia increased resistin promoter activity and the binding site of NFAT in the resistin promoter is essential for the transcriptional regulation. Taken together, our results indicate that hypoxia may increase the NFAT transcriptional activity in VSMCs. Recently, NFAT has been demonstrated to play a key

Fig. 7

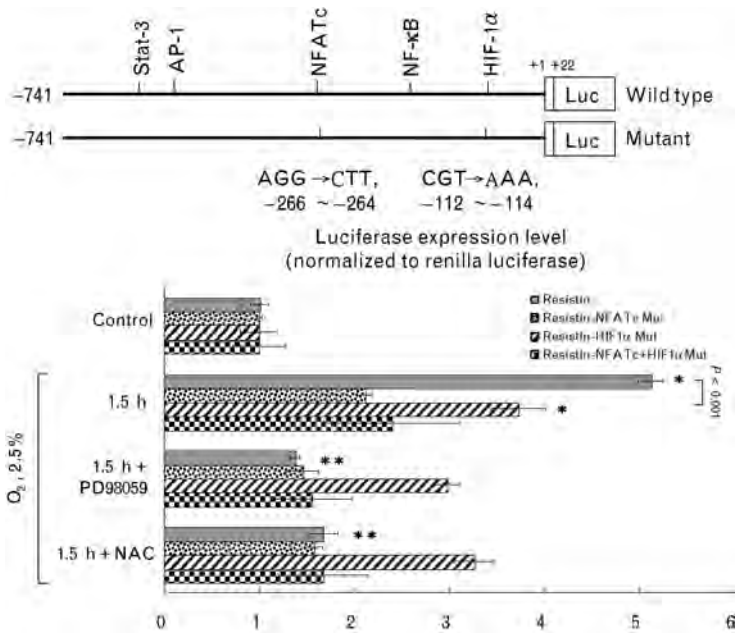

Effect of hypoxia on resistin promoter activity in vascular smooth muscle cells. Upper panel, constructs of resistin promoter gene. Positive +1 demonstrates the initiation site for the resistin transcription. Lower panel, quantitative analysis of resistin promoter activity. VSMCs were transiently transfected with pResistin-Luc by gene gun. The luciferase activity in cell lysates was measured and was normalized with renilla activity ($n = 3$ per group). $*P < 0.001$ vs. control. $**P < 0.001$ vs. 1.5 h. NAC, *N*-acetylcysteine; VSMC, vascular smooth muscle cell.

Fig. 8

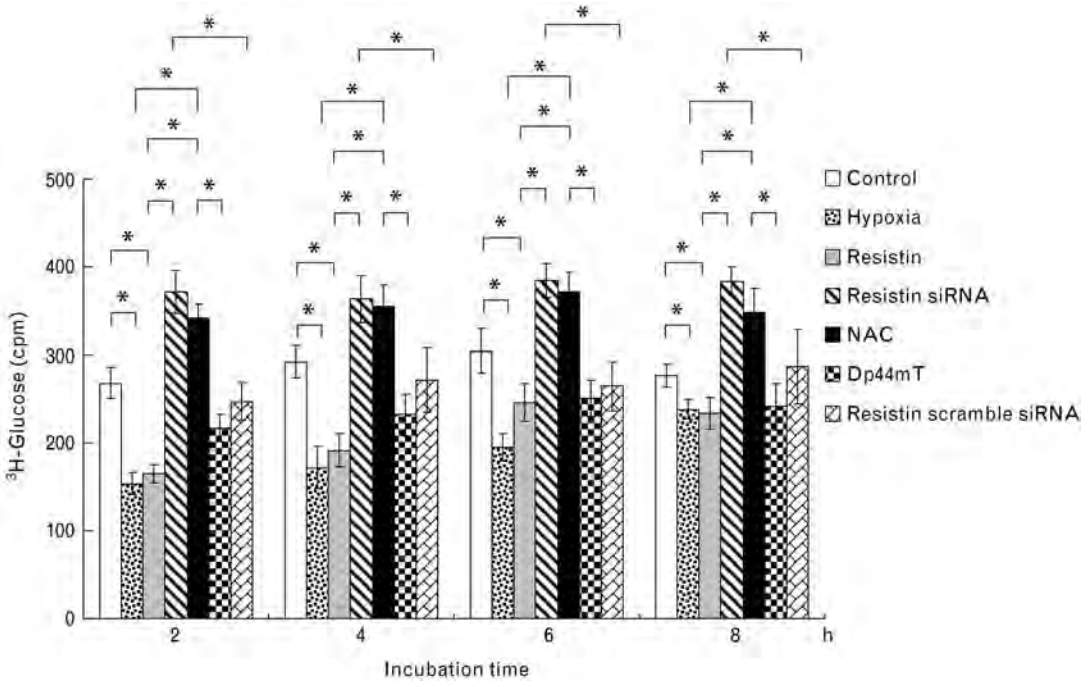

Effect of hypoxia and recombinant resistin on glucose uptake in vascular smooth muscle cells. Glucose uptake was measured in VSMCs treated for 90 min with 20 μg/ml recombinant mouse resistin with or without siRNA or NAC or Dp44mT. $*P < 0.001$. Data are from three independent experiments. NAC, *N*-acetylcysteine; VSMC, vascular smooth muscle cell.

Fig. 9

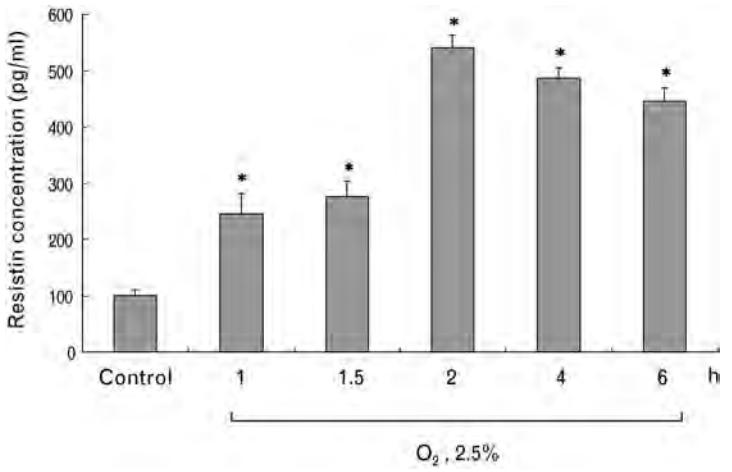

Hypoxia increases release of resistin from vascular smooth muscle cells subjected to 2.5% oxygen for various periods ($n = 3$). $^*P < 0.001$ vs. control.

role in various vasculopathies such as atherosclerosis and restenosis [16–19]. $NFAT_c$ has been demonstrated to mediate hypoxia-induced pulmonary arterial remodeling [19] and blockade of NFAT can reduce SMC proliferation and restenosis [16–18]. The increased NFAT promoter activity by hypoxia may contribute to the vasculopathy induced by hypoxia.

Biomarkers that integrate metabolic and inflammatory signals are powerful candidates for defining risk of atherosclerotic cardiovascular disease [3]. Hyperresistinemia impairs glucose tolerance and induces hepatic insulin resistance in rodents [35], whereas mice deficient in resistin are protected from obesity-associated insulin resistance [36]. Our study using VSMC culture system demonstrated the impaired glucose transport by resistin. The glucose uptake in VSMCs was reduced by resistin upregulation. Impairment of glucose transport may explain the potential mechanism of resistin induction of insulin resistance. Recently, Yang *et al.* [37] have reported that NFAT contributes to glucose and insulin homeostasis and NFAT regulates resistin expression upon insulin stimulation. In the present study, we demonstrated that hypoxia increased resistin secretion from VSMCs, indicating that resistin plays an autocrine or paracrine function in VSMCs. We also demonstrated that the binding site of $NFAT_c$ in the resistin promoter is essential for the transcriptional regulation. We have demonstrated significant reduction in resistin promoter activity after mutation of HIF-1α binding site as compared with the wild-type promoter under hypoxic conditions. This may indicate that HIF-1α binding site in the resistin promoter is also involved in the regulation of resistin expression under hypoxia in VSMCs. However, combing mutation of NFATC and HIF-1α binding sites did not further reduce the promoter activity as compared with mutation of NFATC binding site alone. This finding indicates that the HIF-1α binding site is not the major part for the transcriptional regulation of resistin expression in the hypoxic model of VSMC. The link between resistin and NFAT may contribute to glucose homeostasis in VSMCs. The present study suggests resistin as a metabolic link between hypoxia, inflammation and atherosclerosis.

In summary, our study reports for the first time that hypoxia enhances resistin expression in cultured rat VSMCs. The hypoxia-induced resistin is mediated through ROS, ERK kinase and NFAT pathway. Glucose uptake in VSMCs is reduced by resistin upregulation. The resistin induced by hypoxia may contribute to the pathogenesis of atherosclerosis under hypoxia.

Acknowledgement

This study was sponsored in part by a grant from National Science Council, Taipei, Taiwan.

There are no conflicts of interest.

References

1 Xu H, Barnes GT, Yang Q, Tan G, Yang D, Chou CJ, *et al.* Chronic inflammation in fat plays a crucial role in the development of obesity-related insulin resistance. *J Clin Invest* 2003; **112**:1821–1830.
2 Lusis AJ. Atherosclerosis. *Nature* 2000; **407**:233–241.
3 Rajala MW, Scherer PE. The adipocyte: at the crossroads of energy homeostasis, inflammation, and atherosclerosis. *Endocrinology* 2003; **144**:3765–3773.
4 Kim KH, Lee K, Moon YS, Sul HS. A cysteine-rich adipose tissue-specific secretory factor inhibits adipocyte differentiation. *J Biol Chem* 2001; **276**:11252–11256.
5 Rajala MW, Qi Y, Patel HR, Takahashi N, Banerjee R, Pajvani UB, *et al.* Regulation of resistin expression and circulating levels in obesity, diabetes, and fasting. *Diabetes* 2004; **53**:1671–1679.
6 Rajala MW, Obici S, Scherer PE, Rossetti L. Adipose-derived resistin and gut-derived resistin-like molecule-beta selectively impair insulin action on glucose production. *J Clin Invest* 2003; **111**:225–230.

7 Bokarewa M, Nagaev I, Dahlberg L, Smith U, Tarkowski A. Resistin, an adipokine with potent proinflammatory properties. *J Immunol* 2005; **174**:5789–5795.

8 Kougias P, Chai H, Lin PH, Lumsden AB, Yao Q, Chen C. Adipocyte-derived cytokine resistin causes endothelial dysfunction of porcine coronary arteries. *J Vasc Surg* 2005; **41**:691–698.

9 Burnett MS, Lee CW, Kinnaird TD, Stabile E, Durrani S, Dullum MK, *et al.* The potential role of resistin in atherogenesis. *Atherosclerosis* 2005; **182**:241–248.

10 Calabro P, Samudio I, Willerson JT, Yeh ETH. Resistin promotes smooth muscle cell proliferation through activation of extracellular signal-regulated kinases 1/2 and phosphatidylinositol 3-kinase pathways. *Circulation* 2004; **110**:3335–3340.

11 Cae D, Yuan M, Frantz DF, Melendez PA, Hansen L, Lee J, Shoelson SE. Local and systemic insulin resistance resulting from hepatic activation of IKK-β and NF-κB. *Nat Med* 2005; **11**:183–190.

12 Jung HS, Park KH, Cho YM, Chung SS, Cho JJ, Cho SY, *et al.* Resistin is secreted from macrophages in atheroma and promotes atherosclerosis. *Cardiovasc Res* 2006; **69**:76–85.

13 Reilly MP, Lehrke M, Wolfe ML, Rohatgi A, Lazar MA, Rader DJ. Resistin is an inflammatory marker of atherosclerosis in humans. *Circulation* 2005; **111**:932–939.

14 Tamm M, Bihl M, Eickelberg O, Stulz P, Perruchoud AP, Roth M. Hypoxia-induced interleukin-6 and interlerkin-8 production is mediated by platelet-activating factor and platelet-derived growth factor in primary human lung cells. *Am J Respir Cell Mol Biol* 1998; **19**:653–661.

15 Blaschke F, Stawowy P, Goetze S, Hintz O, Grafe M, Kintscher U, *et al.* Hypoxia activates beta(1)-integrin via ERK 1/2 and p38 MAP kinase in human vascular smooth muscle cells. *Biochem Biophys Res Commun* 2002; **296**:890–896.

16 Liu Z, Zhang C, Dronadula N, Li Q, Rao GN. Blockade of nuclear factor of activated T cells activation signaling suppresses balloon injury-induced neointima formation in a rat carotid artery model. *J Biol Chem* 2005; **280**:14700–14708.

17 Yu H, Sliedregt-Bol K, Overkleeft H, van der Marel GA, van Berkel TJC, Biessen EAL. Therapeutic potential of a synthetic peptide inhibitor of nuclear factor of activated T cells as antirestenotic agent. *Arterioscler Thromb Vasc Biol* 2006; **26**:1531–1537.

18 Nilsson LM, Sun ZW, Nilsson J, Nordstrom I, Chen YW, Molkentin JD, *et al.* Novel blocker of NFAT activation inhibits IL-6 production in human myometrial arteries and reduces vascular smooth muscle cell proliferation. *Am J Physiol Cell Physiol* 2007; **292**:C1167–C1178.

19 De Frutos S, Spangler R, Alo D, Gonzalez Bosc LV. NFATc3 mediates chronic hypoxia-induced pulmonary arterial remodeling with α-actin up-regulation. *J Biol Chem* 2007; **282**:15081–15089.

20 Sato H, Sato M, Kanai H, Uchiyama T, Iso T, Ohyama Y, *et al.* Mitochondrial reactive oxygen species and c-Src play a critical role in hypoxic response in vascular smooth muscle cells. *Cardiovasc Res* 2005; **67**:714–722.

21 Huang C, Li J, Costa M, Zhang Z, Leonard SS, Castranova V, *et al.* Hydrogen peroxide mediates activation of nuclear factor of activated T cells (NFAT) by nickel subsulfide. *Cancer Res* 2001; **61**:8051–8057.

22 Liu Y, Borchert GL, Surazynski A, Hu CA, Phang JM. Proline oxidase activates both intrinsic and extrinsic pathways for apoptosis: the role of ROS/superoxides, NFAT and MEK/ERK signaling. *Oncogene* 2006; **25**:5640–5647.

23 Stavri GT, Zachary IC, Baskerville PA, Martin JF, Erusalimsky JD. Basic fibroblast growth factor upregulates the expression of vascular endothelial growth factor in vascular smooth muscle cells: synergistic interaction with hypoxia. *Circulation* 1995; **92**:1–14.

24 Shyu KG, Chao YM, Wang BW, Kuan P. Regulation of discoidin domain receptor 2 by cyclic mechanical stretch in cultured rat vascular smooth muscle cells. *Hypertension* 2005; **46**:614–621.

25 Shyu KG, Wang BW, Yang YH, Tsai SC, Lin S, Lee CC. Amphetamine activates connexin43 gene expression in cultured neonatal rat cardiomyocytes through JNK and AP-1 pathway. *Cardiovasc Res* 2004; **63**:98–108.

26 Chang H, Shyu KG, Wang BW, Kuan P. Regulation of hypoxia-inducible factor 1-α by cyclical mechanical stretch in rat vascular smooth muscle cells. *Clin Sci* 2003; **105**:447–456.

27 McLennan HR, Degli Esposti M. The contribution of mitochondrial respiratory complexes to the production of reactive oxygen species. *J Bioenegr Biomembr* 2000; **32**:153–162.

28 Shyu KG, Wang BW, Kuan P, Chang H. RNA interference for discoidin domain receptor 2 attenuates neointimal formation in balloon injured rat carotid artery. *Arterioscler Thromb Vasc Biol* 2008; **28**:1447–1453.

29 Graveleau C, Zaha VG, Mohajer A, Banerjee RR, Duedley-Rucker N, Steppan CM, *et al.* Mouse and human resistins impair glucose transport in primary mouse cardiomyocytes, and oligomerization is required for this biological action. *J Biol Chem* 2005; **280**:31679–31685.

30 Crawford DW, Blankebhorm DH. Arterial wall oxygenation, oxyradicals, and atherosclerosis. *Atherosclerosis* 1991; **89**:97–108.

31 Larrieu D, Thiebaud P, Duplaa C, Sibon I, Theze N, Lamaziere JMD. Activation of Ca^{2+}/calcineurin/NFAT2 pathway controls smooth muscle cell differentiation. *Exp Cell Res* 2005; **310**:166–175.

32 Rao A, Luo C, Hogan PG. Transcription factors of the NFAT family: regulation and function. *Annu Rev Immunol* 1997; **15**:707–747.

33 Wada H, Hasegawa K, Morimoto T, Kakita T, Yanazume T, Abe M, *et al.* Calcineurin-GATA-6 pathway is involved in smooth muscle-specific transcription. *J Cell Biol* 2002; **156**:983–991.

34 Gonzalez Bosc LV, Layne J, Nelson MT, Hill-Eubanks DC. Intraluminal pressure is a stimulus for NFATc3 nuclear accumulation: role of calcium, endothelium-derived nitric oxide, and cGMP-dependent protein kinase. *J Biol Chem* 2004; **280**:26113–26120.

35 Banerjee RR, Rangwala SM, Shapiro JS, Rich AS, Rhoades B, Qi Y, *et al.* Regulation of fasted blood glucose by resistin. *Science* 2004; **303**:1195–1198.

36 Rothwell SE, Richards AM, Pemberton CJ. Resistin worsens cardiac ischemia-reperfusion injury. *Biochem Biophys Res Commun* 2006; **349**:4000–4007.

37 Yang TTC, Suk HY, Yang XY, Olabis O, Yu RYL, Durand J, *et al.* Role of transcription factor NFAT in glucose and insulin homeostasis. *Mol Cell Biol* 2006; **26**:7372–7387.

Cancer Gene Therapy (2009), 1–9
 0929-1903/09 $32.00
www.nature.com/cgt

An HDAC inhibitor enhances the antitumor activity of a CMV promoter-driven DNA vaccine

M-D Lai[1,2,3], C-S Chen[4], C-R Yang[5], S-Y Yuan[5], J-J Tsai,[6,7], C-F Tu[1], C-C Wang[8], M-C Yen[2] and C-C Lin[7,8]

[1]Department of Biochemistry and Molecular Biology, College of Medicine, National Cheng Kung University, Tainan, Taiwan, ROC; [2]Institute of Basic Medicine, College of Medicine, National Cheng Kung University, Tainan, Taiwan, ROC; [3]Center for Gene Regulation and Signal Transduction Research, National Cheng Kung University, Tainan, Taiwan, ROC; [4]Division of Medicinal Chemistry and Pharmacognosy, College of Pharmacy, The Ohio State University, Columbus, OH, USA; [5]Division of Urology, Department of Surgery, Taichung Veterans General Hospital, Taichung, Taiwan, ROC; [6]Division of Allergy, Immunology and Rheumatology, Taichung Veterans General Hospital, Taichung, Taiwan, ROC; [7]Department of Medical Education and Research, Taichung Veterans General Hospital, Taichung, Taiwan, ROC and [8]Institute of Medical Technology, College of Life Science, National Chung Hsing University, Taichung, Taiwan, ROC

The cytomegalovirus (CMV) promoter is considered to be one of the strongest promoters for driving the *in vivo* expression of genes encoded by DNA vaccines. However, the efficacy of DNA vaccines has so far been disappointing (particularly in humans), and this might be explained in part by histone deacetylase (HDAC)-mediated chromatin condensation. Hence, we sought to investigate whether increasing the expression of DNA vaccine antigens with the HDAC inhibitor OSU-HDAC42 would enhance the efficacy of DNA vaccines *in vivo*. A luciferase assay was used to determine the effects of OSU-HDAC42 on CMV promoter-driven DNA plasmids *in vitro* and *in vivo*. Three HDAC inhibitors were able to activate expression from the CMV promoter in NIH3T3 cells and MBT-2 bladder cancer cells. The expression of luciferase was significantly enhanced by co-administration of pCMV-luciferase and OSU-HDAC42 in mice. To explore whether OSU-HDAC42 could enhance the specific antitumor activity of a neu DNA vaccine driven by the CMV promoter, we evaluated therapeutic effects and immune responses in a mouse tumor natively overexpressing HER2/neu. Mice receiving OSU-HDAC42 in combination with the CMV-promoter neu DNA vaccine exhibited stronger antitumor effects than mice given the DNA vaccine only. In addition, a correlation between the antitumor effects and the specific cellular immune responses was observed in the mice receiving the DNA vaccine and OSU-HDAC42.
Cancer Gene Therapy advance online publication, 23 October 2009; doi:10.1038/cgt.2009.65

Keywords: histone deacetylase inhibitor; cytomegalovirus promoter; DNA vaccine; tumor

Introduction

DNA vaccines offer a new and powerful approach for generating antigen-specific cancer vaccines and immunotherapies. Naked plasmid DNA is cost-effective, thermostable, easy to construct, and can be easily prepared on a large scale with high purity.[1,2] Two common routes of immunization have been developed for delivering DNA vaccines for genetic immunization: intramuscular needle injection of DNA[3] and epidermal gene gun bombardment with DNA-coated gold particles.[4] Many studies have shown that gene gun-mediated immunization is far more efficient than intramuscular injection, as it elicits similar levels of antibody and cellular responses with less DNA.[5]

The cytomegalovirus (CMV) promoter is considered to be one of the strongest promoters for driving the expression of genes encoded by DNA vaccines *in vivo*.[6] Many studies have showed the therapeutic efficacy of virus promoter-driven DNA vaccines in preclinical animal models. For example, our previous study showed that CMV promoter-driven cDNA encoding the extracellular domain of the human HER-2/neu gene had a therapeutic effect on established HER-2/neu-expressing tumors.[7] However, the therapeutic efficacy of virus promoter-driven DNA vaccines to date has mostly been disappointing in large animal models and in human

Correspondence: Dr C-C Lin, Institute of Medical Technology, College of Life Science, National Chung Hsing University, Taichung 402, Taiwan, ROC.
E-mail: lincc@dragon.nchu.edu.tw
Received 12 April 2009; revised 16 June 2009; accepted 1 August 2009

clinical trials.[8–10] One possible cause for these disappointing results may be the inactivation of the virus promoter by histone deacetylase (HDAC)-mediated chromatinization of the process of transcription.[11] HDACs are enzymes that catalyze removal of acetyl groups from the ε-amino group of specific lysine residues present within the histone tails. On histone deacetylation, tight packaging of the DNA because of chromatin condensation takes place,[12] which decreases the binding of transcription factors to promoters and ultimately causes gene silencing.

Many compounds that inhibit HDAC activity have been developed and characterized. On the basis of their chemical structures, major HDAC inhibitors can be classified into four categories: short-chain fatty acids, cyclic peptides, benzamide derivatives, and hydroxamic acids.[13] The availability of HDAC inhibitors accounts in large part for the identification and characterization of HDACs and the rapid advances in our understanding how HDACs repress gene transcription.[14] Recently, several studies have also showed that HDAC inhibitors can influence virus promoter-driven DNA transcription units introduced into mammalian cells or mice. For example, the HDAC inhibitors butyrate and tricostatin A both activated CMV promoter-controlled glycosyltransferase and β-galactosidase glycogenes.[15] In addition, the HDAC inhibitor trichostatin A (TSA) upregulated SV40 and CMV promoter activity in mice.[16] The HDAC inhibitor FR901228 and TSA greatly enhanced the transcriptional activity of the SV40 promoter in an enhancer-dependent manner.[17] Hence, the HDAC inhibitor-mediated upregulation of virus promoter-driven gene expression may be applicable in many research fields.

In this study, we hypothesized that addition of an HDAC inhibitor could enhance expression of the CMV promoter-driven neu DNA vaccine and thereby improve its therapeutic effects in an animal tumor model. To evaluate the effects of an HDAC inhibitor on the induction of antitumor immune responses by DNA vaccination, local subcutaneous injection of the HDAC inhibitor OSU-HDAC42 was evaluated in conjunction with neu DNA vaccination against a mouse tumor naturally overexpressing HER-2/neu. OSU-HDAC42 is a novel hydroxamate-tethered phenylbutyrate derivative HDAC inhibitor, and it possesses potent cytotoxicity toward prostate cancer cells and hepatocarcinoma.[18,19] The results indicate that OSU-HDAC42 increased the expression of the neu DNA vaccine and enhanced its antitumor effects, which were associated with increases in lymphocyte infiltration and specific cytotoxic T cells.

Materials and methods

Tissue culture and chemical compounds

NIH 3T3 fibroblasts (American Type Culture Collection, Manassas, VA) and MBT-2 cells (a mouse transitional cell carcinoma cell line) were grown in Dulbecco's modified Eagle's medium supplemented with 10% fetal calf serum and 1% penicillin–streptomycin. Sodium butyrate and TSA were purchased from the Sigma Chemical Company (St Louis, MO). OSU-HDAC42 (NSC 736012) is a gift from Dr Ching-Shih Chen, and it is a novel hydroxamate-tethered phenylbutyrate derivative that has received IND approval from the FDA, and it is scheduled to enter clinical trials later this year.[18,19]

NIH3T3 and MBT-2 cell transfection

NIH3T3 and MBT-2 cells were transfected with 0.5 μg of pCMV-luciferase in the presence of Lipofectamine 2000 (Invitrogen, Carlsbad, CA). Forty-eight hours after transfection (24 h after HDAC inhibitor treatment), the cells were collected for luciferase assays.

Luciferase assay

Cells were collected 24 h after HDAC inhibitor treatment and the luciferase activity of the cell lysate was determined using a Promega luciferase assay kit (Promega, Madison, WI). The samples were counted for 10 s and the luciferase activity values were normalized per unit (relative light unit per second) of total protein

Mice

BALB/c and C3H/He mice (6–8 weeks of age) were obtained from National Cheng Kung University and approved by the National Cheng Kung University animal welfare committee.

DNA administration by gene gun with non-coated DNA

The protocol and delivery device for DNA plasmid administrations by gene gun have been described earlier.[20] Briefly, for naked DNA vaccination, 1 μg of DNA plasmid dissolved in 20 μl of autoclaved double-distilled water was directly added to the loading hole near the nozzle and then delivered to the shaved abdominal region of mice at a discharge pressure of 60 psi using a low-pressure-accelerated gene gun (GDS-80) (Wealtec Technologies Co. Ltd, Taipei, Taiwan).

Bioluminescence reporter imaging

BALB/c mice were administered pCMV-luciferase and received the HDAC inhibitor OSU-HDAC42 by local intraperitoneal subcutaneous injection 1 day after DNA plasmid administration. The luciferase activity on the skin of the mice was measured at 48 and 72 h after bombardment with pCMV-luciferase. The distribution of luciferase activity in treated mice was visualized using a night owl imaging unit (Berthold Technologies, Bad Wildbad, Germany) consisting of a peltier-cooled CCD slow-scan camera mounted on a light-tight specimen chamber. Images were generated by WinLight software (Berthold Technologies). For the detection of bioluminescence, mice received 100 μl D-luciferin in saline at a dose of 100 mg kg^{-1} (Synchem OHG, Altenburg, Germany). Mice were placed in the light-tight chamber and a grayscale photo was first taken with dimmed light. Photon emission was then integrated over a period of 5 min. Luminescence measurements are expressed as the integration of the average brightness/pixel unit expressed as photon counts emitted per second.

Detection of green fluorescent protein (GFP)-positive dendritic cells in inguinal lymph nodes from mice

This protocol was modified from one reported earlier.[20] In brief, C3H/He mice were inoculated with 1 μg pCMV-EGFP

DNA plasmid (pEGFR-N1; Clontech Laboratories, Inc., Palo Alto, CA) with the HDAC inhibitor OSU-HDAC42. Inguinal lymph nodes were collected 48 h after DNA plasmid administration. The dendritic cell (DC) population was determined by staining with monoclonal anti-DC-PE antibody (eBioscience). FACSCalibur flow cytometry (BD Bioscience, Mountain View, CA) was used to determine the percentage of GFP-positive DCs in a DC-gated population.

Therapeutic efficacy of the DNA vaccine

C3/HeN mice were injected subcutaneously in the flank with 1×10^6 MBT-2 cells in 0.5 ml PBS. At day 10, 1 μg of naked DNA vaccine in 20 μl of autoclaved double-distilled water was gene gun administered into the skin three times at weekly intervals. Control mice were injected with 1 μg pRc/CMV in 20 μl of autoclaved double-distilled water. The mice were treated with OSU-HDAC42 1 day after DNA vaccination. Tumor size was determine using a caliper at 3 day intervals and calculated using the formula for a rational ellipse: $(m_1^2 \times m_2 \times 0.5236)$, where m_1 represents the short axis and m_2 the longer axis. Mice were killed when the mean diameter of the tumor exceeded 2000 mm^3 or the mouse was in poor condition and expected shortly to become moribund. Statistically significant differences were revealed by Kaplan–Meier analysis of survival.

Measurement of antineu antibody titers

The level of neu cross-reactive antibodies was determined by testing sera from the immunized mice by ELISA with human recombinant erbB2 (R&D, Minneapolis, MN)-coated wells as described elsewhere.[20] Serum immunoglobulin (Ig) G antibody response was carried out with alkaline phosphatase-conjugated rat antimouse IgG secondary antibodies (Calbiochem, Darmstadt, Germany). Color development was facilitated using 3,3′,5,5′-tetramethylbenzidine (Sigma). After a 15-min incubation, the reaction was stopped by the addition of 100 μl of 2 N H_2SO_4, and the OD_{450} nm was determined in an ELISA micro plate reader (Dynatech MR5000 plate reader, Dynatech Lab Inc., Chantilly, VA).

In vitro *cytotoxic T lymphocytes induction and activity*

This protocol was modified from one reported earlier.[20] DNA-vaccinated mice were killed 1 week after the last DNA vaccination, and spleens were isolated and RBCs were removed from single-cell splenocyte suspensions using a NH_4Cl–KCl lysis buffer. A total of 7×10^6 washed splenocytes was then stimulated with 20 μg ml^{-1} human recombinant ErbB2 protein in RPMI 1640 medium containing 10% FBS, 20 μg ml^{-1} streptomycin, 20 U ml^{-1} penicillin, and 50 μM 2-ME (Life Technologies, Rockville, MD). On day 5, the splenocytes (effector cells) were collected and co-incubated with MBT-2-luciferase cells (target cells) at various effector: target ratios in a 96-well U-bottomed plate. After a 12-h incubation, 100 μl of supernatant was collected from each well, and released luciferase activity was assayed with luciferin using a luminometer (EG&G, Berthold, MiniLumat LB9506 luminometer, Bad Wildbad, Germany).

Immunohistochemistry

The infiltration of tumors by T cells in vaccinated mice was analyzed by immunohistochemistry using anti-CD8 antibody (53-6.7, Pharmingen, San Diego, CA) or anti-CD4 antibody (GK1.5; BD PharMingen, San Diego, CA) as described earlier.[21] The average number of infiltrating T cells was quantified by light microscopy with a $\times 10$ eyepiece and a $\times 40$ objective lens. The total number of cells in five high-power fields was counted. Three samples from three mice were analyzed.

Results

An HDAC inhibitor enhances the transcriptional activity of the CMV promoter in vitro *and* in vivo

As the human CMV immediate-early promoter/enhancer is one of the strongest mammalian promoters,[7] we first determined whether HDAC inhibitors would enhance CMV promoter activity *in vitro*. MBT-2 cells and NIH3T3 cells were co-transfected with a CMV promoter-driven luciferase plasmid and three different HDAC inhibitors, TSA, OSU-HDAC42, and sodium butyrate, and luciferase activity was assessed. CMV promoter activity was strongly enhanced in MBT-2 (Figure 1a) and NIH3T3 cells (Figure 1b) by each of these three different HDAC inhibitors in a dose-dependent manner. Therefore, we further investigated whether an HDAC inhibitor would increase the protein expression of a DNA plasmid under control of the CMV promoter *in vivo*. Luciferase was used as a reporter gene to monitor the expression of the DNA vaccine plasmid. The HDAC inhibitor OSU-HDAC42 was injected subcutaneously at the site of DNA vaccination 1 day after administration of CMV-luciferase DNA, and the luciferase activity was recorded with *in vivo* imaging at 48 and 72 h after DNA administration. Mice that received both OSU-HDAC42 and CMV-luciferase plasmid DNA exhibited stronger luciferase activity than mice that received plasmid DNA only (Figure 2a). Quantitation of the luciferase expression is shown in Figure 2b. The strength of the immune response induced by a DNA vaccine usually correlates with the number of migrated DC in the inguinal lymph nodes. A greater percentage of GFP-positive DC cells were present in lymph nodes from mice injected with both pCMV-EGFP and OSU-HDAC42 (Figure 3a). A graphic representation of the number of GFP-positive DC cells is depicted in Figure 3b. In addition, the difference between mice given 10 μg versus 100 μg OSU-HDAC42 in combination with CMV-EGFP DNA plasmid was also statistically significant ($P < 0.05$).

Therapeutic efficacy of naked HER-2/neu DNA vaccine with or without an HDAC inhibitor on established tumors in syngeneic mice

OSU-HDAC42 is a novel hydroxamate-tethered phenylbutyrate with a low nanomolar IC_{50} for HDAC inhibition. In addition, it has been tested in a prostate cancer animal model and showed promising antitumor activity.[18] Therefore, we further tested the effects of OSU-HDAC42 on the therapeutic effect of HER-2/neu DNA vaccination

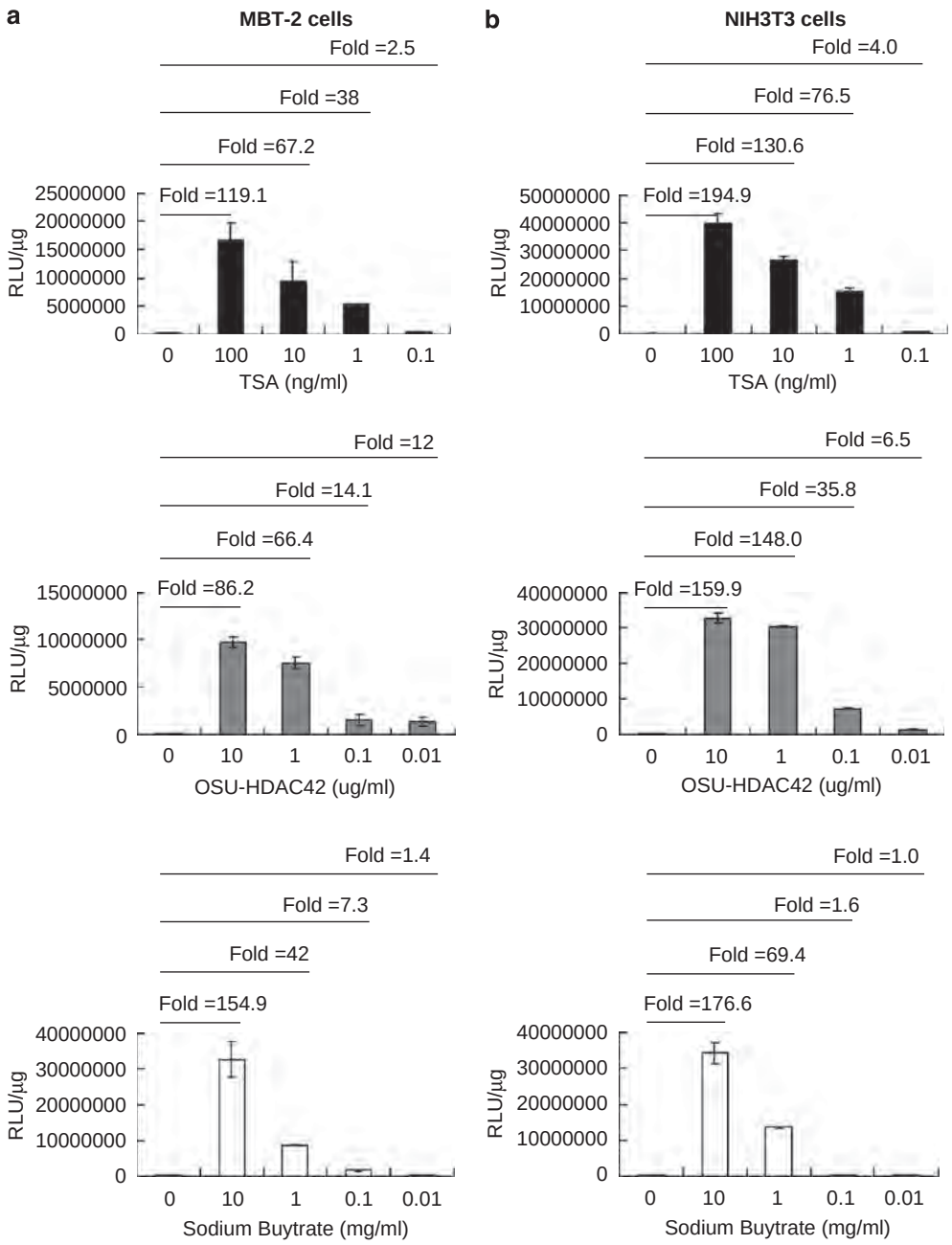

Figure 1 Activation of the CMV promoter by three different HDAC inhibitors *in vitro*. (**a**) MBT-2 cells or (**b**) NIH3T3 cells were transfected with plasmid DNA containing a CMV promoter-driven luciferase reporter plasmid and supplemented with increasing doses of three different HDAC inhibitors: TSA, OSU-HDAC42, or sodium butyrate. The luciferase activity was determined. Lane 1 shows pGL3-basic DNA plasmid transfection (control). Experiments were carried out in triplicate and repeated two times with similar results.

against MBT-2 bladder tumor cells in C3H/HeN mice. The mice that received 100 µg OSU-HDAC42 in combination with a human HER-2/neu naked DNA vaccine exhibited growth delay of MBT-2 tumors (Figure 4a) and had extended survival times relative to mice given the DNA vaccine alone (Figure 4b). In addition, mice receiving 100 µg OSU-HDAC42 and the DNA vaccine had significantly longer lifespans than the mice receiving 10 µg OSU-HDAC42 and DNA vaccine ($P<0.05$).

HDAC inhibition enhanced the HER2-specific cellular immune response induced by neu DNA vaccine

To examine the immunological responses induced by the combination of OSU-HDAC42 and HER-2/neu DNA vaccine, we measured total anti-p185^{neu} IgG in mouse serum. Anti-p185^{neu} IgG was detected in all mice receiving human HER-2/neu DNA vaccine with or without OSU-HDAC42. A minor increase in p185^{neu} antibody was observed when mice were treated with the

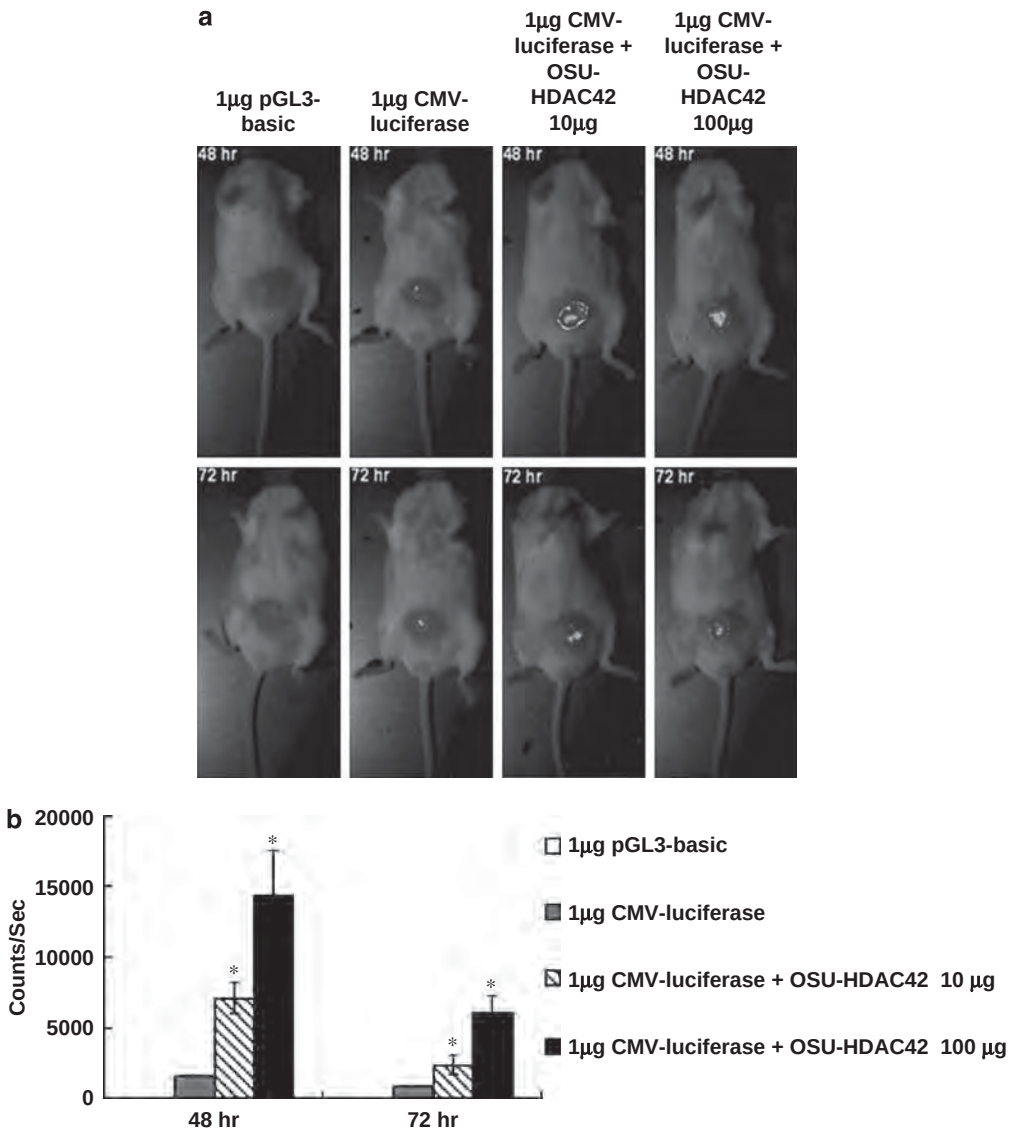

Figure 2 The HDAC inhibitor OSU-HDAC42 enhanced the expression of genes controlled by the CMV promoter in mice. (**a**) Expression of luciferase in skin. Mice were inoculated with 1 μg of pCMV-luciferase DNA alone or with different doses of OSU-HDAC42. *In vivo* images showing luciferase activity at 48 and 72 h after inoculation (taken with a Night Owl imaging unit). (**b**) Histogram showing the quantification of luciferase activity. The symbol * indicates a statistically significant difference when compared with the 1 μg naked CMV-luciferase DNA group ($P<0.05$). The data are from one representative experiment of two independent experiments.

HER-2/neu DNA vaccine and OSU-HDAC42 (10 or 100 μg), but the difference was not statistically significant in comparison with the HER-2/neu DNA vaccine treatment alone (Figure 5). As our previous study indicated that cell-mediated cytotoxic immune responses had a major role in combating MBT-2 cells in the C3H animal model,[21] we further examined whether OSU-HDAC42 enhanced HER2-specific cellular immunity. Tumors form the group of mice receiving neu DNA vaccine plus 100 μg OSU-HDAC42 showed a greater infiltration of $CD4^+$ and $CD8^+$ lymphocytes when compared with tumors from the other treatment groups or the control group (Table 1). Therefore, a correlation between the antitumor effect of HER-2/neu DNA vaccine exposed to OSU-HDAC42 and the ErbB2-specific cellular immune responses was suggested. We then examined whether the HDAC inhibitor would enhance cytotoxic immune responses. At 1 week after the last vaccination, higher cell-mediated cytotoxic immune responses to MBT-2 were observed in mice given 100 μg OSU-HDAC42 and HER-2/neu DNA vaccine when compared with mice given HER-2/neu DNA vaccine only (Figure 6). Therefore, HDAC inhibition may increase the therapeutic effect of neu DNA vaccine by enhancing the expression of the encoded gene product and inducing stronger cellular immunity.

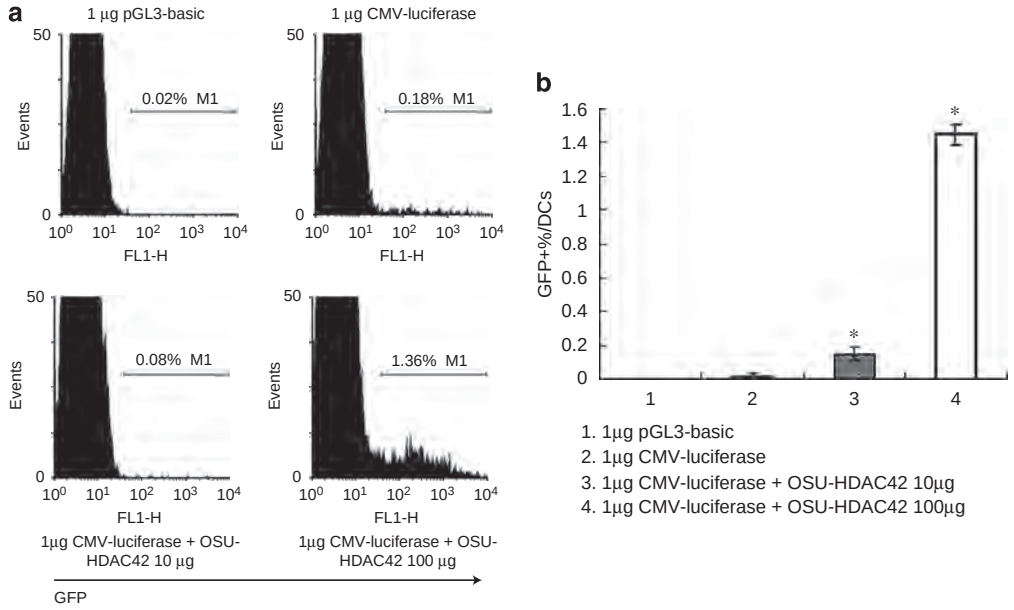

Figure 3 The HDAC inhibitor OSU-HDAC42 enhanced the homing of dendritic cells (DC) to lymph nodes by DNA vaccination. (**a**) Mice were given either 1 μg pCMV-EGFP DNA and OSU-HDAC42, 1 μg pCMV-EGFP alone, or 1 μg pRc/CMV DNA plasmid. The inguinal lymph nodes were removed 48 h later, and the ratio of GFP positive to total DCs was measured using flow cytometry. (**b**) Histogram showing the quantification of the ratio of GFP positive to total DCs. The symbol * indicates a statistically significant difference when compared with the mice that were given 1 μg pCMV-EGFP DNA plasmid only ($P<0.05$). The data presented in this figure are from one representative experiment of two that were performed.

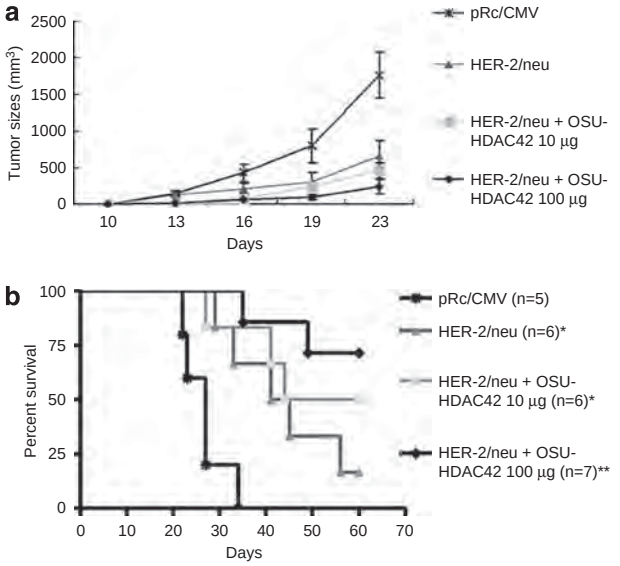

Figure 4 The HDAC inhibitor OSU-HDAC42 enhanced the antitumor efficacy of an HER-2/neu DNA vaccine driven by the CMV promoter. (**a**) Tumor volume was measured at the indicated times. The average tumor volume represents the mean of the tumors from each group until the animals were killed because of excess tumor burden. (**b**) Lifespan of C3H/HeN mice after subcutaneous challenge with MBT-2 cells. The survival data were subjected to Kaplan–Meier analysis. The number of mice in each experiment is in parenthesis. The symbol (*) indicates a statistically significant difference when compared with the control group ($P<0.01$). The symbol (**) indicates a statistically significant difference when compared with the mice that were given HER-2/neu DNA vaccine only ($P<0.05$). Experiments were repeated two times with similar results.

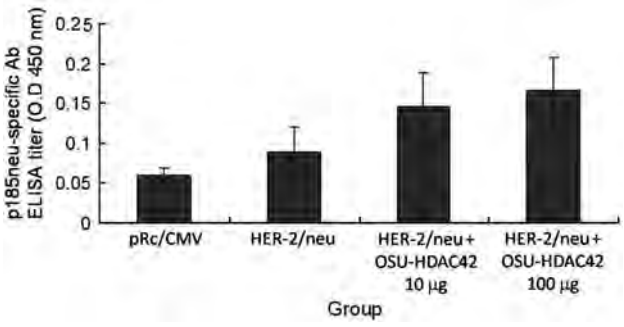

Figure 5 Serum antibody against human recombinant Her2/neu antigen in mice. One week after the last DNA vaccination, $p185^{neu}$-specific IgG antibody titers (± s.e.) were determined by ELISA**.** The data represent the average titer of three mice.

Discussion

To improve the expression of DNA vaccine-encoded antigens such as neu, usually transcription is enhanced with the CMV promoter or translation is made more efficient by improving amino acid codon preference.[8] CMV promoter-driven HER-2/neu DNA vaccine in combination with OSU-HDAC42 caused significant delays in tumor progression and extended lifespan in our mouse model. Immune infiltration analysis revealed that the HDAC inhibitor enhanced the antitumor effects of HER-2/neu DNA vaccine at least in part by increasing antitumor cellular immune responses. Our results show a novel method of enhancing the therapeutic efficacy of

Table 1 Infiltrated lymphocytes at tumor sites within cryosectioned samples

Vaccine group	*$CD4^+$ T cells*	*$CD8^+$ T cells*
Control	3 ± 1	2 ± 1
HER-2/neu DNA vaccine	13 ± 5*	14 ± 5*
HER-2/neu DNA vaccine+ OSU-HDAC42 10 μg	23 ± 4*	16 ± 3*
HER-2/neu DNA vaccine+ OSU-HDAC42 100 μg	33 ± 11**	29 ± 7**

Cell counting was performed at × 400 magnification. Three samples and five randomly chosen fields per sample were evaluated. Results are expressed as the mean ± s.d. of immunohistochemically positive cells in the cryosection. GG, gene gun. The symbol (*) indicates a statistically significant difference when compared with the control group ($P<0.01$). The symbol (**) indicates a statistically significant difference when compared with the HER-2/neu DNA vaccine group ($P<0.05$). Similar results were obtained in two more repeated experiments ($n=3$ per group).

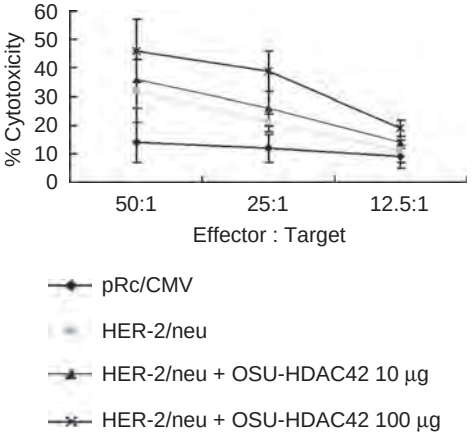

Figure 6 The HDAC inhibitor enhanced DNA vaccine-induced cellular immune responses. Spleen cell-mediated cytotoxicity was determined in mice 1 week after their last DNA vaccination. The target cells were MBT-2-luciferase cells cultured *in vitro*. The effector cells were lymphocytes from mice vaccinated with HER-2/neu DNA vaccine with or without OSU-HDAC42. Effector cells were incubated with serial dilutions of target cells, and cytotoxicity was determined by the release of luciferase. Each point represents the average of triplicate wells.

DNA vaccines expressed by the CMV-promoter. Combining the HDAC inhibitor and the DNA vaccine significantly improved therapeutic efficacy. As HDAC inhibitors are clinically new anticancer target therapy drugs, DNA vaccines will certainly be a promising adjuvant cancer therapy.

Several studies have showed that one type of DC in skin, Langerhans cells, migrate rapidly to draining lymph nodes after skin irritation,[22] infection[23] or painting with antigen.[24–26] In addition, DNA plasmid containing CpG motifs induced Langerhans cell migration in skin sheets, with 50% depletion occurring within 2 h.[27] It was surprising to observe that administration of OSU-HDAC42 1 day after that of CMV-enhanced green fluorescent protein (EGFP) plasmid significantly increased the number of GFP^+ DCs in distal lymph nodes 48 h after plasmid administration. The elevated number of GFP^+ DCs may be because of enhancement of GFP cross-presentation in keratinocytes. As OSU-HDAC42 increased antigen protein expression in transfected keratinocytes, the antigenic proteins were secreted into the surrounding environment of antigen-presenting cells and cross-presented by professional antigen-presenting cells, which in turn migrated to draining lymph nodes and induced T cells.

Administration of OSU-HDAC42 enhanced the luciferase activity because of CMV promoter-driven luciferase for only a short interval (Figure 4), as the fold enhancement significantly decreased 48 h after OSU-HDAC42 injection. One of possible reasons for such a short-term effect is that OSU-HDAC42 exhibited apoptogenic potency and caused greater reductions in phosphor-AKT, Bcl-xl, and survivin.[19] The death of cells expressing plasmid DNA would decrease the observed luciferase activity. Co-administration of DNA encoding anti-apoptotic proteins[28–30] may avoid this cell death and further enhance the effect of OSU-HDAC42 on the induction of CMV promoter-controlled gene expression.

Our previous results indicated that combination of an HSP90 inhibitor and a DNA vaccine had additive cancer-therapeutic effects.[31] However, the enhancing effect was only observed at low doses of the HSP90 inhibitor geldanamycin, as high doses inhibited the immune response. It was interesting to note that the HDAC inhibitor enhance the therapeutic effect of the DNA vaccine in a dose-dependent manner. The effects of HDAC inhibition on immune responses have been investigated before. Histone acetylation was shown to enhance memory CD8 T cells.[32,33] Therefore, HDAC inhibition may enhance CD8 immune responses through direct immune regulation in addition to increasing antigen expression.

Although we have shown that the combination of an HDAC inhibitor and neu DNA vaccine is an effective cancer therapy, the effects of HDAC inhibition on the tumor itself and immune cells warrant detailed further study. The HDAC inhibitor TSA can downregulate MHC class I presentation of self-antigens.[34] Furthermore, HDAC11 regulates the expression of interleukin 10, which is important in immune tolerance. Inactivation of HDAC 11 in antigen-presenting cells led to impairment of T-cell responses.[35] Therefore, the selection of appropriate HDAC inhibitors specific for certain HDACs will be important for the successful development of effective DNA vaccine combination therapies.

In summary, application of the HDAC inhibitor OSU-HDAC42 during immunization significantly enhanced the vaccine's antitumor efficacy by increasing antigen expression and the antigen-specific cellular immune response to MBT-2 tumor cells. The combination of locally applied HDAC inhibitors and skin-administered naked DNA

vaccines is feasible and will be of both research and clinical interest.

Conflict of interest

Dr Chen conducts a clinical trial on OSU-HDAC42 currently.

Acknowledgements

This study was supported by Grants from the Taichung Veterans General Hospital and National Chung Hsing University (TCVGH-NCHU-987614) Taichung, Taiwan, and in part by the Ministry of Education, Taiwan, ROC under the ATU plan.

References

1 Lowe DB, Shearer MH, Kennedy RC. DNA vaccines: successes and limitations in cancer and infectious disease. *J Cell Biochem* 2006; **98**: 235–242.
2 Cui Z. DNA vaccine. *Adv Genet* 2005; **54**: 257–289. Review.
3 Wolff JA, Malone RW, Williams P, Chong W, Acsadi G, Jani A *et al*. Direct gene transfer into mouse muscle *in vivo*. *Science* 1990; **247**: 1465–1468.
4 Tang DC, Devit M, Johnston SA. Genetic immunization is a simple method for eliciting an immune response. *Nature* 1992; **356**: 152–154.
5 Pertmer TM, Eisenbraun MD, McCabe D, Prayaga SK, Fuller DF, Haynes JR. Gene gun-based nucleic acid immunization: elicitation of humoral and cytotoxic T lymphocyte responses following epidermal delivery of nanogram quantities of DNA. *Vaccine* 1995; **13**: 1427–1430.
6 Feltquate DM. DNA vaccines: vector design, delivery, and antigen presentation. *J Cell Biochem Suppl* 1998; **30–31**: 304–311.
7 Tu CF, Lin CC, Chen MC, Ko TM, Lin CM, Wang YC *et al*. Autologous neu DNA vaccine can be as effective as xenogenic neu DNA vaccine by altering administration route. *Vaccine* 2007; **25**: 719–728.
8 Wang RJ, Epstein FM, Baraceros EJ, Gorak Y, Charoenvit DJ, Carucci RC *et al*. Induction of $CD4^+$ T cell-dependent $CD8^+$ type 1 responses in humans by a malaria DNAvaccine. *Proc Natl Acad Sci USA* 2001; **98**: 10817–10822.
9 MacGregor RR, Boyer JD, Ugen KE, Lacy KE, Gluckman SJ, Bagarazzi ML *et al*. First human trial of a DNA-based vaccine for treatment of human immunodeficiency virus type 1 infection: safety and host response. *J Infect Dis* 1998; **178**: 92–100.
10 Wang R, Doolan DL, Le TP, Hedstrom RC, Coonan KM, Charoenvit Y *et al*. Induction of antigen-specific cytotoxic T lymphocytes in humans by a malaria DNAvaccine. *Science* 1998; **282**: 476–480.
11 Murphy JC, Fischle W, Verdin E, Sinclair JH. Control of cytomegalovirus lytic gene expression by histone acetylation. *EMBO J* 2002; **21**: 1112–1120.
12 Chen WY, Townes TM. Molecular mechanism for silencing virally transduced genes involves histone deacetylation and chromatin condensation. *Proc Natl Acad Sci USA* 2000; **97**: 377–382.
13 Lin HY, Chen CS, Lin SP, Weng JR, Chen CS. Targeting histone deacetylase in cancer therapy. *Med Res Rev* 2006; **26**: 397–413.
14 Taunton J, Hassig CA, Schreiber SL. A mammalian histone deacetylase related to the yeast transcriptional regulator Rpd3p. *Science* 1996; **272**: 408–411.
15 Choi KH, Basma H, Singh J, Cheng PW. Activation of CMV promoter-controlled glycosyltransferase and beta -galactosidase glycogenes by butyrate, tricostatin A, and 5-aza-2′-deoxycytidine. *Glycoconj J* 2005; **22**: 63–69.
16 Vanniasinkam T, Ertl H, Tang Q. Trichostatin-A enhances adaptive immune responses to DNA vaccination. *J Clin Virol* 2006; **36**: 292–297.
17 Nakajima H, Kim YB, Terano H, Yoshida M, Horinouchi S. FR901228, a potent antitumor antibiotic, is a novel histone deacetylase inhibitor. *Exp Cell Res* 1998; **241**: 126–133.
18 Kulp SK, Chen CS, Wang DS, Chen CY, Chen CS. Antitumor effects of a novel phenylbutyrate-based histone deacetylase inhibitor, OSU-HDAC42, in prostate cancer. *Clin Cancer Res* 2006; **12**: 5199–5206.
19 Lu YS, Kashida Y, Kulp SK, Wang YC, Wang D, Hung JH *et al*. Efficacy of a novel histone deacetylase inhibitor in murine models of hepatocellular carcinoma. *Hepatology* 2007; **46**: 1119–1130.
20 Lin CC, Yen MC, Lin CM, Huang SS, Yang HJ, Chow NH *et al*. Delivery of noncarrier naked DNA vaccine into the skin by supersonic flow induces a polarized T helper type 1 immune response to cancer. *J Gene Med* 2008; **10**: 679–689.
21 Lin CC, Chou CW, Shiau AL, Tu CF, Ko TM, Chen YL *et al*. Therapeutic HER2/Neu DNA vaccine inhibits mouse tumor naturally overexpressing endogenous neu. *Mol Ther* 2004; **10**: 290–301.
22 Watkins C, Hopkins J, Harkiss G. Reporter gene expression in dendritic cells after gene gun administration of plasmid DNA. *Vaccine* 2005; **23**: 4247–4256.
23 Johnston LJ, Halliday GM, King NJ. Langerhans cells migrate to local lymph nodes following cutaneous infection with an arbovirus. *J Invest Dermatol* 2000; **114**: 560–568.
24 Macatonia SE, Knight SC, Edwards AJ, Griffiths S, Fryer P. Localization of antigen on lymph node dendritic cells after exposure to the contact sensitizer fluorescein isothiocyanate. Functional and morphological studies. *J Exp Med* 1987; **166**: 1654–1667.
25 van Wilsem EJ, Breve J, Kleijmeer M, Kraal G. Antigen-bearing Langerhans cells in skin draining lymph nodes: phenotype and kinetics of migration. *J Invest Dermatol* 1994; **103**: 217–220.
26 Knight S, Krejci J, Malkovsky M, Colizzi V, Gautam A, Asherson G. The role of dendritic cells in the initiation of immune responses to contact sensitizers. I. *In vivo* exposure to antigen. *Cell Immunol* 1985; **94**: 427–434.
27 Ban E, Dupre L, Hermann E, Rohn W, Vendeville C, Quatannens B *et al*. CpG motifs induce Langerhans cell migration *in vivo*. *Int Immunol* 2000; **12**: 737–745.
28 Kim TW, Hung CF, Ling M, Juang J, He L, Hardwick JM *et al*. Enhancing DNA vaccine potency by coadministration of DNA encoding antiapoptotic proteins. *J Clin Invest* 2003; **112**: 109–117.
29 Cheng WF, Chang MC, Sun WZ, Lee CN, Lin HW, Su YN *et al*. Connective tissue growth factor linked to the E7 tumor antigen generates potent antitumor immune responses mediated by an antiapoptotic mechanism. *Gene Ther* 2008; **15**: 1007–1016.
30 Huang B, Mao CP, Peng S, He L, Hung CF, Wu TC. Intradermal administration of DNA vaccines combining a strategy to bypass antigen processing with a strategy to prolong dendritic cell survival enhances DNA vaccine potency. *Vaccine* 2007; **25**: 7824–7831.

31 Lin CC, Tu CF, Yen MC, Chen MC, Hsieh WJ, Chang WC *et al*. Inhibitor of heat-shock protein 90 enhances the antitumor effect of DNA vaccine targeting clients of heat-shock protein. *Mol Ther* 2007; **15**: 404–410.
32 Kato Y, Yoshimura K, Shin T, Verheul H, Hammers H, Sanni TB *et al*. Synergistic *in vivo* antitumor effect of the histone deacetylase inhibitor MS-275 in combination with interleukin 2 in a murine model of renal cell carcinoma. *Clin Cancer Res* 2007; **13**: 4538–4546.
33 Araki Y, Fann M, Wersto R, Weng NP. Histone acetylation facilitates rapid and robust memory CD8 T cell response through differential expression of effector molecules (eomesodermin and its targets: perforin and granzyme B). *J Immunol* 2008; **180**: 8102–8108.
34 Pellicciotta I, Cortez-Gonzalez X, Sasik R, Reiter Y, Hardiman G, Langlade-Demoyen P *et al*. Presentation of telomerase reverse transcriptase, a self-tumor antigen, is down-regulated by histone deacetylase inhibition. *Cancer Res* 2008; **68**: 8085–8093.
35 Villagra A, Cheng F, Wang HW, Suarez I, Glozak M, Maurin M *et al*. The histone deacetylase HDAC11 regulates the expression of interleukin 10 and immune tolerance. *Nat Immunol* 2009; **10**: 92–100.

Genetic Vaccines and Therapy

BioMed Central

Research

Open Access

The effects of DNA formulation and administration route on cancer therapeutic efficacy with xenogenic EGFR DNA vaccine in a lung cancer animal model

Ming-Derg Lai[1,2,3], Meng-Chi Yen[2], Chiu-Mei Lin[4,5], Cheng-Fen Tu[1], Chun-Chin Wang[6], Pei-Shan Lin[6], Huei-Jiun Yang[1] and Chi-Chen Lin*[6,7]

Address: [1]Department of Biochemistry and Molecular Biology, College of Medicine, National Cheng Kung University, Taiwan, [2]Institute of Basic Medicine, College of Medicine, National Cheng Kung University, Taiwan, [3]Center for Gene Regulation and Signal Transduction Research, National Cheng Kung University, Tainan, Taiwan, [4]School of Medicine, College of Medicine, Taipei Medical University, Taipei, Taiwan, [5]Department of Emergency Medicine, Shin Kong Wu Ho-Su Memorial Hospital, Taipei, Taiwan, R.O.C, [6]Institute of Medical Technology, College of Life Science, National Chung Hsing University, Taiwan and [7]Department of Medical Research and Education, Taichung-Veterans General Hospital, Taichung, Taiwan

Email: Ming-Derg Lai - a1211207@mail.ncku.edu.tw; Meng-Chi Yen - iqri@hotmail.com; Chiu-Mei Lin - james@bioware.com.tw; Cheng-Fen Tu - dnavaccine@hotmail.com; Chun-Chin Wang - tony10600@yahoo.com.tw; Pei-Shan Lin - butterfly7557@hotmail.com; Huei-Jiun Yang - snowangel0209@hotmail.com; Chi-Chen Lin* - lincc@dragon.nchu.edu.tw

* Corresponding author

Published: 30 January 2009

Genetic Vaccines and Therapy 2009, **7**:2 doi:10.1186/1479-0556-7-2

Received: 29 October 2008
Accepted: 30 January 2009

This article is available from: http://www.gvt-journal.com/content/7/1/2

Abstract

Background: Tyrosine kinase inhibitor gefitinib is effective against lung cancer cells carrying mutant epidermal growth factor receptor (EGFR); however, it is not effective against lung cancer carrying normal EGFR. The breaking of immune tolerance against self epidermal growth factor receptor with active immunization may be a useful approach for the treatment of EGFR-positive lung tumors. Xenogeneic EGFR gene was demonstrated to induce antigen-specific immune response against EGFR-expressing tumor with intramuscular administration.

Methods: In order to enhance the therapeutic effect of xenogeneic EGFR DNA vaccine, the efficacy of altering routes of administration and formulation of plasmid DNA was evaluated on the mouse lung tumor (LL2) naturally overexpressing endogenous EGFR in C57B6 mice. Three different combination forms were studied, including (1) intramuscular administration of non-coating DNA vaccine, (2) gene gun administration of DNA vaccine coated on gold particles, and (3) gene gun administration of non-coating DNA vaccine. LL2-tumor bearing C57B6 mice were immunized four times at weekly intervals with EGFR DNA vaccine.

Results: The results indicated that gene gun administration of non-coating xenogenic EGFR DNA vaccine generated the strongest cytotoxicty T lymphocyte activity and best antitumor effects. CD8(+) T cells were essential for anti-tumor immunityas indicated by depletion of lymphocytes in vivo.

Conclusion: Thus, our data demonstrate that administration of non-coating xenogenic EGFR DNA vaccine by gene gun may be the preferred method for treating EGFR-positive lung tumor in the future.

Background

The epidermal growth factor receptor (EGFR) is a transmembrane glycoprotein, which consists of three domains: an extracellular ligand-binding domain that recognizes and binds to specific ligands, a hydrophobic membrane-spanning region, and an intracellular catalytic domain that serves as the site of tyrosine kinase activity [1,2]. High EGFR protein expression was observed in several types of cancer including breast, bladder, colon and lung carcinomas [3-6]. This involvement in cancer progression and a negative prognosis makes EGFR an attractive target for molecule therapy [7]. Various therapeutic strategies have been developed to block EGFR signaling, with the most frequent strategies involving monoclonal antibodies and small molecule tyrosine kinase inhibitors that are designed to directly against receptor or specifically inhibit EGFR enzymatic activity [8-10]. However, some clinical studies indicated that tumors overexpressing EGFR did not show a significant clinical response to antibody-based or small molecule inhibitor therapy in lung cancer, Searching for correlates, it has been found that the presence of certain kinase domain mutations in EGFR gene appear to predict responsiveness [11-13]. Hence, new strategies are required to treat tumors overexpressing normal EGFR.

Antigen-specific active immunotherapy is another potential therapeutic approach for the treatment of EGFR-positive tumor cells by breaking of immune tolerance against wild type or mutant-type EGFR. Since the anti-EGFR antibody was not effective, the active immunotherapy may need to induce both humoral and cellular immunity. DNA vaccine apparently fulfills such a requirement [14]. Furthermore, DNA vaccine offer many advantages including induction of a long-lived immune response, better stability, and easy preparation in large quantities than other conventional vaccines such as peptide or attenuated live or killed pathogens [15]. In addition, several studies have indicated that tolerance to self antigens on cancer cells can be overcome using active therapeutic immunization strategies in preclinical animal model [16,17].

Intramuscular administration of xenogenic EGFR DNA vaccine has been shown to break immune tolerance and induce the specific antitumor immunity against EGFR-positive tumors in a therapeutic preclinical model [18]. Two common routes of immunization have been for DNA vaccination: needle intramuscular injection and epidermal gene gun bombardment. Many studies have shown that gene gun-mediated immunization is more efficient than needle intramuscular injection as it elicits similar levels of humoral and cellular response [19,20]. However, intramuscular injection of DNA induces a predominantly Th1 response, whereas gene gun immunization with DNA coated on gold evokes mainly Th2 response. The route of immunization can influence the outcome of the immune response through altering the interaction between the vaccine and different APCs at the site of injection [21]. Our previous results suggested that gold particles used in gene gun bombardment affected the induced-immune response [22], because gene gun administration using non-coating naked DNA vaccine elicited Th1-bias immune response. Hence, the choice of the route of DNA immunizations and formulation of DNA could thus represent an important element in the design of EGFR DNA vaccine against EGFR-positive tumor.

In the present study, we aimed to determine how different route of administration and formulation of plasmid DNA could influence the efficacy of xenogenic EGFR DNA vaccine on a mouse lung tumor LL2 naturally overexpressing endogenous EGFR. We analyzed and compared the immunological and antitumor responses generated by the plasmid DNA encoding extracellular domain of human EGFR(a.a 1–621, Sec-N'-EGFR) administrated through three different methods: needle intramuscular administration using non-coating DNA (i.m), gene gun administration using gold-coated DNA and gene gun administration using non-coating DNA. Our results indicated that the routes of administration and formulation of DNA clearly affected the therapeutic response by altering immune pathway. Gene gun administration using non-coating plasmid DNA induced the best anti-tumor immune response in LLC2 animal lung cancer animal model, which may provide the basis for the design of DNA vaccine in human clinical trial in the future.

Methods

Animals, Cell lines and antibodies

Inbred female C57BL/6 mice (6–8 weeks of age) weighing 18–20 g were used. Animal experiments were approved by the National Cheng Kung University animal welfare committee. LL2 is a cell line derived from Lewis lung carcinoma passaged routinely in C57BL/6 mice [23]. B-16 F10 melanoma cell line and colon carcinoma cell line CT-26 were obtained from American Type Culture Collection (Manassas, VA, USA). Antibody against the extracellular domain of mouse EGFR (N20; Santa cruz) was used for Western blotting analysis of the expression of EGFR in these cell lines. Antibody against mouse extracellular EGFR (N20; Santa cruz) and FITC-conjugated donkey against goat IgG secondary Ab (Jackson Immuno Research Laboratories, Inc) were used for detection of surface EGFR in LL2 cells. Flow cytometry analysis was performed with a FACSCalibur (BD Bioscience, Mountain View, CA, USA).

Construction and Preparation of DNA vaccine

A431 cells were harvested and total RNA was isolated using a total RNA extraction kit (Viogene-Biotek Corp., Hsichih, Taiwan) according to the manufacturer's instructions. The RNA was subjected to reverse transcriptase

polymerase chain reaction (RT-PCR) for amplification of the extracellular domain of the human EGFR gene (Sec-N'-EGFR) using the primers GCAATCAAGCTTATGCGAC-CCTCCG GGACGG and GCAATCTCTAGACACA GGT-GGCACACATGGCC The PCR product of the expected size was isolated, digested with HindIII and XbaI, and cloned into the multiple cloning site of pcDNA3.1B+myc-his (Invitrogen, San Diego, CA, USA). The plasmid DNA was transformed into Escherichia coli DH5 and purified from large-scale cultures using a QIAGEN Endofree Mega Kit (Qiagen, Chatsworth, CA, USA).

In vitro transfection and Western blotting

COS-7 cells were transiently transfected with DNA plasmids by Lipofactamine 2000 (Invitrogen, San Diego, CA, USA), and cells were harvested 18 h post transfection. Total cell lysates were prepared by using 2× SDS gel loading buffer(Tris-HCl pH 8.45, 90 mM, Glycerol 24%, SDS 4%). Equal amounts of cell lysates (30 μg of total protein) were separated by sodium dodecyl sulfate-polyacrylamide gel electrophoresis and transferred onto PVDF membranes (minipore). The membrane was blocked for 1 h at room temperature in PBS containing 5% nonfat dried milk and 0.1% Tween 20 under gentle shaking. The membrane was then incubated overnight with EGFR-specific monoclonal antibody and the ound antibody was detected with a 1:2,000 dilution of horseradish peroxidase-conjugated goat anti-mouse immunoglobulin G (Cell Signaling Technology, Inc, Danvers, MA, USA). The immobilon Western chemiluminescent HRP substrate (Millipore Corporation, Billerica, U.S.A) was used for Western blotting. The intensity of each band was read by using a B UVP Biospectrum AC System (UVP, Upland, CA, U.S.A)

Therapeutic efficacy of DNA vaccine on tumor growth

Mice were injected subcutaneously in the flank with 1 × 10^6 LL2 cells in 0.5 ml of PBS. At day 5, Sec-N'-EGFR DNA vaccine was administered by three different methods four times at weekly intervals when tumors were palpable. Control mice were injected with water containing no plasmid DNA. Tumor growth was monitored using caliper twice a week. Subcutaneous tumor volumes were calculated using the formula for a rational ellipse: (m1 × m2 × m2 × 0.5236), where m1 represents the longer axis and m2 the shorter axis. Mice were sacrificed when the tumor volume exceeded 2500 mm^3 or the mouse was in poor condition and death was expected shortly. Significance of differences in mice survival was tested by Kaplan-Meier analysis.

DNA vaccination by needle intramuscular injection

For intramuscular needle-mediated DNA vaccination, 100 μg/mouse of Sec-N'-EGFR DNA vaccines or pcDNA3.1B+myc-his DNA plasmid were administered intramuscularly by syringe needle injection.

DNA vaccination by gene gun gold-coated DNA or naked non-coating DNA

The protocol and delivery device for DNA vaccination by gene gun have been described previously [22]. Briefly, for gold-coated DNA vaccination, plasmid DNA was coated on gold particles (Bio-Rad, Hercules, CA, USA) at the ratio of 1–2 μg of DNA per mg of gold particles, and was dissolved in 20 μl of 100% ethanol. The gold-coated DNA was delivered to the shaved abdominal region of C57BL/6 mice using a helium-driven low pressure gene gun (Bio Ware Technologies Co. Ltd, Taipei, Taiwan) with a discharge pressure of 40 psi. For non-coating DNA vaccination, 1–2 μg of Sec-N'-EGFR DNA in 20 μl of autoclaved double-distilled water was directly added to the loading hole near the nozzle, and delivered to the shaved abdominal of mice using the same low pressure gene gun with a discharge pressure of 60 psi.

Determination of anti-EGFR antibody titer in serum

Recombinant extracellular domain protein of human EGFR (0.25 μg/well) (R&D Systems Inc) in 100 μl coating buffer (sodium carbonate, pH 9.6) was added to microtiter plates (Nunc, Roskilde, Denmark) and incubated overnight at 4°C. Nonspecific binding was blocked with 1% BSA in PBS buffer for 2 h and washed with PBS containing 0.05% Tween 20 for three times. Mouse monoclonal anti-human EGFR antibody (20E12; Santa cruz) was used to generate the standard curve. The titer of anti-EGFR antibody in experimental mouse sera were determined by serial dilution and added to wells. Plates were incubated for 2 h at 37°C, washed, and then incubated with HRP-conjugated anti-mouse IgG (Cell Signaling Technology). TMB substrate was used for colour development. Absorbance was measured at 450 nm with an ELISA reader (Sunrise, Tecan, Austria).

Serum passive transfer

LL2 tumor bearing B6 mice were immunized with DNA vaccine four times. Blood was collected 4, 7, 10 days after the last immunization, and serum was collected and pooled within each group of mice. A 300 μl of the polled sera was transferred by intraperitoneal injection into recipient mice which was s.c challenged with 1 × 10^6 LL2 tumor cells 5 day before. Blood collected from LL2 tumor bearing B6 mice without DNA vaccination was used as control.

Intracellular staining

Spleen or lymph node cells(2.5 × 10^6 cells/ml) were harvested a day after last immunization and cultured in 48 well tissue culture plates (BD Biosciences) in the presence of 5 μg/ml of recombinant EGFR protein and incubated at 37°C in a 5% CO_2 humidified atmosphere for 18 h. Thereafter, 5 μg/ml brefeldin A (BFA; Sigma, St. Louis, MO) was added, and the cultures were incubated for an

additional 6 hr. Cells were harvested and stained with PE-anti-CD4 (eBioscience) and PE-anti-CD8 (eBioscience) and then fixed with 4% paraformaldehyde for 30 min at 4°C. The cells were permeabilized with PBS containing 0.1% saponin for 5 min, after which FITC-anti-IFN-γ (eBioscience) antibody was added for detection of intracellular cytokine in the presence of saponin for 45 min at 4°C. For analysis, 100000 cells were acquired on a Facscalibur. The results were analyzed using CellQuest (BD Biosciences).

In vivo CTL assay

Spleen and inguinal lymph node cells from naive C57BL/6 mice were labeled with 5 or 0.5 μM CFSE. Cells labeled with 5 μM CFSE were pulsed with 5 μg/ml recombinant EGFR protein at 37°C for 1 hr as target cells while the cells labeled with 0.5 μM CFSE were left unpulsed as control cells. Equal number (1×10^7) of the two target populations were mixed together and injected into mice i.v., such that each mouse was injected i.v with a total of 2×10^7 cells in 150 μl of PBS. Spleens and inguinal lymph nodes in recipient mice were harvested 18 hrs later and single-cell suspensions were prepared. The proportions of differentially CFSE-labeled target cells were analyzed by flow cytometry. To calculate specific lysis, the following formula was used: ratio = (percentage CFSE low/percentage CFSE high). Percentage of specific lysis = [1 - (ratio for unimmunized mice/ratio for immunized mice) × 100]

Histological analysis of lymphocyte infiltration

Tumor tissues were removed from mice one week after the last vaccination and embedded in OCT compound (Sakura Finetek Inc., USA) and then frozen in liquid nitrogen. Cryosections (5-μm) were made and fixed with 3.7% formaldehyde and acetone. Endogenous peroxidase was removed with 3.7% hydrogen peroxide, washed with PBS three times and incubated with primary antibody anti-CD4 (GK1.5;BD Biosciences Pharmingen, San Jose, CA), or anti-CD8 (53-6.7; Pharmingen), overnight at 4°C. After further reaction with peroxidase-conjugated secondary antibody, aminoethyl carbazole substrate kit (Zymed Laboratories, San Francisco, CA) was used for color developing. For quantification of immune infiltrating cells, the cells were counted with a light microscope with a 10× eyepiece and a 40× objective lens. Three samples from three mice were taken and analyzed for statistical significance test.

Depletion of CD8+ or CD4+ T cells

T cell-depletion experiments have been described previously[16]. Briefly, C57BL/6 mice were injected i.p with rat anti-mouse CD8 (2.43; 500 g), rat anti-mouse CD4 (GK 1.5; 300 μg), or control antibody (purified rat IgG; 500 μg). The depletions started 2 day before DNA vaccination, followed by multiple injections at 7-day intervals. To confirm the efficiency of T cell depletion, flow cytometry analysis revealed that the >95% of the appropriate subset was depleted

Statistical Analysis

The animal experiments to evaluate immune responses were repeated at least two times ($n = 3$ per group). SE values were calculated with GraphPad Prism 4 software (GraphPad Software; San Diego, CA, USA), and P value less than 0.05 was considered statistically significant. Comparison of the survival rate was carried out by using Kaplan-Meier method and log-rank test in GraphPad Prism 4 software.

Results

The expression of EGFR in Mouse Cancer Cell Lines

The expression of EGFR in several cancer cell lines was determined by Western blotting using antibodies that recognize the N-terminus of mouse EGFR (Fig. 1A). The expression of EGFR in LL2 lung tumor cells was the highest among three cell lines examined. In addition, we further confirmed surface expression of EGFR with flow cytometry (Fig. 1B). Therefore, the LL2 lung tumor in B6 mice is a good animal model to study the efficacy of the EGFR DNA vaccine.

Construction and Characterization of Sec-N'-EGFR DNA vaccine

We first constructed the plasmid encoding the N-terminal extracellular domain of human EGFR (a.a. 1–621) and named the plasmid "Sec-N'-EGFR" (Fig. 2). The COS-7 cells were transfected with Sec-N'-EGFR DNA and the expression of extracellular domain of human EGFR was determined with western blotting. The Sec-N'-EGFR DNA plasmids expressed the extracellular domain of human EGFR in vitro (Fig. 2).

Efficacy of Sec-N'-EGFR DNA Vaccine in Mice with Established Tumors

At day 0, we injected mice subcutaneously with 1×10^6 LL2 tumor cells. At day 5, when the tumor was palpable, we immunized the mice with Sec-N'-EGFR DNA vaccine four times at weekly intervals via three different methods: intramuscular injection (i.m), gene gun administration of gold-coated DNA, and gene gun administration of non-coating DNA. Non-coating Sec-N'-EGFR DNA vaccine administered by gene gun statistically delayed the growth of LL2 tumors when compared with control mice (Fig. 3A). In addition, the survival portion of vaccinated mice indicated that the therapeutic efficacy appeared to be in the order: g.g non-coating DNA vaccine mice group > g.g-DNA coated gold particels or i.m DNA vaccine mice groups >> control mice group (Fig 3B). The survival rate of mice showed significant differences between the control mice and all three vaccinated mice groups ($p < 0.01$).

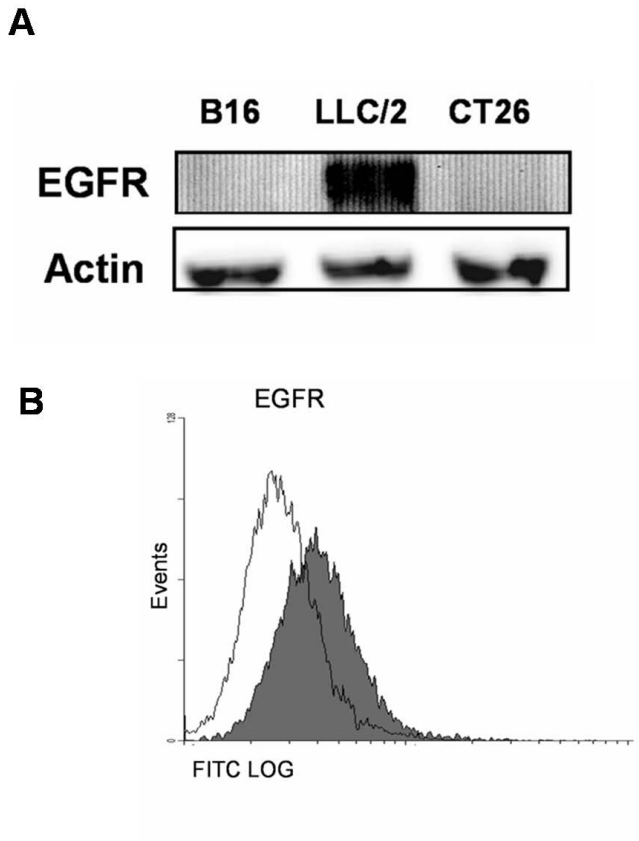

Figure 1
Overexpression of EGFR in LL2 lung cancer cell line. The expression of EGFR in various cell lines was analyzed by Western blotting with monoclonal antibody against EGFR. (B) Flow cytometry analysis of membrane EGFR in LL2 cells. LL2 cells were stained with monoclonal antibody against the extracellular domain of mouse EGFR, followed by FITC-conjugated mouse anti-goat secondary antibody (gray histogram). Normal mouse IgG mAb was used as the negative control (white histogram).

Furthermore, the difference between g.g non-coating DNA and the other two mice groups (i.m or g.g-DNA coated gold particles) is also statistically significant ($P < 0.05$)(Fig 3B)

Humoral Immunity

To investigate the immunological mechanism underlying the therapeutic effect of Sec-N'-EGFR DNA vaccine, the induction of anti-EGFR antibodies was examined in mice serum. Specific antibodies against EGFR proteins in mice serum samples were tested by ELISA using recombinant extracellular domain human EGFR proteins. The results showed that anti-EGFR antibodies were detected in all mice vaccinated with Sec-N'-EGFR DNA vaccine; however, the serum from g.g DNA coated gold particles and i.m mice groups contained higher levels of anti-EGFR antibodies than g.g-non-coating DNA mice group (Fig 4A). To further confirm the role of antibody in this therapeutic Sec-N'-EGFR DNA vaccine approach, the immune sera from mice vaccinated with DNA vaccine was passively transferred into mice with established LL2 tumors. The result showed that mice receiving serum from i.m mice group ($p = 0.08$) and g.g-DNA coated gold particles mice group($p < 0.05$) showed prolong mice survival compared with mice injected with serum from control animals (Fig. 4B). The anti-EGFR antibody induced by Sec-N'-EGFR DNA played a role in delay tumor progression although the amount of antibody may not be correlated with anti-tumor effects of three forms of therapeutic EGFR DNA vaccine.

Cellular Immunity

To examine the specific immunologic cellular response to Sec-N'-EGFR DNA vaccine using different administration methods, spleen and lymph nodes were isolated from vaccinated mice. The lymphocytes were stained for the surface CD4 and CD8 marker and intracellular IFN-γ after recombinant human EGFR antigen stimulation. Non-coating Sec-N'-EGFR administration by gene gun generated most functional EGFR-specific CD8+ T cell cells as evidenced by their production of intracellular IFN-γ in the lymph node(Fig 5A, B). In contrast, splenic lymphocytes isolated from intramuscular injection of Sec-N'-EGFR mice group had higher functional EGFR-specific CD4+ and CD8+ T cells when compared with i.m and g.g DNA coated gold particles vaccinated mice groups, respectively(Fig 5A, B). In addition, we also measured cytotoxic T lymphocytes(CTLs) activity in mice immunized with Sec-N'-EGFR DNA vaccine by three different methods. The cytotoxic T lymphocytes(CTLs) effector function in spleen appeared to be in the order i.m mice group > g.g-DNA coated gold particles and g.g-non coating DNA mice groups>> control group (illustrated in an individual mouse in Fig. 6A and as group means in Fig. 6B). In contrast, the percent of specific cytotoxic T lymphocytes lysis in inguinal lymph node of vaccinated mice indicated that only non-coating Sec-N'-EGFR DNA administrated via gene gun is sufficient to induce CTL effector function (Fig 6A, B). Hence, taken together, the number of functional CD4+, CD8+ T cell and level of CTL activity in spleen and inguinal lymph node were differentially affected by the routes of administration and formulation of DNA vaccine.

To further demonstrate the importance of cellular immunity in cancer therapy, we examined the histology of the tumors. We observed CD4+ lymphocyte tumor infiltrations were detected in all mice groups (Fig. 7A and Table 1). However, tumors form g.g DNA coated gold particles mice group showed a greater infiltration of CD4+ lymphocytes compared with other treatment groups and con-

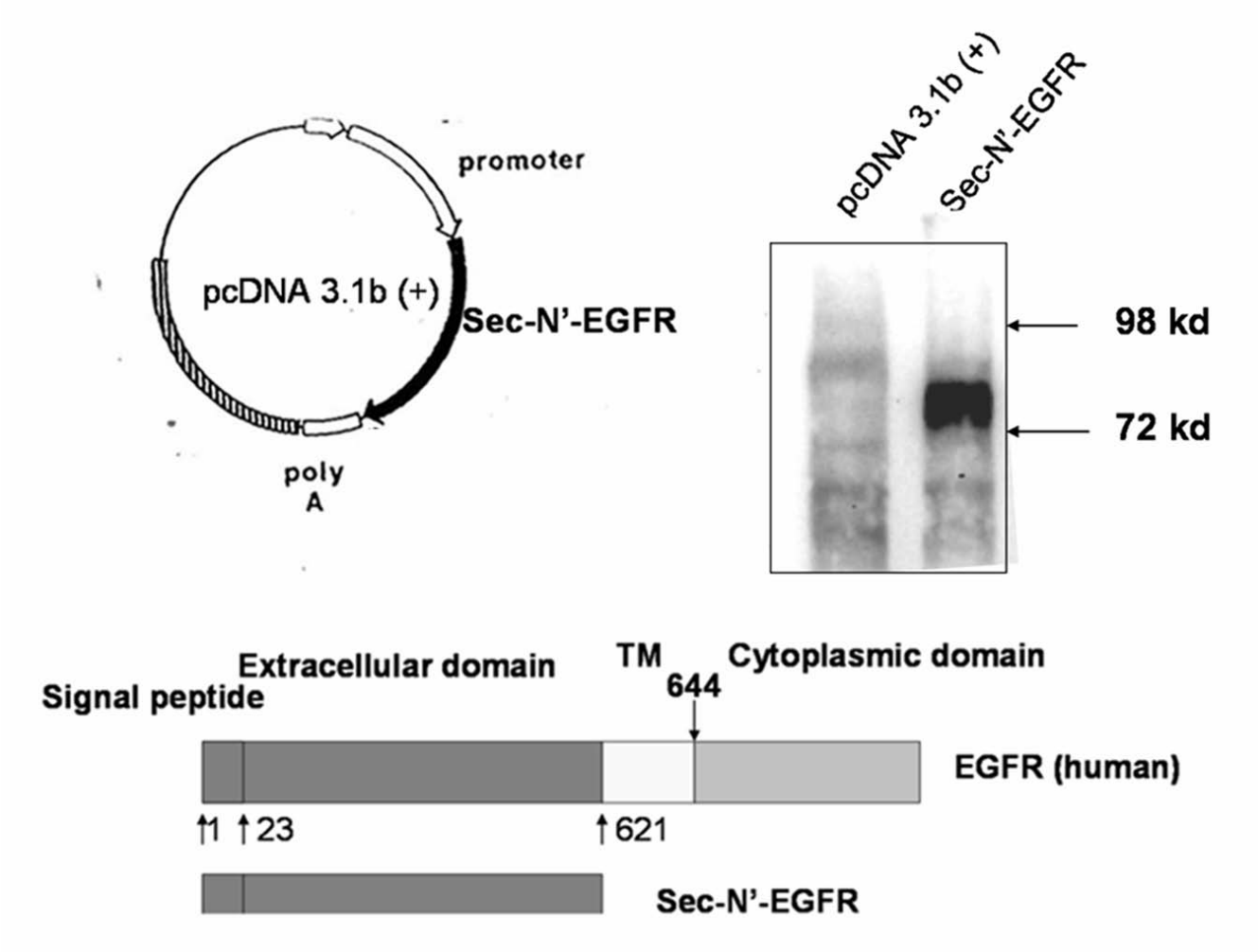

Figure 2

Characterization of Sec-N'-EGFR DNA vaccines. (A) Schematic diagram of the Sec-N'-EGFR expressing vectors. The N-terminal extracellular portion of the human EGFR gene was constructed to pcDNA3.1B+myc-his plasmid. Transcription is directed by cytomegalovirus (CMV) early promoter/enhancer sequences. The plasmid was named Sec-N'-EGFR (B) Expression of Sec-N'-EGFR was evaluated with transient transfection into COS-7 cells in vitro., and western blot analysis of sec-N-terminal EGFR protein. Whole cell lysates were collected from Cells transfected with Sec-N'-EGFR (lane 2), or control pcDNA3.1B+myc-his plasmid (lane 1), and analyzed with western blotting.

trol group. As for tumor infiltration of CD8+ T cell, we observed considerably increase of CD8+ lymphocyte in the g.g-non coating DNA mice group (Fig. 7B and Table 1) and minor increase of CD8+ lymphocytes in the i.m and g.g-gold mice group in comparison with control mice group. Hence, the results suggested a correlation between the therapeutic efficacy of gene gun administration of non-coating EGFR DNA vaccine and the amount of CD8+ T cell tumor infiltration.

The effects of CD8+ T Cell- Depletion or CD4+ T Cell- Depletion on the Efficacy of Gene Gun Administration of Non-coating EGFR DNA vaccine

The efficacy of gene gun administration of non-coating EGFR DNA vaccine was the best among three types of EFEGFR DNA vaccines, and seemed to correlate with CD8+ T cells. Therefore, CD8+ T cells were depleted with monoclonal antibody 2.43 to determine whether CD8+ lymphocytes were required for the therapeutic efficacy. We performed CD8+ T cell-depletion at weekly intervals during the entire experiment, and the protocol is shown in Fig. 8A. Depletion of CD8+ lymphocytes completely

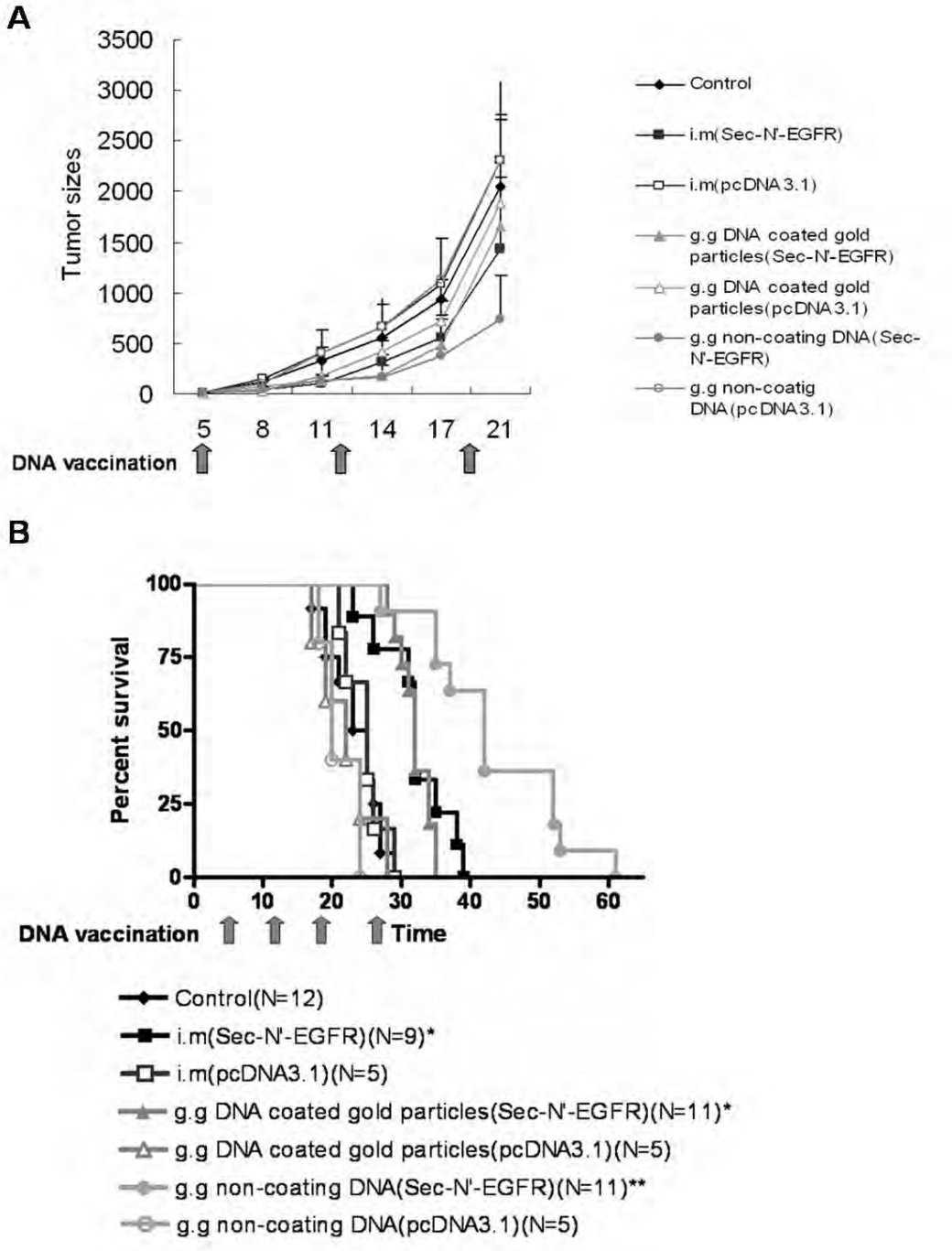

Figure 3

Therapeutic effects of Sec-N'-EGFR DNA vaccine administered by three different methods on established tumor in B6 mice. Five days after subcutaneous tumor implantation with 1 × 10^6 LL2 tumor cells., mice were administrated with DNA vaccine four times (day 5, 12, 19, 26) at weekly intervals; (A) tumor volume was measured at the indicated time. Data are means of the animals per group; bars, ± S.D. (B) lifespan of mice after subcutaneous challenge. The survival data were subjected to Kaplan-Meier analysis. The digit in the parenthesis is the number of mice in the experiment. The symbol (*) indicates a statistically significant difference when compared with the control saline mice ($P < 0.01$). The symbol (**) indicates a statistically significant difference when compared with the i.m and g.g gold-coated DNA group mice ($P < 0.05$) or control mice ($P < 0.001$). The experiments were repeated 2 times with similar results.

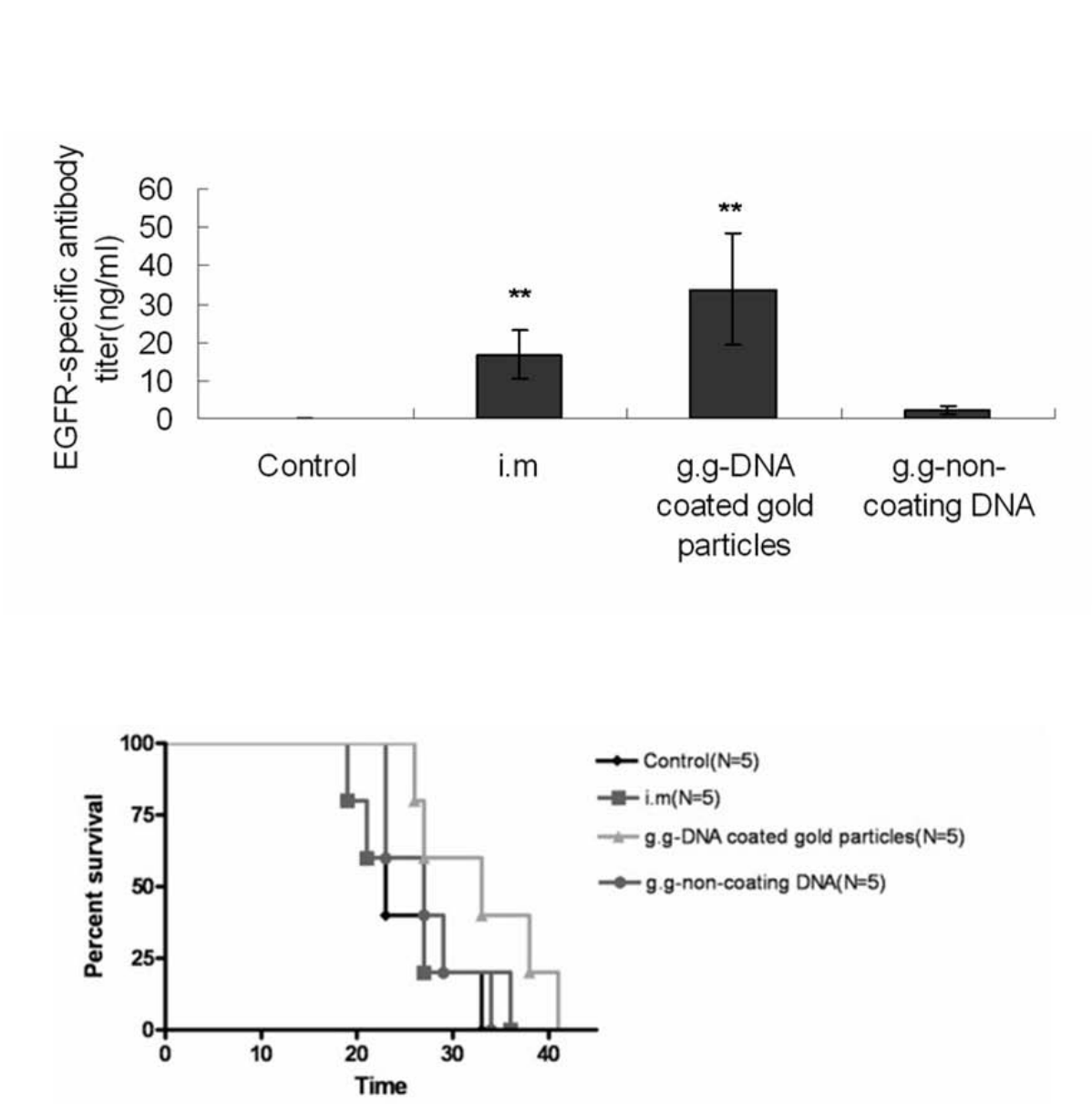

Figure 4

The presence and the therapeutic efficacy of anti-EGFR antibody in serum from the DNA vaccine group of mice. A) Anti-EGFR antibody titer in the mice serum. The serum anti-EGFR antibody in mice was determined with ELISA on dishes coated with the recombinant extracellular domain of human EGFR protein. The data represent the average titer of the sera from three mice in each group. The symbol (**) indicates a statistically significant difference when compared with the g.g non-coating DNA group mice ($P < 0.05$) or control mice ($P < 0.001$). B) B6 mice were treated with serum from control or vaccinated mice on day 5, 12, 19, 26 after s.c challenge with LL2 cells. The survival data were subjected to Kaplan-Meier analysis The symbol (*) indicates a statistically significant difference when compared with control mice group($P < 0.05$). The experiments were repeated 2 times with similar results.

abolished the therapeutic efficacy of Sec-N'-EGFR DNA vaccine delivered via g.g non-coating DNA method (Fig. 8B). On the other hand, it is known that CD4+ T cells have important regulatory functions for CD8+ CTL and antibody responses [24]. Hence, we also depleted CD4 +T cells with monoclonal antibodies GK1.5 and at weekly intervals during the entire experiment. The results showed that depletion of CD4+ T cell in mice did not affect the

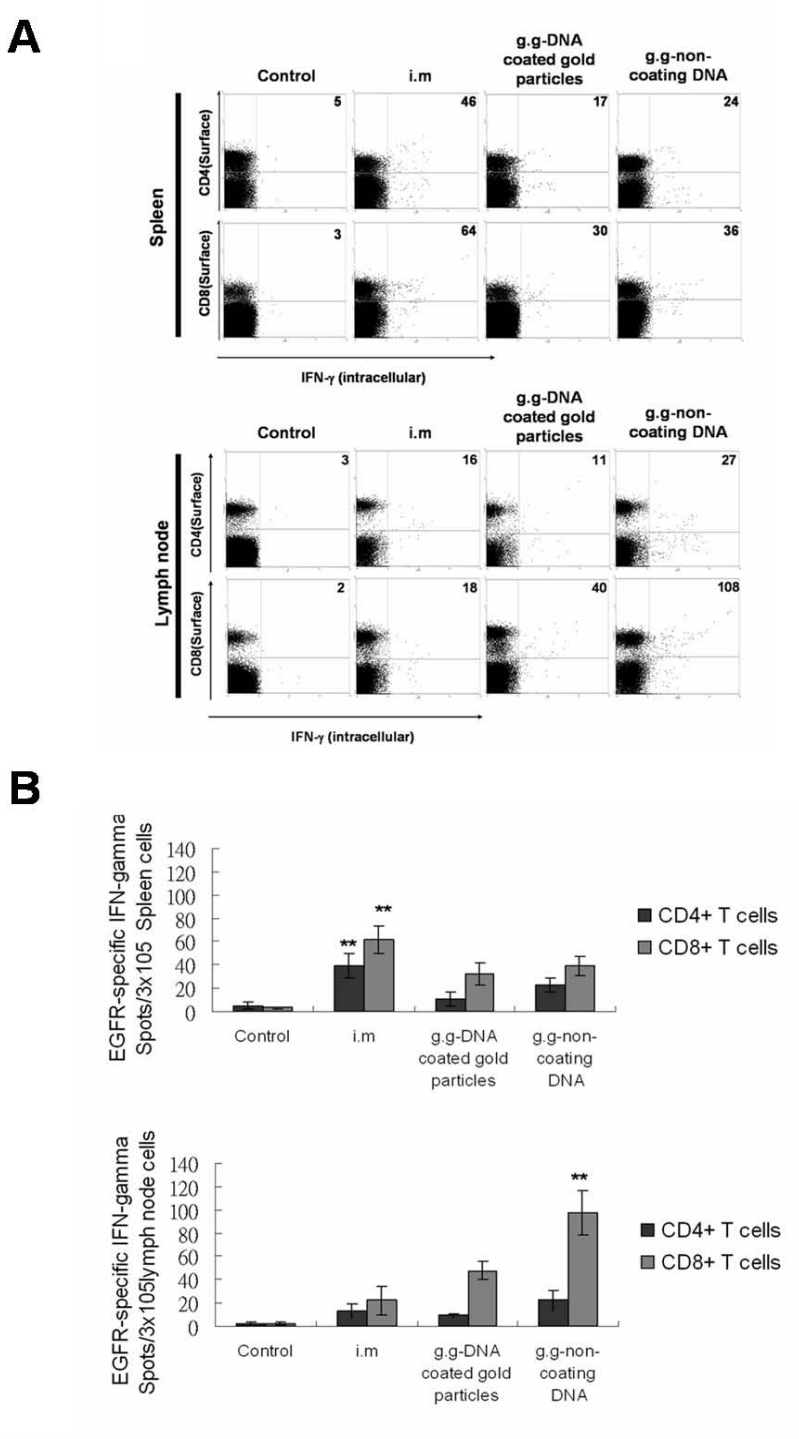

Figure 5

Flow cytometry analysis EGFR-specific CD4⁺ and CD8⁺ T cells that functionally secrete IFN-γ in vaccinated mice. A) the number of IFN-γ-producing EGFR-specific CD4+ and CD8+ T cells in both spleens and inguinal lymph node was determined using flow cytometry in the presence of recombinant extracellular domain of human EGFR. B). Data are expressed as the mean numbers of $CD4^+$ (black sqaure) and $CD8^+$ (black sqaure)IFN-γ^+ cells/3 × 105 spleen cells or inguinal lymph node cells; *bars*, SE. The symbol(**)indicates a statistically significant difference when compared with other treatment groups($P < 0.05$). The data presented in this figure are from one representative experiment of two performed.

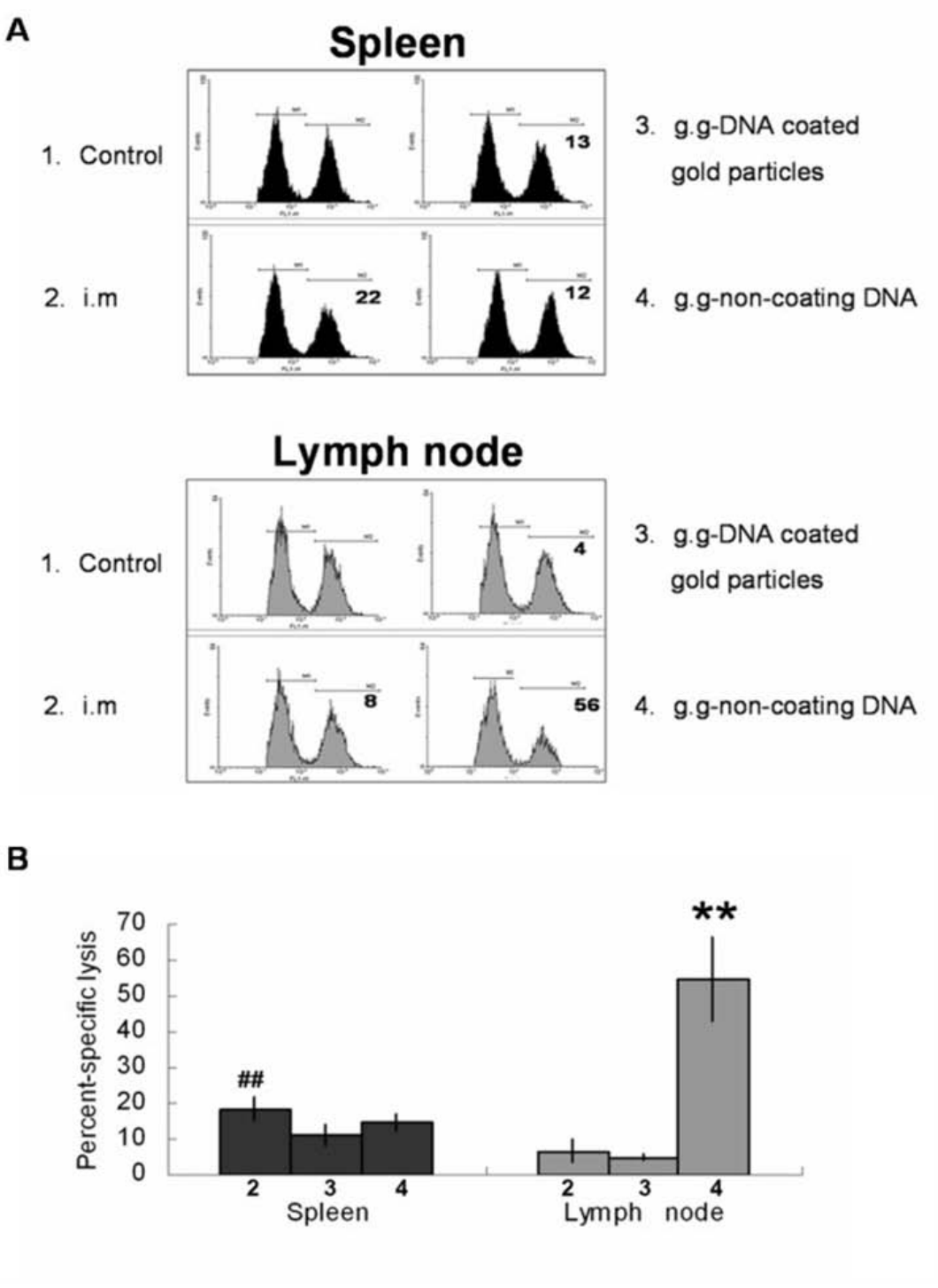

Figure 6

In vivo CTL activity in vaccinated mice. (A) In vivo EGFR-specific effector CTL are located throughout the secondary lymphoid system. A week after last DNA vaccination, an in vivo CTL using recombinant human EGFR protein pulsed splenocytes or inguinal lymph node as targets was performed to assess in vivo CTL activity. (B) The percentages of specific lysis were calculated to obtain a numerical value of cytotoxicity with data from each experimental group of three mice averaged. The symbol(##) and the symbol(**)indicates a statistically significant difference when compared with other treatment groups($P < 0.05$). Similar results were obtained from two more repeated experiments (n = 3 per group).

Table 1: Infiltrated lymphocytes at tumor sites within cryosectioned samples

Vaccine group	$CD4^+$ T cells	$CD8^+$ T cells
Control	6 ± 1	0
i.m	17 ± 2**	11 ± 5#
g.g -DNA coated gold particles	118 ± 24***	4 ± 3#
g.g-non coating DNA	7 ± 2	23 ± 4##

Note: Cell count was performed at 400× magnification. Three samples and five randomly chosen fields/sample were evaluated. Results are expressed as mean ± standard deviation of immunohistochemical positive cells in the cryosection. GG: gene gun. The symbol (**) indicates a statistically significant difference when compared with the g.g non-coating DNA and control group ($P < 0.05$). The symbol (***) indicates a statistically significant difference when compared with the i.m and g.g non-coating DNA group ($P < 0.05$). The symbol (#) indicates a statistically significant difference when compared with the control group ($P < 0.01$). The symbol (##) indicates a statistically significant difference when compared with the i.m and g.g DNA coated gold particles group($P < 0.05$).

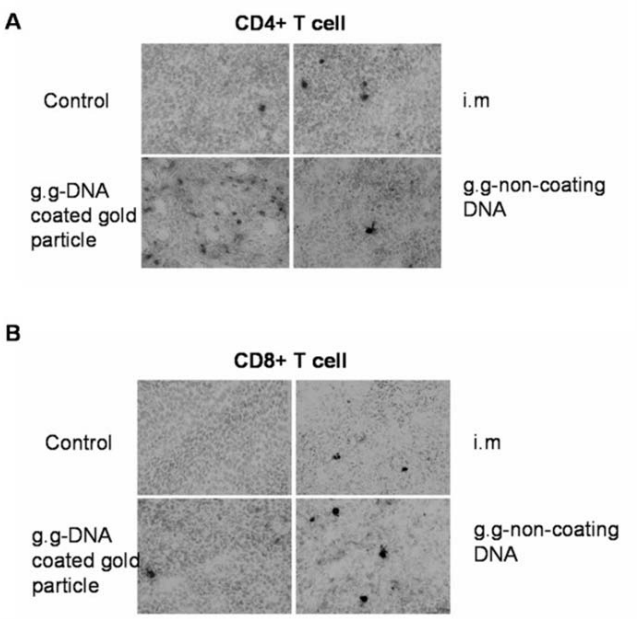

Figure 7
Tumor infiltration of CD4+ and CD8+ T cells. Tumors were excised from mice administrated with Sec-N'-EGFR, or control DNA vector by different delivery methods. Analysis of (A) CD4+ and (B) CD8+ T cells in cryosections of tumors was performed with staining with primary antibody specific for CD4+ and CD8+ cells respectively. Peroxidase-conjugated antibody was used as secondary antibody. Dark spots, peroxidase-stained cells. Similar results were obtained from two more repeated experiments (n = 3 per group).

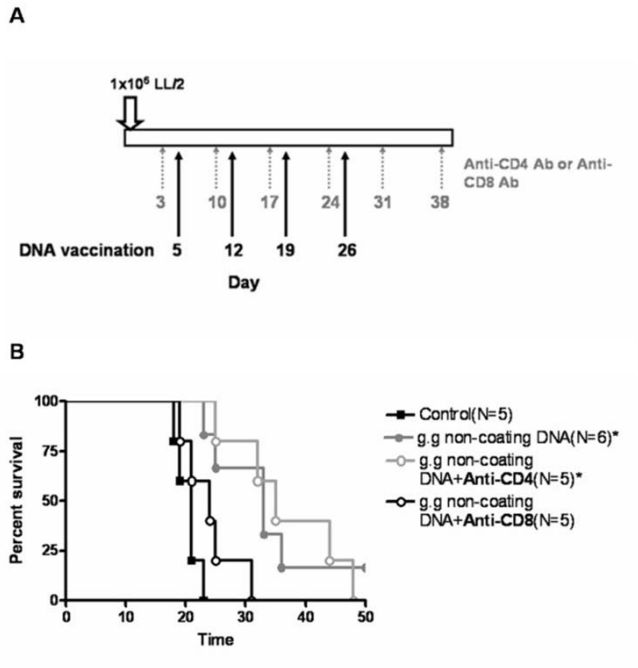

Figure 8
The effects of CD8+ T cell-depletion or CD4+ T cell-depletion on the therapeutic effects of non-coating EGFR DNA vaccine by gene gun administration (A) Protocol for depletion of CD8+ or CD4+ T cells in vivo. Tumor-bearing mice were injected i.p with 500 μg of anti-CD8 antibody or 300 μg of anti-CD4 antibody at weekly intervals starting from 2 days before the first inoculation of DNA vaccine. (B) Life span of B6 mice after sc challenge with LL2 tumor cells. ** represents statistically significant difference when compared to the control saline group of mice ($P < 0.01$). The experiments were repeated twice with experimental groups.

overall survival of mice administrated with non-coating DNA vaccine via g, g (Fig. 8B). Thus, these results suggested that CD8+ T cell played a major role in mediating therapeutic efficacy of gene gun administration of non-coating EGFR DNA vaccine

Discussion

In this study, we assessed the immunologic responses and therapeutic antitumor effects of EGFR DNA vaccine delivered by three different methods: needle intramuscular administration using non-coating DNA (i.m), gene gun administration using DNA coated on gold particles (g.g-coated gold particles) and gene gun administration using non-coating DNA (g.g-non coating DNA) in an EGFR-overexpressing LL2 lung tumor animal model. Our results showed that non-coating Sec-N'-EGFR DNA vaccine administrated via gene gun represents the most potent regime for DNA administration. In addition, gene gun administration using non-coating Sec-N'-EGFR DNA vac-

cine generated higher EGFR-specific functional CD8+ T cell and EGFR-specific CTL activity in vivo comparing to other treatment groups. T cell-depletion experiment indicated that CD8+ T cell played a major role in mediating therapeutic efficacy of gene gun administration of non-coating EGFR DNA vaccine

In this study, we observed that gold-coated Sec-N'-EGFR DNA vaccine by gene gun generated higher antibody in the serum than g.g-non-coating DNA mice group. In addition, mice receiving serum from g.g-DNA coated gold particles mice group($p < 0.05$) showed prolong mice survival when compared with mice injected with serum from control animals. These results suggested that anti-EGFR antibody produced also might be effective against EGFR-overexpressing tumor in LL2 model. However, clinical reports indicated that EGFR overexpression as detected by immunohistochemistry has not been correlated with response to small molecule EGFR inhibitor or anti-EGFR antibody therapy. The presence of certain EGFR kinase domain mutation appears to predict responsiveness better [11-13]. It is possible that the mutations present in EGFR precipitate the altered oncogenic signal and make EGFR indispensable for tumor growth, which make the inhibitor or antibody function to inhibit tumor growth. On the other hand, the reaction of CTLs does not depend whether the target molecules are indispensable or essential for the growth of tumor cells. Therefore, CTL effector cell may be useful against lung tumor with expressing wild type EGFR or mutant type EGFR protein. Hence, our results suggest that increase of Th1-like CTL immune response by administration of non-coating EGFR DNA vaccine may be the most potential application of EGFR DNA vaccine in the further clinical trials.

It was interesting to observe that administration route and forms of DNA affected the CTL activity in the spleen and inguinal lymph node differentially. Administration of Sec-N'-EGFR DNA vaccine by needle intramuscular injection can induce stronger CTL activity in spleen than gene gun administration of Sec-N'-EGFR DNA. In contrast, administration of non-coating Sec-N'-EGFR DNA vaccine via gene gun induced stronger CTL activity in inguinal lymph node than other treatments The different outcome of CTL activity may at least be explained by two reasons. First, i.m and g.g administrations of DNA may induce immune responses in different lymphoid compartments. Skin administration of DNA by gene gun appears to initiate responses by virtue of transfected epidermal Langerhans cells or antigen loaded epidermal Langerhans cells moving into draining inguinal lymph nodes [25-27]. By contrast, intramuscular injection of DNA initiated mainly by cells that has moved in the blood to the spleen [25,28]. Second, Th1 immunity is critical for the induction of specific cell-mediated cytotoxic cells including tumor-specific cytotoxic T lymphocytes in tumor-bearing mice. Our previous study demonstrated that administration of non-coating DNA via gene gun induced a predominantly T helper type 1 (Th1) response, whereas administration of gold-coated DNA by gene gun elicited predominantly T helper type 2 (Th2) responses [22]. Combination of these two factors may determine the final CTL activity in spleen and lymph nodes.

Conclusion

In summary, the therapeutic efficacy of Sec-N'-EGFR DNA vaccine was dependent on the route of administration and formulation of plasmid DNA (gold-coating or non-coating). More importantly, we have shown that non-coating Sec-N'-EGFR DNA administration via gene gun represents the most potent regimen for EGFR DNA vaccine against EGFR-positive LL2 lung tumor and may be the preferred choice in the future clinical trial.

Competing interests

The authors declare that they have no competing interests.

Authors' contributions

MDL helped with the design of the experiments and prepared the draft manuscript, MCY, CFT, CCW, PSL and HJY performed the experiments; CML provided advice on the design of the study and commented on the manuscript; CCL conceived and supervised the study, participated in the preparation of and commented on the manuscript.

Acknowledgements

This study was supported by Grants NSC89-2318-B-006-017-M51, NSC-97-2320-B-005-004 from the National Science Council, Taiwan, Republic of China and in part by the Ministry of Education, Taiwan, R.O.C. under the ATU plan

References

1. Zandi R, Larsen AB, Andersen P, Stockhausen MT, Poulsen HS: **Mechanisms for oncogenic activation of the epidermal growth factor receptor.** *Cell Signal* 2007, **19:**2013-23.
2. Yarden Y: **The EGFR family and its ligands in human cancer: signaling mechanisms and therapeutic opportunities.** *Eur J Cancer* 2001, **37:**S3-8.
3. Nicholson S, Richard J, Sainsbury C, Halcrow P, Kelly P, Angus B, Wright C, Henry J, Farndon JR, Harris AL: **Epidermal growth factor receptor (EGFR); results of a 6 year follow-up study in operable breast cancer with emphasis on the node negative subgroup.** *Br J Cancer* 1991, **63:**146-50.
4. Lipponen P, Eskelinen M: **Expression of epidermal growth factor receptor in bladder cancer as related to established prognostic factors, oncoprote in (c-erbB-2, p53) expression and long-term prognosis.** *Br J Cancer* 1994, **69:**1120-5.
5. Galizia G, Lieto E, Ferraraccio F, De Vita F, Castellano P, Orditura M, Imperatore V, La Mura A, La Manna G, Pinto M, Catalano G, Pignatelli C, Ciardiello F: **Prognostic significance of epidermal growth factor receptor expression in colon cancer patients undergoing curative surgery.** *Ann Surg Oncol* 2006, **13:**823-835.
6. Mountain CF: **New prognostic factors in lung cancer: biologic prophets of cancer cell aggression.** *Chest* 1995, **108:**246-254.
7. Schiff BA, McMurphy AB, Jasser SA, Younes MN, Doan D, Yigitbasi OG, Kim S, Zhou G, Mandal M, Bekele BN, Holsinger FC, Sherman SI, Yeung SC, El-Naggar AK, Myers JN: **Epidermal growth factor receptor (EGFR) is overexpressed in anaplastic thyroid can-**

cer, and the EGFR inhibitor gefitinib inhibits the growth of anaplastic thyroid cancer. *Clin Cancer Res* 2004, **10:**8594-8602.
8. Dancey J: **Epidermal growth factor receptor inhibitors in clinical development.** *Int J Radiat Oncol Biol Phys* 2004, **58:**1003-7. Review
9. Harari PM: **Epidermal growth factor receptor inhibition strategies in oncology.** *Endocr Relat Cancer* 2004, **11:**689-708.
10. Metro G, Finocchiaro G, Toschi L, Bartolini S, Magrini E, Cancellieri A, Trisolini R, Castaldini L, Tallini G, Crino L, Cappuzzo F: **Epidermal growth factor receptor (EGFR) targeted therapies in non-small cell lung cancer (NSCLC).** *Rev Recent Clin Trials* 2006, **1:**1-13. Review
11. Giaccone G: **HER1/EGFR-targeted agents: predicting the future for patients with unpredictable outcomes to therapy.** *Ann Onc* 2005, **16:**538-548.
12. Huang SF, Liu HP, Li LH, Ku YC, Fu YN, Tsai HY, Chen YT, Lin YF, Chang WC, Kuo HP, Wu YC, Chen YR, Tsai SF: **High frequency of epidermal growth factor receptor mutations with complex patterns in non-small cell lung cancers related to gefitinib responsiveness in Taiwan.** *Clin Cancer Res* 2004, **10:**8195-203.
13. Valentini AM, Pirrelli M, Caruso ML: **EGFR-targeted therapy in colorectal cancer: does immunohistochemistry deserve a role in predicting the response to cetuximab?** *Curr Opin Mol Ther* 2008, **10:**124-31.
14. Berzofsky JA, Terabe M, Oh S, Belyakov IM, Ahlers JD, Janik JE, Morris JC: **Progress on new vaccine strategies for the immunotherapy and prevention of cancer.** *J Clin Invest* 2004, **113:**1515-25. Review
15. Choo AY, Choo DK, Kim JJ, Weiner DB: **DNA vaccination in immunotherapy of cancer.** *Cancer Treat Res* 2005, **123:**137-56. Review
16. Lin CC, Chou CW, Shiau AL, Tu CF, Ko TM, Chen YL, Yang BC, Tao MH, Lai MD: **Therapeutic HER2/Neu DNA vaccine inhibits mouse tumor naturally overexpressing endogenous neu.** *Mol Ther* 2004, **10:**290-301.
17. Curcio C, Di Carlo E, Clynes R, Smyth MJ, Boggio K, Quaglino E, Spadaro M, Colombo MP, Amici A, Lollini PL, Musiani P, Forni G: **Non-redundant roles of antibody, cytokines, and perforin in the eradication of established Her-2/neu carcinomas.** *J Clin Invest* 2003, **111:**1161-70.
18. Lu Y, Wei YQ, Tian L, Zhao X, Yang L, Hu B, Kan B, Wen YJ, Liu F, Deng HX, Li J, Mao YQ, Lei S, Huang MJ, Peng F, Jiang Y, Zhou H, Zhou LQ, Luo F: **Immunogene therapy of tumors with vaccine based on xenogeneic epidermal growth factor receptor.** *J Immunol* 2003, **170:**3162-70.
19. Pertmer TM, Eisenbraun MD, McCabe D, Prayaga SK, Fuller DH, Haynes JR: **Gene gun-based nucleic acid immunization: elicitation of humoral and cytotoxic T lymphocyte responses following epidermal delivery of nanogram quantities of DNA.** *Vaccine* 1995, **13:**1427-1430.
20. Barry MA, Johnston SA: **Biological features of genetic immunization.** *Vaccine* 1997, **15:**788-791.
21. Feltquate DM, Heaney S, Webster RG, Robinson HL: **Different T helper cell types and antibody isotypes generated by saline and gene gun DNA immunization.** *J Immunol* 1997, **158:**2278-84.
22. Lin CC, Yen MC, Lin CM, Huang SS, Yang HJ, Chow NH, Lai MD: **Delivery of noncarrier naked DNA vaccine into the skin by supersonic flow induces a polarized T helper type 1 immune response to cancer.** *J Gene Med* 2008, **10:**679-89.
23. Duś D, Budzyński W, Radzikowski C: **LL2 cell line derived from transplantable murine Lewis lung carcinoma – maintenance in vitro and growth characteristics.** *Arch Immunol Ther Exp (Warsz)* 1985, **33:**817-23.
24. Wyatt LS, Earl PL, Eller LA, Moss B: **Highly attenuated smallpox vaccine protects mice with and without immune deficiencies against pathogenic vaccinia virus challenge.** *Proc Natl Acad Sci USA* 2004, **101:**4590-4595.
25. Robinson HL, Torres CA: **DNA vaccine.** *Semin Immunol* 1997, **9:**271-283.
26. Condon C, Watkins SC, Celluzzi CM, Thompson K, Falo LD Jr: **DNA-based immunization by in vivo transfection of dendritic cells.** *Nat Med* 1996, **2:**1122-1128.
27. Boyle CM, Morin M, Webster RG, Robinson HL: **Role of different lymphoid tissues in the initiation and maintenance of DNA-raised antibody responses to the influenza virus H1 glycoprotein.** *J Virol* 1996, **70:**9074-9078.
28. Winegar RA, Monforte JA, Suing KD, O'Loughlin KG, Rudd CJ, MacGregor JT: **Determination of tissue distribution of an intramuscular plasmid vaccine using PCR and in situ DNA hybridization.** *Hum Gene Ther* 1996, **7:**2185-2194.

PMMA particle-mediated DNA vaccine for cervical cancer

Pei-Jen Lou,[1] Wen-Fang Cheng,[2] Yi-Chen Chung,[3] Che-Yuan Cheng,[4] Lien-Hua Chiu,[5] Tai-Horng Young[3,4]
[1]*Department of Otolaryngology, National Taiwan University Hospital and National Taiwan University College of Medicine, Taipei 100, Taiwan*
[2]*Graduate Institute of Clinical Medicine, College of Medicine, National Taiwan University, Taipei 100, Taiwan*
[3]*Institute of Polymer Science and Engineering, National Taiwan University, Taipei 106, Taiwan*
[4]*Institute of Biomedical Engineering, College of Medicine and College of Engineering, National Taiwan University, Taipei 100, Taiwan*
[5]*Department of Textile Technology and Product Development, Taiwan Textile Research Institute, Taipei Hsien 236, Taiwan*

Received 18 June 2007; revised 22 November 2007; accepted 30 November 2007
Published online 20 March 2008 in Wiley InterScience (www.interscience.wiley.com). DOI: 10.1002/jbm.a.31919

Abstract: DNA vaccination is a novel immunization strategy that possesses many potential advantages over other vaccine strategies. One of the major difficulties hindering the clinical application of DNA vaccination is the relative poor immunogenicity of DNA vaccines. Poly(methyl methacrylate) (PMMA) is a synthetic polymer approved by the Food and Drug Administration for certain human clinical applications such as the bone cement. *In vivo*, PMMA particles are phagocytosable and have the potential to initiate strong immune responses by stimulating the production of inflammatory cytokines. In this study, we synthesized a series of PMMA particles (PMMA 1–5) with different particle sizes and surface charges to test the feasibility of implementing such polymer particles for DNA vaccination. To our knowledge, this is the first report to show that the gene gun can deliver DNA vaccine by propelling PMMA particles mixed with plasmid DNA for cervical cancer. It was found that PMMA 4 particles (particle size: 460 ± 160 nm, surface charge: +11.5 ± 1.8 mV) stimulated the highest level of TNF-α production by macrophages *in vitro* and yielded the best result of antitumor protection *in vivo*. Therefore, our results possess the potential for translation and implementation of polymer particles in gene gun delivering DNA vaccination. © 2008 Wiley Periodicals, Inc. J Biomed Mater Res 88A: 849–857, 2009

Key words: poly(methyl methacrylate) (PMMA) particles; DNA vaccine; gene gun; cervical cancer

INTRODUCTION

Cancer vaccine targeting tumor antigens has attracted much attention in recent years because of its higher specificity and less toxicity than traditional modalities such as radiotherapy and chemotherapy.[1] Among the various vaccine strategies currently being investigated, DNA vaccination possesses many potential advantages over other vaccine strategies and its efficacy has been successfully observed in murine settings.[2] DNA vaccines employ genes encoding proteins of interest, rather than using the proteins themselves and represent a novel means of expressing antigens *in vivo* for producing both humoral and cellular immune responses.[3,4] Several measures have been used to deliver DNA vaccines, including the intramuscular and the intradermal routes. The former uses conventional needle/syringe for immunization, whereas the latter employs a gene gun to propel gold particles coated with DNA into the epidermis.[5] Generally, gold particle-mediated epidermal delivery of DNA vaccines is based on the acceleration of DNA-coated gold directly into the cytoplasm of antigen-presenting cells (APCs) in the epidermis, resulting in antigen presentation via direct transfection and cross-priming mechanisms.[5] Only a low DNA dose and a small number of cells are needed for transfection to elicit humoral, cellular, and memory responses.[5]

Despite extensive studies of DNA vaccination using gold particles, it is unclear whether we can use the gene gun to propel polymer particles instead of gold particles to deliver DNA vaccine. Therefore, the purpose of this study is to assess the feasibility of using the gene gun to propel poly(methyl methacrylate) (PMMA) particles to deliver DNA vaccine

Correspondence to: T.-H. Young; e-mail: thyoung@ha.mc.ntu.edu.tw
Contract grant sponsor: National Science Council of the Republic of China

for cervical cancer. PMMA, one of the few synthetic polymers approved by the Food and Drug Administration (FDA) for human clinical applications, has been used successfully in bone cements to fix total joint prostheses for a number of years. In cemented implants, wear debris particles have been isolated from periprosthetic tissues during revision surgery and found to be less than 3 μm.[6] A number of studies have investigated the cytokine secretion by macrophages when PMMA particles are phagocytosed.[7–9] *In vivo*, these particles have the potential to initiate strong immune responses by stimulating the production of inflammatory cytokines, such as tumor necrosis factor alpha (TNF-α) and interleukin-6 (IL-6), by macrophages.[10–12] Local cellular and tissue response to the wear cement particles have thought to play an important role in determining the survival of orthopedic implants.[10–12]

Although the efficacy of DNA vaccine has been successfully observed in murine settings, DNA vaccination within human systems has achieved little success because of the inability of DNA vaccines to elicit robust immune responses during the course of early clinical trials.[13,14] PMMA particles from orthopedic joint implants have been postulated to initiate cellular and tissue responses[7–12]; thus, it is reasonable to assume these events are advantageous for PMMA particles to mediate the host immune responses of DNA vaccine. To test this hypothesis, we performed an *in vivo* tumor protection experiment using a previously characterized cervical cancer animal model and vaccination strategy.[15] PMMA particles were coupled with a DNA vaccine encoding calreticulin and HPV-16 E7 (CRT-E7) to test the tumor protection effects against TC-1 cells that express the HPV-16 E7 oncoprotein.[15] Furthermore, the murine macrophage cell line J774A.1 was used to examine the effects of PMMA particles alone or with CRT-E7 DNA, for the production of inflammatory cytokines. Our results showed that different sizes and surface charges of PMMA particles have different capabilities to stimulate the production of inflammatory cytokines. When coupled with the CRT-E7 DNA, PMMA 4 (particle size: 460 ± 160 nm; surface charge: +11.5 ± 1.8 mV) particles stimulated the highest level of TNF-α production and yielded the best results of tumor protection.

MATERIALS AND METHODS

Preparation and characterization of PMMA particles

In this work, five PMMA particles were prepared by changing the emulsion process, identified by the numbers 1–5. PMMA 1 and 2 particles were prepared by emulsion polymerization of methyl methacrylate (MMA, Acros), using sodium dodecyl sulfate (SDS, Wako) as an emulsifier. The recipe for PMMA 1 and 2 particles was 5.1 g of MMA, 0.14 g of initiator, 10 g of SDS, and 100 g of water. PMMA 3 and 4 particles were prepared in the absence of emulsifier. The recipe for PMMA 3 and 4 particles was 10.9 g of MMA, 0.08 g of initiator, and 100 g of water. First, the reaction mixture without initiator was heated to 60°C under nitrogen atmosphere, stirred at a speed of 300 rpm. Subsequently, the initiator, anionic potassium persulfate (Aldrich) for PMMA 1 and 3 particles, and cationic 2, 2-azobis (2-methyl propionamide) dihydrochloride (Acros) for PMMA 2 and 4 particles was added. Polymerization was allowed to proceed for 1 h at 60°C, stirred continuously at 300 rpm with nitrogen gas passed continuously through the reactor. These particles were purified by dialysis using Spectra/Pro molecular porous membrane tubing (molecular weight cutoff: 8000, Spectrum Laboratories) for 1 week. PMMA 5 particles were prepared by dropwise addition of 0.01 mg/mL PMMA (ChiMei CM-211) solution in dimethyl sulfoxide (DMSO, Acros) into water, stirred at a speed of 300 rpm. After 10 min of stirring, larger particles with the micron-size range was obtained by free precipitation.

The morphology of the produced PMMA particles was observed by using a JOEL-JEM 1230 transmission electron microscope (TEM). The average size of particles was obtained from measurements using a Coulter counter N4-PLUS. The surface charge of particles was determined by the measurement of zeta potential using a Zetasizer 3000 HS (Malvern Instruments) based on the laser-Doppler microelectrophoresis.

Gel retardation assays

The generation of pcDNA3-CRT-E7 has been described previously.[15] Plasmid constructs were confirmed by DNA sequencing.

PMMA/CRT-E7 DNA complexes were prepared in Hank's buffered saline (HBS) by mixing 0.675 mg of PMMA particles with 2 μg of CRT-E7 DNA. After 30-min incubation at room temperature for complex formation, the samples were electrophoresed on a 0.8% (w/v) agarose gel containing ethidium bromide (0.5 μg/mL in the gel) and analyzed with an UV illuminator.

Cell culture

The murine macrophage cell line J774A.1 (ATCC, Rockville, MD) was maintained in Dulbecco's modified Eagle's medium (DMEM) supplemented with 10% fetal calf serum (Gibco-RBL Life Technologies, Paisley, UK) and antibiotic/antimycotic (penicillin G sodium 100 U/mL, streptomycin 100 μg/mL, amphotericin B 0.25 μg/mL, Gibco-BRL Life Technologies, Paisley, UK). J774A.1 cells were trypsinized using 0.2% trypsin and 0.2% ethylenediaminetetraacetic acid for 5 min, centrifuged at 1500 rpm for 5 min, and resuspended in the medium.

The metabolic activity of cells was determined by the MTT [3-(4,5-dimethylthiazol-2-yl)-diphenyl tetrazolium

bromide, Sigma] colorimetric assay.[16] To enhance the response of J774A.1 cells to PMMA particles and plasmid DNA, 2×10^4 J774A.1 cells were exposed to PMMA particles (3.375 mg) or PMMA (3.375 mg)/CRT-E7 DNA (10 μg) complexes in 24-well tissue culture polystyrene plates (Costar, USA). Untreated cells were used as a control group. After culturing in a humidified atmosphere with 5% CO_2 at 37°C for 7 days, the culture medium was removed and the cells were incubated with 0.1 mL of MTT solution (2 mg/mL in phosphate-buffered saline) for 3 h at 37°C. Subsequently, the MTT solution was aspirated and the formazan reaction products were dissolved in DMSO and shaken for 20 min. The optical density of the formazan solution was read on an ELISA plate reader (ELx 800, BIO-TEK) at 570 nm.

DNA vaccination and *in vivo* tumor protection experiments

PMMA/CRT-E7 DNA complexes were prepared by incubating 0.675 mg of PMMA particles with 2 μg of plasmid DNA in HBS for 30 min at room temperature. Subsequently, the complexes of PMMA particles and plasmid DNA were delivered to the shaved abdominal region of C57BL/6 mice (five per group) using a helium-driven gene gun (BioWare Technologies, Taipei, Taiwan) as described previously.[15] One week later, mice were boosted with the same regimen as the second vaccination. One week after the last vaccination, mice were subcutaneously challenged with 5×10^4 TC-1 cells/mouse in the right leg. Mice were monitored for evidence of tumor growth by palpation and inspection twice a week until they were sacrificed at day 60.

Cytokine assay

For determination of cytokine release of J774A.1 cells after exposure to PMMA particles and CRT-E7 DNA, 1 mL medium of cell suspension (2×10^4 cells) plus PMMA particles (3.375 mg) or PMMA (3.375 mg)/CRT-E7 (10 μg) complexes were cultured in 24-well tissue culture polystyrene plates. Untreated cells were used as a control group. After incubation for 1 day, the supernatant was harvested and the cytokines (IL-6 and TNF-α) released by cells into the media were measured by ELISA following the manufacturer's protocol (Endogen, Boston, MA).

Cell transfection

J774A.1 and HeLa cells were transfected using PMMA particles or polyethyleneimine (PEI) reagent (ExGen500, Fermentas) as the DNA vector. Plasmid pEGFP-N1 (Clontech), containing the cDNA for enhanced green fluorescent protein (EGFP) under the control of the cytomegalovirus promoter, was used for the tests of transfection. Briefly, cells were seeded onto 24-well tissue culture polystyrene plates at 5×10^4 cells/well and incubated at 37°C in 5% CO_2 for 24 h. Subsequently, EGFP DNA (1 μg) mixed with the PMMA particles (0.337 mg) or PEI reagent (3.3 μL) was added into the culture wells for transfection, which were incubated at 37°C in 5% CO_2 for 24 h. The EGFP expression was assessed using a fluorescent microscope (Axiovert 100TV, ZEISS, USA) equipped with green fluorescent filter set, and cell counts were manually taken (100–200 cells for each treatment group) to determine the percentage of cells displaying EGFP expression.

Statistical analysis

The data of MTT and cytokine assay presented as the mean ± standard deviation are representative of at least four independent experiments. Statistical significance was calculated using one-way analysis of variance followed by Student's t test. In the tumor protection experiment, the principal outcome of interest was time to development of tumor. The event time distributions for different mice were compared by Kaplan and Meier and by log-rank analyses.

RESULTS

Particle size and surface potential

Figure 1 illustrates the morphology of synthesized PMMA particles from TEM. Excluding PMMA 5, PMMA 1–4 were all quite globular. Table I summarizes the particle sizes and surface charges of different PMMA particles. For PMMA 1 and 2, which were obtained by the emulsion polymerization with SDS surfactant, the average size was about 50 and 150 nm, respectively. On the other hand, emulsifier-free emulsion polymerization yielded a diameter of about 340 and 460 nm for PMMA 3 and 4, respectively. Clearly, the diameter of PMMA particles was significantly reduced from >300 nm without a surfactant to <200 nm upon the addition of SDS during the polymerization. For PMMA 5, which was prepared by dropwise addition of PMMA solution into water, the particle size was in the micron range. Table I also shows the surface charge, determined by the measurement of zeta potential, of prepared PMMA particles. Reasonably, PMMA 1, 3, and 5, prepared from anionic initiators, exhibited a negative zeta potential, whereas PMMA 2 and 4, prepared from cationic initiators, exhibited a positive zeta potential.

Gel retardation of PMMA/CRT-E7 DNA complexes

Two micrograms of CRT-E7 was incubated with equivalent weight of various PMMA particles and the formation of stable PMMA/plasmid DNA complexes was checked by the gel retardation assay. As shown in Figure 2, PMMA 4 could retard the

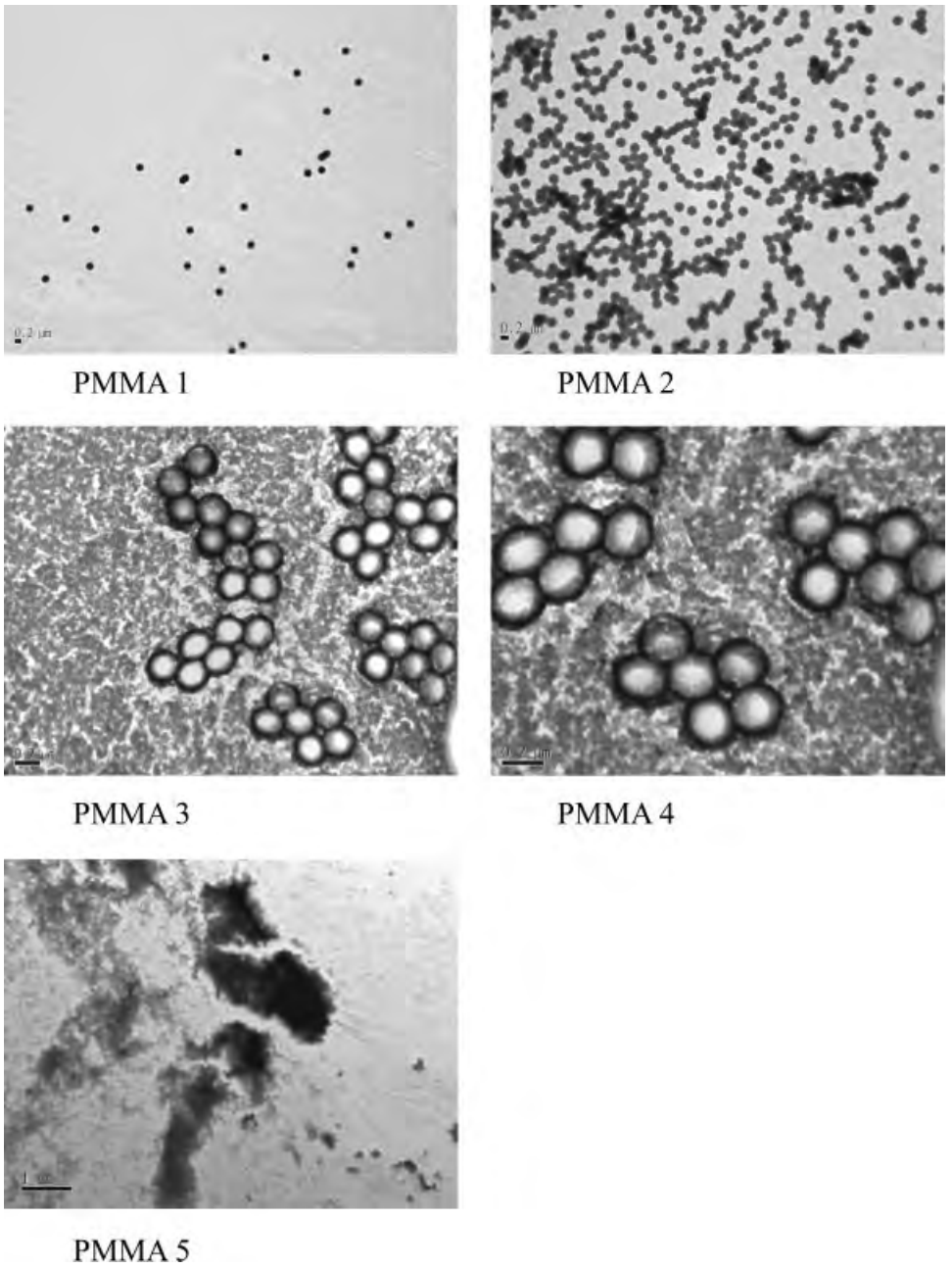

Figure 1. TEM photographs of PMMA particles: PMMA 1, PMMA 2, PMMA 3, PMMA 4, and PMMA 5.

migration of CRT-E7 DNA completely whereas other PMMA particles failed to do so. This result indicates that the PMMA 4 may form the most stable complex with plasmid DNA when compared with the other PMMA particles under such experimental conditions.

MTT assay

To investigate if PMMA particles and PMMA/CRT-E7 DNA complexes affect the survival of J774A.1 cells, 3.375 mg of PMMA particles without or with 10 μg of CRT-E7 DNA were incubated with 2×10^4 J774A.1 cells for 7 days and then assayed the cells' metabolic activity by the MTT test. Control

TABLE I
Size and Surface Charge of Synthesized PMMA Particles

	Particle Size (nm)	Surface Charge (mV)
PMMA 1	50 ± 14	−30.6 ± 4.5
PMMA 2	150 ± 15	+10.5 ± 1.9
PMMA 3	340 ± 80	−37.3 ± 2.2
PMMA 4	460 ± 160	+11.5 ± 1.8
PMMA 5	1000 ± 250	−28.7 ± 3.1

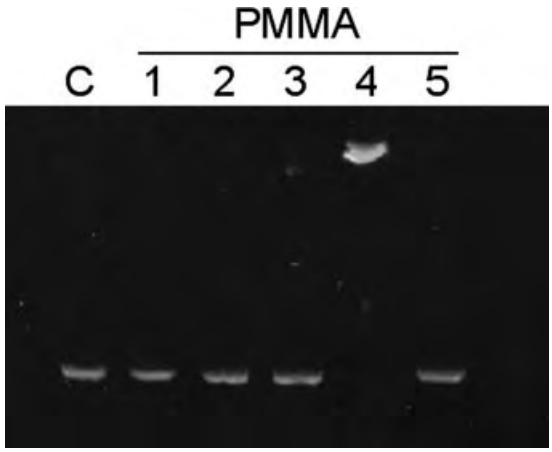

Figure 2. Gel retardation of PMMA/CRT-E7 DNA complexes. C: plasmid DNA only.

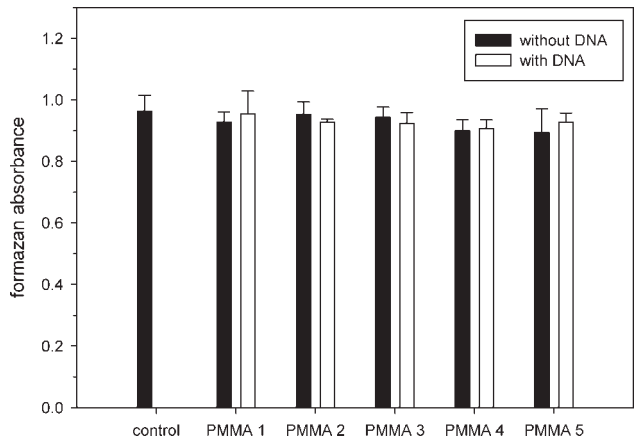

Figure 3. The metabolic activity, determined by the MTT assay, of J774A.1 cells exposed to PMMA particles without and with CRT-E7 DNA after incubation for 7 days. Data are presented as mean ± standard deviation ($n = 6$). Statistical significance was calculated using one way analysis of variance (ANOVA) followed by Student's t test ($p < 0.05$ was considered significant).

cells were cultivated without adding PMMA particles and DNA. As shown in Figure 3, the mean formazan absorbance obtained was comparable for all prepared PMMA particles and was not significantly different from the control cell population, regardless of the presence or absence of CRT-E7 DNA. When MTT assay was measured for 1 and 3 days of incubation, it also showed the similar result (not shown here). This indicated that the PMMA particles, even in the presence of CRT-E7 DNA, did not affect the survival of J774A.1 cells.

In vivo tumor protection

To assess the feasibility of using the gene gun to propel prepared PMMA particles to deliver DNA vaccine, we performed an *in vivo* tumor protection experiment using a previously characterized tumor model and vaccination strategy.[15] All of the mice without treatment developed tumors within 10 days after tumor challenge (data not shown). Similarly, mice only receiving PMMA particles also developed tumors within 10 days after tumor challenge, indicating PMMA itself did not show an antitumor effect (data not shown). Figure 4 shows that 20% of the mice receiving CRT-E7 DNA alone or PMMA 5/CRT-E7 DNA complex vaccination, and 40% of the mice receiving either PMMA 1/, PMMA 2/, or PMMA 3/CRT-E7 DNA complex vaccination remained tumor-free 60 days after TC-1 challenge. The best result was observed in mice vaccinated with the PMMA 4/CRT-E7 DNA complex. Sixty percent of the mice were still tumor-free at the end of this study, which was significantly better than the control group ($p = 0.0027$).[15] The operating parameters used in the gene gun of this study were for the delivery of gold particles. Therefore, better tumor protection effects are anticipated if appropriate operating parameters for PMMA particles are developed. As shown in Figure 4, the protection rate can be up to 100% by using gold particle-mediated DNA vaccination, which is consistent with the result of the previously characterized cervical cancer animal model.[15]

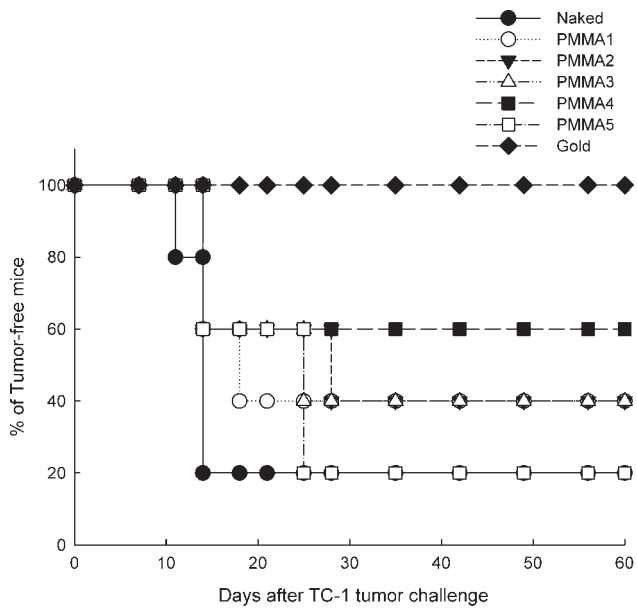

Figure 4. *In vivo* tumor protection experiments in mice vaccinated with various DNA vaccines. Mice were immunized with naked DNA alone, PMMA 1–5/plasmid DNA, and gold/plasmid DNA (five per group) as indicated and challenged as described in the "Materials and Methods" section to assess the antitumor effect generated by each DNA vaccine. The Kaplan–Meier product-limit method for survival was assessed for significance using the log-rank test.

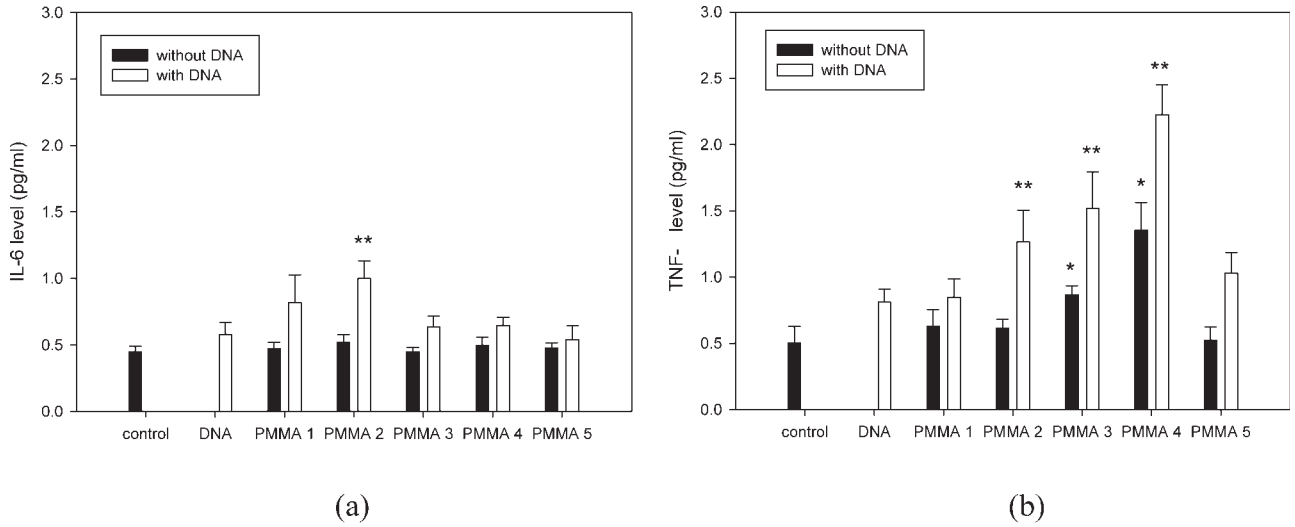

Figure 5. The level of IL-6 (a) and TNF-α (b) released by J774A.1 cells exposed to PMMA particles without and with CRT-E7 DNA after incubation for 1 day. Data are presented as mean ± standard deviation ($n = 4$). Asterisk and double asterisks denote significant differences of $p < 0.05$ and $p < 0.01$ of the cytokine release compared with control cells, respectively, which were calculated using one-way analysis of variance (ANOVA) followed by Student's t test.

Cytokine production

We next investigated the release of inflammatory cytokines TNF-α and IL-6 by J774A.1 cells to gain further insights as to how PMMA particles and PMMA/CRT-E7 DNA complexes were involved in regulating the immune responses. We still used 3.375 mg of PMMA particles and 10 μg of plasmid DNA, five times the concentrations of *in vivo* tumor protection tests were added, to enhance the response of J774A.1 cells. As shown in Figure 5(a), all PMMA particles tested in this study did not induce significant IL-6 release by J774A.1 cells in the absence of CRT-E7 DNA. However, in the presence of CRT-E7 DNA, PMMA 2 significantly increased the level of IL-6 secretion by J774A.1 cells when compared with control cells ($p < 0.01$). On the contrary, Figure 5(b) shows PMMA 3 and PMMA 4 significantly induced the TNF-α secretion by J774A.1 cells even in the absence of CRT-E7 DNA, compared with control cells ($p < 0.05$). After coupling with CRT-E7 DNA, the levels of TNF-α in the culture supernatants of PMMA 2/, PMMA 3/, and PMMA 4/CRT-E7 DNA complexes treated cells were significantly higher than the control cells ($p < 0.01$). In this study, PMMA 4/CRT-E7 DNA complex was the most potent inducer of TNF-α secretion by J774A.1 cells.

Transfection of macrophages

Taken together, our data showed that the combination of PMMA 4 particles and CRT-E7 DNA had the best tumor protection effect to augment the host immune responses, but we did not know whether PMMA 4/plasmid DNA complexes could be taken up into macrophages and expressed. To assess this possibility, we used another plasmid DNA encoding EGFP to complex with PMMA 4 particles to transfect J774A.1 macrophages. For comparison, another nonviral vector PEI with superior transfection performance and another cell type HeLa cells with good transfection activity were used in this study. Figure 6 shows J774A.1 macrophages were very resistant to transfection that could be ascribed to EGFP expression, regardless of using PMMA 4 particle or PEI reagent to complex with EGFP DNA. After 24 h of transfection, we could not observe any cells showing

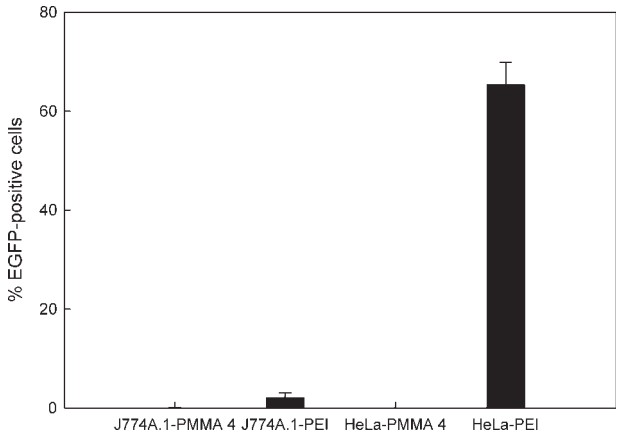

Figure 6. Transfection of J774A.1 macrophages and HeLa cells with EGFP DNA using PMMA 4 particles and PEI reagent as the DNA vector. The assessment of EGFP expression using a fluorescent microscope equipped with green fluorescent filter set, and cell counts were manually taken (100–200 cells) from three independent wells to determine the percentage of cells displaying EGFP expression.

EGFP fluorescence using PMMA 4 particles and only a small fraction (<3%) of transfected cells were found using PEI. In contrast, we could observe obvious EGFP fluorescence of HeLa cells using PEI reagent. However, PMMA 4 still had no detectable gene transfer activity in HeLa cells. These results suggested that PMMA 4 particles were not a potent DNA delivery vehicle in gene transfection. In addition, compared with that HeLa cells could be transfected using PEI reagent, J774A.1 macrophages exhibited very low transfection efficiency, which was in agreement with previous reports.[17,18]

DISCUSSION

Currently, DNA vaccines have been safely administered in several human studies. Intramuscular injection and transdermal particle bombardment are the two routes commonly used for DNA vaccination. Intramuscular injection results in plasmid DNA uptake by myocytes, which present antigen through MHC-I pathways.[19] However, the efficiency of transfection is probably low, because the requirement for cellular uptake of DNA and myocytes do not promote costimulatory molecules to function as efficient APCs. Unlike vaccination by intramuscular injection of DNA, vaccination by particle bombardment transfects cells of the epidermis and dermis by direct deposition of DNA-coated particles. The skin is a rich source of somatic cells such as keratinocytes and fibroblasts as well as potent bone-marrow-derived APCs such as Langerhans cells, the resident "professional APCs" of the skin. These APCs are directly transfected and then migrate to the draining lymph nodes.[20] It has been proposed that this mechanism is the predominant means of priming cytotoxic T-lymphocytes of using gene gun to deliver DNA vaccine into the epidermis and dermis.[21]

Gold particles are the most extensively used in gene gun to accelerate DNA vaccines into the cytoplasm of cells, facilitating DNA delivery and gene expression. In this study, we tried to use gene gun to propel PMMA particles to deliver DNA vaccine. A series of PMMA particles with different particle size and surface charge were prepared. The concentrations of PMMA particles used in our *in vitro* studies were not toxic to mouse J774A.1 cells. Although such particle concentrations were five times higher than the concentrations used in our *in vivo* studies, we still were not sure if the particle concentrations in our *in vivo* studies would have any detrimental effects to the mice. Nevertheless, PMMA is a biomaterial that has already been widely used in orthopedic implant devices. Furthermore, PMMA nanoparticles have been used for DNA vaccination by the route of intramuscular injection and already been shown to be nontoxic for the cells and well tolerated *in vivo*.[22–28] It might be argued that PMMA particle preparation was not a new technique, but, to our knowledge, this is the first report to show that the gene gun can deliver DNA vaccine by propelling PMMA particles mixed with DNA. The best result was PMMA 4 particles with the size of 460 ± 160 nm and surface charge of 11.5 ± 1.8 mV. Sixty percent of the vaccinated mice were still tumor-free 60 days after the tumor challenge. It is noted that the protection rate can be up to 100% by using gold particle-mediated DNA vaccination. As mentioned earlier, the operating parameters for the delivery of PMMA particles used in the gene gun were for gold particles. Therefore, better tumor protection effects are anticipated if appropriate operating parameters for PMMA particles are developed.

Because of the relatively poor immunogenicity of DNA in humans, several strategies have been employed to improve the immunogenicity of DNA vaccines. Among them, the use of adjuvants (e.g., aluminum salts, cytokines, lipopolysaccharide) alongside DNA immunization is effective in enhancing the level of immune response to a target antigen.[1,5] Adjuvants serve to activate innate immune cell subsets in order to better promote adaptive immunity through T-cell interaction. In this study, we took advantage of the proinflammatory cytokine inducing effects of PMMA particles and test if this property of PMMA could serve it as an effective adjuvant in DNA vaccination. As shown in Figure 5(b), TNF-α production by macrophages was significantly increased when the cells were treated with PMMA 3 and PMMA 4 particles. Coupling with CRT-E7 DNA seemed to increase the TNF-α-stimulating effects of all PMMA particles, although in PMMA 1 and PMMA 5 the difference did not reach statistical significance. PMMA 4/CRT-E7 DNA complexes induced the highest level of TNF-α production by mouse macrophage cells [Fig. 5(b)] and the best tumor protection effects *in vivo* (Fig. 4). It is known that TNF-α can promote antibody-dependent cytotoxicity and upregulate the expression of MHC class II molecules.[29] Thus, in this study, PMMA particles serve as a potent adjuvant to enhance host immune responses. In addition to the TNF-α, IL-6 is another potent proinflammatory cytokine that has been involved in a wide spectrum of biological events. However, overproduction of IL-6 may have detrimental effects to DNA vaccination because IL-6 suppresses MHC-II expression on dendritic cells and attenuates T-cell activation.[30] Our results showed that, except for the PMMA 2/CRT-E7 DNA complexes, PMMA particles and other PMMA/CRT-E7 DNA complexes did not induce significant IL-6 production by mouse macrophage cells [Fig. 5(a)]. This

might be another potential advantage of using PMMA particles as adjuvants for DNA vaccination. In fact, PMMA, in the form of nanoparticles, has recently been shown to be very attractive as an adjuvant in protein and DNA vaccine applications.[22–26] Therefore, phagocytic uptake of the PMMA/CRT-E7 DNA complexes by macrophages with subsequent production of cytokines such as TNF-α shown in this study might play an adjuvant role in enhancing the immune responses toward the target antigen.

It is known that both direct transfection of epidermal APCs and cross-priming mechanisms that occur between APCs and macrophages are involved in the generation of antitumor immunity in gold particle-mediated epidermal delivery of DNA vaccines.[5] In addition to the direct transfection of DNA to APCs by using the gene gun, it may be possible to increase delivery of DNA to APCs by using a particulate formulation of DNA because of the nonspecifically phagocytic capacity of such cells. In support of this hypothesis, Singh and coworkers showed that intramuscular injection of poly(lactide-*co*-glycolide) microspheres of about 1 μm diameter with surface-adsorbed DNA substantially induced higher levels of immune responses compared with that of naked DNA.[31] Theoretically, the PMMA 4/EGFP DNA complexes can be easily phagocytosed by macrophages.[7–9] However, Figure 6 shows that PMMA 4 particle-mediated transfection on macrophages was not satisfactory. Therefore, the observed tumor protection in this study might not due to phagocytic uptake of DNA with subsequent transfection of target antigen by the macrophages. The mechanism for PMMA particle-mediated DNA vaccine in suppressing cervical cancer is not clear at this time. It is postulated that the increased cytokine production after phagocytic uptake of the PMMA/CRT-E7 DNA complexes by macrophages [Fig. 5(b)] might improve the "cross-priming" effects that occur through the crosstalk between macrophages and professional APCs. Direct delivery of PMMA/CRT-E7 DNA complexes into professional APCs through the gene gun is another possible explanation for the observed tumor protection effects in this study.

CONCLUSION

A series of PMMA particles (PMMA 1–5) were synthesized in this study for a DNA vaccination study. It was found that PMMA particles with different sizes and surface charges could result in different tumor protection effects. Among them, PMMA 4 particles (particle size: 460 ± 160 nm; surface charge: +11.5 ± 1.8 mV) stimulated the highest level of TNF-α production by macrophages *in vitro* and yielded the best results of tumor protection *in vivo*. Although the underlying mechanism remains elusive, our results possess the potential for great translation and implementation of polymer particles in DNA vaccination because the safety of many polymer biomaterials has been approved by the FDA.

References

1. Berzofsky JA, Terabe M, Oh SK, Belyakov IM, Ahlers JD, Janik JE, Morris JC. Progress on new vaccine strategies for the immunotherapy and prevention of cancer. J Clin Invest 2004;113:1515–1525.
2. Weiner DB, Kennedy RC. Genetic vaccines. Sci Am 1999; 281:50–57.
3. Donnelly JJ, Ulmer JB, Shiver JW, Liu MA. DNA vaccines. Annu Rev Immunol 1997;15:617–648.
4. Gurunathan S, Klinman DM, Seder RA. DNA vaccines: Immunology, application, and optimization. Annu Rev Immunol 2000;18:927–974.
5. Dean HJ, Haynes J, Schmaljohn C. The role of particle-mediated DNA vaccines in biodefense preparedness. Adv Drug Deliv Rev 2005;57:1315–1342.
6. Maloney WJ, Smith RL, Schmalzried TP, Chiba J, Huene D, Rubash H. Isolation and characterization of wear particles generated in patients who have had failure of a hip arthroplasty without cement. J Bone Joint Surg Am 1995;77:1301–1310.
7. Gelb H, Schumacher HR, Cuckler J, Ducheyne P, Baker DG. In vivo inflammatory response to polymethylmethacrylate particulate debris: Effect of size, morphology and surface area. J Orthop Res 1994;12:83–92.
8. Gonzalez O, Smith RL, Goodman SB. Effect of size, concentration, surface area, and volume of Polymethylmethacrylate particles on human macrophages in vitro. J Biomed Mater Res 1996;30:463–473.
9. Prabhu A, Shelburne CE, Gibbons DF. Cellular proliferation and cytokine responses of murine macrophage cell line J774A.1 to polymethylmethacrylate and cobalt–chrome alloy particles. J Biomed Mater Res 1998;42:655–663.
10. Lohmann CH, Dean DD, Köster G, Casasola D, Buchhorn GH, Fink U, Schwartz Z, Boyan BD. Ceramic and PMMA particles differentially affect osteoblast phenotype. Biomaterials 2002;23:1855–1863.
11. Haynes DR, Hay SJ, Rogers SD, Ohta S, Howie DW, Graves SH. Regulation of bone cells by particle-activated mononuclear phagocytes. J Bone Joint Surg Br 1997;79:988–994.
12. Haynes DR, Rogers SD, Hay S, Pearcy MJ, Howie DW. The differences in toxicity and release of bone-resorbing mediators induced by titanium and cobalt-chromium-alloy wear particles. J Bone Joint Surg Am 1993;75:825–834.
13. Rosenberg SA, Yang JC, Sherry RM, Hwu P, Topalian SL, Schwartzentruber DJ, Restifo NP, Haworth LR, Seipp CA, Freezer LJ, Morton KE, Mavroukakis SA, White DE. Inability to immunize patients with metastatic melanoma using plasmid DNA encoding the gp100 melanoma-melanocyte antigen. Hum Gene Ther 2003;14:709–714.
14. Triozzi PL, Aldrich W, Allen KO, Carlisle RR, LoBuglio AF, Conry RM. Phase I study of a plasmid DNA vaccine encoding MART-1 in patients with resected melanoma at risk for relapse. J Immunother 2005;28:382–388.
15. Cheng WF, Hung CF, Chai CY, Hsu KF, He L, Ling M, Wu TC. Tumor-specific immunity and antiangiogenesis generated by a DNA vaccine encoding calreticulin linked to a tumor antigen. J Clin Invest 2001;166:6218–6226.

16. Mosmann T. Rapid colorimetric assay for cellular growth and survival: Application of proliferation and cytotoxicity assays. J Immunol Methods 1983;65:55–63.
17. Kusumawati A, Commes T, Liautard JP, Widada JS. Transfection of myelomonocytic cell lines, cellular response to a lipid-based reagent and electroporation. Anal Biochem 1999;269, 219–221.
18. Arkusz J, Stepnik M, Trzaska D, Dastych J, Rydzynski K. Assessment of usefulness of J774A.1 macrophages for the assay of IL-1b promoter activity. Toxicol In Vitro 2006;20:109–116.
19. Kutzler MA, Weiner DB. Developing DNA vaccines that call to dendritic cells. J Clin Invest 2004;114:1241–1244.
20. Condon C, Watkins SC, Celluzi CM, Thompson K, Falo LD. DNA-based immunization by in vivo transfection of dendritic cells. Nat Med 1996;2:1122–1128.
21. Porgador A, Irvine KR, Iwasaki A, Barber BH, Restifo NP, Germain RN. Predominant role for directly transfected dendritic cells in antigen presentation to CD8+ T cells after gene gun immunization. J Exp Med 1998;188:1075–1082.
22. Castaldello A, Brocca-Cofano E, Voltan R, Triulzi C, Altavilla G, Laus M, Sparnacci K, Ballestri M, Tondelli L, Fortini C, Gavioli R, Ensoli B, Caputo A. DNA prime and protein boost immunization with innovative polymeric cationic core-shell nanoparticles elicits broad immune responses and strongly enhance cellular responses of HIV-1 Tat DNA vaccination. Vaccine 2006;24:5655–5669.
23. Caputo A, Brocca-Cofano E, Castaldello A, De Michele R, Altavilla G, Marchisio M, Gavioli R, Rolen U, Chiarantini L, Cerasi A, Dominici S, Magnani M, Cafaro A, Sparnacci K, Laus M, Tondelli L, Ensoli B. Novel biocompatible anionic polymeric microspheres for the delivery of the HIV-1 Tat protein for vaccine application. Vaccine 2004;22:2910–2924.
24. Shephard MJ, Todd D, Adair BM, Po AL, Mackie DP, Scott EM. Immunogenicity of bovine parainfluenza type 3 virus proteins encapsulated in nanoparticle vaccines, following intranasal administration to mice. Res Vet Sci 2003;74:187–190.
25. Kreuter J. Nanoparticles as adjuvants for vaccines. Pharm Biotechnol 1995;6:463–472.
26. Stieneker F, Lower J, Kreuter J. Different kinetics of the humoral immune response to inactivated HIV-1 and HIV-2 in mice: Modulation by PMMA nanoparticle adjuvant. Vaccine Res 1993;2:111–118.
27. Kreuter J. Physicochemical characterization of nanoparticles and their potential for vaccine preparation. Vaccine Res 1992;1:93–98.
28. Stieneker F, Kreuter J, Lower J. High antibody titres in mice with polymethylmethacrylate nanoparticles as adjuvant for HIV vaccines. AIDS 1991;5:431–435.
29. Sigal LH, Ron YR. Immunology and Inflammation: Basic Mechanism and Clinical Consequences. New York: McGraw-Hill; 1994.
30. Kitamura H, Kamon H, Sawa S, Park SJ, Katunuma N, Ishihara K, Murakami M, Hirano T. IL-6-STAT3 controls intracellular MHC class II alpha beta dimmer level through cathepsin S activity in dendritic cells. Immunity 2005;23:491–502.
31. Singh M, Briones M, Ott G, O'Hagan D. Cationic microparticles: A potent delivery system for DNA vaccines. Proc Natl Acad Sci USA 2000;97:811–816.

Journal of Biomedical Science

BioMed Central

Research

Open Access

Mechanism of inhibitory effect of atorvastatin on resistin expression induced by tumor necrosis factor-α in macrophages

Kou-Gi Shyu[1,2], Su-Kiat Chua[1], Bao-Wai Wang[1] and Peiliang Kuan*[1]

Address: [1]Division of Cardiology, Shin Kong Wu Ho-Su Memorial Hospital, Taipei, Taiwan and [2]Graduate Institute of Clinical Medicine, College of Medicine, Taipei Medical University, Taipei, Taiwan

Email: Kou-Gi Shyu - shyukg@ms12.hinet.net; Su-Kiat Chua - benchua1131@yahoo.com.tw; Bao-Wai Wang - m002018@ms.skh.org.tw; Peiliang Kuan* - t002558@ms.skh.org.tw

* Corresponding author

Published: 27 May 2009

Journal of Biomedical Science 2009, **16**:50 doi:10.1186/1423-0127-16-50

Received: 21 December 2008
Accepted: 27 May 2009

This article is available from: http://www.jbiomedsci.com/content/16/1/50

Abstract

Atorvastatin has been shown to reduce resistin expression in macrophages after pro-inflammatory stimulation. However, the mechanism of reducing resistin expression by atorvastatin is not known. Therefore, we sought to investigate the molecular mechanisms of atorvastatin for reducing resistin expression after proinflammatory cytokine, tumor necrosis factor-α (TNF-α) stimulation in cultured macrophages. Cultured macrophages were obtained from human peripheral blood mononuclear cells. TNF-α stimulation increased resistin protein and mRNA expression and atorvastatin inhibited the induction of resistin by TNF-α. Addition of mevalonate induced resistin protein expression similar to TNF-α stimulation. However, atorvastatin did not have effect on resistin protein expression induced by mevalonate. SP600125 and JNK small interfering RNA (siRNA) completely attenuated the resistin protein expression induced by TNF-α and mevalonate. TNF-α induced phosphorylation of Rac, while atorvastatin and Rac-1 inhibitor inhibited the phosphorylation of Rac induced by TNF-α. The gel shift and promoter activity assay showed that TNF-α increased AP-1-binding activity and resistin promoter activity, while SP600125 and atorvastatin inhibited the AP-1-binding activity and resistin promoter activity induced by TNF-α. Recombinant resistin and TNF-α significantly reduced glucose uptake in cultured macrophages, while atorvastatin reversed the reduced glucose uptake by TNF-α. In conclusion, JNK and Rac pathway mediates the inhibitory effect of atorvastatin on resistin expression induced by TNF-α.

Background

Resistin is an adipocyte-secreted molecule induced during adipocyte differentiation. Recombinant resistin up-regulates cytokines and adhesion molecule expression on human endothelial cells [1,2], suggesting a potential role in atherosclerosis. Resistin has been shown to have potent proinflammatory properties [3]. Resistin promotes endothelial cell activation and causes endothelial dysfunction of porcine coronary arteries [4]. Recently, resistin was found to have a potential role in atherosclerosis because resistin increases MCP-1 and sVCAM-1 expression in vascular endothelial cells and resistin promotes vascular smooth muscle cell proliferation [5,6]. More recently, resistin was found to be secreted from macrophages in atheromas and promotes atherosclerosis [7]. Plasma resistin levels are correlated with markers of inflammation and are predictive of coronary atherosclerosis in humans, independent of plasma C – reactive protein. Resistin may represent a novel link between metabolic signals, inflammation, and atherosclerosis [8].

NSC The cost of publication in *Journal of Biomedical Science* is bourne by the National Science Council, Taiwan.

The 3-hydroxy 3-methyl glutaryl-CoA reductase (HMG-CoA reductase) inhibitors or statins have been proved to reduce inflammation and exert beneficial effects in the prevention of atherosclerosis progression [9]. The pleiotropic effect of statins, independent of their lipid-lowering effects have been described to improve endothelial function, stabilize atheroslerotic plaque, inhibit vascular smooth muscle cell proliferation as well as platelet aggregation, and reduce vascular inflammation [9]. Ichida et al reported that atorvastatin decreases resistin expression in adipocytes and monocytes/macrophages [10]. Atorvastatin decreased resistin mRNA expression in a dose- and time-dependent manner. However, the mechanism of reducing resistin expression by atorvastatin is not known. Therefore, we sought to investigate the molecular mechanisms of atorvastatin for reducing resistin expression after proinflammatory cytokine, TNF-α stimulation in macrophages.

Materials and methods

Drugs

Atorvastatin, a calcium salt of a pentasubstituted pryole, was supplied by Pfizer. A 10-mmole/l stock solution was made in 100% DMSO. Recombinant TNF-α protein and mevalonate were purchased from Sigma; Polyclonal Rac, and polyclonal phospho-Rac1 (Ser71) antibodies from Cell Signaling; Resistin antibody from R&D Systems; Rac 1 inhibitor, PD 98059, SB 203580, and anisomycin from CALBIOCHEM; Resistin siRNA from Invitrogen.

Cell culture

Human peripheral mononuclear cells (PBMCs) were isolated from heparinized whole blood obtained from normal healthy volunteers by Ficoll-Hypaque gradient centrifugation. The cells were washed three times with sterile PBS and resuspended in RPMI 1640 supplemented with 10% fetal calf serum, 2 mmol/l L-glutamate and 1% penicillin/streptomycin. Monocytes were purified from PBMCs by positive selection using anti-CD14 magnetic beads according to the manufacturer's instructions. The cells were cultured for 4 days in RPMI 1640 supplemented with 10% fetal calf serum, 2 mmol/l L-glutamate and 1% penicillin/streptomycin. For experimental use, purified monocytes/macrophages were changed to serum-free RPMI-1640 supplemented with 2 mmol/l L-glutamate and 1% penicillin/streptomycin for 6 h, then treated with either 1 or 10 μmol/l of atorvastatin for 24 and 48 h.

Western blot analysis

Cells were homogenized in modified RIPA buffer. Equal amounts of protein (15 μg) were loaded into a 12.5% SDS-polyacrylamide minigel, followed by electrophoresis. Protein samples were mixed with sample buffer, boiled for 10 min, separated by SDS-PAGE under denaturing conditions, and electroblotted to nitrocellulose membranes. The blots were incubated overnight in Tris-buffered saline (TBS) containing 5% milk to block non-specific binding of the antibody. Proteins of interest were revealed with specific antibodies as indicated (1:1000 dilution) for 1 hour at room temperature followed by incubation with a 1:5000 dilution of horseradish peroxidase-conjugated polyclonal anti-rabbit antibody for 1 h at room temperature. Signals were visualized by chemiluminenescent detection. Equal protein loading of the samples was further verified by staining monoclonal antibody GAPDH. All Western blots were quantified using densitometry.

RNA isolation and reverse transcription

Total RNA was isolated from cultured macrophages using the single-step acid guanidinium thiocyanate/phenol/chloroform extraction method. Total RNA (1μg) was incubated with 200U of Moloney-Murine Leukemia Virus reverse transcriptase in a buffer containing a final concentration of 50 mmol/L TrisCl (pH 8.3), 75 mmol/L KCl, 3 mmol/$MgCl_2$, 20 U of RNase inhibitor, 1 μmol/L polydT oligomer, and 0.5 mmol/L of each dNTP in a final volume of 20 μL. The reaction mixture was incubated at 42°C for 1 h and then at 94°C for 5 min to inactivate the enzyme. A total of 80 μL of diethyl pyrocarbonate treated water was added to the reaction mixture before storage at -70°C.

Real-time PCR

A Lightcycler (Roche Diagnostics, Mannheim, Germany) was used for real-time PCR. cDNA was diluted with nuclease-free water. 2 μL of the solution was used for the Lightcycler SYBR-Green mastermix (Roche Diagnostics): 0.5 μmol/L primer, 5 mmol/L magnesium chloride, and 2 μL Master SYBR-Green in nuclease-free water in a final volume of 20 μL. The primer used for mouse resistin was: forward, 5'-d(GTACCCACGGGATGAAGAACC)-3'; reverse, 5'-d(GCAGACCCACAGGAGCAG)-3'. The primer used for human resistin was: forward, 5'-d(TAAGCAGCATTGGCCTGG)-3'; reverse, 5'-d(CTGTGGCTCGTGGGATGT)-3'. GAPDH: forward, 5'-d(CATCACCATCTTCCAGGAGC)-3'; reverse, 5'-d(GGATGATGTTCTGGGCTGCC)-3'. The initial denaturation phase was 10 min at 95°C followed by an amplification phase as detailed below: denaturation at 95°C for 10 sec; annealing at 55°C for 5 sec; elongation at 72°C for 15 sec and for 30 cycles. Amplification, fluorescence detection, and post-processing calculation were performed using the Lightcycler apparatus. Individual PCR products were analyzed for DNA sequence to confirm the purity of the product.

Electrophoretic mobility shift assay (EMSA)

Nuclear protein concentrations from macrophages were determined by Biorad protein assay. Consensus and control oligonucleotides (Santa Cruz Biotechnology Inc.)

were labeled by polynucleotides kinase incorporation of [γ^{32}P]-ATP. Oligonucleotides sequences included the activating protein 1 (AP-1) consensus 5'-CGCTTGATGACTCAGCCGGAA-3'. The AP-1 mutant oligonucleotides sequences were 5'-CGCTTGATGACTTGGCCGGAA-3'. After the oligonucleotide was radiolabeled, the nuclear extracts (4 μg of protein in 2 μl of nuclear extract) were mixed with 20 pmol of the appropriate [γ^{32}P]-ATP-labeled consensus or mutant oligonucleotide in a total volume of 20 μl for 30 min at room temperature. The samples were then resolved on a 4% polyacrylamide gel. Gels were dried and imaged by autoradiography. Controls were performed in each case with mutant oligonucleotides or cold oligonucleotides to compete with labeled sequences.

Promoter activity assay

A-741 to +22 bp rat resistin promoter construct was generated as follows. Rat genomic DNA was amplified with forward primer (ACGCGTCTCAGCGGTAGAGCTCTTG) and reverse primer (AGATCTGGAGAAATGAAAGGTTCTTCATC). The amplified product was digested with MluI and BglII restriction enzymes and ligated into pGL3-basic luciferase plasmid vector (Promega Corp. Madison, Wisconsin, USA) digested with the same enzymes. The resistin promoter contains AP-1 conserved sites (CT) at -51 to -52 bp. For the mutant, the AP-1 binding sites were mutated using the mutagenesis kit (Stratagene, La Jolla, California, USA). Site-specific mutations were confirmed by DNA sequencing. Plasmids were transfected into macrophages using a low pressure-accelerated gene gun (Bioware Technologies, Taipei, Taiwan) essentially following the protocol from the manufacturer. Test plasmid at 2 μg and control plasmid (pGL4-Renilla luciferases) 0.02 μg were cotransfected with gene gun in each well, and then replaced by normal culture medium. Following 4 hours of TNF-α stimulation, cell extracts were prepared using Dual-Luciferase Reporter Assay System (Promega) and measured for dual luciferase activity by luminometer (Turner Designs).

Measurement of resistin concentration

Conditioned media from cultured macrophages under TNF-α stimulation and those from control cells were collected for resistin measurement. The level of resistin was measured by a quantitative sandwich enzyme immunoassay technique (R&D Systems). The lower limit of detection of resistin was 5 pg/mL. Both the intra-observer and inter-observer coefficient of variance were < 10%.

Glucose uptake in macrophages

Macrophages were seeded on ViewPlate for 60 min (Packard Instrument Co., Meriden, Connecticut, USA) at a cell density of 5 × 10^3 cells/well in serum free medium with transferring 5 μg/mL, insulin 5. μg/mL for overnight. Recombinant TNF-α protein or conditioned medium were added to the medium. Glucose uptake was performed by adding 0.1 mmol/L 2-deoxy-D-glucose and 3,33 nCi/mL 2- [1,2-^{3}H]-deoxy-D-glucose for various periods of time. Cells were washed with PBS twice. Non-specific uptake was performed in the presence of 10 μM cytochalasin B and subtracted from all of the measured value. MicroScint-20 50 μl was added and the plate was read with TopCount (Packard Instrument Co.). The radioactivity was counted and normalized to protein amount measured with a protein assay kit.

Statistical analysis

The data were expressed as mean+S.E.M. Statistical significance was performed with analysis of variance followed by Dunnett's test for experiments consisting of more than two groups and with Student's t test for stretch at 10% and 20%. A value of $P < 0.05$ was considered to denote statistical significance.

Results

TNF-α increases resistin expression in human macrophages

Western blot was used first to investigate the effect of TNF-α on resistin expression in human macrophages. As shown in Fig. 1, resistin protein expression was significantly induced at 4 h after TNF-α (1 ng/mL) stimulation, maximally induced at 18 h, and remained elevated for 48 h. The expression of resistin messenger RNA was significantly induced by TNF-α from 4 to 18 h of stimulation (Fig. 1C).

Atorvastatin inhibited the effect of TNF-α on resistin expression

To test whether atorvastatin can inhibit the effect of TNF-α on resistin expression in human macrophages, different doses of atorvastatin was added before TNF-α stimulation. As shown in Fig. 2, atorvastatin inhibited the resistin protein expression induced by TNF-α in a dose-dependent manner. Addition of mevalonate at 200 μM for 18 h induced resistin protein expression similar to TNF-α stimulation (Fig. 3A and 3B). However, atorvastatin did not have effect on resistin protein expression induced by mevalonate. Atorvastatin alone had neutral effect on resistin expression similar to control cells. Exogenous mevalonate did not reverse the resistin protein expression induced by TNF-α stimulation. This finding implicated that mevalonate has proinflammatory effect on resistin expression in human macrophages and atorvastatin inhibited the TNF-α-induced resistin expression not via HMG-CoA reductase pathway. SP600125, a potent inhibitor of JNK, completely attenuated the resistin protein expression induced by TNF-α and mevalonate (Fig. 4A and 4B). PD98059, a potent inhibitor of p42/p44 MAP kinase, and SB203580, a potent inhibitor of p38 MAP kinase, partially attenuated the resistin protein expression

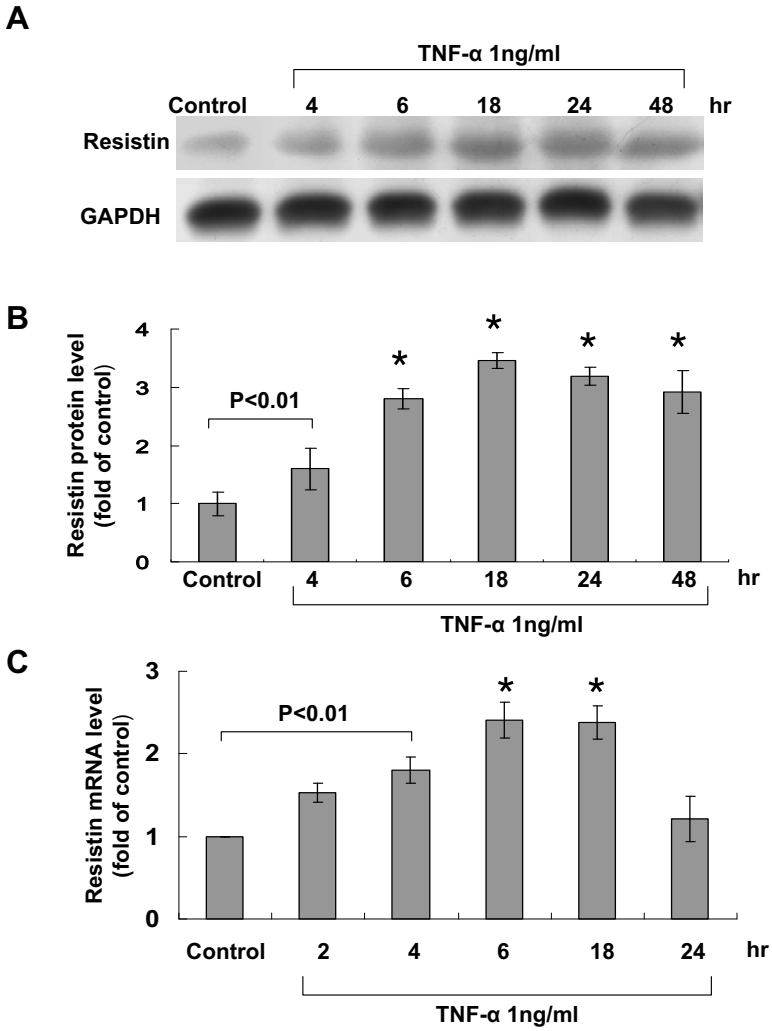

Figure 1

Effect of pro-inflammatory cytokine, tumor necrosis factor-α (TNF-α) on resistin expression in cultured macrophages. (A) Representative Western blots for resistin in macrophages treated with TNF-α for different periods of time. (B and D) (B) Quantitative analysis of resistin protein levels. The values from treated macrophages have been normalized to values in control cells. (n = 4 per group). *P < 0.01 vs. control. (C) Quantitative analysis of resistin mRNA levels. The mRNA level was measured by real-time PCR. The values from treated macrophages have been normalized to matched actin measurement and then expressed as a ratio of normalized values to mRNA in control cells (n = 3 per group). *P < 0.01 vs. control.

induced by TNF-α and mevalonate. NAC, an antioxidant scavenger, did not affect the resistin protein expression induced by TNF-α and mevalonate. TNF-α stimulation increased phosphorylation of JNK (Additional file 1), while TNF-α stimulation did not increase phosphorylation of p38 kinase and increased phosphorylation of ERK only after stimulation for 2 h. SP 60025 and Rac1 inhibitor significantly attenuated the phosphorylation of JNK induced by TNF-α stimulation. Atorvastatin also significantly reduced the phosphorylated JNK induced by TNF-α stimulation. These findings indicate that JNK pathway is the main signal pathway mediating the induction of resistin protein expression by TNF-α. Our data also demonstrated that Rac was also involved in TNF-α induced JNK activation.

Rac pathway mediates the inhibitory effect of atorvastatin on resistin expression induced by TNF-α

To investigate the atorvastatin inhibitory mechanism on induction of resistin by TNF-α, rac pathway was studied. As shown in Fig. 5, TNF-α induced phosphorylation of Rac in a dose-dependent manner. TNF-α did not have

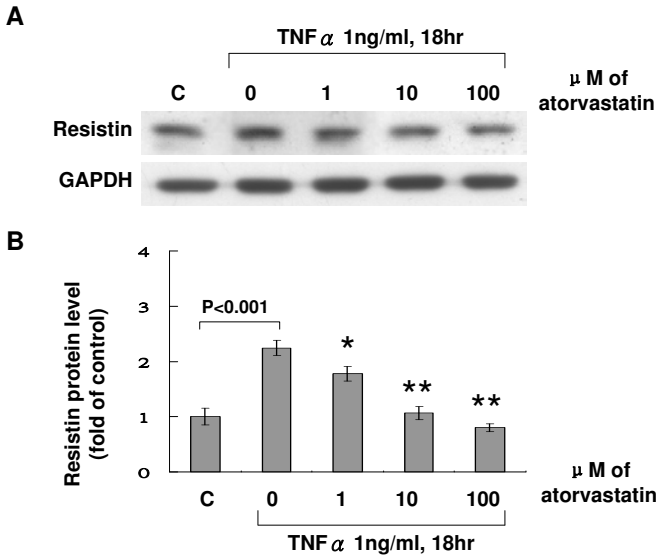

Figure 2

Atorvastatin inhibits the resistin protein expression induced by TNF-α in a dose-dependent manner. A, Representative Western blots for resistin in macrophages treated with TNF-α with or without atorvastatin. B, Quantitative analysis of resistin protein levels. The values from treated macrophages have been normalized to values in control cells. (n = 4 per group). *P < 0.05 vs. TNF-α. **P < 0.001 vs. TNF-α.

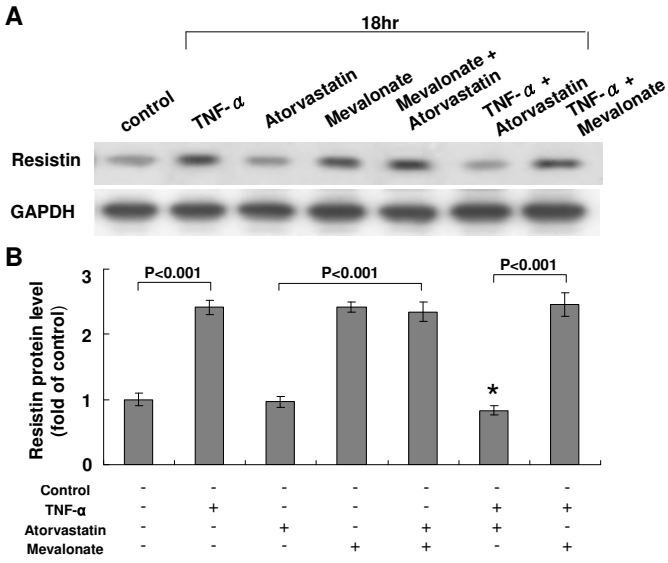

Figure 3

Atorvastatin inhibits the TNF-α-induced resistin expression not via HMG-CoA reductase pathway. A. Representative Western blots for resistin in macrophages treated with TNF-α, mevalonate with or without atorvastatin. B, Quantitative analysis of resistin protein levels. The values from treated macrophages have been normalized to values in control cells. (n = 4 per group). *P < 0.001 vs. TNF-α.

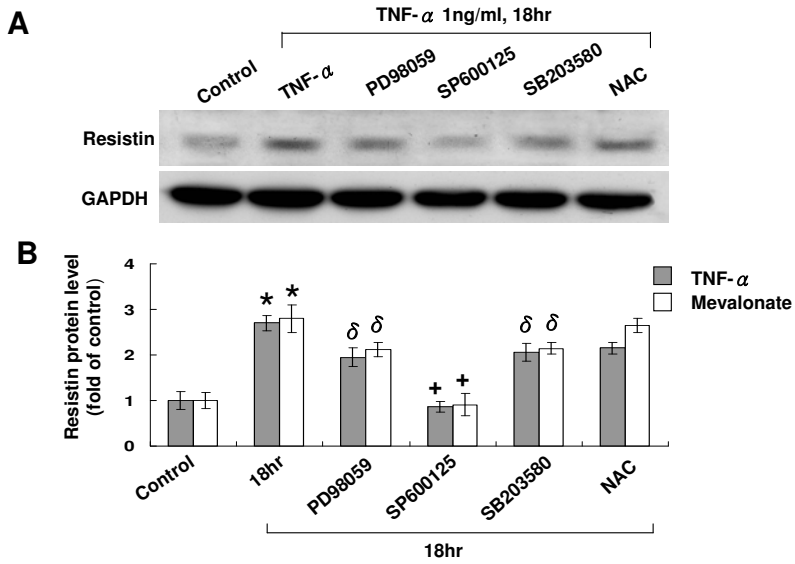

Figure 4
JNK pathway is the main signal pathway mediating the induction of resistin protein expression by TNF-α and mevalonate. A. Representative Western blots for resistin in macrophages treated with TNF-α with or without different inhibitors. B, Quantitative analysis of resistin protein levels. The values from treated macrophages have been normalized to values in control cells. (n = 4 per group).

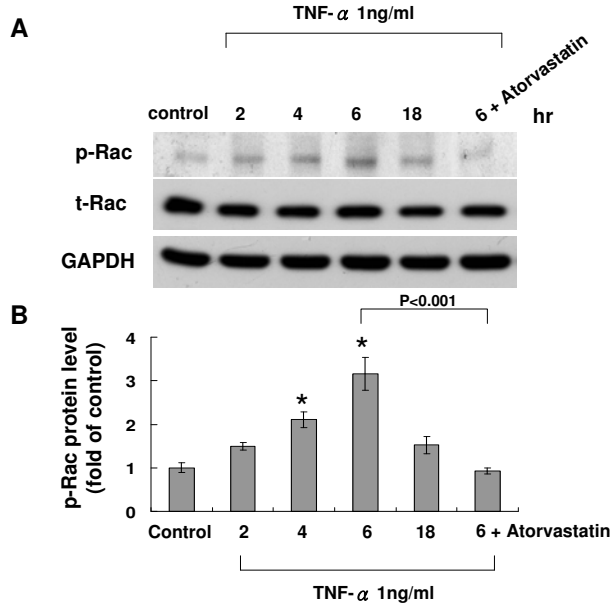

Figure 5
TNF-α induces phosphorylation of rac protein expression in cultured macrophages. A. Representative Western blots for phospho-rac and total rac in macrophages treated with TNF-α with or without atorvastatin. B, Quantitative analysis of phospho-rac protein levels. The values from treated macrophages have been normalized to values in control cells. (n = 4 per group). *P < 0.001 vs. control.

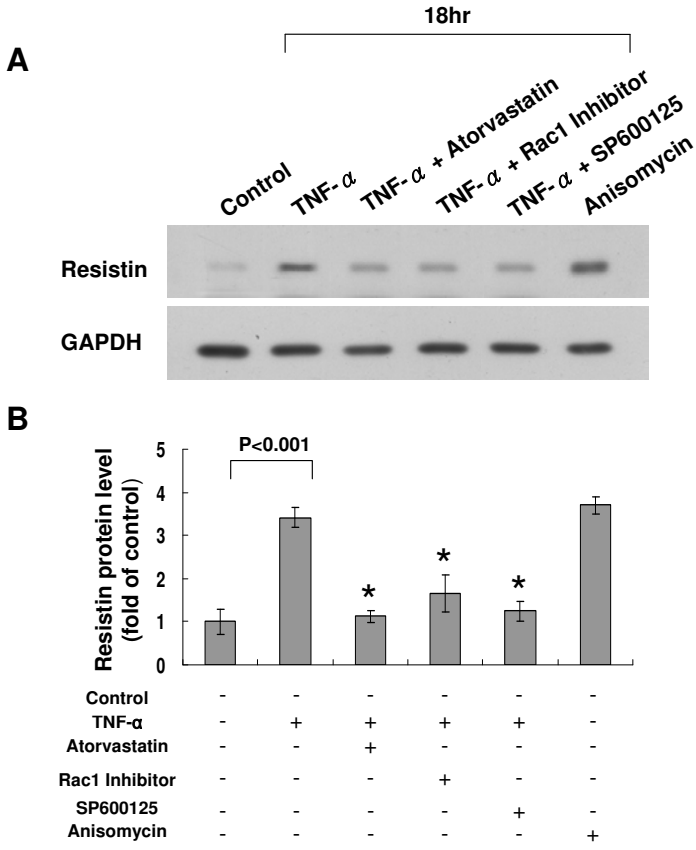

Figure 6
Rac pathway mediates the inhibitory effect of atorvastatin on resistin expression induced by TNF-α. A. Representative Western blots for resistin in macrophages treated with TNF-α with or without atorvastatin and different inhibitors. B, Quantitative analysis of resistin protein levels. The values from treated macrophages have been normalized to values in control cells. (n = 3 per group). *P < 0.001 vs.*P < 0.01 vs. TNF-α.

effect on total Rac. Addition of atorvastatin inhibited the phosphorylation of Rac induced by TNF-α. Rac-1 inhibitor almost completely attenuated the effect of TNF-α on resistin induction (Fig. 6). Anisomycin, an agonist of Rac, significantly increased the resistin protein expression similar to TNF-α. Rac1 inhibitor attenuated the induction of resistin protein expression by TNF-α, while rac1 inhibitor did not alter the resistin protein expression induced by anisomycin. As shown in Additional file 2, addition of mevalonate did not induce phosphorylation of Rac and total rac protein expression.

TNF-α increases AP-1-binding activity and resistin promoter activity

The EMSA assay showed that TNF-α increased AP-1 DNA-protein binding activity (Fig. 7). An excess of unlabeled AP1 oligonucleotide competed with the probe for binding AP1 protein, whereas an oligonucleotide containing a 2-bp substitution in the AP1 binding site did not compete for binding. Addition of SP600125 and atorvastatin 30 min before TNF-α stimulation abolished the DNA-protein binding activity induced by TNF-α. DNA-binding complexes induced by TNF-α could be supershifted by a monoclonal AP-1 antibody, indicating the presence of this protein in these complexes.

To study whether the resistin expression induced by TNF-α is regulated at the transcriptional level, we cloned the promoter region of rat resistin (-741~+22), and constructed a luciferase reporter plasmid (pGL3-Luc). The resistin promoter construct contains Stat-3, SRE, NF-κB, and AP1 binding sites. As shown in Fig. 7B and 7C, transient transfection experiment in macrophages using this reporter gene revealed that TNF-α stimulation for 4 h significantly caused resistin promoter activation. This result indicates that resistin expression is induced at transcrip-

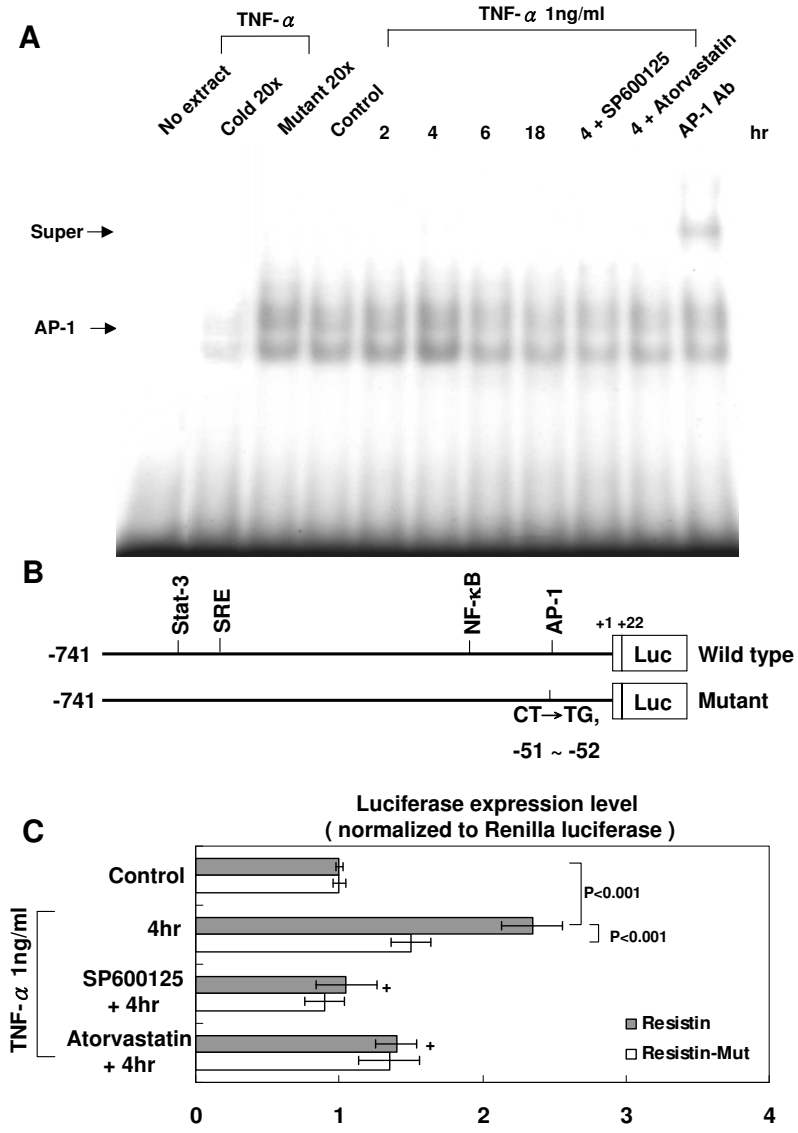

Figure 7

TNF-α increases AP-1-binding activity and resistin promoter activity. A. Representative EMSA showing protein binding to the AP-1 oligonucleotide in nuclear extracts of macrophages after TNF-α treatment in the presence or absence of atorvastatin or JNK inhibitor. Similar results were observed in another two independent experiments. A significant supershifted complex (super) after incubation with AP-1 antibody was observed. Cold oligo means unlabeled AP-1 oligonucleotides. B. Constructs of resistin promoter gene. Positive +1 demonstrates the initiation site for the resistin transcription. Mutant resistin promoter indicates mutation of AP-1 binding sites in the resistin promoter as indicated. C. Quantitative analysis of resistin promoter activity. Cultured macrophages were transiently transfected with pResistin-Luc by gene gun. The luciferase activity in cell lysates was measured and was normalized with renilla activity (n = 3 per group). *$P < 0.001$ vs. control. $^{+}P < 0.01$ vs. 4 h.

tional level by TNF-α. When the AP1 binding sites were mutated, the increased promoter activity induced by TNF-α was abolished. Moreover, addition of SP600125 and atorvastatin caused an inhibition of transcription. These results suggested that AP1 binding site in the resistin promoter is essential for the transcriptional regulation by TNF-α and that TNF-α regulates resistin promoter via JNK pathways.

TNF-α stimulates secretion of resistin from macrophages and reduces glucose uptake

As shown in Fig. 8A, TNF-α significantly increased the resistin secretion from cultured macrophages from 4 to 24

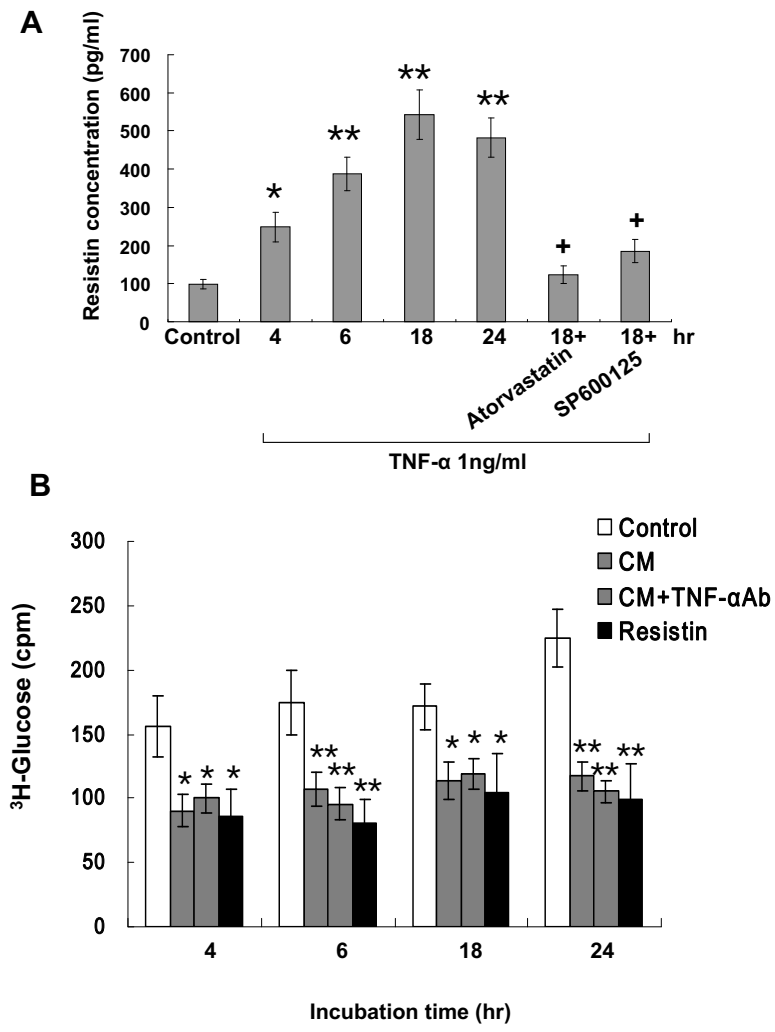

Figure 8

TNF-α stimulates secretion of resistin from macrophages and reduces glucose uptake. (A) TNF-α at 1 ng/mL significantly increasesd release of resistin from cultured macropghes at different stimulation periods. SP600125 and atorvastatin attenuated the effect induced by TNF-α (n = 3). *P < 0.01 vs. control. **P < 0.001 vs. control.+P < 0.001 vs. 18 hr. (B) Resistin and conditioned medium (CM) after TNF-α treatment had similar effect on reducing glucose uptake. Glucose uptake was measured in macrophages treated for 90 min with 20 μg/mL recombinant resisitn protein or conditioned medium from cultured macrophages after 1 ng/mL TNF-α stimulation with or without TNF-α antibody (TNF-α Ab). *P < 0.05 vs. control. **P < 0.01 vs. control. Data are from 3 independent experiments.

h. The mean concentration of resistin rose from 98 ± 13 pg/mL before TNF-α stimulation to 542 ± 64 pg/mL after TNF-α stimulation for 18 h (P < 0.01). Pretreatment with atorvastatin or SP600125 significantly attenuated the secretion of resistin induced by TNF-α

Recombinant TNF-α protein at 1 ng/mL significantly reduced glucose uptake at various periods of incubation as compared to control macrophages without treatment (Additional file 3). As shown in Figure 8B, exogenous addition of conditioned medium from TNF-α stimulated macrophages and resisitn also increased glucose uptake in cultured macrophages. To eliminate the TNF-α effect on glucose uptake, anti-rat TNF-α antibody (5 μg/ml, purchased form R&D Systems) was added to the medium 1 hour before 2- [1,2-^{3}H]-deoxy-D-glucose was added. The effect of cultured medium obtained from macrophages after TNF-α antibody treatment on reducing glucose

uptake was similar to that of resistin. Addition of resistin siRNA or atorvastatin before recombinant resistin treatment reversed the glucose uptake to baseline levels (Additional file 3). This data indicates that resistin secreted from macrophage after TNF-α stimulation is functional.

Discussion

Atherosclerosis has been considered an inflammatory disease. Inflammatory mediators such as TNF-α, interleukin-1 and C-reactiv protein paly an important role in atheogenesis. Resistin could stimulate expression of TNF-α, interleukin-1, 6 and 12 in cultured macrophages [3,11]. We have previously demonstrated a remarkable induction of resistin protein level even after stimulation with low level of TNF-α in vascular smooth muscle cells [12]. In this study, we further demonstrated that resistin protein and mRNA levels can be induced by TNF-α in cultured human macrophages. Macrophages and vascular smooth muscle cells are important components in the atheroma. These findings indicate that resistin is a promising target for controlling atherosclerotic disease.

Biomarkers that integrate metabolic and inflammatory signals are attractive candidates for defining risk of atherosclerotic cardiovascular disease [13]. Hyperresistinemia impairs glucose tolerance and induces hepatic insulin resistance in rodents [14], whereas mice deficient in resistin are protected from obesity associated insulin resistance [15]. In this study, we also demonstrated that recombinant resistin protein and TNF-α reduced glucose uptake in human macrophages and atorvastatin reversed the abnormal glucose uptake induced by resistin and TNF-α. Resistin may represent a novel link between metabolic signals, inflammation, and atherosclerosis [16].

Norata et al. have reported that plasma resistin levels are increased in the presence of metabolic syndrome and are associated with increased cardiovascular risk [17]. Lubos et al. have also reported that resistin levels are elevated in patients with acute coronary syndrome and might play a role as a diagnostic marker [18]. Recently, resistin was found to induce lipolysis and re-esterification of triacylglycerol stores and increase cholesteryl ester deposition in human macrophages [19]. Therefore, resistin contributes macrophage form cell formation. Statins have been shown to reduce lipid lowering effects as well as pleiotropic properties. Although statin cannot alter resistin levels in patients with type 2 diabetic and in healthy men [20-22], statins have been shown to reduce resistin expression in human monocytes and adipocytes [10,23]. These data implicate that statins may control inflammatory responses by inhibiting resistin expression.

Indeed, our study demonstrated that TNF-α induced resistin protein and mRNA expression in human macrophages and atorvastatin decreased TNF-α-induced resistin expression in a dose-dependent manner. The induction of resistin protein by TNF-α was largely mediated by JNK kinase pathway because the specific and potent inhibitors of an upstream JNK kinase, SP600125, inhibited the induction of resistin protein. Atorvastatin also inhibited the phosphorylation of rac induced by TNF-α. In this study, we demonstrated that TNF-α stimulation of AP-1-DNA binding activity required at least phosphorylation of the JNK since JNK inhibitor abolished the AP-1 binding activity. Atorvastatin also attenuated the AP-1 binding activity induced by TNF-α. The promoter activity of wild resistin promoter after TNF-α was significantly higher than that of AP-1 mutant resistin promoter. This finding indicates that TNF-α regulates resistin in human macrophages at transcriptional level and that AP-1 binding sites in the resistin promoter is essential for the transcriptional regulation. Taken together, our results indicate that TNF-α may increase the AP-1 transcriptional activity in macrophages. Resistin induced by TNF-α was largely though JNK, rac and resistin promoter pathways and atorvastatin could inhibit resistin expression through inhibition of rac phosphorylation, reduced AP-1 binding activity and resistin promoter activity.

In our study, we demonstrated that inhibition of the TNF-α-induced resistin expression by atorvastatin was independent of HMG-CoA reductase. Downregulation of resistin expression induced by CRP by simvastatin was independent of HMG-CoA reductase [23]. Rac pathway mediates the signal trasndcution by isoprenoid intermediates, such as farnesylpyrophosphate and geranylgeranylpyrophosphate. In this study, we did not test the effect of isoprenoid intermediate on inhibition of TNF-α-induced resistin expression by atorvastatin. We demonstrated that TNF-α and mevalonate induce resisitn at the similar level. However, atorvastatin only blocks TNF-α but not mevalonate induced resistin. TNF-α but not mevalonate induces rac phosphorylation in cultured macrophages. JNK specific inhibitor S600125 blocked both TNF-α and mevalonate induced resistin expression. This data suggests that mevalonate plays a proinflammatory role and atorvastatin attenuates resistin expression induced by TNF-α is independent of HMG-CoA reductase but through inhibition of Rac and JNK pathway.

In conclusion, our study confirmed previous findings that TNF-α could induce resistin expression in human macrophages and atorvastatin could inhibit the resistin expression induced by TNF-α. The inhibitory effect of atorvastatin on TNF-α-induced resistin expression was mediated by rac and resistin promoter. Our findings provide another evidence of pleiotropic effect of statin. Statin therapy may become another therapeutic strategy for con-

trolling resistin-associated pathologic cardiovascular disease in humans.

Abbreviations

AP-1: activating protein 1; EMSA: electrophoretic mobility shift assay; HMG-CoA reductase: 3-hydroxy 3-methyl glutaryl-CoA reductase; PBMCs: peripheral mononuclear cells; TNF-α: tumor necrosis factor-α.

Competing interests

The authors declare that they have no competing interests.

Authors' contributions

KGS has participated in the design of the study and drafted the manuscript. SKC has made substantial contributions to conception and design, or acquisition of data, or analysis and interpretation of data. BWW has made substantial contributions to conception and design, or acquisition of data, or analysis and interpretation of data. PK has given final approval of the version to be published.

Additional material

Additional file 1

***Figure S1**. Expression of JNK, ERK and p38 MAP kinase in cultured macrophages. (A) Representative Western blot for phosphorylated and total JNK, ERK, and p38 MAP kinase in macrophages after treatment with TNF-α for various periods of time with or without inhibitor. (B) Quantitative analysis of phosphorylated protein levels. The values from treated macrophages have been normalized to matched GAPDH and corresponding total protein measurement and then expressed as a ratio of normalized values to each phosphorylated protein in control cells (n = 3 per group). **P < 0.001 vs. control. *P < 0.01 vs. control. ‡P < 0.001 vs. 6 hr.*
Click here for file
[http://www.biomedcentral.com/content/supplementary/1423-0127-16-50-S1.ppt]

Additional file 2

***Figure S2**. Expression of Rac in cultured macrophages. (A) Representative Western blot for phosphorylated and total Rac in macrophages after treatment with mevalonate for various periods of time. (B) Quantitative analysis of phosphorylated protein levels. The values from treated macrophages have been normalized to matched GAPDH and corresponding total protein measurement and then expressed as a ratio of normalized values to each phosphorylated protein in control cells (n = 3 per group).*
Click here for file
[http://www.biomedcentral.com/content/supplementary/1423-0127-16-50-S2.ppt]

Additional file 3

***Figure S3**. Effect of recombinant resistin and TNF-α on glucose uptake in macrophages. Glucose uptake was measured in macrophages treated for 90 min with 20 μg/mL recombinant mouse resistin or 1 ng/mL TNF-α with or without resistin siRNA or atorvastatin. *P < 0.001. Data are from 3 independent experiments.*
Click here for file
[http://www.biomedcentral.com/content/supplementary/1423-0127-16-50-S3.ppt]

Acknowledgements

This study was sponsored in part from Pfizer Limited, Taiwan and Shin Kong Wu Ho-Su Memorial Hospital, Taipei, Taiwan.

References

1. Verma S, Li SH, Wang CH, Fedak PW, Li RK, Weisel RD, Mickle DA: **Resistin promotes endothelial cell activation: further evidence of adipokine-endothelial interaction.** *Circulation* 2003, **108:**736-740.
2. Kawanami D, Maemura K, Takeda N, Harada T, Nojiri T, Imai Y, Manabe I, Utsunomiya K, Nagai R: **Direct reciprocal effects of resistin and adiponectin on vascular endothelial cells: a new insight into adipocytokine-endothelial cell interactions.** *Biochem Biophys Res Commun* 2004, **314:**415-419.
3. Bokarewa M, Nagaev I, Dahlberg L, Smith U, Tarkowski A: **Resistin, an adipokine with potent proinflammatory properties.** *J Immunol* 2005, **174:**5789-5795.
4. Kougias P, Chai H, Lin PH, Lumsden AB, Yao Q, Chen C: **Adipocyte-derived cytokine resistin causes endothelial dysfunction of porcine coronary arteries.** *J Vasc Surg* 2005, **41:**691-698.
5. Burnett MS, Lee CW, Kinnaird TD, Stabile E, Durrani S, Dullum MK, Devaney JM, Fishman C, Stamou S, Canos D, Zbinden S, Clavijo LC, Jang GJ, Andrews JA, Zhu J, Epstein SE: **The potential role of resistin in atherogenesis.** *Atherosclerosis* 2005, **182:**241-248.
6. Calabro P, Samudio I, Willerson JT, Yeh ET: **Resistin promotes smooth muscle cell proliferation through activation of extracellular signal-regulated kinases 1/2 and phosphatidylinositol 3-kinase pathways.** *Circulation* 2004, **110:**3335-3340.
7. Jung HS, Park KH, Cho YM, Chung SS, Cho HJ, Cho SY, Kim SJ, Kim SY, Lee HK, Park KS: **Resistin is secreted from macrophages in atheromas and promotes atherosclerosis.** *Cardiovasc Res* 2006, **69:**76-85.
8. Reilly MP, Lehrke M, Wolfe ML, Rohatgi A, Lazar MA, Rader DJ: **Resistin is an inflammatory marker of atherosclerosis in humans.** *Circulation* 2005, **111:**932-939.
9. Arnaud C, Braunerseuther V, Mach F: **Toward immunomodulatory and anti-inflammatory properties of statins.** *Trends Cardiovasc Med* 2005, **15:**202-206.
10. Ichida Y, Hasegawa G, Fukui M, Obayashi H, Ohta M, Fujinami A, Ohta K, Nakano K, Yoshikawa T, Nakamura N: **Effect of atorvastatin on in vitro expression of resistin in adipocytes and monocytes/macrophages and effect of atorvastatin treatment on serum resistin levels in patients with type 2 diabetes.** *Pharmacology* 2006, **76:**34-39.
11. Silswal N, Singh AK, Aruna B, Mukhopadhyay S, Ghosh S, Ehtesham NZ: **Human resistin stimulates the pro-inflammatory cytokines TNF-alpha and IL-12 in macrophages by NF-kappa B-dependnet pathway.** *Biochem Biophys Res Commun* 2005, **334:**1092-1101.
12. Hung HF, Wang BW, Chang H, Shyu KG: **The molecular regulation of resistin expression in cultured vascular smooth muscle cells under hypoxia.** *J Hypertens* 2008, **26:**2349-2360.
13. Rajala MW, Scherer PE: **The adipocyte: at the crossroads of energy homeostasis, inflammation, and atherosclerosis.** *Endocrinology* 2003, **144:**3765-3773.
14. Banerjee RR, Rangwala SM, Shapiro JS, Rich AS, Rhoades B, Qi Y, Wang J, Rajala MW, Pocai A, Scherer PE, Steppan CM, Ahima RS, Obici S, Rossetti L, Lazar MA: **Regulation of fasted blood glucose by resistin.** *Science* 2004, **303:**1195-1198.
15. Rothwell SE, Richards AM, Pemberton CJ: **Resistin worsens cardiac ischemia-reperfusion injury.** *Biochem Biophys Res Commun.* 2006, **349(1):**4000-4007.
16. Reilly MP, Lehrke M, Wolfe ML, Rohatgi A, Lazar MA, Rader DJ: **Resistin is an inflammatory marker of atherosclerosis in humans.** *Circulation* 2005, **111:**932-939.
17. Norata GD, Ongari M, Garlaschelli K, Raselli S, Grigore L, Catapano AL: **Plasma resistin levels correlate with determinants of the metabolic syndrome.** *Eur J Endocrinol* 2007, **156:**279-284.
18. Lubos E, Messow CM, Schnabel R, Rupprecht HJ, Espinola-Klein C, Bickel C, Peetz D, Post F, Lackner K, Tiret L, Munzel T, Blankenberg S: **Resistin, acute coronary syndrome and prognosis results from the AtheroGene study.** *Atherosclerosis* 2007, **193:**121-128.
19. Rac C, Roberston SA, Taylor JM, Graham A: **Resistin induces lipolysis and re-esterification of triacylglycerol stores, and**

increases cholesteryl ester deposition, in human macrophages. *FEBS Lett* 2007, **581:**4877-4883.
20. Shetty G, Economides PA, Horton ES, Mantzoros CS, Veves A: **Circulating adiponectin and resistin levels in relation to metabolic factors, inflammatory markers, and vascular reactivity in diabetic patients and subjects at risk for diabetes.** *Daibetes Care* 2004, **27:**2450-2457.
21. Otto C, Frost RJ, Vogeser M, Pfeiffer AF, Spranger J, Parhofer KG: **Short-term therapy with atorvastatin or fenofibrate does not affect plasma ghrelin, resistin or adiponectin levels in type 2 diabetic patients with mixed hyperlipoproteinaemia.** *Acta Diabetol* 2007, **44:**65-68.
22. Gouni-Berthold I, Berthold HK, Chamberland JP, Krone W, Mantzoros CS: **Short-term ttreatment with ezetimibe, simvastatin or their combination does not alter circulating adiponectin, resistin or leptin levels in healthy men.** *Clin Endocrinol* 2008, **68:**536-541.
23. Hu WL, Qian SB, Li JJ: **Decreased C-reactive protein-induced resistin production in human monocytes by simvastatin.** *Cytokine* 2007, **40:**201-206.

A Novel Cancer Therapy by Skin Delivery of Indoleamine 2,3-Dioxygenase siRNA

Meng-Chi Yen,[1,3] Chi-Chen Lin,[6] Yi-Ling Chen,[5] Shih-Shien Huang,[1] Huei-Jiun Yang,[1] Chih-Peng Chang,[2,3] Huan-Yao Lei,[2,3] and Ming-Derg Lai[1,3,4]

Abstract

Purpose: Indoleamine 2,3-dioxygenase (IDO), an enzyme that degrades tryptophan, is a negative immune regulatory molecule of dendritic cells. IDO-expressing dendritic cells suppress T cell responses and may be immunosuppressive *in vivo*. We hypothesized that silencing the IDO expression in skin dendritic cells *in vivo* could elicit antitumor activity in tumor-draining lymph nodes.

Experimental Design: The efficiency of IDO-specific small interfering RNA (siRNA) was evaluated *in vitro* and *in vivo*. The therapeutic effect was evaluated in MBT-2 murine bladder tumor model and CT-26 colon tumor models.

Results: IDO expression was down-regulated in CD11c-positive lymphocytes after IDO siRNA treatment. *In vivo* skin administration of IDO siRNA inhibited tumor growth and prolonged survival in both tumor models. The number of infiltrated T cells and neutrophils increased at tumor sites, which are correlated with therapeutic efficacy. The T cells may be mainly responsible for the immunologic rejection because the effect was abolished by depletion of CD8-positive T cells. Adoptive transfer of CD11c-positive dendritic cells from vaccinated mice delayed tumor progression. The cancer therapeutic effect was reproducibly observed with another IDO siRNA targeting at different site, suggesting the effect was not due to off-target effect. In a neu-overexpressing MBT-2 tumor model, IDO siRNA enhanced the therapeutic efficacy of Her2/Neu DNA vaccine. Down-regulation of IDO2, an IDO homologue, with siRNA also generated antitumor immunity *in vivo*.

Conclusions: Antitumor immunity can be effectively elicited by physical delivery of siRNAs targeting immunoregulatory genes in skin dendritic cells *in vivo*, as shown by IDO and IDO2 in this report.

Dendritic cells are specific immune cells that can present antigens and affect T cell differentiation and activation. Dendritic cells are divided into two subpopulations: myeloid dendritic cells or conventional dendritic cells and plasmacytoid dendritic cells. Conventional dendritic cells are subtyped according to their tissue distribution into Langerhans cells in the epidermis, dermal dendritic cells in the dermis, liver dendritic cells, lung dendritic cells, etc. Dendritic cells process antigen at their local tissue sites and migrate to lymphoid organs where they present the antigens to naïve T cells and induce primary T cell and B cell responses (1–4). In addition, dendritic cells are important regulators of tolerance to self-antigens (5). Tumors develop through the accumulation of multiple genetic mutations, which leads to the production of mutated proteins. Despite their potential as tumor-associated antigens, these mutated proteins rarely induce sufficient immunity to eradicate the tumor (6). Many mechanisms have been proposed to explain the ineffectiveness of the immune response against cancer. One important mechanism is the modulation of dendritic cells in the tumor microenvironment and lymph nodes by cancer cells (7).

Indoleamine-2,3-dioxygenase (IDO) catalyzes the first step in the kynurenine pathway, the main pathway of tryptophan metabolism (8). It is involved in many activities including microbial infectivity and maternal T-cell immunity during pregnancy (5, 9). The establishment of tolerance may be mediated through either localized depletion of tryptophan or accumulation of toxic metabolites. Tryptophan catabolism also affects naïve T cell proliferation and memory CD8 T cell generation (10). IDO also plays an important role in immune escape in cancer (5, 11–13). Overexpression of IDO is

Authors' Affiliations: Departments of [1]Biochemistry and Molecular Biology, and [2]Microbiology and Immunology, [3]Institute of Basic Medicine, College of Medicine, and [4]Center for Gene Regulation and Signal Transduction Research, National Cheng Kung University, No. 1, and [5]Department of Childhood Education and Nursery, Chia Nan University of Pharmacy and Science, No. 60, Sec.1, Jen-Te, Tainan, Taiwan; and [6]Institute of Medical Technology, College of Life Sciences, National Chung Hsing University, No. 250, Taichung, Taiwan

Received 7/31/08; revised 9/18/08; accepted 9/22/08.

Grant support: Grants NSC-93-3112-B-006-006 and 94-3112-B-006-011 to Dr. Ming-Derg Lai from the National Science Council.

The costs of publication of this article were defrayed in part by the payment of page charges. This article must therefore be hereby marked *advertisement* in accordance with 18 U.S.C. Section 1734 solely to indicate this fact.

Note: Supplementary data for this article are available at Clinical Cancer Research Online (http://clincancerres.aacrjournals.org/).

Requests for reprints: Ming-Derg Lai, Department of Biochemistry and Molecular Biology, College of Medicine, National Cheng Kung University, Tainan, Taiwan, R.O.C. Phone: 886-6-235-3535, ext. 5549; Fax: 886-6-2741694; E-mail: a1211207@mail.ncku.edu.tw.

doi:10.1158/1078-0432.CCR-08-1988

Translational Relevance

Dendritic cells are usually prepared *ex vivo* and pulsed with tumor antigens to generate antitumor immunity. In this article, we have shown that physical delivery of small interfering RNA (siRNA) targeting indoleamine 2,3-dioxygenase (IDO) *in vivo* can produce an effective antitumor immune response without loading specific tumor antigens. This simple nonviral method reduces lengthy work in preparation of dendritic cells *ex vivo*, and may be useful in treating various types of tumors because the immune response is not limited to a particular tumor antigen. Furthermore, the immune response can be directed to a tumor-associated antigen as shown by codelivery of neu DNA vaccine and IDO siRNA. Based on these preclinical data, skin delivery of siRNA targeting IDO has the therapeutic potential in treating many cancers by itself and can function as an adjuvant to boost other immunotherapy.

observed in tumors of many organs and tissues and in tumor-draining lymph nodes (11, 14–17). The induction of IDO in tumor is linked to the mutation of a tumor suppressor gene, *Bin 1*. Inactivation of the *Bin 1* gene results in superinduction of the *IDO* gene by IFN-γ. Treatment with the IDO inhibitor 1-methyl-tryptophan suppressed the growth of Bin1-null tumor in immunologically intact mice, but not in nude mice (18). Expression of IDO in tumor endothelial cells also correlates with disease progression (19). A subset of dendritic cells expressing IDO was identified in tumor-draining lymph nodes. These dendritic cells can activate resting CD4-positive CD25-positive Foxp3-positive regulatory T cells that can mediate immunosuppression (16, 20). The induction of IDO in dendritic cells seems to be mediated through the noncanonical nuclear factor-kB pathway, which is strictly dependent on IKKα homodimers (21). IDO may not be essential for self-tolerance because IDO-knockout mice did not develop spontaneous autoimmune diseases (16, 22). IDO may serve as a good immunologic target for cancer therapy.

The IDO competitive inhibitor L-1-methyl-tryptophan (L-1MT) significantly reduced tumor size in animal experiments (15). On the other hand, the dextro stereoisomer (D-1MT) had better antitumor activity (23). It was also shown that the small interfering RNA (siRNA) against IDO in tumor cells can restore antitumor immunity (24). However, the effects of silencing IDO in dendritic cells have not been investigated *in vivo*. Recently, an IDO homologue protein, IDO2, was identified and may be the preferred target of the antitumor compound D-1MT (25, 26). Interestingly, D-1MT had no antitumor activity in IDO-knockout mice (23). Furthermore, L-1MT, but not D-1MT, blocked tryptophan catabolism through abrogation of IDO activity in dendritic cells (27). IDO and IDO2 may have different biological interactions in various cell types (28). Some discrepancies in these previous results may also be attributed to the broad effects of 1-MT, which can interfere with Toll-like receptor signaling in dendritic cells, independent of IDO activity (29).

Because IDO is expressed in dendritic cells in tumor-draining lymph nodes, modulating this expression may have antitumor effects. Modulation can be achieved by *ex vivo* loading and *in vivo* targeting. Directly modifying the dendritic cells *in vivo* has several advantages, including low cost, uniformity of the products of dendritic cell synthesis, and activation of dendritic cells within their natural environment (30). In our previous study, supersonic flow was used effectively to deliver DNA into skin dendritic cells (31). Therefore, we hypothesized that delivery of IDO siRNA into skin dendritic cells may stimulate low-IDO-expressing dendritic cells to migrate into tumor-draining lymph nodes, activate the antitumor immune response, and thereby delay progression of established tumors (Fig. 1). In this report, we show that delivery of IDO siRNA into skin dendritic cells can generate antitumor immune responses in two different murine tumor models. Furthermore, IDO siRNA combined with other gene therapy regimens can further increase cancer therapeutic efficacy.

Materials and Methods

Animals. Female 4- to 6-wk C3H/HeN and BALB/c mice were obtained from the Laboratory Animal Center at National Cheng Kung University. All study protocols involving mice were approved by the Animal Welfare Committee at National Cheng Kung University. L-1MT (Sigma-Aldrich) was dissolved in sterile water (5 mg/mL) and adjusted to pH 9.9 by NaOH. Animal water bottles were filled with L-1MT–supplemented water, and replaced with fresh L-1MT water every 2 to 3 d until mice were sacrificed.

Cell lines and antibodies. The MBT-2 murine bladder carcinoma cell line has been described (32). The CT-26 colon tumor cell line was a kind gift from Dr. Huan-Yao Lei. The following antibodies were used in Western blotting: neu (Ab-20; Lab Vision Corp.) against extracellular domain of neu; c-MYC (OP10; Calbiochem) against the myc-tag of pcDNA3.1-IDO and pcDNA3.1-IDO2; and β-actin–specific mouse monoclonal antibody (Chemicon).

Plasmid construction and preparation of DNA vaccine. siRNA was constructed within pHsU6 vector as described previously (33). The targets were 5′-GCA CTG CAC GAC ATA GCT A-3′ (for IDO siRNA); 5′-GCA ATA TTG CTG TTC CCT A-3′ (for IDO siRNA-2); 5′-GCA ATA GTA GAT ACT TAC A-3′ (for IDO siRNA-3); 5′-GCA GAT TCC TAA AGA GTT A (for IDO2 siRNA); 5′-GGC CAT CTA CCC ATG AAG A-3′ (for scramble IDO siRNA). IDO and IDO2 full-length genes were cloned from C3H/HeN mouse lymph node lymphocytes and liver, respectively, and subcloned into pcDNA3.1/myc-His-B(+) vector (Invitrogen). The resulting plasmids were named IDO-myc and IDO2-myc. Neu-IDO-siRNA plasmid was constructed by subcloning U6 promoter/IDO siRNA fragment into the plasmid containing the extracellular domain of human neu driven by CMV promoter (Invitrogen). Plasmid DNA was purified with Endofree Qiagen Plasmid Mega Kits (Qiagen). DNA was precipitated and suspended in sterile water at the concentration of 1 mg/mL.

IDO activity. Cos-7 cells (2×10^6) were transfected with 2 μg of IDO-myc, and cells were harvested from 18-h cultures. Cells were subjected to three freeze/thaw cycles in 200 μL of PBS buffer and the supernatant was removed after centrifugation at $3000 \times g$. The reaction solution for measuring IDO activity contained potassium phosphate buffer (50 mmol/L, pH 6.5), ascorbic acid (20 mmol/L, neutralized with NaOH), catalase (200 μg/mL), methylene blue (10 μmol/L), L-tryptophan (400 μmol/L). One hundred microliters of reaction solution and 100 μL of cell lysate were mixed and incubated at 37°C for 60 min. Twenty microliters of 30% w/v trichloroacetic acid were added to stop reaction at 65°C for 15 min, and the reaction mixture was centrifuged at $6000 \times g$ for 5 min. Twenty microliters of supernatants were analyzed by a high performance liquid chromatography system with a reverse-phase column (Mightysil RP-18 GP 4.6 × 250 mm; Kanto Chemical Co. Inc). L-Kynurenine (5-100 μmol/L) was used as the standard.

Histologic analysis of lymphocytes infiltrating tumor. One week after the third vaccination, the mice were sacrificed and the tumors were removed and cryosectioned (5 μm). The immune cells in cryosections were detected with anti-CD4 (GK 1.5; Pharmingen), anti-CD8 (53-6.7; Pharmingen), anti-pan-NK (DX5; Pharmingen), or anti-neutrophil (GR-1; Pharmingen) antibodies.

Therapeutic efficacy of IDO siRNA on established tumor. Mice were injected s.c. in the flank with 1×10^6 MBT-2 cells or 1×10^5 CT-26 cells in 0.5 mL of PBS. At day 8, the same flank was bombarded with 10 μg of plasmid DNA diluted in 20 μL of water, using a low-pressure-accelerated gene gun (BioWare Technologies Co. Ltd.) at 50 psi of helium gas pressure. Tumor size was measured using a caliper twice a week. Tumor volume was calculated using the formula: volume = $(A^2 \times B \times 0.5236)$, where A and B represent the shortest and longest diameter, respectively. Mice were sacrificed when the volume of tumor grew larger than 2,500 mm^3 or the mouse was in poor condition and expected shortly to become moribund. Significant differences were revealed by Kaplan-Meier analysis of survival rates.

Depletion of CD8-positive T cells. Five hundred micrograms of murine antimouse CD8 (2.43) or control antibody (purified rat IgG) was injected i.p. into mice. The depletion was done at weekly intervals until the end of the experiment. The specific depletion was >90% as determined by flow cytometric analysis.

Isolation of CD11c-positive cells. Inguinal lymph nodes were collected from mice 48 h after vaccination. Cd11c-positive cells were enriched with CD11c (N418) microbeads (Miltenyi Biotec). The enriched cells were routinely >90% CD11c positive.

Detection of IDO expression in IDO siRNA transfected cells in inguinal lymph nodes. The protocol was based on the previous report (31) with minor modification. C3H/HeN mice were inoculated with 5 μg of pEGFP-N1 plasmid (Clontech) and 15 μg of IDO siRNA or scramble IDO siRNA. Lymphocytes were harvested from inguinal lymph nodes 48 h later. Lymphocytes were stained with IDO polyclonal antibody (Adipogen) and then stained with Alexa Fluor goat antirabbit IgG (Invitrogen Life Technologies). FACS Calibur flow cytometry (BD Bioscience) was used to determine expression of IDO. Briefly, the lymphocytes were gated according to side-scatter and forward-scatter characteristics of monocytes. Enhanced green fluorescence protein fluorescence-positive cells were further gated according to their FL-1 intensity and forward scatter. IDO expression was shown in histogram plots, and the IDO quantitative analysis was done on geometric means.

CD11c-positive cells adoptive transfer. CD11c-positive dendritic cells were isolated from the inguinal lymph nodes of mice vaccinated three times with IDO siRNA or scramble siRNA. Recipient mice were challenged with 1×10^6 MBT-2 cells, and 5×10^4 dendritic cells were injected s.c. into each recipient on the same flank where tumor cells were injected.

Reverse transcription-PCR and quantitative reverse transcription-PCR. CD11c-positive cells were harvested for RNA extraction with TRIZOL (Invitrogen Life Technologies). cDNA was synthesized from 2 μg of RNA using MMLV-Reverse Transcriptase (Promega) according to the manufacturer's directions. Primers were as follows: IDO forward: 5′-TGT GGC TAG AAA TCT GCC TGT-3′; and reverse: 5′-CTG CGA TTT CCA CCA ATA GAG-3′; IDO2 forward: 5′-GGC TTT CTC CTT CCA AAT CC-3′ and reverse: TTG TCA GCA CCA GGT CAG AG-3′; hypoxanthine phosphoribosyltransferase forward: 5′-GTT GGA TAC AGG CCA GAC TTT GTT G-3′ and reverse: 5′-GAT TCA ACT TGC GCT CAT CTT AGG C-3′; IDO primer of quantitative PCR forward: 5′-CGG ACT GAG AGG ACA CAG GTT AC-3′ and reverse 5′-ACA CAT ACG CCA TGG TGA TGT AC-3′ (34). cDNA was amplified by Protaq DNA polymerase (PROtech Technology, Inc.). The PCR products were electrophoresed on 2.0% agarose gels and visualized by ethidium bromide staining under UV light. Quantitative PCR was done on ABI 7500 Fast Real-Time system (Applied Biosystems) using SYBR Green PCR Master Mix (Applied Biosystems). Cycling conditions were 95°C for 5 min, followed by 45 cycles of 95°C for 15 s and 60°C for 1 min.

In vitro *CTL induction and activity.* Spleen cells were harvested 7 d after the third DNA vaccination. Spleen cells (2×10^7) were incubated with 10 μg of MBT-2 cell lysate for 48 h, and the suspended cells were harvested as effector cells. MBT-2 luciferase cells were used as target cells (35). Target cells (1×10^4 cells/well) were incubated for 6 h with serial dilutions of effector cells in 200 μL of RPMI 1640 medium at 37°C. The specific lysis of splenocytes was assessed in the supernatant using a conventional luciferase detection system (Promega) in a Lumat LB9506 luminometer (Berthold Technologies).

Statistics. Graphs were generated and two-tailed t-tests were done using GraphPad Prism version 4.00 for Windows (GraphPad Software).

Results

The efficacy of silencing IDO with IDO siRNA. We constructed U6 promoter plasmid-based siRNA targeting at

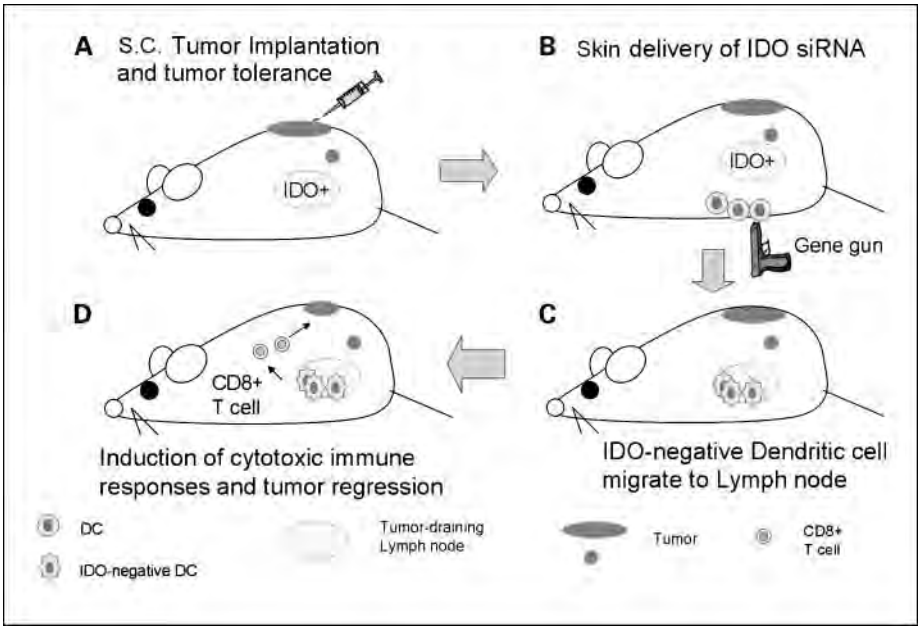

Fig. 1. Outline of anticancer therapy with skin delivery of the immune regulator IDO siRNA. *A,* tumor implantation induced increase of IDO-positive cells in tumor-draining lymph node which may cause tumor tolerance. *B,* skin delivery of IDO siRNA repressed the expression of IDO in dendritic cells and some skin cells. *C,* IDO-negative (low-expression) dendritic cells migrated to lymph node. *D,* IDO-negative dendritic cells produced antitumor immune response and delayed tumor progression.

nucleotides 607 to 625 on the *IDO* gene. To evaluate the efficacy of IDO siRNA, liposome transfection was used to deliver IDO siRNA and myc-tagged IDO (IDO-myc) into COS-7 cells *in vitro*. U6 vector or scramble IDO siRNA was used as a negative control. IDO siRNA significantly attenuated the mRNA expression level of IDO, but not the mRNA expression level of IDO2, a related enzyme of IDO (Fig. 2A and data not shown; ref. 26). Decrease in IDO protein and total abolition of IDO

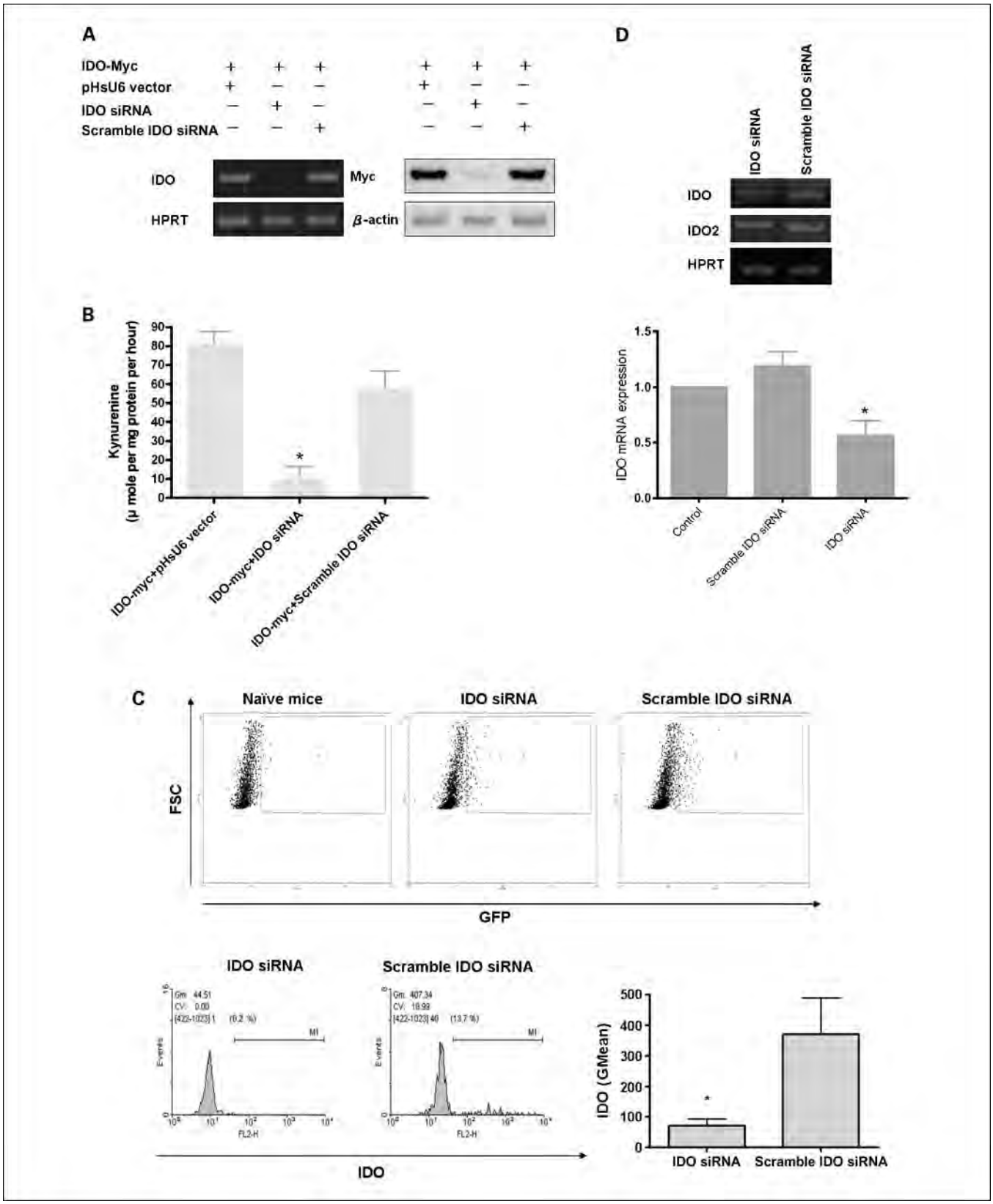

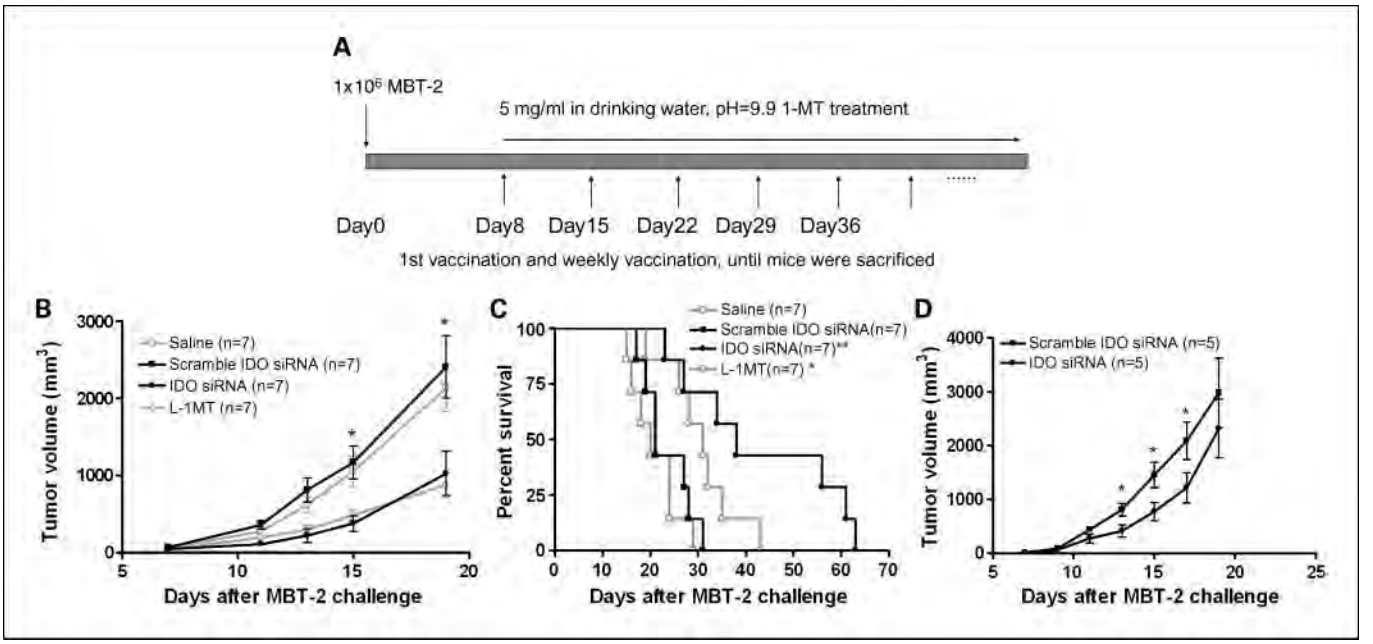

Fig. 3. Skin delivery of IDO siRNA had anticancer therapeutic effect in the C3H/HeN mouse tumor model. *A,* protocol for DNA vaccination. Eight days after s.c. tumor implantation of 1×10^6 of MBT-2 cells, mice were vaccinated using a biolistic device at weekly intervals. *B,* MBT-2 tumor volume in C3H/HeN mice; bars, ± S.D. *, a statistically significant difference when compared with the saline and scramble IDO siRNA groups ($P < 0.05$). *C,* Kaplan-Meier survival analysis of IDO siRNA – vaccinated mice. The number in parentheses is the number of mice in the experiment. *, a statistically significant difference when compared with the saline and scramble IDO siRNA groups ($P < 0.05$); **, a statistically significant difference when compared with the L-1MT groups ($P < 0.05$). *D,* adoptive transfer of dendritic cells from vaccinated mice delayed tumor progression. CD11c-positive dendritic cells were isolated from IDO siRNA mice or scramble siRNA mice and assayed for delay of tumor progression in naïve tumor-bearing mice.

enzyme activity by IDO siRNA were shown on Western blots and Kynurenine production, respectively (Fig. 2B).

To further examine the influence of IDO siRNA on the expression of IDO in skin dendritic cells *in vivo*, IDO siRNA or scramble IDO siRNA was codelivered with green fluorescence protein (GFP)-encoding plasmid to C3H/HeN mice via bombardment using gene gun, and GFP-positive CD11c-positive lymphocytes were isolated from inguinal lymph nodes 48 hours after bombardment (Fig. 2C, *top*). IDO siRNA significantly decreased the IDO-high-expression cells in total GFP-positive cells (Fig. 2C, *bottom*). The expression of IDO mRNA in CD11c-positive lymphocytes was significantly repressed by IDO siRNA, but not by scramble siRNA. IDO2 expression was only weakly affected (Fig. 2D). These data indicate that IDO siRNA could significantly down-regulate IDO expression *in vitro* and *in vivo*.

Therapeutic effect of IDO siRNA. To determine whether silencing IDO expression in skin dendritic cells leads to an antitumor effect, we first evaluated the therapeutic efficacy of IDO siRNA in an animal tumor model (i.e., the MBT-2 bladder tumor model in syngeneic C3H/HeN mice; refs. 31, 35). Because the L isoform of 1-MT is reported to be a specific inhibitor of IDO (26, 27), the therapeutic effect of IDO siRNA was compared with that of L-1MT (5 mg/mL in drinking water). The protocol of IDO siRNA vaccination is shown in Fig. 3A. L-1MT and IDO siRNA significantly delayed tumor growth when compared with scramble IDO siRNA (Fig. 3B). Furthermore, mice vaccinated with IDO siRNA or treated with L-1MT survived significantly longer than control mice ($P = 0.003$ and 0.013, respectively; Fig. 3C). It was interesting to note that skin delivery of IDO siRNA was even better than systemic administration of L-1MT. To further show that the therapeutic effects are mediated by dendritic cells in lymph nodes, CD11c-positive cells from vaccinated mice were harvested and transferred to recipient mice with established MBT-2 tumors. Adoptive transfer of

Fig. 2. The expression of IDO was down-regulated by IDO siRNA *in vitro* and *in vivo*. *A,* left panel, COS-7 cells (2×10^5) were cotransfected with different combinations of 0.5 μg IDO-myc (c-myc-tagged) and 1.5 μg U6 vector, IDO siRNA, or scramble IDO siRNA. IDO expression was determined with reverse transcription-PCR (RT-PCR). Hypoxanthine phosphoribosyltransferase was used as RNA internal control. Right panel, total cell lysates were subjected to Western blotting and detected with anti-myc antibody. β-Actin was used as internal control. *B,* tryptophan catabolism activity was repressed by IDO siRNA. Cells were harvested 24 h after transfection and the level of kynurenine was determined by high performance liquid chromatography. *, a statistically significant difference when compared with the U6 vector control and scramble IDO siRNA group ($P < 0.05$). *C,* IDO siRNA knockdown IDO expression in skin DC cells. Mice were vaccinated with plasmids encoding enhanced GFP (EGFP) plus IDO siRNA or scramble IDO siRNA. The expression of IDO was analyzed by flow cytometry 48 h after vaccination. Upper panel, EGFP positive cells were gated. Lower panel, the IDO expression in EGFP-positive cells. One representative of three independent experiments is shown. The IDO quantitative analysis was done on geometric means. *D,* IDO siRNA inhibited IDO expression of CD11c-positive cells in lymph node. CD11c-positive cells were isolated from 2×10^7 inguinal lymph node 48 h after vaccination. The mRNA level of IDO, IDO2, and hypoxanthine phosphoribosyltransferase was analyzed by RT-PCR (*top*). IDO mRNA was measured by quantitative real-time RT-PCR. Data were normalized to hypoxanthine phosphoribosyltransferase expression in each sample (*bottom*). *, a statistically significant difference when compared with control or the scramble IDO siRNA group ($P < 0.05$).

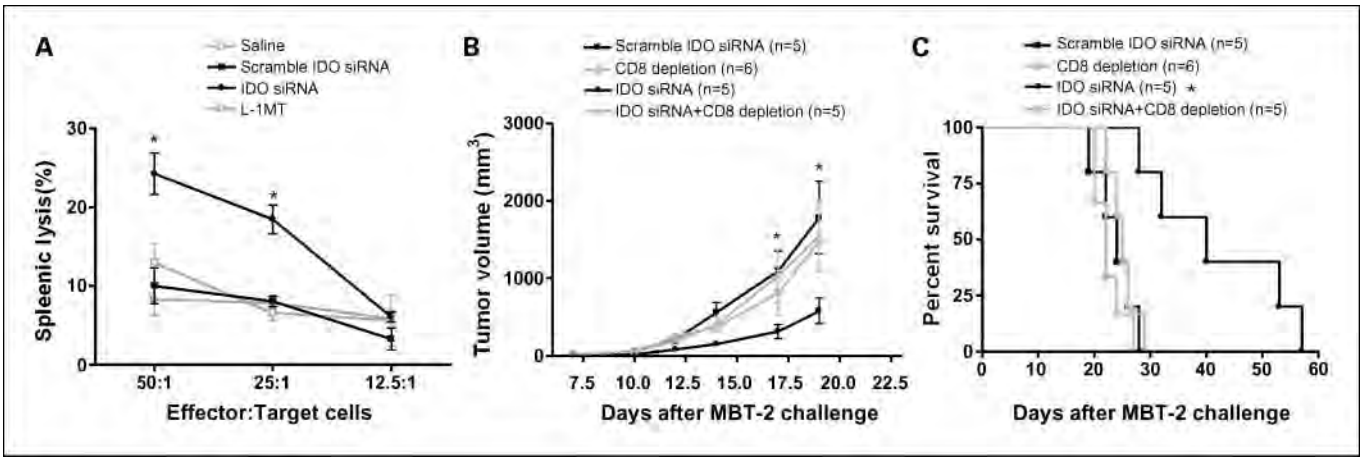

Fig. 4. The immunologic mechanism of tumor rejection. *A,* cytotoxicity assay of lymphocytes. Effector cells were lymphocytes derived from mice with the indicated treatments. MBT-2-luciferase cells (1×10^4) were used as target cells. Cytotoxicity was determined by the luciferase release. Each point represents the average of triplicate wells. *B,* tumor volume of C3H/HeN mice bearing MBT-2 tumor without or with CD8 depletion. Data are means of the animals per group; bars, $\pm$ S.D. *C,* the effects of CD8-positive T cell depletion on the mouse survival. The survival data were subjected to Kaplan-Meier survival analysis. The number in parentheses is the number of mice in the experiment. *, a statistically significant difference when compared with the scramble IDO siRNA and CD8-positive depletion group ($P < 0.05$).

CD11c-positive dendritic cells produced antitumor effects in recipient mice (Fig. 3D).

Cellular immunity induction by IDO siRNA. To examine the immunologic response induced by IDO siRNA, we determined the number of lymphocytes infiltrating tumor sites (Supplementary Table S1). CD4-positive, CD8-positive T cells and neutrophils were significantly increased in both IDO siRNA- and L-1MT–treated mice. We further evaluated the cytotoxic activity of splenocytes of vaccinated mice. The cytotoxic lysis activity in splenocytes was highest in the IDO siRNA-vaccinated group compared with all other groups, including the L-1MT group (Fig. 4A). The cytotoxic activity was significantly correlated with the number of infiltrating CD8-positive T cells in the IDO siRNA and L-1MT groups ($P = 0.0034$). This result suggests that CD8-positive T cells may play an essential role in the therapeutic effect of IDO siRNA vaccination. Depletion of CD8-positive T cells with monoclonal antibody (hybridoma 2.43) completely abolished the therapeutic effect of IDO siRNA (Fig. 4B and C).

Therapeutic effects of various IDO siRNA are correlated with their silencing efficacy. Because the siRNA may have off-target effects, i.e., attenuate other genes besides the target gene, we constructed two other IDO siRNAs, i.e., IDO siRNA-2 and IDO siRNA-3, targeting the sequences 326-344 and 1053-1072 of mouse IDO, respectively. The relative silencing efficacy of IDO siRNA-2 and IDO siRNA-3 was evaluated by cotransfection with c-myc IDO in COS-7 cells. Similar silencing efficacy for IDO siRNA-2 and IDO siRNA, and lower silencing efficacy for IDO siRNA-3, were shown by Western blotting with c-myc tag antibody (Fig. 5A). Likewise, the therapeutic effects of IDO siRNA-2 and IDO siRNA-1 were similar. On the other hand, IDO siRNA-3 had less efficacy in delaying tumor progression and prolonging mouse survival (Fig. 5B and C). The therapeutic effect of individual IDO siRNAs was thus correlated with its silencing effects on IDO gene expression, which suggested that the therapeutic effects of IDO siRNA is due to the reduction of IDO expression *in vivo*.

IDO siRNA had therapeutic efficacy in another animal tumor model. To determine whether IDO siRNA was functional in another animal tumor model, the CT-26 colon tumor in BALB/c mice was used. IDO siRNA exerted similar antitumor effects in mice bearing the CT-26 tumor. Vaccination with IDO siRNA reduced tumor burden and prolonged survival. Interestingly, L-1MT did not have a therapeutic effect in this model (Supplementary Fig. S1). Histologic analysis of infiltrating cells revealed that numbers of CD4-positive and CD8-positive T cells were significantly elevated in IDO siRNA–vaccinated mice (Supplementary Table S2). Taken together, our results indicate that IDO siRNA has antitumor therapeutic efficacy in BALB/c mice with CT-26 tumors.

IDO siRNA enhanced antitumor therapeutic efficacy of neu DNA vaccine. IDO is an immune regulatory molecule of dendritic cells, which are the main targets of the DNA vaccine. We then tested whether IDO siRNA could be used as an immunologic adjuvant to boost response to the DNA vaccine. Previously, the antitumor effect of neu DNA vaccine on the MBT-2 tumor (a tumor that endogenously overexpresses Her-2/Neu) was shown in C3H mice (32). Fusion of the NH_2-terminal neu DNA vaccine with IDO siRNA or scramble IDO siRNA had no effect on the IDO silencing by IDO siRNA and no effect on the expression of the truncated neu *in vitro* (Fig. 6A). The fusion product of neu DNA vaccine and IDO siRNA had significantly greater therapeutic efficacy than either component (neu DNA or IDO siRNA) separately (Fig. 6B and C).

IDO2 siRNA. To investigate the role of IDO2-expressing dendritic cells in tumor-bearing mice, we also treated C3H/HeN mice with IDO2-specific siRNA. The silencing efficacy of IDO2 siRNA was evaluated in COS-7 cells *in vitro*. IDO2 siRNA specifically suppressed IDO2 expression, but did not affect IDO1 expression (Supplementary Fig. S2). The expression of IDO2 mRNA in CD11c-positive lymphocytes was significantly repressed by skin delivery of IDO2 siRNA, but not by scramble siRNA. IDO expression was only weakly affected. Skin delivery of IDO2 siRNA had antitumor effects, but was less efficacious than IDO in the MBT2/C3H model (Supplementary Fig. S2).

Discussion

In this report, we have shown that skin delivery of IDO siRNA reduced the expression of IDO in dendritic cells and significantly delayed tumor progression *in vivo*. Increased infiltration of T cells and neutrophils were observed in mice vaccinated with IDO siRNA. The increase in neutrophils might induce tumor-specific T cell proliferation (36). The cancer therapeutic effects were probably mainly due to the enhancement of T cell immune responses against cancer because depletion of T cells abolished the therapeutic response to IDO siRNA.

The antitumor effects are unlikely to be due to the leakage of IDO siRNA to the tumor site because no GFP-positive cells were detected at these sites when GFP-encoding plasmid was delivered by gene gun to the skin.[7] Furthermore, adoptive transfer of IDO-knockdown CD11c-positive lymph node dendritic cells can provide antitumor immunity in naïve mice. These results support the notion that knockdown of IDO in dendritic cells mediates the antitumor immunity. Plasmid DNA delivered by biolistic device may transfect cells other than dendritic cells in skin, such as keratinocytes. IDO siRNA could down-regulate the expression of IDO in these cells. Because the biolistic device, unlike the viral delivery, can only transfect a limited amount of skin cells (31), the amounts of IDO alteration and metabolite change are minimal, and may not be sufficient to alter the skin environment to activate the dendritic cells. Altogether, down-regulation of IDO in skin dendritic cells is probably mainly responsible for the observed antitumor response.

Dendritic cells are important for priming immune responses to foreign antigen and can be recruited and activated by coadministration of plasmids encoding the chemokine macrophage inflammatory protein 1-α. In addition, the fms-like tyrosine kinase 3 ligand can potentiate the immunogenicity of plasmid DNA vaccines *in vivo* (37). Our experiments further expand the use of DNA as a tool for targeting regulatory genes in dendritic cells. In the absence of codelivered antigen, IDO siRNA alone can overcome immune tolerance and induce immunity directed against tumor-associated antigens expressed on MBT-2 or CT-26 cells. The enhancement of CTL responses to whole MBT-2 cells has been observed, although the specific tumor-associated antigens responsible for the cytotoxic responses have not been identified. In the presence of codelivered antigen, such as neu, IDO siRNA can further boost the specific adaptive immunity toward the tumor-associated antigen neu.

Skin dendritic cells are essential for mediating immune responses to infectious agents and cancer, and our experimental approaches can be used for other genes expressed in skin dendritic cells as well. In this report, we showed that either IDO or IDO-2 siRNA can produce antitumor effects *in vivo*. ATP has been shown to induce IDO and down-regulate thrombospondin-1 in dendritic cells (38). Based on this rationale, skin delivery of thrombospondin-1 siRNA can also be expected to induce an antitumor immune response, although thrombospondin-1 is classified as an antiangiogenesis molecule. Our preliminary results indicate that thrombospondin-1 siRNA indeed induces an antitumor immune response *in vivo*. Skin delivery of immunoregulatory siRNA may be a novel therapeutic method for treating cancer and other diseases. However, the success of this application depends on two important parameters. Firstly, down-regulation of a single immunoregulatory gene may not be sufficient to generate antitumor response in certain cases because tumor cells may create immune suppression through multiple pathways. One potential solution for this limitation is to inactivate several immune regulatory genes by multiple siRNAs. Secondly, the strength of antitumor immunity is determined by two factors: the efficacy of siRNA and the amounts of transfected dendritic cells. An IDO siRNA with less efficacy would not produce enough antitumor immunity to prolong mouse survival (Fig. 5C). On the other hand, optimization of immunization regimen or delivery device may enhance the amounts of transfected dendritic cells and the resultant antitumor immunity. PowerMed delivery device has been reported to deliver several folds more DNA into a larger delivery site than the conventional gene gun, which may provide another alternative in the clinical trial with human patients (39).

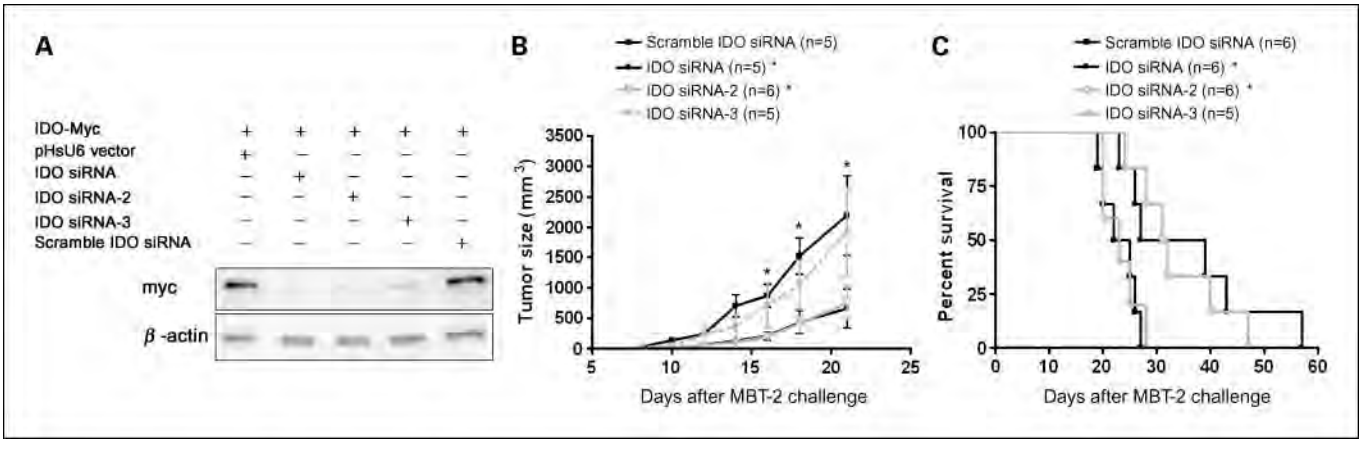

Fig. 5. The therapeutic effects of IDO siRNA are correlated with its silencing efficacy. *A,* the silencing effects of three IDO siRNAs. COS-7 cells were transfected with IDO siRNA, IDO siRNA-2, or IDO siRNA-3 targeted to different sequences, and cell lysates were analyzed with Western blotting to evaluate the silencing efficacy. *B,* MBT-2 tumor volume in C3H mice vaccinated with the three different IDO siRNAs. Data are expressed as group means. The number in parentheses is the number of mice in the experiment; bars, ± S.D. *, a statistically significant difference when compared with the saline and scramble IDO siRNA groups ($P < 0.05$). *C,* Kaplan-Meir analysis of survival of mice vaccinated with different IDO siRNAs.

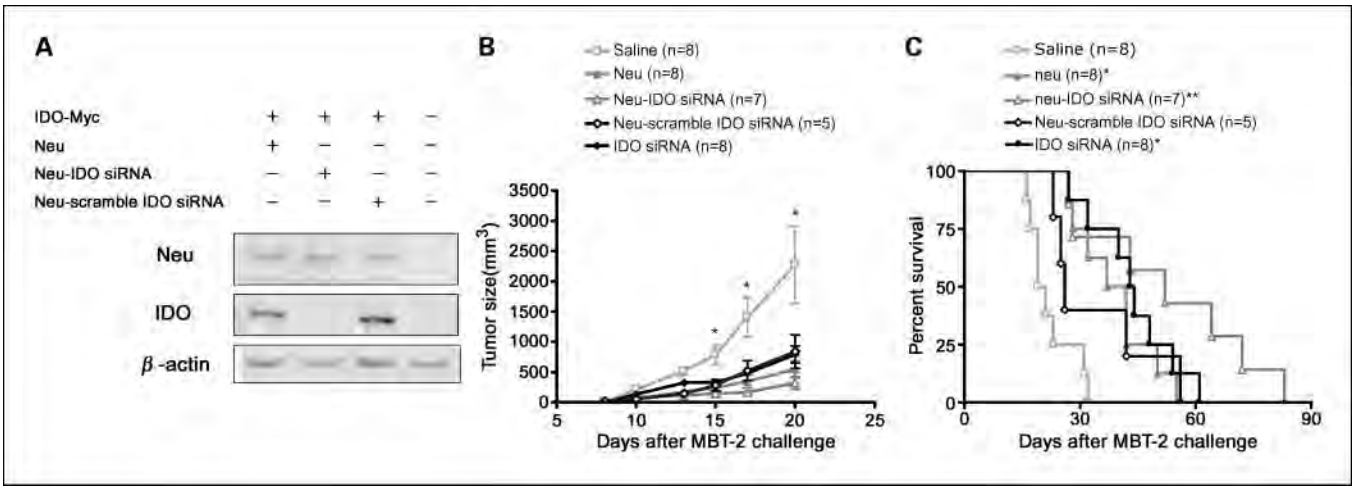

Fig. 6. Enhancement of the therapeutic effect of neu DNA vaccine after fusion with IDO siRNA. *A,* the fusion plasmid expressed truncated neu product and silenced IDO *in vitro*. COS-7 cells were transfected with neu, neu-IDO siRNA, or neu-scramble IDO siRNA. Cell lysates were subjected to Western blotting with respective antibodies. *B,* tumor-bearing mice were inoculated with the indicated siRNAs, and the tumor sizes were measured. Data are expressed as group means; bars, ± S.D. *, a statistically significant difference when compared with the saline and scramble IDO siRNA groups ($P < 0.05$). *C,* survival data were subjected to Kaplan-Meier analysis. The number in parentheses is the number of mice in the experiment. *, a statistically significant difference when compared with the saline group ($P < 0.05$); **, a statistically significant difference when compared with the saline, IDO siRNA, and neu groups ($P < 0.05$).

IDO siRNA was apparently more effective than IDO-2 siRNA in inducing antitumor immune responses. Because it is difficult to assess the relative silencing efficiency in dendritic cells, it is inappropriate to deduce that IDO is more effective than IDO2 in skin dendritic cells. In addition, the keratinocytes in skin were also transfected with the DNA delivered by gene gun inoculation. The activation of dendritic cells by either IDO or IDO2 siRNA suppressed IDO in both dendritic cells and surrounding skin keratinocytes. Our results clearly indicate, however, that IDO plays an important immunologic role in skin dendritic cells. Because the D-form of 1-MT has better antitumor activity and preferentially inhibits IDO2 activity in 293T cells, the role of IDO in dendritic cells has been questioned recently (26). Paradoxically, D-1MT loses its therapeutic effect in IDO-knockout mice, indicating IDO is required for D-1MT to exert its antitumor effects (23). Prendergast has proposed that IDO2 acts upstream of IDO in a common pathway, which would explain these discrepancies (40). These discrepancies may also result from differences between *in vitro* and *in vivo* observation. Moreover, the effect of D- or L-1MT may vary among the many different types of dendritic cells. Munn and Mellor have suggested that inappropriate antitumor responses may be largely due to plasmacytoid dendritic cells with constitutive expression of IDO in tumor-draining lymph nodes (16). In our experimental system, change in the expression of IDO in Langerhan cells and dermal dendritic cells are sufficient to reverse immune tolerance. Although the role of IDO2 in tryptophan catabolism in human dendritic cells may not be essential (27), skin delivery of IDO2 siRNA in mouse dendritic cells exerted a moderate anticancer effect. Taken together, our results support the concept that both IDO and IDO2 are important immune regulators in skin dendritic cells (39), but do not show whether IDO2 acts upstream of IDO.

Interestingly, epidermal gene gun administration of IDO siRNA is more potent than systemic administration of L-1MT (Fig. 3). Because three IDO siRNAs targeting different sites have been used in our experiments, the off-target effects of siRNA may be less likely to occur in our animal experiment. There are four possibilities for the observed effects. Firstly, the low palatability of pH9 water containing L-1MT may decrease the water consumption by mice, and the concentration of L-1MT in mice may not reach the maximal effective therapeutic range. Secondly, IDO inhibitor can diffuse systemically and therefore its effects on other tissues and organs may affect its therapeutic efficacy. Thirdly, 1-MT acts on other targets in addition to IDO1 or IDO2, and these side effects may affect its therapeutic efficacy. 1-MT interferes with toll-like receptor signaling in dendritic cells independent of IDO activity and can affect tryptophan transport through cell membranes (30, 41). Fourthly, part of IDO's effect may be independent of enzymatic activity. There are several carbohydrate metabolism enzymes that may act similarly (42, 43), and amino acid metabolism enzymes may do the same. Microarray comparison of IDO siRNA with other IDO inhibitors may help to resolve this difference (44).

It is very interesting and important to note that transfection of a small population of dendritic cells in lymph nodes can exert antitumor effects at a different site. One possibility is that this small population of dendritic cells presents the tumor-specific antigen to both peripheral tissue and lymph nodes and activates the immune response. Another possibility is that the small population of activated dendritic cells alters the properties of resident dendritic cells and other immune cells in lymph nodes. Previous results from Robbiani's group have indicated that single intranodal administration of C274 produced local and systemic effects on lymph node cell functions (45). In conclusion, the skin administration of immune regulatory molecules can induce a systemic antitumor immune response without targeting specific tumor-associated antigens.

Disclosure of Potential Conflicts of Interest

No potential conflicts of interest were disclosed.

References

1. Kadowaki N. Dendritic cells: a conductor of T cell differentiation. Allergol Int 2007;56:193–9.
2. Wu L, Liu YJ. Development of dendritic-cell lineages. Immunity 2007;26:741–50.
3. Tuyaerts S, Aerts JL, Corthals J, et al. Current approaches in dendritic cell generation and future implications for cancer immunotherapy. Cancer Immunol Immunother 2007;56:1513–37.
4. Tan JK, O'Neill HC. Concise review: dendritic cell development in the context of the spleen microenvironment. Stem Cells 2007;25:2139–45.
5. Grohmann U, Fallarino F, Puccetti P. Tolerance, DCs and tryptophan: much ado about IDO. Trends Immunol 2003;24:242–8.
6. Zou W. Regulatory T cells, tumour immunity and immunotherapy. Nat Rev Immunol 2006;6:295–307.
7. Mantovani A, Romero P, Palucka AK, Marincola FM. Tumour immunity: effector response to tumour and role of the microenvironment. Lancet 2008;371:771–83.
8. Takikawa O. Biochemical and medical aspects of the indoleamine 2,3-dioxygenase-initiated L-tryptophan metabolism. Biochem Biophys Res Commun 2005;338:12–9.
9. Mellor AL, Munn DH. IDO expression by dendritic cells: tolerance and tryptophan catabolism. Nat Rev Immunol 2004;4:762–74.
10. Liu Z, Dai H, Wan N, et al. Suppression of memory CD8 T cell generation and function by tryptophan catabolism. J Immunol 2007;178:4260–6.
11. Munn DH, Mellor AL. Indoleamine 2,3-dioxygenase and tumor-induced tolerance. J Clin Invest 2007;117:1147–54.
12. Munn DH, Sharma MD, Baban B, et al. GCN2 kinase in T cells mediates proliferative arrest and anergy induction in response to indoleamine 2,3-dioxygenase. Immunity 2005;22:633–42.
13. Belladonna ML, Grohmann U, Guidetti P, et al. Kynurenine pathway enzymes in dendritic cells initiate tolerogenesis in the absence of functional IDO. J Immunol 2006;177:130–7.
14. Friberg M, Jennings R, Alsarraj M, et al. Indoleamine 2,3-dioxygenase contributes to tumor cell evasion of T cell–mediated rejection. Int J Cancer 2002;101:151–5.
15. Uyttenhove C, Pilotte L, Theate I, et al. Evidence for a tumoral immune resistance mechanism based on tryptophan degradation by indoleamine 2,3-dioxygenase. Nat Med 2003;9:1269–74.
16. Munn DH, Sharma MD, Hou D, et al. Expression of indoleamine 2,3-dioxygenase by plasmacytoid dendritic cells in tumor-draining lymph nodes. J Clin Invest 2004;114:280–90.
17. Karanikas V, Zamanakou M, Kerenidi T, et al. Indoleamine 2,3-dioxygenase (IDO) expression in lung cancer. Cancer Biol Ther 2007;6:1258–62.
18. Muller AJ, DuHadaway JB, Donover PS, Sutanto-Ward E, Prendergast GC. Inhibition of indoleamine 2,3-dioxygenase, an immunoregulatory target of the cancer suppression gene Bin1, potentiates cancer chemotherapy. Nat Med 2005;11:312–9.
19. Riesenberg R, Weiler C, Spring O, et al. Expression of indoleamine 2,3-dioxygenase in tumor endothelial cells correlates with long-term survival of patients with renal cell carcinoma. Clin Cancer Res 2007;13:6993–7002.
20. Sharma MD, Baban B, Chandler P, et al. Plasmacytoid dendritic cells from mouse tumor-draining lymph nodes directly activate mature Tregs via indoleamine 2,3-dioxygenase. J Clin Invest 2007;117:2570–82.
21. Tas SW, Vervoordeldonk MJ, Hajji N, et al. Noncanonical NF-κB signaling in dendritic cells is required for indoleamine 2,3-dioxygenase (IDO) induction and immune regulation. Blood 2007;110:1540–9.
22. Mellor AL, Baban B, Chandler P, et al. Cutting edge: induced indoleamine 2,3 dioxygenase expression in dendritic cell subsets suppresses T cell clonal expansion. J Immunol 2003;171:1652–5.
23. Hou DY, Muller AJ, Sharma MD, et al. Inhibition of indoleamine 2,3-dioxygenase in dendritic cells by stereoisomers of 1-methyl-tryptophan correlates with antitumor responses. Cancer Res 2007;67:792–801.
24. Zheng X, Koropatnick J, Li M, et al. Reinstalling antitumor immunity by inhibiting tumor-derived immunosuppressive molecule IDO through RNA interference. J Immunol 2006;177:5639–46.
25. Ball HJ, Sanchez-Perez A, Weiser S, et al. Characterization of an indoleamine 2,3-dioxygenase-like protein found in humans and mice. Gene 2007;396:203–13.
26. Metz R, Duhadaway JB, Kamasani U, Laury-Kleintop L, Muller AJ, Prendergast GC. Novel tryptophan catabolic enzyme IDO2 is the preferred biochemical target of the antitumor indoleamine 2,3-dioxygenase inhibitory compound D-1-methyl-tryptophan. Cancer Res 2007;67:7082–7.
27. Lob S, Konigsrainer A, Schafer R, Rammensee HG, Opelz G, Terness P. Levo- but not dextro-1-methyl tryptophan abrogates the IDO activity of human dendritic cells. Blood 2008;111:2152–4.
28. Ball HJ, Yuasa HJ, Austin CJ, Weiser S, Hunt NH. Indoleamine 2,3-dioxygenase-2; a new enzyme in the kynurenine pathway. Int J Biochem Cell Biol 2008. Epub 2008 Jan 11.
29. Agaugue S, Perrin-Cocon L, Coutant F, Andre P, Lotteau V. 1-Methyl-tryptophan can interfere with TLR signaling in dendritic cells independently of IDO activity. J Immunol 2006;177:2061–71.
30. Tacken PJ, de Vries IJ, Torensma R, Figdor CG. Dendritic-cell immunotherapy: from *ex vivo* loading to *in vivo* targeting. Nat Rev Immunol 2007;7:790–802.
31. Lin CC, Yen MC, Lin CM, et al. Delivery of noncarrier naked DNA vaccine into the skin by supersonic flow induces a polarized T helper type 1 immune response to cancer. J Gene Med 2008;10:679–89.
32. Lin CC, Chou CW, Shiau AL, et al. Therapeutic HER2/Neu DNA vaccine inhibits mouse tumor naturally overexpressing endogenous neu. Mol Ther 2004;10:290–301.
33. Lu TJ, Lai WY, Huang CY, et al. Inhibition of cell migration by autophosphorylated mammalian sterile 20-like kinase 3 (MST3) involves paxillin and protein-tyrosine phosphatase-PEST. J Biol Chem 2006;281:38405–17.
34. De Luca A, Montagnoli C, Zelante T, et al. Functional yet balanced reactivity to Candida albicans requires TRIF, MyD88, and IDO-dependent inhibition of Rorc. J Immunol 2007;179:5999–6008.
35. Lin CC, Tu CF, Yen MC, et al. Inhibitor of heat-shock protein 90 enhances the antitumor effect of DNA vaccine targeting clients of heat-shock protein. Mol Ther 2007;15:404–10.
36. Kousis PC, Henderson BW, Maier PG, Gollnick SO. Photodynamic therapy enhancement of antitumor immunity is regulated by neutrophils. Cancer Res 2007;67:10501–10.
37. Sumida SM, McKay PF, Truitt DM, et al. Recruitment and expansion of dendritic cells *in vivo* potentiate the immunogenicity of plasmid DNA vaccines. J Clin Invest 2004;114:1334–42.
38. Marteau F, Gonzalez NS, Communi D, Goldman M, Boeynaems JM. Thrombospondin-1 and indoleamine 2,3-dioxygenase are major targets of extracellular ATP in human dendritic cells. Blood 2005;106:3860–6.
39. Fuller DH, Loudon P, Schmaljohn C. Preclinical and clinical progress of particle-mediated DNA vaccines for infectious diseases. Methods 2006;40:86–97.
40. Prendergast GC. Immune escape as a fundamental trait of cancer: focus on IDO. Oncogene 2008;27:3889–900.
41. Kudo Y, Boyd CA. The role of L-tryptophan transport in L-tryptophan degradation by indoleamine 2,3-dioxygenase in human placental explants. J Physiol 2001;531:417–23.
42. Kim JW, Dang CV. Multifaceted roles of glycolytic enzymes. Trends Biochem Sci 2005;30:142–50.
43. Zheng L, Roeder RG, Luo Y. S phase activation of the histone H2B promoter by OCA-S, a coactivator complex that contains GAPDH as a key component. Cell 2003;114:255–66.
44. Kumar S, Malachowski WP, Duhadaway JB, et al. Indoleamine 2,3-dioxygenase is the anticancer target for a novel series of potent naphthoquinone-based inhibitors. J Med Chem 2008;51:1706–18.
45. Teleshova N, Kenney J, Van Nest G, et al. Local and systemic effects of intranodally injected CpG-C immunostimulatory-oligodeoxyribonucleotides in macaques. J Immunol 2006;177:8531–41.